

**Akeem Olapade  
Mufutau**

**Fronthaul Móvel para Redes de Acesso Rádio de  
Próxima Geração**

**Mobile Fronthaul for Next Generation Radio Access  
Networks**



**Akeem Olapade  
Mufutau**

**Fronthaul Móvel para Redes de Acesso Rádio de  
Próxima Geração**

**Mobile Fronthaul for Next Generation Radio Access  
Networks**



**Akeem Olapade  
Mufutau**

## **Fronthaul Móvel para Redes de Acesso Rádio de Próxima Geração**

Tese apresentada às Universidades de Aveiro, Porto e Minho para cumprimento dos requisitos necessários à obtenção do grau de Doutor no âmbito do programa doutoral em Telecomunicações, MAP-Tele, realizada sob a orientação do **Professor Doutor Paulo Miguel Nepomuceno Pereira Monteiro**, Professor Associado do Departamento de Eletrónica, Telecomunicações e Informática da Universidade de Aveiro e Instituto de Telecomunicações de Aveiro, e sob a co-orientação do **Professor Doutor Arnaldo Silva Rodrigues de Oliveira**, Professor Auxiliar do Departamento de Eletrónica, Telecomunicações e Informática da Universidade de Aveiro e Instituto de Telecomunicações de Aveiro.

Apoio financeiro da Fundação para a Ciência e a Tecnologia (FCT) através do Programa Operacional Regional do Centro (CENTRO 2020) do enquadramento Portugal 2020, proporcionado pelos projectos ORCIP (CENTRO-01-0145-FEDER-022141), 5GO (POCI-01-0247-FEDER-024539), SOCA (CENTRO-01-0145-FEDER-000010), Projeto, RETIOT (POCI-01-0145-FEDER-016432) e LandMark (POCI-01-0145-FEDER-031527)

**FCT** Fundação para a Ciência e a Tecnologia

MINISTÉRIO DA CIÊNCIA, TECNOLOGIA E ENSINO SUPERIOR Portugal

Instituição de acolhimento:



Programa doutoral:





**Akeem Olapade  
Mufutau**

## **Mobile Fronthaul for Next Generation Radio Access Networks**

A thesis submitted to the Unversidade do Minho, Aveiro and Porto in partial fulfilment of the requirements for Doctoral degree in Engenharia Eletrotécnica/Telecomunicações under the MAP-Tele doctoral program. The thesis was conducted under the supervisions of Professor Dr. Paulo Miguel Nepomuceno Pereira Monteiro, Associate Professor in the Department of Electronics, Telecommunications and Informatics at the University of Aveiro and the Institute of Telecommunications of Aveiro, and under the co-supervision of Professor Dr. Arnaldo Silva Rodrigues de Oliveira, Assistant Professor at the Department of Electronics, Telecommunications and Informatics at the University of Aveiro and the Institute of Telecommunications of Aveiro.

Financial support from the Fundação para a Ciência e a Tecnologia (FCT) através do Programa Operacional Regional do Centro (CENTRO 2020) do enquadramento Portugal 2020, proporcionado pelos projectos ORCIP (CENTRO-01-0145-FEDER-022141), 5GO (POCI-01 -0247-FEDER-024539), SOCA (CENTRO-01-0145-FEDER-000010), Projeto, RETIOT (POCI-01-0145-FEDER-016432) e LandMark (POCI-01-0145-FEDER-031527)

**FCT** Fundação para a Ciência e a Tecnologia

MINISTÉRIO DA CIÊNCIA, TECNOLOGIA E ENSINO SUPERIOR Portugal

Instituição de acolhimento:



Programa doutoral:







**o júri / the jury**

presidente / president

**Doutor João Filipe Colardelle da Luz Mano**

Professor Catedrático  
Universidade de Aveiro

vogais / examiners committee

**Doutora Maria do Carmo Raposo de Medeiros**

Professora Associada  
Universidade de Coimbra

**Doutor Henrique Manuel de Castro Faria Salgado**

Professor Associado  
Universidade do Porto

**Doutor Paulo Miguel Nepomuceno Pereira Monteiro  
(Orientador)**

Professor Associado  
Universidade de Aveiro

**Doutor Mário José Neves de Lima**

Professor Auxiliar  
Universidade de Aveiro

**Doutor Fernando José da Silva Velez**

Professor Auxiliar  
Universidade da Beira Interior



## **agradecimentos / acknowledgements**

First and foremost, I would like to thank God for granting me uncountable blessings and mercies to accomplish this research work.

I would like to express sincere gratitude to my supervisor, Professor Paulo Miguel Nepomuceno Pereira Monteiro and my co-supervisor, Professor Arnaldo Silva Rodrigues de Oliveira for their unflinching support, guidance, availability, advice, and encouragement throughout my research. I sincerely thank my supervisors for giving me the opportunity to work with them and learn from their wealth of knowledge, which has led to interesting research directions.

Besides my supervisors, I am deeply indebted to Dr. Fernando Pedro Pereira Guiomar, a true friend and an excellent mentor, for his tireless efforts, encouragement, innovative ideas, and productive discussions. Words are not enough to eulogise and appreciate him for always motivating and inspiring me when the going got tough. Without his unstinting supports, guidance and valuable feedback, this work would not have come to fruition.

I am also grateful to Professor Dr. Antonio Luis Jesus Teixeira for his unceasing encouragement, unrelenting support, and attention. I am indeed indebted to you, sir.

My profound gratitude to Dr. Wasiu Tomori and Prof. Albert Adebayo for their encouragement, supports and serving as my guarantors.

I would like to thank Prof. B. Kareem, Prof. W. Akinlabi, Prof. O. A. Dahunsi, Dr. W. O. Apena, Dr. (Mrs) F.M. Dahunsi, Dr. Oluyomi Aboderin, Dr. Sheriff Busari, Dr. Shahid Mumtaz, Dr. Abdelgader Mahmoud, Dr Daud Folarin, Dr Kayode Taiwo, Mr. Steven Ogodo, Mr. Taiwo Adewusi, Mr. Adebayo Abejide, Mr. Abdelghafour Abraray, Mr. Patel Kantibhai, Mr. Samuel Pereira, Mr. Marco Fernandes, Miss Sulikha Yunus, and Miss Sanaa Finich for their contributions, directly or indirectly towards this feat.

I would like to sincerely thank my friend, Bruno Brandão, for translating the abstract of this thesis to Portuguese.

I sincerely thank Dr Isiaka Ajewale Alimi, who introduced the MAP-tele Doctoral Program to me, for his love, supports, encouragement and contributions towards the success of my doctoral research.

I would also like to acknowledge the MAP-Tele Doctoral Program in Telecommunications for offering an excellent doctoral program in telecommunications engineering, which is greatly beneficial to me.

My special thanks go to the Instituto de Telecomunicações de Aveiro (IT), University of Aveiro for providing excellent working conditions and funding for my research. I would also like to thank all the administrative and technical staff in IT for their supports.

I must also thank the management of Federal University of Technology, Akure for approving my study leave.

Lastly, I would like to thank my wife, Khadijah and my children for their invaluable love, support, perseverance, encouragement, patience and understanding throughout the duration of this work.



**palavras-chave**

Sistemas de transmissão ótica, fronthaul móvel, convergência ótica sem fio, rádio sobre FSO, Fronthaul flexível, rede de acesso de rádio.

**resumo**

A constante procura por melhores serviços de banda larga fixa e móvel é evidente e despoleta uma necessidade de desenvolver novas redes móveis com requisitos mais exigentes. As redes 5G e 6G já preveem a utilização de sistemas de comunicação heterogêneos que suportem novas aplicações e tecnologias wireless. De entre as várias arquiteturas propostas para as redes rádio de acesso, a Cloud Radio Access Network (C-RAN) tem sido considerada com o uma solução viável para as redes de próxima geração. No entanto, esta solução exige elevada largura de banda e baixa latência na ligação de fronthaul (MFH) devido ao uso da interface CPRI.

Considerando a procura por alta capacidade, a fibra ótica é o meio de transmissão mais adequado para a implementação de links transparentes dada a sua baixa atenuação, insensibilidade a interferência eletromagnética e grande largura de banda. No entanto, a transmissão de sinais wireless de alta velocidade na fibra ótica apresenta um desafio, especialmente quando é exigida baixa latência e jitter. Dados estes requisitos, neste trabalho são estudadas possíveis soluções para tecnologias óticas de transporte que evitem o uso do CPRI. Finalmente, uma ligação de fronthaul flexível baseada numa arquitetura C-RAN modificada é realizada recorrendo a uma plataforma de código aberto, demonstrando convergência entre domínios ótico-wireless com resultados promissores.



**keywords**

Optical transmission systems, mobile fronthaul, Radio over FSO, Flexible Fronthaul, radio access network

**abstract**

The ever-increasing demand for better fixed and mobile broadband connectivity is evident and necessitates the search for new mobile networks with new requirements. Heterogeneous communication systems that can support various innovative wireless technologies, services and applications are envisioned for fifth-generation (5G) and upcoming sixth-generation (6G) networks. While there are several proposed architectures for radio access networks, the Cloud Radio Access Network (C-RAN), which has been widely considered as a promising and viable solution for the next generation network, has been criticized for its stringent mobile fronthaul (MFH) requirements due to the Common Public Radio Interface (CPRI) to achieve seamless connectivity.

Considering the desired high capacities, optical fiber is an obvious transmission medium for building transparent links due to its low attenuation, insensitivity to electromagnetic interference, and enormous bandwidth. Nevertheless, the transmission of high-speed wireless channels over optical fibers poses a great challenge, especially when low latency and jitter are required. To overcome these challenges, optical transport technologies are used in this work. Moreover, considering the above requirements, possible transport solutions without CPRI for mobile fronthaul are investigated. Finally, to realize a flexible mobile fronthaul, a modified C-RAN prototype architecture is developed based on the extensive use of an open-source platform to demonstrate optical wireless convergence is demonstrated and promising results are presented in this thesis.





# Contents

<b>Contents</b>	<b>i</b>
<b>List of Figures</b>	<b>v</b>
<b>List of Tables</b>	<b>vii</b>
<b>List of acronyms</b>	<b>ix</b>
<b>List of Symbols</b>	<b>xv</b>
<b>1 Introduction</b>	<b>1</b>
1.1 Evolution of Radio Access Network . . . . .	3
1.1.1 Pre-5G Era . . . . .	3
1.1.2 5G and Beyond Network . . . . .	5
1.2 Optical Technologies for Mobile Transport . . . . .	7
1.2.1 Optical Transport Technologies . . . . .	7
1.2.2 Optical Wireless Communication for Mobile Fronthaul . . . . .	7
1.3 Motivation and Objectives . . . . .	8
1.4 Thesis outline . . . . .	9
1.5 Main Contribution . . . . .	9
1.6 List of publications . . . . .	10
References . . . . .	12
<b>2 Evolution of Radio Access Network Towards 5G and Beyond</b>	<b>17</b>
2.1 Cloud-RAN (C-RAN) . . . . .	17
2.2 Virtualized Cloud RAN . . . . .	21
2.3 Heterogeneous Cloud RAN (H-CRAN) . . . . .	24
2.4 Fog RAN . . . . .	27
2.5 Fronthaul Interface Requirements . . . . .	30
2.6 Functional Splits . . . . .	32
2.6.1 RF/PHY Split . . . . .	34
2.6.2 Low PHY Split . . . . .	36
2.6.3 Low PHY/High PHY Split . . . . .	36
2.6.4 High PHY Split . . . . .	37
2.6.5 PHY-MAC Split . . . . .	37

2.6.6	Intra-MAC Split . . . . .	38
2.6.7	MAC-RLC Split . . . . .	38
2.6.8	Intra-RLC Split . . . . .	39
2.6.9	RLC-PDCP Split . . . . .	39
2.6.10	PDCP-RRC Split . . . . .	40
2.7	Flexible Functional Split . . . . .	40
2.8	The 5G Radio Access Network . . . . .	41
2.9	5G NR Base station Architecture . . . . .	43
2.10	Architecture Options . . . . .	43
2.11	Evolving Open RAN and Smart RAN . . . . .	45
2.12	Summary . . . . .	47
	References . . . . .	47
<b>3</b>	<b>Transport Solutions for the Evolving RAN</b>	<b>55</b>
3.1	Millimeter-Wave and Terahertz Technologies . . . . .	56
3.2	Radio over Fiber Techniques . . . . .	58
3.2.1	Basic Structure of RoF System . . . . .	58
3.2.2	Types of RoF Transport Schemes . . . . .	59
3.2.2.1	Analog RoF Transport Schemes . . . . .	59
3.2.2.2	Digitized RoF Transport Schemes . . . . .	60
3.3	Optical-Wireless Communication Based Mobile Transport Solutions . . . . .	63
3.3.1	Free-space optical communication system . . . . .	64
3.3.2	Basic Structure of a FSO System . . . . .	64
3.3.3	Free Space Optics (FSO) Transport Schemes . . . . .	65
3.3.3.1	Hybrid RF/FSO System . . . . .	66
3.3.3.2	Relay-assisted FSO Transmission System . . . . .	67
3.4	Optical Access Transport Solution . . . . .	68
3.4.1	Passive Optical Network . . . . .	68
3.4.2	PON Based Mobile Transport Solution . . . . .	69
3.4.3	Low latency PON Based Solution . . . . .	73
3.5	Ethernet Based Mobile Fronthaul . . . . .	73
3.6	Time-Sensitive Network . . . . .	74
3.7	Summary . . . . .	76
	References . . . . .	76
<b>4</b>	<b>Open-Source enabled Real-time RAN with a PON Based Fronthaul</b>	<b>85</b>
4.1	An overview of the ORCIP Project . . . . .	86
4.2	Softwarization and Virtualization of RAN . . . . .	87
4.3	Virtualization Paradigm . . . . .	88
4.4	Software-Enabled RAN . . . . .	89
4.4.1	srsLTE Implementation . . . . .	91
4.4.2	SDR based srsUE . . . . .	92
4.4.3	OpenAirInterface Enabled Network Realization . . . . .	93
4.4.4	OAI-Based Baseband Processing . . . . .	95
4.4.5	Prototyping of a Non-Monolithic RAN . . . . .	98

4.4.6	Functional Split Based Architecture . . . . .	98
4.4.7	Building and Operating the Functional Split Setup . . . . .	99
4.4.8	OAI based 5G NR Experimental Demonstration . . . . .	100
4.4.9	Building gNodeB . . . . .	101
4.5	The Overall Setup Description . . . . .	101
4.6	Real-time Transmission over PON . . . . .	102
4.7	Results and Discussions . . . . .	104
4.8	Summary . . . . .	106
	References . . . . .	107
<b>5</b>	<b>Hybrid Optical Fiber–Wireless 5G and 4G fronthaul coexistence</b>	<b>113</b>
5.1	4G-5G Combined Transmission over Optical Fiber–Wireless Fronthaul . .	114
5.2	FSO Fronthaul Integration . . . . .	115
5.3	Experimental Setup . . . . .	115
5.3.1	Open-source Based RAN . . . . .	116
5.3.2	Optical–Wireless Mobile Fronthaul . . . . .	118
5.4	Experimental results . . . . .	119
5.5	Summary . . . . .	122
	References . . . . .	124
<b>6</b>	<b>Conclusions and Future Work</b>	<b>129</b>
6.1	Conclusions . . . . .	129
6.2	Future Work . . . . .	131
	References . . . . .	132
	<b>Appendices</b>	<b>133</b>
<b>A</b>	<b>OpenAirInterface Monolithic eNB with USRP NI-2953R</b>	<b>133</b>
<b>B</b>	<b>OpenAirInterface with Functional Split 7.2</b>	<b>147</b>
<b>C</b>	<b>Sample of OAI eNB, CU, DU and gNB Configuration files</b>	<b>159</b>
C.1	OAI eNB Configuration script . . . . .	160
C.2	OAI CU Configuration script . . . . .	165
C.3	OAI DU Configuration script . . . . .	171
C.4	OAI gNB Configuration script . . . . .	175



# List of Figures

1.1	Global Mobile Data Traffic Growth . . . . .	2
1.2	Mobile generations landmark. . . . .	4
2.1	A representation of traditional macro base station. . . . .	18
2.2	A traditional D-RAN architecture. . . . .	19
2.3	An example of a C-RAN architecture. . . . .	21
2.4	Basic structure of a V-CRAN. . . . .	23
2.5	Basic structure of a H-CRAN. . . . .	25
2.6	Basic structure of a F-RAN. . . . .	28
2.7	An overview of functional split options. . . . .	33
2.8	Overall architecture . . . . .	42
2.9	A generic structure of the gNB . . . . .	42
2.10	Baseline architecture options for NR deployment . . . . .	44
2.11	An O-RAN reference architecture. . . . .	46
3.1	An illustration of IAB deployment. . . . .	57
3.2	A simple illustration of RoF transport (Downlink). . . . .	59
3.3	A representation of analog RoF transport configurations. . . . .	61
3.4	A representation of digital RoF transport configurations. . . . .	62
3.5	A basic schematic to illustrate hybrid RF/FSO transmission. . . . .	66
3.6	An illustration of relay-assisted FSO transmission. . . . .	67
3.7	A simple representation of a PON based backhaul scheme. . . . .	70
3.8	A simple representation of a PON based fronthaul scheme. . . . .	71
4.1	Schematic representation of ORCIP research infrastructure . . . . .	86
4.2	Virtualization approach . . . . .	91
4.3	A Simple Representation of srsLTE Based Testbed exemplifying Monolithic Baseband processing . . . . .	93
4.4	OAI Communication Stack . . . . .	94
4.5	Monolithic OAI-LTE RAN . . . . .	96
4.6	Basic representation of OAI based functional split architecture . . . . .	99
4.7	Laboratory Setup for OAI based functional split architecture . . . . .	99
4.8	Overall setup showcasing virtualization approach . . . . .	102
4.9	Demonstration of real-time transmission over PON. . . . .	103
4.10	Measured data rate for TCP traffic. . . . .	103

4.11	Measured data rate for UDP traffic. . . . .	104
4.12	Over-the-Air signal capture by the VSA, showing modulation constellation points, signal waveform and error vector magnitude (EVM) while data traffic is being transmitted. . . . .	105
5.1	Emulated RAN with functional splits adopted for the experimental setup.	117
5.2	Experimental setup for the demonstration of heterogeneous 5G and 4G LTE fronthaul over a hybrid fiber-FSO link. The inset shows a photo of a mobile terminal downloading a 4K video using our end-to-end (E2E) OAI-based LTE implementation. . . . .	118
5.3	Snapshot of the FSO devices consisting of two fiber collimators and a two-inch mirror. . . . .	119
5.4	Measured spectra of both LTE signals measured with an antenna combined with the 5G signal after the photodetector. . . . .	120
5.5	Measured EVM vs time for the 64QAM, 100 MHz 5G signal. . . . .	121
5.6	RF power vs time for the 5G signal. . . . .	121
5.7	Measured constellation of the 5G signal after 8 km fiber and 55 m free-space optics link. The different points correspond to user data in the physical downlink shared channel (PDSCH), PDSCH demodulation reference signal (PDSCH-DMRS), primary and secondary synchronization channels (PSS and SSS), and physical broadcast channel (PBCH). . . . .	122

# List of Tables

1.1	Minimum performance requirements for 5G by IMT 2020 . . . . .	6
2.1	CPRI and eCPRI compared . . . . .	32
2.2	Comparison of the three categories of functional split . . . . .	35
3.1	Comparison of PON baseline systems . . . . .	72
3.2	Summary of IEEE standards for Ethernet Fronthauls . . . . .	75
4.1	Summary of some virtualization solutions . . . . .	90
4.2	System parameter and configuration of the developed E2E OAI-LTE testbed	97
4.3	System parameter and configuration for functional split testbed . . . . .	100
5.1	Hardware component for the setup . . . . .	116





# List of acronyms

<b>2G</b>	second-generation
<b>3G</b>	third-generation
<b>3GPP</b>	3rd Generation Partnership Project
<b>4G</b>	fourth-generation
<b>5G</b>	fifth-generation
<b>5GC</b>	5G core
<b>6G</b>	sixth-generation
<b>ADC</b>	analog-to-digital converter
<b>ARoF</b>	analog radio over fiber
<b>ARQ</b>	automatic repeat request
<b>B5G</b>	Beyond-5G
<b>BBoF</b>	baseband-over-fiber
<b>BBU</b>	baseband unit
<b>BER</b>	bit error rate
<b>BS</b>	base station
<b>BSC</b>	base station controller
<b>BTS</b>	base transceiver station
<b>CA</b>	carrier aggregation
<b>CAPEX</b>	capital expenditures
<b>CC</b>	cloud centre
<b>CM</b>	control and management
<b>CMRI</b>	China Mobile Research Institute
<b>CN</b>	core network
<b>CO</b>	central office
<b>CoE</b>	CPRI over ethernet
<b>CoMP</b>	coordinated multi-point
<b>COTS</b>	commercial off-the-shelf

<b>CP</b>	cyclic prefix
<b>CPRI</b>	Common Public Radio Interface
<b>C-RAN</b>	cloud radio access networks
<b>CU</b>	central unit
<b>DAC</b>	digital-to-analog converter
<b>DBA</b>	dynamic bandwidth allocation
<b>DIFoF</b>	digitized intermediate frequency-over-fiber
<b>DAS</b>	distributed antenna system
<b>DL</b>	downlink
<b>DRoF</b>	digitized radio over fiber
<b>DS</b>	downstream
<b>DU</b>	distributed unit
<b>E2E</b>	end-to-end
<b>eMBB</b>	enhanced mobile broadband
<b>eNB</b>	evolved NodeB
<b>eCPRI</b>	enhanced CPRI
<b>E-O</b>	electrical-to-optical
<b>EPC</b>	evolved packet core
<b>EVM</b>	error vector magnitude
<b>FFT</b>	fast Fourier transform
<b>FH</b>	fronthaul
<b>FHI</b>	fronthaul interface
<b>FSO</b>	free space optics
<b>FTTB</b>	fiber-to-the-building
<b>FTTH</b>	fiber-to-the-home
<b>GbE</b>	Gigabit Ethernet
<b>Gbps</b>	gigabits per second
<b>gNB</b>	gNodeB
<b>GPP</b>	general purpose processor
<b>GPRS</b>	general packet radio service
<b>GSM</b>	global system for mobile communication
<b>HARQ</b>	hybrid automatic repeat request
<b>HSPA</b>	high-speed packet access
<b>HSS</b>	home subscriber services

<b>I</b>	In-phase
<b>IEEE</b>	Institute of Electrical and Electronics Engineers
<b>iFFT</b>	inverse Fast Fourier Transform
<b>IFoF</b>	intermediate frequency-over-fiber
<b>IMSI</b>	international mobile subscriber identity
<b>IMT</b>	International Mobile Telecommunication system
<b>IoT</b>	internet of things
<b>IP</b>	internet protocol
<b>IT</b>	information technology
<b>ITU-T</b>	International Telecommunications Union – Telecommunications Sector
<b>KPI</b>	key performance indicator
<b>LoS</b>	Line-of-sight
<b>LTE</b>	Long Term Evolution
<b>MAC</b>	media access control
<b>MFH</b>	mobile fronthaul
<b>MIMO</b>	multiple-input multiple-output
<b>MME</b>	mobile management entity
<b>M-MIMO</b>	massive multiple-input, multiple-output
<b>mMTC</b>	massive machine type communications
<b>mm-wave</b>	millimeter wave
<b>MNO</b>	mobile network operator
<b>MSC</b>	mobile service switching center
<b>MTU</b>	maximum transmission unit
<b>NAS</b>	non access stratum
<b>NFV</b>	network function virtualization
<b>NGFI</b>	Next Generation Fronthaul Interface
<b>NGMN</b>	next generation mobile networks
<b>NG-PON2</b>	next-generation passive optical network stage 2
<b>NIC</b>	network interface card
<b>NSA</b>	non-standalone
<b>NR</b>	new radio
<b>OAI</b>	OpenAirInterface
<b>OAI-CN</b>	OAI core network
<b>OAISIM</b>	OAI Simulation

<b>OBSAI</b>	Open Base Station Architecture Initiative
<b>OFDM</b>	orthogonal frequency division multiplexing
<b>OLT</b>	optical line terminal
<b>ONU</b>	optical network unit
<b>OS</b>	operating system
<b>O-RAN</b>	open radio access network
<b>OPEX</b>	operational expenditure
<b>ORCIP</b>	optical radio convergence infrastructure for communications and power delivering
<b>ORI</b>	Open Radio Interface
<b>OSA</b>	OpenAirInterface Software Alliance
<b>OTN</b>	optical transport network
<b>OWC</b>	optical wireless communication
<b>PBCH</b>	physical broadcast channel
<b>PCFICH</b>	physical control format indicator channel
<b>PDCCH</b>	physical downlink control channel
<b>PDCP</b>	packet data convergence protocol
<b>PDSCH</b>	physical downlink shared channel
<b>PDU</b>	protocol data unit
<b>PGW</b>	packet data network gateway
<b>PHICH</b>	physical hybrid ARQ indicator channel
<b>PHY</b>	physical
<b>PON</b>	passive optical network
<b>PRACH</b>	physical random access channel
<b>PRB</b>	physical resource block
<b>PSS</b>	primary synchronization signal
<b>PtMP</b>	point to multipoint
<b>PtP</b>	point to point
<b>PUCCH</b>	physical uplink control channel
<b>PUSCH</b>	physical uplink shared channel
<b>Q</b>	Quadrature
<b>QoE</b>	quality of experience
<b>QoS</b>	quality of service
<b>R15</b>	release 15

<b>RAN</b>	radio access networks
<b>RAT</b>	radio access technology
<b>RAU</b>	remote antenna unit
<b>RCC</b>	radio cloud center
<b>RF</b>	radio frequency
<b>RLC</b>	radio link control
<b>RNC</b>	radio network controller
<b>RoF</b>	radio-over-fiber
<b>RoFSO</b>	radio-over-Free Space Optics
<b>RRC</b>	radio resource control
<b>RRH</b>	remote radio head
<b>RRU</b>	remote radio unit
<b>RU</b>	radio unit
<b>SCF</b>	small cell forum
<b>SDU</b>	service data unit
<b>SDAP</b>	service data adaptation protocol
<b>SDMN</b>	software defined mobile network
<b>SDN</b>	software-defined networking
<b>SDR</b>	software defined radio
<b>SFP</b>	small form-factor pluggable
<b>SGW</b>	serving gateway
<b>SISO</b>	single input single output
<b>SMF</b>	single-mode fiber
<b>SNR</b>	signal-to-noise ratio
<b>SRP</b>	stream reservation protocol
<b>SRS</b>	sounding reference signal
<b>srsLTE</b>	software radio system long term evolution
<b>SSS</b>	secondary synchronization signal
<b>SA</b>	standalone
<b>TCO</b>	total cost of ownership
<b>TCP</b>	transmission control protocol
<b>TDM</b>	time division multiplexing
<b>THz</b>	terahertz
<b>TRx</b>	transceiver

<b>TSN</b>	time-sensitive network
<b>TWDM-PON</b>	time wavelength division multiplexing-passive optical network
<b>UDP</b>	user datagram protocol
<b>UE</b>	user equipment
<b>UHD</b>	USRP hardware driver
<b>UL</b>	uplink
<b>UMTS</b>	universal mobile telecommunications service
<b>URLLC</b>	ultra-reliable and low latency communications
<b>USIM</b>	UMTS subscriber identity module
<b>US</b>	upstream
<b>USRP</b>	universal software radio peripheral
<b>V-CRAN</b>	virtualized cloud RAN

# List of Symbols

Symbol	Designation
$A(\lambda)$	total radiation attenuation
$B_i$	bandwidth of the $i^{th}$ channel
$c$	speed of light in vacuum
$C$	coding factor
$C_w$	factor of CPRI control word
$f$	frequency of the transmitted signal
$F1$	interface for inter-connection of a gNB-CU and a gNB-DU
$M$	number of antennas per sector
$N$	sample width (bits/sample)
$N_p$	noise power
$S_i$	signal power of the $i^{th}$ channel
$S_r$	sampling rate for digitization (sample/s/carrier)
$S1$	interface between RAN node and core network
$X_n$	interface between RAN nodes in SA operation (between ng-eNB & ng-eNB/gNB)
$\alpha$	attenuation coefficient
$\alpha_{fog}$	attenuation due to fog
$\alpha_{rain}$	attenuation due to rain
$\alpha_{snow}$	attenuation due to snow
$\alpha_{scattering}$	attenuation due to scattering effect
$\lambda$	wavelength of the transmitted optical wave
$\tau$	latency





# Chapter 1

## Introduction

The subscribers demand for better fixed and mobile broadband services is growing rapidly. This is due to the increasing use of information technology (IT), among other things, to enable low latency, high data rate services and applications, including emerging tactile communications and other cutting-edge technologies. In line with this, global data mobile traffic is escalating at exponential rate and according to Cisco, it is expected to reach 77 Exabytes per month by year 2022 as shown in Figure 1.1 [1]. Furthermore, with unprecedented high data rate requirements, fifth-generation (5G) and future mobile is envisaged to support diverse services and application scenarios, while also addressing spectra efficiency at a reduced total cost of ownership (TCO) and ultimately enabling green revolution by lowering energy consumption at the base stations [2]. In line with this, there have been persistent improvements in mobile network generation from earlier to the upcoming, 5G and even beyond to support the evolving services and applications.

Furthermore, International Mobile Telecommunication system (IMT) has classified the diverse services into three broad use cases for multitudes of possible application scenarios [3]:

- enhanced mobile broadband (eMBB), which is an improvement to the fourth-generation (4G) Long Term Evolution (LTE) broadband communication;
- ultra-reliable and low latency communications (URLLC) for services that require tight latency, high degree of reliability and availability, for instance remote medical surgery and tactile internet; and
- massive machine type communications (mMTC) which will involve a very large number of low cost devices with some content of non-delay-sensitive data.

Now, with the forthcoming sixth-generation (6G), several use cases with new requirements for unprecedented performance, are being identified by researchers [4–9], generally reflecting improved ultra reliable low latency communications and extreme capacity enhancements with envisioned better quality of service (QoS) for mobile broadband, internet of things (IoT), pervasive connectivity, augmented reality / virtual reality, holographic telepresence, unmanned mobility, eHealth, industry 4.0 and robotics.

Considering the foregoing, 5G and beyond mobile networks are deemed to involve disparate multiple technologies. Therefore, it is imperative that the mobile networks are designed to be flexible and adaptable to the dynamic services and applications. Furthermore, considering the requirements for 5G use cases, the 3rd Generation Partnership Project (3GPP) and other stake-holders in the telecommunication industry are standardizing the design of 5G network [10]. This effort which receives tremendous collaboration is yielding standards for defining 5G and beyond mobile network in phases. Likewise, the significant progress made on release 15 (R15) of the 3GPP, especially as regards eMBB has resulted to the first commercial deployment of 5G on R15 standard. The success of R15 motivates further development of releases 16 and 17, which are currently undergoing full standardization in response to the recurring need to improve on the eMBB while also adding more enhanced features of mMTC and URLLC [11].

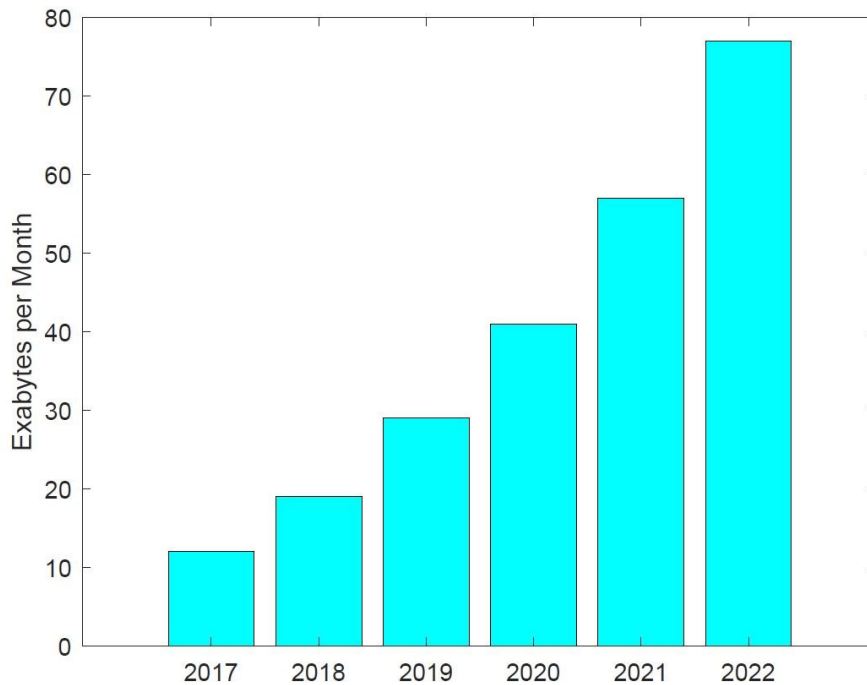


**Figure 1.1:** Global Mobile Data Traffic Growth [1].

Encouraged by the challenges associated with the increasing mobile data traffic, researchers in the industry and academics are continually developing and improving on the limitations of the existing technologies to achieve evolutionary networks that are capable of supporting the prevailing services and applications. Consequently, these research efforts have led to a paradigm shift in network architecture and supporting technologies, and hence the fundamental elements of existing mobile network architecture are being redefined, thus paving way for new terminology for some network elements.

Moreover, evolving from the existing 4G RAN architecture, some research works have identified cloud radio access networks (C-RAN) as a potential candidate for driving the 5G. C-RAN is a cloud computing-based architecture for radio access networks that splits the conventional cell-based network architecture into a centralized baseband unit and remote radio heads, while these two units are connected by a transport segment called

mobile fronthaul. The C-RAN architecture is proposed to enable centralized processing, collaborative radio, and real-time radio networking. However, C-RAN has been heavily criticized for its stringent requirements of high data rate and latency on the Fronthaul. Consequently, this limitation has excited several proposals geared towards redefining RAN entities for relaxing these stringent requirements imposed by the C-RAN. Among these techniques are the concept of functional decomposition of base-band processing, which has been widely investigated as a measure to circumvent the Fronthaul limitations of C-RAN and consideration for alternatives for the traditional Common Public Radio Interface (CPRI). Consequently, several flavors of RAN architectures have been proposed and extensively investigated based on different functional split options [12–16].

## 1.1 Evolution of Radio Access Network

Radio access networks (RAN) are identified as the most significant asset of mobile network operator (MNO) to deliver a variety of services required by subscribers [17, 18]. To continuously deliver services that meet prevalent demand, radio access networks (RAN) is continually being redesigned for renovation or outright development of new network entities to improve on QoS and quality of experience (QoE). Consequently, there have been significant improvements in the network architecture from global system for mobile communication (GSM) to 4G. Sequentially, technology standards are evolving from GSM, universal mobile telecommunications service (UMTS) for third-generation (3G) to LTE (4G) and 5G, including subsequent releases by 3GPP to meeting the increasing mobile traffic and also ensuring improvement in key performance indicator (KPI). Responding to the utmost need to provide mobile networks that match seamless dynamics pattern of global mobile data growth, it is becoming a tradition that new mobile network generation is surfacing every decade as evidenced over the years. As shown in Figure 1.2, evolution to 6G with KPI improvement is graphically illustrated [9]. For now, the era of 6G is emerging and stakeholders are currently defining and investigating enabling technologies for 6G.

### 1.1.1 Pre-5G Era

From generation to generation of mobile network, there has been an obvious progressive trend in terms of overall performance of the network. From the era of 2G when digital voice and circuit-switched data were delivered at rather low rates of 14.4 Kbps with enhancement featured by 2.5G general packet radio service (GPRS) achieving 170 Kbps data rate to 4G LTE achieving a maximum of 100 Mbps (single input single output (SISO)) [19]. Each mobile network generation has its peculiar RAN architecture in response to the prevailing service requirements. For instance, a GSM network comprises base transceiver station (BTS) that are connected to a base station controller (BSC). The BTS consists of radio transceiver (TRx) Modules which are responsible for signal processing, while the BSC coordinates the handovers, radio frequency (RF) power of the BTSs and also aggregates/desegregates the traffic prior to communicating with the mobile service switching center (MSC) in core network (CN).

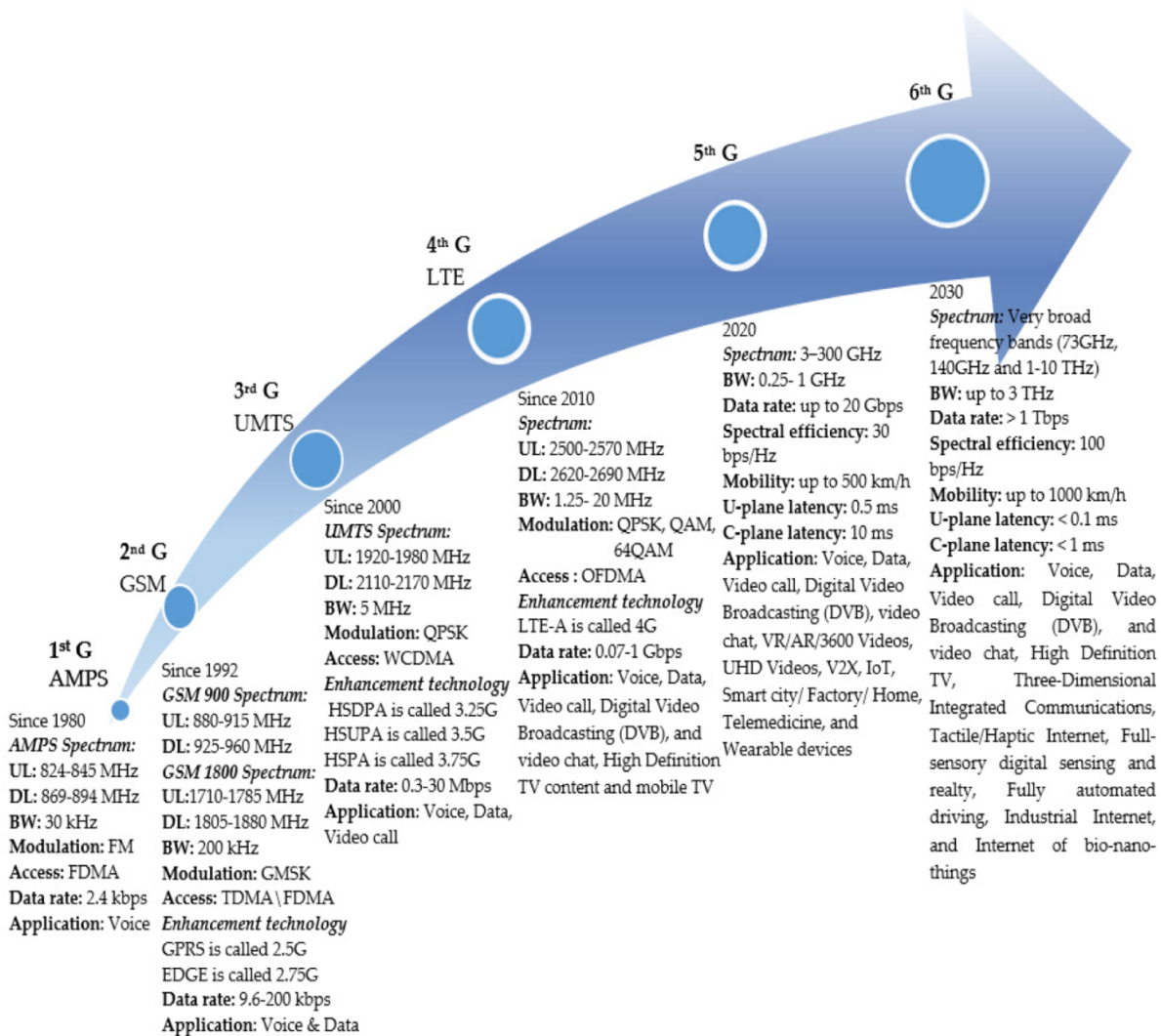


**Figure 1.2:** Mobile generations landmark [9].

After GSM, further enhanced features came through the introduction of 3G. Using enhanced data rates for GSM evolution (EDGE) and universal mobile telecommunications system (UMTS), 3G brought advanced improvement to data rates up to a higher peak rate of 14 Mbps with the support of evolution data optimized (EVDO) and high speed downlink packet access (HSDPA) at enhanced spectral efficiency. The architecture of 3G is composed of a base station (BS) called NodeB which is managed by a radio network controller (RNC). For 3G, the use of high-speed packet access (HSPA) and HSPA+ facilitate improved throughput and latency reduction [20].

Conversely, the 4G LTE series of 3GPP came with a more advanced architecture and offers a higher capacity per cell, improved throughput, lower latency and more frequency agility. LTE uses orthogonal frequency division multiplexing (OFDM) and allows 1.4 MHz, 3 MHz, 5 MHz, 10 MHz, 15 MHz and 20 MHz channel bandwidths. The BS is called evolved NodeB (eNB) and it is directly connected to the evolved packet

core (EPC) via an “*S1*” logical interface. The eNB to eNB link is established through the “*X2*” interface. Each eNB offers services to mobile devices or user equipment (UE) in one or more cells. By way of functionality, the BS that is communicating with a UE is called its serving eNB.

Fast forward to 5G network era, the 3GPP standards are undergoing consistent upgrading the LTE network as pathway to the 5G and beyond. The 3GPP release 10, for instance, refers to as LTE-Advance and emerges with more enhanced features and aimed at achieving a theoretical data rate of 1 Gbps and 500 Mbps in the downlink (DL) and uplink (UL), respectively. Furthermore, LTE uses carrier aggregation (CA) and coordinated multi-point (CoMP) to improve the quality of radio coverage within the entire network. Likewise, the LTE release 11 provided further improvements basically to mitigate the effects of interference and increase user throughput by equipping UE with mechanism that rejects interference [21], while release 15 emerges as the first version of 5G [11, 22].

### 1.1.2 5G and Beyond Network

Unlike the previous mobile network generations, 5G comes with unprecedented performance and some basic set of requirements to revolutionize telecommunications technology. Each generation of mobile networks is targeted at supporting communication services according the prevailing demands. For example, while voice and messaging services were supported by second-generation (2G) and mobile broadband is promoted by 4G, 5G is designed to offer enhanced flexibility and configurability to support more advanced capabilities than that of 4G LTE. Currently, 5G is being rolled out and its impacts in the society are gradually becoming conspicuous as it is deemed to support the three major use case classes: enhanced Mobile Broadband (eMBB), massive machine type communications (mMTC) and ultra-reliable low latency (URLLC). As presented in Table 1.1 [10], 5G is capable to deliver 20 times peak data rate, about 10% reduction of latency and improved spectral efficiency compared to 4G LTE.

The progression to 5G mobile network has aroused tremendous interests from the industries and academics. These efforts are yielding substantial research outputs to meeting the objectives of the novel 5G network. However, with the success achieved on the Rel-15 (first 5G version) on the enhanced mobile broadband (eMBB), the 3rd Generation Partnership Project (3GPP) is advancing with its further Releases 16 and 17 standards to improve on Ultra-Reliable Low Latency Communication (URLLC) and massive machine type communications (mMTC) use cases [11, 23, 24]. Considering the complexity arising from the delivering use case services, it becomes imperative to have robust radio access networks with flexibility that could the 5G and beyond 5G (B5G) services and applications, for instance support for network slicing [25]. Against this background, while there is significant research work directed at achieving good quality of service provisioning, tremendous efforts are ongoing in the improvement of the design and provisioning of radio access network (RAN) architecture for 5G and B5G network [11, 26, 27]. In particular, the transport segment of RAN has received considerable attention because of its peculiar importance in conveying the radio streams for the aforementioned

use cases.

**Table 1.1:** Minimum performance requirements for 5G by International Mobile Telecommunication system (IMT) 2020 [10]

KPI	Use Case	Values
Peak Data Rate	eMBB	DL: 20 <i>Gbps</i> , UL: 10 <i>Gbps</i>
Peak Spectral Efficiency	eMBB	DL: 30 <i>bps/Hz</i> , UL: 15 <i>bps/Hz</i>
User Experienced Data Rate	eMBB	DL: 100 <i>Mbps</i> , UL: 50 <i>Mbps</i> (Dense Urban)
5% User Spectral Efficiency	eMBB	DL: 0.3 <i>bps/Hz</i> , UL: 0.21 <i>bps/Hz</i> (Indoor Hotspot); DL: 0.225 <i>bps/Hz</i> , UL: 0.15 <i>bps/Hz</i> (Dense Urban); DL: 0.12 <i>bps/Hz</i> , UL: 0.045 <i>bps/Hz</i> (Rural)
Average Spectral Efficiency	eMBB	DL: 9 <i>bps/Hz/TRxP</i> , UL: 6.75 <i>bps/Hz/TRxP</i> (Indoor Hotspot); DL: 7.8 <i>bps/Hz/TRxP</i> , UL: 5.4 <i>bps/Hz/TRxP</i> (Dense Urban); DL: 3.3 <i>bps/Hz/TRxP</i> , UL 1.6 <i>bps/Hz/TRxP</i> (Rural)
Area Traffic Capacity	eMBB	DL: 10 <i>Mbps/m<sup>2</sup></i> (Indoor Hotspot)
User Plan Latency	eMBB, URLLC	4 <i>ms</i> for eMBB and 1 <i>ms</i> for URLLC
Control Plane Latency	eMBB, URLLC	20 <i>ms</i> for eMBB and URLLC
Energy Efficiency	eMBB	Capacity to support high sleep ratio and long sleep duration to enable low energy consumption when there is no data
Reliability	URLLC	$1 - 10^{-5}$ success probability of transmitting a layer-2 protocol data unit of 32 bytes within 1 <i>ms</i> in channel quality of coverage edge
Bandwidth	eMBB	At least 100 <i>MHz</i> ; Up to 1 <i>GHz</i> for operation in higher frequency bands (e.g. above 6 <i>GHz</i> )
Mobility	eMBB	Up to 500 <i>km/h</i>
Mobility Interruption Time	eMBB, URLLC	0 <i>ms</i>
Connection Density	mMTC	1,000,000 devices/ <i>km<sup>2</sup></i>

## 1.2 Optical Technologies for Mobile Transport

Mobile network is obviously evolving on a rapid track, while proactively meeting both the current and long term service requirements. As the era of next generation mobile network is fast approaching; the academia, research communities, MNO and standardization bodies are directing efforts toward the realization of 5G. Similarly, several research efforts are geared towards evolution of RAN to drive the 5G network. Therefore, this section present a brief introductory review of transport technologies for the 5G and future mobile network with emphasis on optical transport solutions and optical wireless communication (OWC) for fronthaul.

### 1.2.1 Optical Transport Technologies

Technologies for high capacity enhancement are desirable for meeting requirements of 5G as well guaranteeing traffic delivery within allowable delay limits. Notably, massive multiple-input, multiple-output (M-MIMO) techniques is projected to be prominently employed for achieving high capacity [28, 29], especially with the envisaged massive deployment of large antenna arrays for high channel capacity enhancement [30–32]. While millimeter wave (mm-wave) is a key driver for 5G air interface to provide high-speed communications, its utilization for M-MIMO with multi-elements arrays is widely investigated for enhanced high capacity transmission [33–35]. A combination of technologies for enabling high data rate communication poses challenges to the transport network to commensurate with air interface traffic. Therefore, considering the abundant bandwidth availability and high speed transmission characteristics, optical channel is an obvious transport technology for 5G and beyond cellular networks.

Optical transport technologies could offer low cost solutions in a particular situation whereby existing infrastructure for optical transport network (OTN) can be reused to deliver eMBB communication, for instance, by enabling transport support to densely populated small cell networks which are envisaged for 5G and beyond. There are significant research works investigating and proposing techniques for maximizing the benefits of using OTN for 5G and future network deployment. Furthermore, passive optical network (PON) as an OTN is being widely investigated for delivering 5G services, most especially the eMBB while considering the timing limitations [36]. Also, by allowing efficient use of the existing fiber infrastructures, there is remarkable saving of power used at the base stations due to reduction of site space. Among PON systems that are being heavily investigated include multi-wavelength based PON, typically time and wavelength division multiplexing PON (TWDM-PON) which is a hybrid of traditional TDM/TDMA and wavelength division multiplexing (WDM) technologies which is adopted by next-generation passive optical network stage 2 (NG-PON2) [37].

### 1.2.2 Optical Wireless Communication for Mobile Fronthaul

Following the increasing utilization of frequency spectrum and gradual congestion of RF allocations coupled with the quest for seamless communication at high data rate, attention is being directed towards the adoption of OWC as alternate or backup

link to wireless, wherever applicable. For 5G and future networks, higher carrier frequencies including the mm-wave (30 – 300 GHz) [33] and THz-wave frequency bands (0.1 – 10 THz) [38, 39] are key enablers to achieving high data rate. Furthermore, OWC channels have propensity to high bit rates, full duplex transmission, simplicity of implementation, license free operation, resistant to electromagnetic interference and high secured transmission. Similarly, OWC offers some benefits over RF in terms of high bandwidth, low power and mass requirements [40, 41]. These benefits are derived from the fibre optic characteristics. Thus, both OWC and fibre optic transmission are similar except that in the case of OWC, unguided channels are involved for transmitting modulated signals. However, as promising as OWC channels are, their reliability depends on requirement for strict line of sight, obstruction of signal propagation by objects within the Line-of-sight (LoS), great influence of weather conditions and dependence on very narrow beam-width to maximize gain. free space optics (FSO), in particular, is affected by background illumination and sun, introducing noise in the photodetector [41].

### 1.3 Motivation and Objectives

Inspired by the increasing data traffic due to the proliferation of connected devices, innovative wireless technologies, services and applications, several research efforts have been directed towards meeting this trend by the academia and industry. Widespread adoption of heterogeneous communication systems are envisaged for beyond 2020 mobile network. Despite the anticipated benefits of CPRI in terms of performance optimization and cost-effectiveness, attention is being drifted to the utilization of CPRI alternative mobile fronthaul (MFH) to avert limitations of tight requirements imposed by CPRI based architectures and consequently facilitating seamless connectivity between the mobile network entities. In view of the aforementioned, high capacities can be achieved by using optical fiber as a transmission medium because of its low attenuation, electromagnetic interference immunity and enormous bandwidth, to provide high capacity. However, the transportation of high speed wireless channels over the fiber attracts substantial challenges, especially when low latency transmission is required for the mobile fronthaul. Considering the prominent role that fronthaul plays in mobile network architectures, this research work is therefore motivated to investigate CPRI alternative MFH by exploiting enabling technologies to achieve a flexible fronthaul. Motivated by the need to support high capacity transmission seamlessly without the use of CPRI on the mobile fronthaul, we propose and investigate transport solutions based on optical-wireless communication and passive optical networks which are validated on our open-source based testbed. Therefore, the main objectives of this thesis are:

1. Study possible alternatives to the classic, bandwidth-hungry fronthaul networks;
2. Develop and demonstrate free space optics (FSO) fronthaul for carrying radio streams of 5G and beyond;
3. Investigate the performance and suitability of passive optical network (PON) as a mobile fronthaul for eMBB communication;



## 1.4 Thesis outline

This thesis is divided into chapters and organized as follows:

- In Chapter 2, a review of radio access network architectures is presented with particular emphasis on cloud radio access networks (C-RAN). Also, the various architectural modifications of C-RAN to 5G and beyond services as proposed in the literature are reviewed. Due to the challenges of conventional C-RAN in meeting diverse 5G services, functional split proposals are subsequently discussed. Finally, open-source technology geared towards a realization of intelligent radio access network and support for network ecosystem are discussed.
- Chapter 3 provides an overview of key enabling technologies for MFH transport solutions, with focus on their compatibility with current and future RAN architecture with emphasis on evolving fiber-optic, optical-wireless communication- and PON-based transport techniques.
- A brief review of softwarization and virtualization technologies are presented in Chapter 4, leading to the development of open-source based testbeds for the purpose of demonstrating, in real-time, the transmission of RF over PON based fronthaul. The same testbed has capability for validating other mobile fronthaul (MFH) solutions, thus exposing its simplicity to support several MFH technologies as added novelty of this research work.
- Chapter 5 presents a hybrid digital-analog fiber-wireless fronthaul architecture supporting a full-fledged 4G LTE and 5G coexistence which adopts both digital and analog radio-over-fiber (ARoF) fronthauling. In addition, this chapter showcases the real-time radio over FSO (RoFSO) transmission for outdoor application.
- Lastly, main conclusions from this work and suggestions for future research topics of interest are summarized in Chapter 6.

## 1.5 Main Contribution

The main contributions of this thesis are summarized as follows

1. This work proposes and experimentally demonstrate PON based mobile fronthaul integrated to a software-defined radio enabled end-to-end (E2E) mobile network which has the flexibility to support other mobile fronthaul solutions. With the developed testbed, an experimental assessment of PON-based fronthaul practically expose the limitation of PON-based MFH, thus providing a ground for further investigation for performance improvement. This work is published in [J3].
2. Another key contribution of this work is reported in [J2], where an hybrid fiber - FSO mobile fronthaul for a modified C-RAN architecture is proposed. The setup for the experiment is developed in-house and consist of a SDR based testbed that

adopts both digital and analog radio-over-fiber (ARoF) techniques. This work also involve an experimental setup which showcases a 5G and 4G coexistence scenario to experimentally demonstrate a success joint transmission of real-time 4G and 100MHz 64QAM-modulated 5G over the hybrid fronthaul comprising of 8 km fiber and 55 m FSO links with EVM measurements generally below 8% limit for 64QAM over uninterrupted period of 80 minutes.

3. To avoid the limitation imposed by the use of CPRI based mobile fronthaul by C-RAN, we propose and experimentally demonstrate Ethernet based fronthaul that is connected between the BBU and RRU. Successful transmission of a full-fledged E2E emulated mobile network is achieved thus exposing the possibility of advancing the use of non-CPRI based MFH. This contribution to research infrastructure is presented in [C1].
4. Propose and develop SDR-based testbed by exploiting open-source platform, contributing research infrastructure within the framework of the optical radio convergence infrastructure for communications and power delivering (ORCIP) project as enunciate in [C2], for testing and validating wireless-, optical fiber-, optical wireless- and hybrid fiber-wireless transport solutions. Use case for experimental assessment of real-time RF over a VLC based MFH is presented in [C3].

## 1.6 List of publications

During the course of this PhD work, the following manuscripts are produced for publication:

### Book Chapters

- [B1] I. Alimi, A. Mahmoud, **A. O. Mufutau**, F. P. Guiomar, J. Rodriguez, P. Monteiro, A. Teixeira, “Energy Efficiency in Cloud Radio Access Network (C-RAN) for 5G Mobile Networks: Opportunities and Challenges, Chapter in, Optical and Wireless Convergence for 5G Networks and Beyond,” Wiley, London, 2019

### Papers in international journals

- [J4] Alimi, I. A., Patel, R. K., **Akeem O. Mufutau.**, Muga, N. J., Pinto, A. N., & Monteiro, P. P. ,”Towards a Sustainable Green Design for Next-Generation Networks.” *Wireless Personal Communications* 121, 1123–1138, November 2021. <https://doi.org/10.1007/s11277-021-09062-2>
- [J3] **Akeem O. Mufutau**, Fernando P. Guiomar, Arnaldo Oliveira, Paulo P. Monteiro, “Software-Defined Radio enabled Cloud Radio Access Network Implementation using OpenAirInterface,” *Wireless Personal Communications*, September, 2021. <https://doi.org/10.1007/s11277-021-09064-0>.

- [J2] **Akeem O. Mufutau**, Fernando P. Guiomar, Marco A. Fernandes, Abel Lorences-Riesgo, Arnaldo Oliveira, Paulo P. Monteiro, “Demonstration of a hybrid optical fiber–wireless 5G fronthaul coexisting with end-to-end 4G networks,” *Journal of Optical Communications and Networking*, Vol. 12, No. 3, pp. 72 - 78, February, 2020.
- [J1] I. Alimi, **A. O. Mufutau**, A. Teixeira, P. Monteiro “Performance Analysis of Space-Air-Ground Integrated Network (SAGIN) Over an Arbitrarily Correlated Multivariate FSO Channel,” *Wireless Personal Communications*, Vol. 100, No. 1, pp. 47 - 66, March, 2018.

### Papers in conference proceedings

- [C3] **Akeem O. Mufutau**, Fernando P. Guiomar, Marco A. Fernandes, Arnaldo Oliveira, Paulo P. Monteiro, “On the Suitability of VLC Enabled Fronthaul for Future Mobile Network,” 11th Conference on Telecommunications, Order of Engineers of Portugal, Lisboa, Portugal, February 2021.
- [C2] P. Monteiro, I. Alimi, F. P. Guiomar, A. Lorences-Riesgo, **A. O. Mufutau**, A. Gameiro, “Flexible Optical and Wireless Testbed for 5G and Beyond Communication Systems,” *OSA Advanced Photonics Congress*, San Francisco, United States, Vol., Page JT4A.15, August, 2019.
- [C1] **Akeem O. Mufutau**, Carlos Borges Lopes; Abel Lorences-Riesgo, Fernando P. Guiomar, Atilio Gameiro; Arnaldo Oliveira, Paulo P. Monteiro, “Implementing a Software-Defined Radio Access Network for an Open 5G Testbed,” 11th Conference on Telecommunications, Order of Engineers of Portugal, Lisboa, Portugal, June, 2019.

---

## References

- [1] Cisco, “Cisco Visual Networking Index: Global Mobile Data Traffic Forecast Update, 2017–2022,” <http://media.mediapost.com/uploads/CiscoForecast.pdf>, [Online; accessed 2020-10-06].
- [2] Y. R. Li, M. Chen, J. Xu, L. Tian, and K. Huang, “Power Saving Techniques for 5G and Beyond,” *IEEE Access*, vol. 8, pp. 108 675–108 690, 2020.
- [3] K. Chang, K. Chu, H. Wang, Y. Lin, and J. Pan, “Energy Saving Technology of 5G Base Station Based on Internet of Things Collaborative Control,” *IEEE Access*, vol. 8, pp. 32 935–32 946, 2020.
- [4] M. Giordani, M. Polese, M. Mezzavilla, S. Rangan, and M. Zorzi, “Toward 6g networks: Use cases and technologies,” *IEEE Communications Magazine*, vol. 58, no. 3, pp. 55–61, 2020.
- [5] I. F. Akyildiz, A. Kak, and S. Nie, “6g and beyond: The future of wireless communications systems,” *IEEE Access*, vol. 8, pp. 133 995–134 030, 2020.
- [6] J. F. Monserrat *et al.*, “Key technologies for the advent of the 6g,” in *2020 IEEE Wireless Communications and Networking Conference Workshops (WCNCW)*, 2020, pp. 1–6.
- [7] L. U. Khan, I. Yaqoob, M. Imran, Z. Han, and C. S. Hong, “6g wireless systems: A vision, architectural elements, and future directions,” *IEEE Access*, vol. 8, pp. 147 029–147 044, 2020.
- [8] T. Nakamura, “5g evolution and 6g,” in *2020 IEEE Symposium on VLSI Technology*, 2020, pp. 1–5.
- [9] M. H. Alsharif *et al.*, “Sixth Generation (6G) Wireless Networks: Vision, Research Activities, Challenges and Potential Solutions,” *Symmetry*, vol. 12, no. 4, 2020.
- [10] M. Shafi *et al.*, “5G: A tutorial overview of standards, trials, challenges, deployment, and practice,” *IEEE Journal on Selected Areas in Communications*, vol. 35, no. 6, pp. 1201–1221, 2017.
- [11] A. Ghosh, A. Maeder, M. Baker, and D. Chandramouli, “5G Evolution: A View on 5G Cellular Technology Beyond 3GPP Release 15,” *IEEE Access*, vol. PP, pp. 1–1, 09 2019.
- [12] 3GPP, “Technical specification group radio access network; study on cu-du lower layer split for nr; (release 15),” 3rd Generation Partnership Project, Tech. Rep., 2017.
- [13] C. Y. Chang, N. Nikaiein, R. Knopp, T. Spyropoulos, and S. S. Kumar, “FlexCRAN: A flexible functional split framework over ethernet fronthaul in Cloud-RAN,” *IEEE International Conference on Communications*, 2017.

- [14] I. A. Alimi, A. L. Teixeira, and P. P. Monteiro, "Toward an Efficient C-RAN Optical Fronthaul for the Future Networks: A Tutorial on Technologies, Requirements, Challenges, and Solutions," *IEEE Communications Surveys Tutorials*, vol. 20, no. 1, pp. 708–769, Firstquarter 2018.
- [15] A. Maeder *et al.*, "Towards a flexible functional split for cloud-RAN networks," in *EuCNC 2014 - European Conference on Networks and Communications*, 2014.
- [16] A. Checko, A. P. Avramova, M. S. Berger, and H. L. Christiansen, "Evaluating C-RAN fronthaul functional splits in terms of network level energy and cost savings," *Journal of Communications and Networks*, vol. 18, no. 2, pp. 162–172, 2016.
- [17] C. I *et al.*, "Recent progress on c-ran centralization and cloudification," *IEEE Access*, vol. 2, pp. 1030–1039, 2014.
- [18] A. Checko *et al.*, "Cloud RAN for Mobile Networks - A Technology Overview," *IEEE Communications Surveys and Tutorials*, vol. 17, no. 1, pp. 405–426, 2015.
- [19] G. Thirunavukkarasu and G. Murugesan, "A comprehensive survey on air-interfaces for 5g and beyond," in *2019 10th International Conference on Computing, Communication and Networking Technologies (ICCCNT)*, 2019, pp. 1–7.
- [20] A. Gupta and R. K. Jha, "A Survey of 5G Network: Architecture and Emerging Technologies," *IEEE Access*, vol. 3, pp. 1206–1232, 2015.
- [21] M. Jaber, M. Imran, R. Tafazolli, and A. Tukmanov, "5G Backhaul Challenges and Emerging Research - A survey," *IEEE Access*, vol. 3536, no. c, pp. 1–1, 2016.
- [22] 3GPP Technical Specifications Groups, "Submission of initial 5G description for IMT-2020."
- [23] J. García-Morales, M. C. Lucas-Estañ, and J. Gozalvez, "Latency-Sensitive 5G RAN Slicing for Industry 4.0," *IEEE Access*, vol. 7, pp. 143 139–143 159, 2019.
- [24] M. A. Habibi, M. Nasimi, B. Han, and H. D. Schotten, "A Comprehensive Survey of RAN Architectures Toward 5G Mobile Communication System," *IEEE Access*, vol. 7, pp. 70 371–70 421, 2019.
- [25] J. García-Morales, M. C. Lucas-Estañ, and J. Gozalvez, "Latency-sensitive 5g ran slicing for industry 4.0," *IEEE Access*, vol. 7, pp. 143 139–143 159, 2019.
- [26] J. Pedreno-Manresa, P. S. Khodashenas, J. Izquierdo-Zaragoza, and P. Pavon-Marino, "Improved user experience by dynamic service handover and deployment on 5g network edge," in *2019 21st International Conference on Transparent Optical Networks (ICTON)*, 2019, pp. 1–4.
- [27] C. Barjau, M. Säily, and D. G. Barquero, "Enabling sfn transmissions in 5g cloud-ran deployments," in *2019 IEEE International Symposium on Broadband Multimedia Systems and Broadcasting (BMSB)*, 2019, pp. 1–5.

- 
- [28] Q. C. Li, H. Niu, A. T. Papathanassiou, and G. Wu, "5G Network Capacity: Key Elements and Technologies," *IEEE Vehicular Technology Magazine*, vol. 9, no. 1, pp. 71–78, 2014.
- [29] S. Yang and L. Hanzo, "Fifty Years of MIMO Detection: The Road to Large-Scale MIMOs," *IEEE Communications Surveys Tutorials*, vol. 17, no. 4, pp. 1941–1988, 2015.
- [30] T. Kashima *et al.*, "Large scale massive mimo field trial for 5g mobile communications system," in *2016 International Symposium on Antennas and Propagation (ISAP)*, 2016, pp. 602–603.
- [31] H. Hu, H. Gao, Z. Li, and Y. Zhu, "A Sub 6GHz Massive MIMO System for 5G New Radio," in *2017 IEEE 85th Vehicular Technology Conference (VTC Spring)*, 2017, pp. 1–5.
- [32] S. Yoshioka, S. Suyama, T. Okuyama, J. Mashino, and Y. Okumura, "5G massive MIMO with digital beamforming and two-stage channel estimation for low SHF band," in *2017 Wireless Days*, 2017, pp. 107–112.
- [33] R. G. Stephen and R. Zhang, "Joint Millimeter-Wave Fronthaul and OFDMA Resource Allocation in Ultra-Dense CRAN," *IEEE Transactions on Communications*, vol. 65, no. 3, pp. 1411–1423, March 2017.
- [34] Y. Huo, X. Dong, W. Xu, and M. Yuen, "Cellular and WiFi Co-design for 5G User Equipment," in *2018 IEEE 5G World Forum (5GWF)*, 2018, pp. 256–261.
- [35] O. Ulgen, U. Ozmat, and E. Gunaydin, "Hybrid Implementation of Millimeter Wave and Visible Light Communications for 5G Networks," in *2018 26th Telecommunications Forum (TELFOR)*, Nov 2018, pp. 1–4.
- [36] M. Kumari, R. Sharma, and A. Sheetal, "Passive Optical Network Evolution to Next Generation Passive Optical Network: A Review," in *2018 6th Edition of International Conference on Wireless Networks Embedded Systems (WECON)*, 2018, pp. 102–107.
- [37] J. S. Wey, "The Outlook for PON Standardization: A Tutorial," *Journal of Lightwave Technology*, vol. 38, no. 1, pp. 31–42, 2020.
- [38] P. T. Dat, A. Kanno, T. Umezawa, N. Yamamoto, and T. Kawanishi, "Millimeter-and terahertz-wave radio-over-fiber for 5G and beyond," in *2017 IEEE Photonics Society Summer Topical Meeting Series (SUM)*, July 2017, pp. 165–166.
- [39] S. A. Busari, K. M. S. Huq, S. Mumtaz, and J. Rodriguez, "Terahertz massive mimo for beyond-5g wireless communication," in *ICC 2019 - 2019 IEEE International Conference on Communications (ICC)*, 2019, pp. 1–6.
- [40] Z. Ghassemlooy, S. Zvanovec, M.-A. Khalighi, W. O. Popoola, and J. Perez, "Optical wireless communication systems," *Optik*, vol. 151, pp. 1–6, dec 2017.
-

- [41] A. Mansour, R. Mesleh, and M. Abaza, “New challenges in wireless and free space optical communications,” *Optics and Lasers in Engineering*, vol. 89, pp. 95 – 108, 2017, 3DIM-DS 2015: Optical Image Processing in the context of 3D Imaging, Metrology, and Data Security.





## Chapter 2

# Evolution of Radio Access Network Towards 5G and Beyond

The tremendous growth of data traffic and the increasing demand for low-latency services require new concepts for the architecture of mobile networks. These arise not only from the need to support an infinite number of different services, but also from the need to allow scalability and upgradeability while maintaining flexibility for service requirements. Over the years, this evolution has led to changes in the architecture of mobile networks from generation to generation. The current pre-5G mobile network architecture is designed to meet the requirements for voice and traditional mobile broadband services. In the previous generation, the architecture of RAN focuses on monolithic network functions in the form of physical network components that are largely inflexible and sufficient to deliver 5G services. As a result, paradigm shift in the organisation of the mobile network are becoming more apparent.

Defined by the need to support diversified services, the 5G mobile network has evolved from the traditional scheme, which has a more obvious impact on the BS functions that include baseband processing and radio functionalities. Several architectures have been proposed and are being studied in detail to enable the provision of 5G and beyond services that meet the envisaged requirements [1, 2]. To this end, radio access network architectures as drivers for 5G and beyond networks are extensively reviewed in this chapter.

### 2.1 Cloud-RAN (C-RAN)

The C-RAN, a well-studied candidate architecture for 5G, has received enormous attention as a possible enabler for 5G. The concept of C-RAN was first proposed and described by the China Mobile Research Institute (CMRI) [3]. The C-RAN is considered as an evolution of the distributed radio access network (D-RAN), which is widely used for 3G and 4G, while the D-RAN is also an evolution of the traditional BS architecture. As a brief summary, the traditional BS and the D RAN architectures are mentioned in this section to provide a basis for understanding the evolution from traditional RAN to C-RAN.

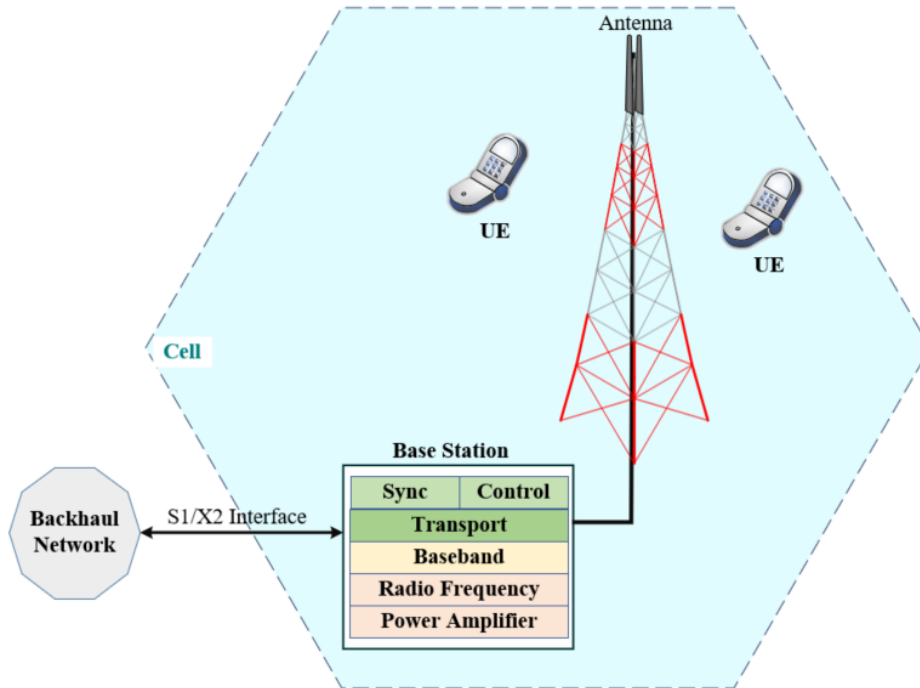


**Figure 2.1:** A representation of traditional macro base station (Adapted from [4, 5]).

The standard deployment for 2G mobile networks is based on the traditional BS, as shown in Figure 2.1. In this RAN architecture, the digital unit and the radio equipment controller (REC) form the base station. While the functions such as amplification, modulation/demodulation, frequency conversion, RF filtering, digital-to-analog/analog-to-digital conversion are performed in the digital unit, the REC handles the baseband signal processing, management and control of BSs and interface with the radio network controller [4]. The BS is mounted at the base of the tower and connected to the antenna at the top via a coaxial cable.

On the other hand, the universal terrestrial radio access network (UTRAN) and the evolved UTRAN (eUTRAN) for 3G and LTE, respectively, are based on the distributed radio access network (D-RAN) architecture as shown in Figure 2.2. In the D-RAN, all radio and baseband processing functions are performed separately in the remote radio head (RRH) or remote radio unit (RRU) and in the baseband unit (BBU). The RRU is usually located near the macro BS, while the BBU is placed such that each RRU is connected to a dedicated BBU via a transport network called a fronthaul, which in turn is connected to the EPC via a backhaul network. Interaction between RRU and BBU is enabled by using the CPRI to transmit in-phase and quadrature (IQ) between RRU and BBU over optical fiber or microwave fronthaul. Data related to handover and coordinated transmission between eNBs are also exchanged over the backhaul link. In an LTE architecture, the connection between master eNB and secondary eNBs is established over the X2 interface. Therefore, inter-cell cooperation between BSs is enabled by performing the control plane and mobility functions at the master BS while the user plane data transmissions and other lower layer functions are distributed [4, 6]. In addition,

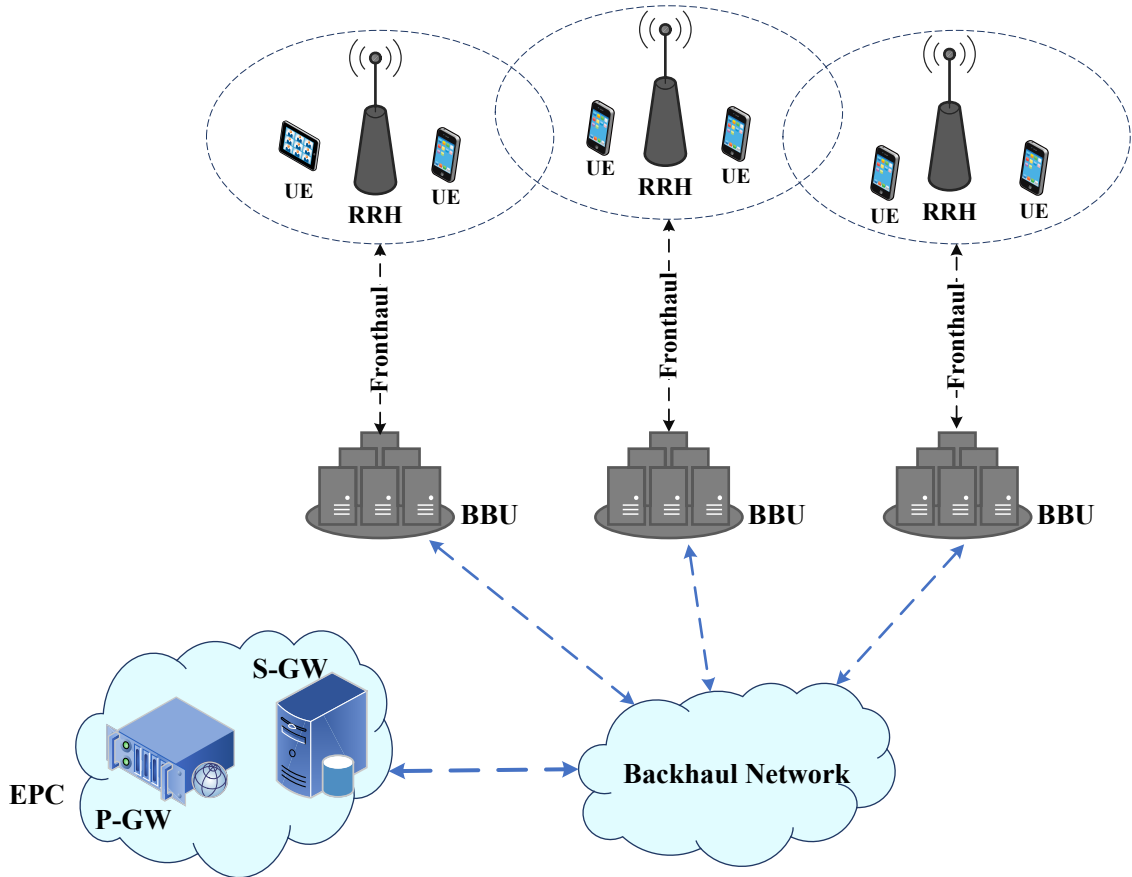


**Figure 2.2:** A traditional D-RAN architecture in which each RRH is connected to a dedicated BBU via the fronthaul (Adapted from [4]).

the UE can establish direct communication with the RRU, which can only perform RF functions [6].

As suitable as the distributed BS architecture is for 3G and 4G, its scalability and ability to deliver 5G services with high bandwidth, low latency and cost efficiency are complicated. Therefore, D-RAN has been modified to allow centralization of baseband processing functions so that network coordination and management can be supported in a way that does not compromise the cost-efficiency and energy efficiency of the cellular network in providing 5G services [7]. In contrast to D-RAN, centralized baseband processing is introduced by having multiple BBU forming a BBU pool or BBU hosting at a concentration point to support multiple connected RRUs. The resulting centralized scheme is shown in Figure 2.3. Hence, this centralized and cloudified RAN, which can be used to pool network resources, is referred to as C-RAN. This scheme promotes the use of advanced computing techniques and virtualization technology for radio and baseband processing functions, leading to the development of variants of C-RAN such as virtualized cloud RAN (V-CRAN), fog RAN (F-RAN), and heterogeneous cloud RAN (H-CRAN). These variants are discussed in the sections 2.2 - 2.4.

Moreover, the impact of the centralization concept introduced in the RAN architecture is pronounced on the coordinated multiple point (CoMP) transmission and reception

which has an influence on the inter-cell interference cancelation in the cellular networks and also on the multiple-input multiple-output (MIMO) functionality of the network [8].

## Basic Types of RAN Centralization

The C-RAN architecture can be configured to perform partial, full, or hybrid centralization depending on which stack layer functions are executed in the BBU pool [9], as described below:

### Fully Centralized

In the fully centralized configuration, all functions of physical (PHY), media access control (MAC), and the network layer are moved to the BBU. This simplifies operation and maintenance, as resource management and processing is handled by the BBU pool. However, this solution results in high bandwidth due to the IQ data exchange between the RRH and the BBU pool. This is an obvious drawback as it causes a significant communication overhead between the BBU and the RRHs, which could limit the performance due to the fronthaul (FH) capacity [9].

### Partially centralized

One attempt to reduce the capacity burden on the fronthaul is a partially centralized solution. In this configuration, the MAC and network layer functions are centralized at the BBUs, while the physical layer functions reside at the RRHs [9]. However, this structure forces complex communication between the MAC and PHY layers, as the sharing of PHY layer resources between different RRHs is significantly limited and CoMP is not optimally supported.

### Hybrid centralized

In the case of the hybrid centralized structure, the functionalities lie between the two extremes mentioned above. This configuration allows the use of some physical layer functions in the BBUs, while other remaining parts are executed in the RRHs, in particular cell signal processing or user-specific functions that are normally executed in the RRHs [9]. The flexibility of this arrangement cannot be underestimated, particularly in terms of the ability to share resources in conjunction with reducing power consumption and communication overhead in the BBUs. Moreover, the hybrid C-RAN supports the proposal to share the processing of BBU functions between the cloud centre (CC) (or central office (CO)) and the RRH pool, also referred to as the edge cloud, an aggregation node that has lower processing efficiency.

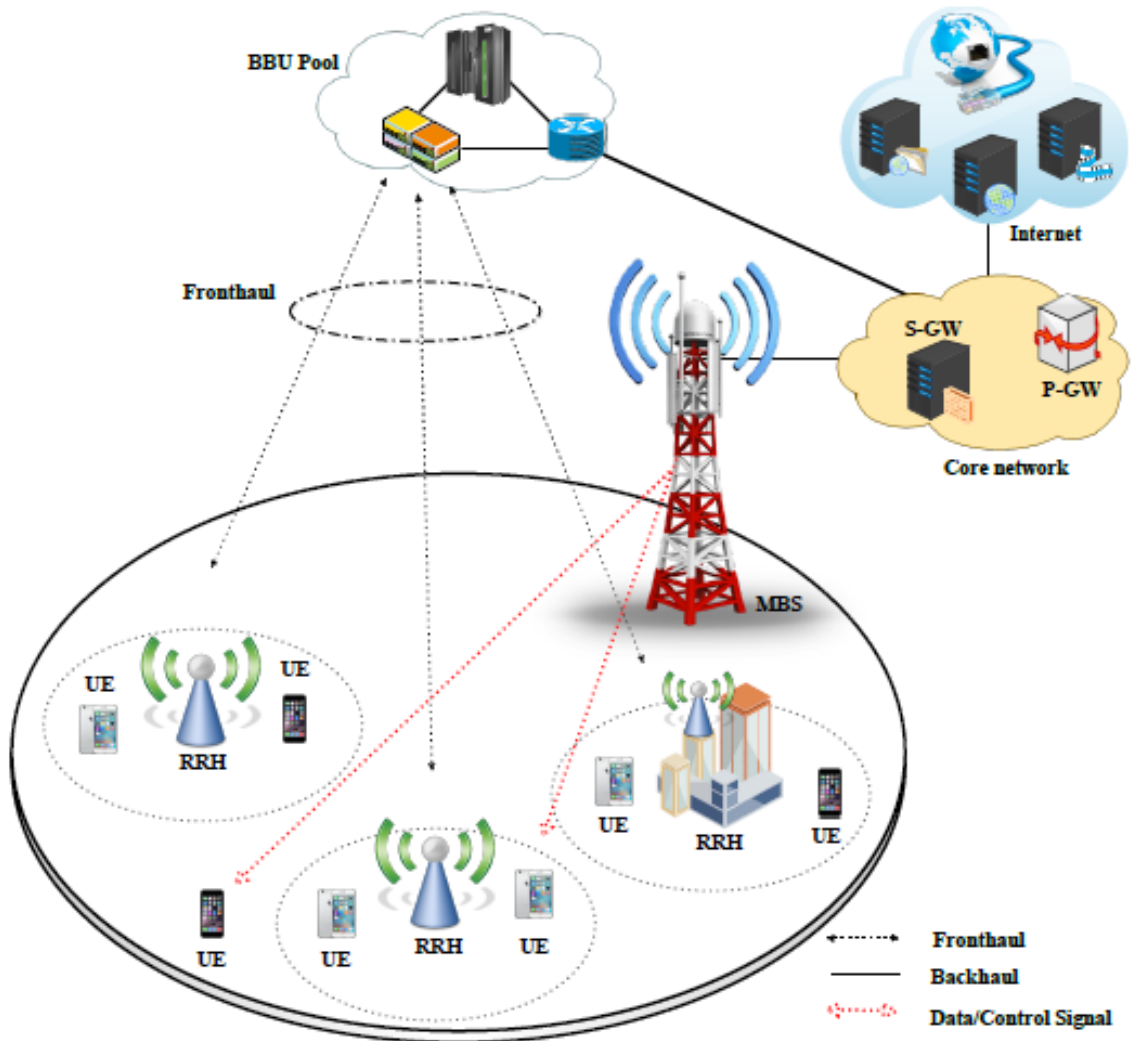


Figure 2.3: An example of a C-RAN architecture [8].

## 2.2 Virtualized Cloud RAN

The centralized architecture provides the ability to move non-real-time functions to the central office while keeping the real-time functions in the cell site. Therefore, the baseband functions can be redefined by separating the real-time critical baseband functions from the non-real-time critical functions. Based on the evolution towards a centralized architecture, virtualization of RAN is necessary as the baseband processing functions can be divided among different network entities. In addition to lowering CAPEX/OPEX for the MNO while potentially centralizing radio and baseband processing, the adoption of robust virtualization technology for mobile networks is widely used in cloud RAN architecture. A notable advantage of RAN virtualization is the ability to execute radio processing intelligence without depending solely on purpose-built hardware to deliver high-quality, real-time communications. Consequently, more

flexible deployment options can be achieved for different cell configurations. In addition, RAN virtualization not only impacts network performance improvement and resource utilization efficiency, but also enables seamless network upgrades. With network function virtualization (NFV) and software-defined networking (SDN), various functionalities of the cellular network can be combined into E2E virtualization. Thus, the components of the cellular network can be virtualized by creating a logical abstraction of the physical hardware for the processing functions of the CN and RAN units.

Despite the benefits attributed to RAN virtualization, its implementation is hindered by scalability and latency complications. One attempt to address this limitation is the use of mobile edge computing or multi-access edge computing (MEC), which focuses on decentralizing the virtual RAN to the edge and fog computing levels [10, 11]. With MEC in radio access, more computing capacity is allocated at the edge near the users. This allows large amounts of connected devices with MEC to serve small cells, as expected for 5G traffic.

## Basic Structure of V-CRAN

A basic structure of a virtualized cloud RAN (V-CRAN) is shown in Figure 2.4. In the V-CRAN virtualization techniques are used to support radio access and core network functions. The V-CRAN includes the BBU cloud, the MFH network that provides communication between the pool of RRH and the BBU cloud. The data and signaling exchange between the BBUs and the RRHs usually requires higher bandwidth and lower latency of the fronthaul. Therefore, transmission over high-capacity optical channels for V-CRAN is desirable to meet these requirements while enabling possible virtualization of the MFH network. In [10], a time wavelength division multiplexing-passive optical network (TWDM-PON)-based fronthaul network enabling optical channel sharing by virtual BBUs is used to describe an end-to-end V-CRAN. Baseband processing including all PHY, MAC, radio link control (RLC), packet data convergence protocol (PDCP), and radio resource control (RRC) functions are centrally processed in the BBU cloud. Interaction between all BBUs in the cloud can be done via high-speed Layer 2 switches to facilitate data exchange and signaling.

Using a TWDM-PON system as a fronthaul, the optical line terminal (OLT) of the PON is connected to the BBU cloud and the multiple optical network units (ONUs) serving the RRHs, which may be co-located but may also be remote from the OLT. The PON between the BBU cloud and the array of RRH can be used advantageously to create virtualized channels [4, 10] and eventually form a Virtualized Passive Optical Network (VPON). For this purpose, each BBU is connected to a VPON via a line card and an optical transceiver to transmit the desired traffic after an optical-to-electrical conversion. Through the VPON, a single BBU located in the BBU cloud can control multiple RHHs or radio units and provide communication-related services. The V-CRAN is an obvious candidate for reducing OPEX and energy consumption while efficiently managing network resources [10, 11].

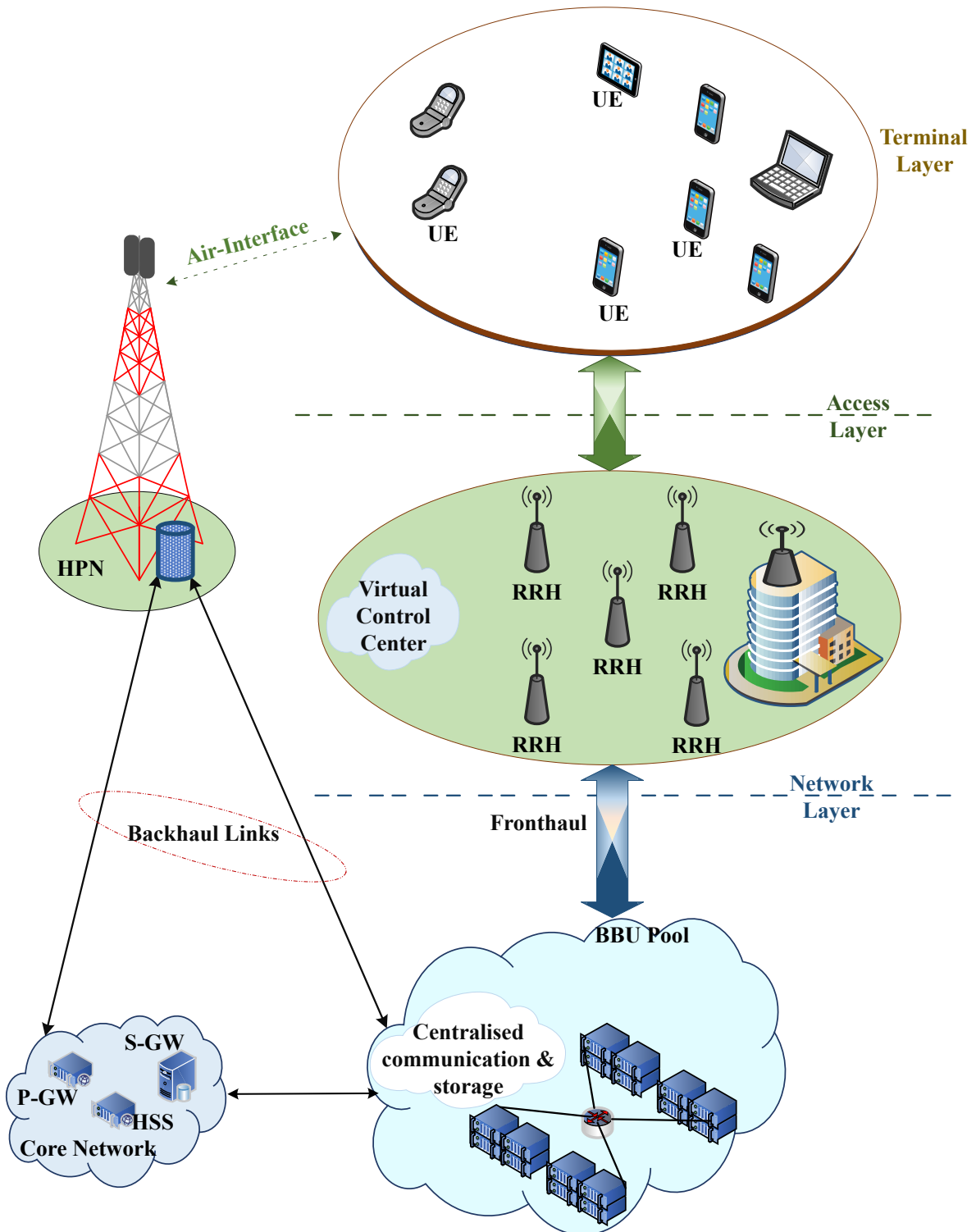


Figure 2.4: Basic structure of a V-CRAN (Adapted from [4]).

## Review of V-CRAN research

Motivated by the potential benefits associated with the use of V-CRAN, several research efforts have focused on its system architecture. In particular, Reference [4]

explores advances in SDN and C-RAN, which are geared towards virtualization of the next-generation wireless networks. Also, in [10], a virtualization architecture for wireless networks is developed to optimize the dynamic allocation of network resources based on the cognitive plane, control plane, and data plane. According to the authors, the proposed architecture provides improvement in network performance and spectrum efficiency while reducing the packet loss rate to 1/20. Similarly, [4] has extensively used container virtualization to develop and demonstrate a fully virtualized end-to-end mobile network implementing 3GPP 7.3 functional split. In addition, [12] presents the architectural characterization for the 5G vRAN including multi-access edge computing (MEC). In the paper, an experimental setup is proposed to demonstrate 5G vRAN including the coexistence of 5G NR and MEC. The authors concluded that the overhead time due to MEC application processing is less threatening to the operation of 5G NR than the system failure.

Regarding the performance of V-CRAN, Reference [13] attempts to identify possible solutions to the problems of network performance, scalability, security, and interoperability. Moreover, in [14] throughput, system stability, and fairness are analyzed based on the strategies of dominant resource fairness (DRF) and proportional fairness (PF) for resource allocation. Similarly, Paper [15] defines macro-level metrics and micro-level metrics as performance metrics for evaluating BS virtualization platforms. According to the authors, all measurements related to real-time performance and virtualization overhead are categorized as micro-level metrics, while macro-level metrics evaluate the virtualization platform's ability to support the BS resource and virtualization function during the process of fulfilling the radio access network requirements. To minimize the total end-to-end delays of C-RAN with a BBU cloud consisting of a set of virtual BBU functions, [16] proposes a combinatorial optimization model and employs two heuristic approaches while meeting the capacity and cost constraints.

Another aspect of V-CRAN, which is extensively studied, is resource allocation. For efficient resource allocation and management, [17] recognizes and discusses user assignment, throughput maximization, RRH selection, spectrum management, network utility, and power allocation. Moreover, in [18], a resource negotiation algorithm for network virtualization is proposed, which, according to the authors, deals with network slicing and on-demand delivery of radio resources. In [15], a resource allocation framework is also proposed and energy consumption for V-CRAN is studied. In terms of energy consumption in V-CRAN, reference [15] provides a cost-effective scheme for V-CRAN, by which the average energy consumption for the distributed baseline (DB), the First Fit Decreasing (FFD) algorithm, and the Heuristic Simulating Annealing (HSA) algorithm can be reduced by 65%, 6%, and 3%, respectively.

## 2.3 Heterogeneous Cloud RAN (H-CRAN)

For 5G and possibly beyond mobile networks, heterogeneous RAN architecture is generally considered to be one of the key enablers for supporting different categories of wireless network services. Basically, heterogeneous networks (HetNets) include different types of BS implementations. Therefore, the seamless coexistence of multiple RANs is



### 2.3. Heterogeneous Cloud RAN (H-CRAN)

not only useful to achieve high capacity, but also to achieve effective network coverage while improving the spectral efficiency of the system. While traditional macro base stations (MBSs) can be used for backward compatibility, the use of MBSs is limited by inter-cell interference, which becomes more pronounced the more densely populated the access nodes are in a realistic cellular network environment. One approach to address this challenge is to deploy a range of low-power cells such as femtocells, picocells, and microcells [19] in a heterogeneous environment to ultimately improve overall network capacity and coverage, increase spectral efficiency, and reduce network cost. Consequently, the total system capacity ( $C_{total}$ ) can be increased as expected in accordance with the popular Shannon theory expressed by the equation 2.1 [4, 20]; where  $B_i$  denotes the bandwidth of the  $i$  th channel,  $S_i$  represents the signal power of the  $i$  th channel, and the noise power is denoted by  $N_p$ .

$$C_{total} \approx \sum_{HetNets} \sum_{Ch} B_i \log_2 \left( 1 + \frac{S_i}{N_p} \right) \quad (2.1)$$

Further improvement in system performance can be achieved by integrating BSs into the C-RAN architecture to meet the requirements of 5G and beyond cellular networks. Under this premise, the heterogeneous cloud RAN (H-CRAN) is a functional and effective blend of cloud computing technology and HetNets.

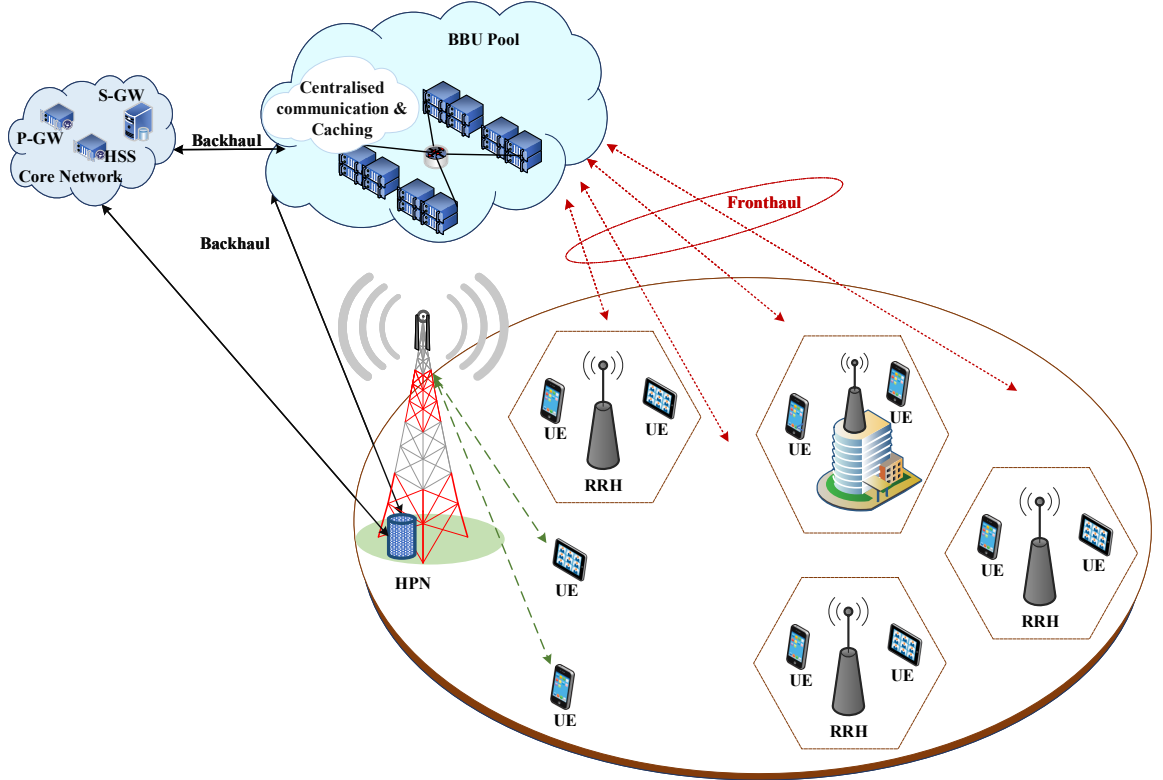


**Figure 2.5:** Basic structure of a H-CRAN (Adapted from [8]).

## Basic Structure of H-CRAN

Heterogeneous-CRAN (H-CRAN) exploits heterogeneous networks and C-RAN to improve the functionality and performance of C-CRAN by decoupling the control and user planes. The H-CRAN architecture consists of a combination of radio infrastructures and cloud computing devices to handle the various end-user QoS requirements, interference levels, and channel state information (CSI) for overall effective resource allocation throughout the cellular network. Basically, the cell layouts of an H-CRAN architecture include the macro BS or high power nodes (HPN) and the small BSs or RRHs cellular layouts [4]. The use of HPNs is essentially to increase network coverage and strengthen the control network signaling.

Basically, the following three functional blocks are identified in the system architecture of H-CRAN [21] as shown in Figure 2.5:

- **Cloud-enabled and real-time virtualized BBU Pool:** In this functional block, cloud computing and powerful virtualization techniques are extensively used to integrate all BBUs into the BBU pool. As mentioned earlier, the HPNs are then connected to the BBU pool to ensure coordination between the RRHs and the HPNs.
- **ultra-reliable transport network:** The connection between RRHs and BBUs is done through low-latency, high-bandwidth fronthaul links, such as fiber. In addition, control and data signaling between the MBSs (HPNs) and BBUs is performed via interfaces  $X_2$  and  $S_1$ , respectively.
- **Densely populated macro-BSs, small BSs and RRHs deployment:** As mentioned earlier, there are cells of different categories, including small base stations (SBSs), macro base stations (MBSs), and RRHs. While MBSs facilitate control network, manage mobility, and improve overall network performance, e.g., by minimizing handover frequency to avoid ping-pong effects that occur with highly mobile users, geographically distributed SBSs are deployed to improve user proximity to the network, increase capacity, and enable instantaneous reduction of transmit power. In H-CRANs, the systematic management of densely deployed mobile networks is facilitated by the functional separation between BBUs and RRHs, including the decoupling of control and data planes, and the cloud-computing-based centralization of BBU processing. Through this scheme, H-CRANs provide more flexibility, support seamless RAN upgrades, and multiple standard operations using an open-source platform.

A critical review of the architecture of H-CRAN, presented in Figure 2.5 shows that H-CRAN shares two key similarities with traditional C-RAN. In addition, some significant differences can be observed between H-CRAN and C-RAN. In both H-CRAN and CRAN, a large number of RRHs are used and connected to a cloud of BBU pools to achieve improved energy efficiency and high cooperative gain. Also, the RF and the processing at other protocol layers processing between the RRHs and the BBU pool are similar in both architectures. Apart from the above similarities, the following differences can

be noted: (a) linking the BBU pool and HPNs in an H-CRAN architecture to reduce the cross-tier interference between RRHs and HPNs; (b) load balancing is supported, in particular, RRHs enter the idle state when the traffic load of an RRH is low; (c) the inclusion of HPNs in the H-CRAN relaxes the fronthaul requirements so that control signalling and system broadcasting data are transmitted to the UEs via HPNs.

## 2.4 Fog RAN

Fog computing technology evolved as a response to the challenges associated with cloud techniques, such as high end-to-end delays, processing large amounts of data, significant traffic congestion, and resulting communication costs. According to Cisco, Fog computing is described as a concept by which the cloud computing can be extended to the network edge [22], moving functions such as communication, control, computation, and decision-making to the edge of the network to minimize delays and process time-sensitive data near the end-users' IoT devices. The need to assign more functions and intelligence to the edge network motivates the concept of mobile edge computing (MEC), which also facilitates the relocation of cloud processing functions to the edge and ultimately supports the creation of many small clouds or cloudlets at the edge by applying fog computing techniques [23, 24].

The introduction of fog computing technology in radio access networks is perceived as an improvement for the C-RAN, especially in an attempt to provide a robust RAN that supports ultra-low latency and high reliability services as considered for 5G wireless network [22]. The fog radio access network (F-RAN) enhances the realization and support for collaboration radio signal processing (CRSP) and cooperative radio resource management (CRRM) in the BBU pool and RRH including the UE [25]. With the provision of CRSP and CRRM, UEs can easily access locally available information contents in the cache through intelligent interaction between RRH peers instead of connecting the BBU pool to download the packets. Therefore, the latency of the traffic will improve significantly. These properties of F-RAN make it robust to mitigate the challenges of H-CRAN. It is worth noting that F-RAN capitalizes on the benefits of fog computing and C-RAN to provide better QoS and an improved QoE to users [4].

### Basic Structure of F-RAN

A basic scheme of F-RAN is shown in Figure 2.6, which includes the cloud computing layer, the network access layer, and the terminal layer [4, 26]. In the network access layer, a prominent feature of the F-RAN, as shown in the Figure is the composition of F-APs and HPNs that are deployed to deliver system information, including signaling, to all F-UEs. Similarly, a fog-computing-based access point (F-AP) replaces the traditional RRH in the network access layer. Likewise, the fog user equipment (F-UE) in the terminal layer can access not only the F-APs but also the HPN to obtain system signaling information. Another interesting aspect of the F-RAN architecture is the promotion of D2D communication in the terminal layer, since neighboring F-UEs can smartly communicate with each other. Meanwhile, all data received from the F-UEs is

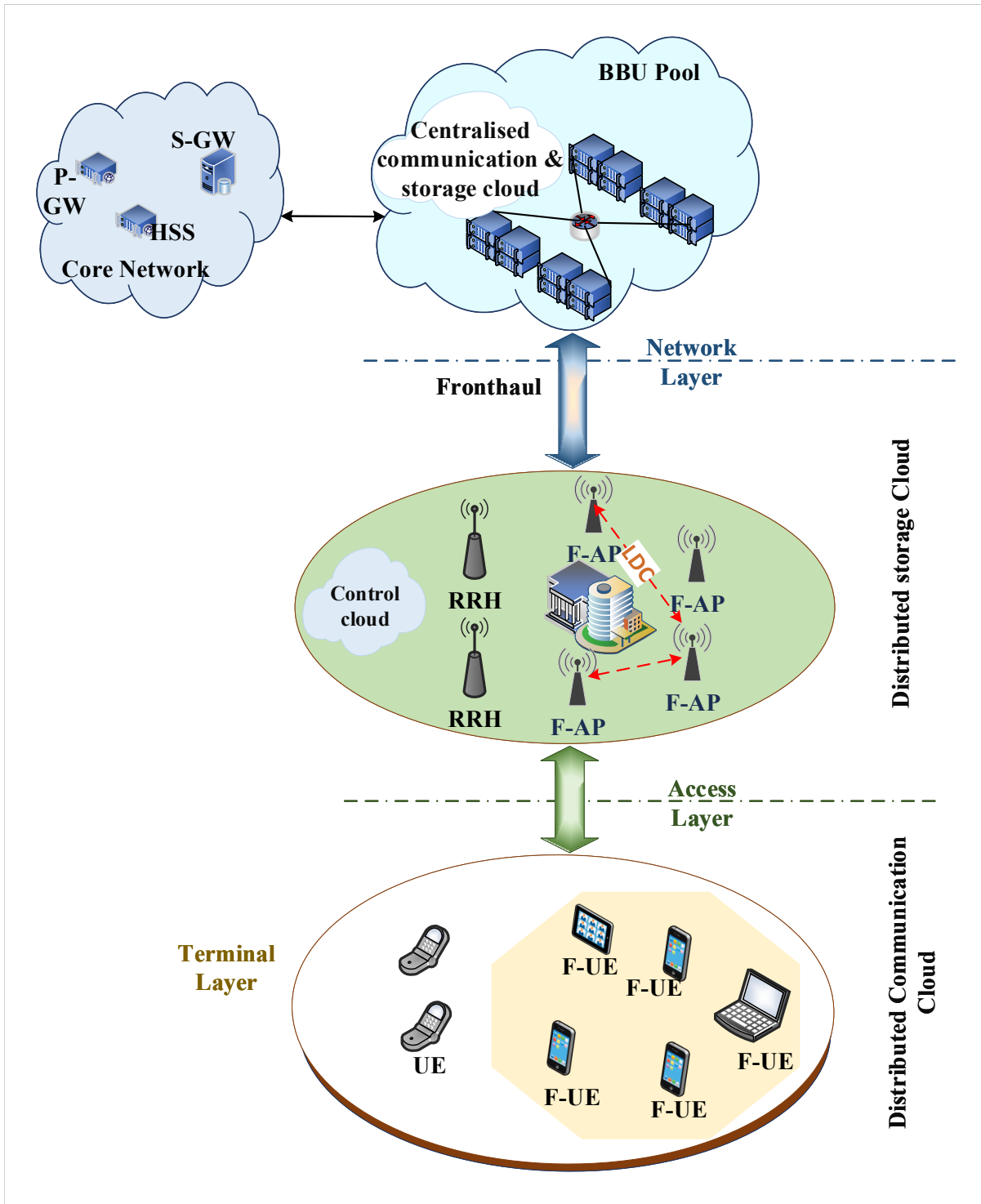


Figure 2.6: Basic structure of a F-RAN (Adapted from [4]).

processed and forwarded by the F-APs. The HPNs and F-APs are connected to the BBU pool, which is located in the cloud computing layer, through the fronthaul and backhaul networks, respectively.

## Review of F-RAN Research

Fog radio access networks (F-RANs) is widely studied due to its potential advantages and characteristics. In [27], the authors propose a model to evaluate the performance of F-RAN, in particular the delay, power consumption and energy efficiency. The authors further claimed that despite apparently substantial power consumption that may contribute to performance degradation depending on the number of fog devices deployed, F-RANs offer improved delay performance compared to conventional C-RAN. Consequently, a joint resource allocation and coordinated offloading method for the F-RAN is investigated in [26] to reduce energy consumption. Moreover, in [28], an energy consumption model that includes analytical and discrete-event modeling is proposed to evaluate the energy consumption of fog nodes when processing applications in a fog computing architecture.

Further studies on the energy consumption of a F-RAN architecture are considered in [29–32]. In [29], the authors propose an algorithm aimed at minimizing the energy consumption in the downlink transmission of a multicast F-RAN based on information compression (soft) and information sharing (hard) fronthauling schemes. Comparing the two schemes, the authors found that soft fronthauling can lead to an increase in the energy efficiency of the network while also contributing to delay reduction. In addition to performing load balancing among serving BBU pools in an F-RAN environment, the authors in [30] present a scheme that could enable energy consumption savings and load balancing during the BBU resource allocation process. Moreover, the authors present in [31] algorithms based on mixed integer linear programming (MILP) to reduce the power consumption of the F-RAN architecture.

Since F-RAN are clusters of interrelating RRHs in a Fog community, allocating sufficient BBU resources is critical for traffic management and user handover. In [33], the authors propose a data-driven framework consisting of a column-reduced integer programming (CLIP) to obtain optimal BBU allocation schemes aimed at optimizing the BBU utilization factor. Focusing on developing a dynamic and autonomous computational resource allocation scheme for F-RAN, the authors in [32] present an algorithm that uses reinforcement learning to optimize latency, energy consumption, and cost in F-RAN. The trade-off between performance, communication cost, and computational cost in F-RAN architecture is investigated in [34] using a mobile augmented reality use case. The authors claim that ultra-low low-latency services can be realized by the F-RAN if the trade-off is managed appropriately.

As network slicing is key to the deployment of 5G and beyond networks, fog RAN slicing is considered in several research activities. One of these works is presented in [35]. In it, the authors propose a Deep Reinforcement Learning algorithm to address content caching and mode selection decision for improving the performance of F-RAN. In addition, the authors in [36] consider a cooperative caching scenario in F-RAN and propose a dueling deep-Q-network framework that offers a delay-aware cache update policy, which is experimentally simulated. As claimed by the authors, the results show improved average cache hit ratio and lower average transmission delay. Paper [37] also states that a jointly optimized task offloading and scheduling technique could help reduce the average task execution delay in fog RAN. Further improvement in the latency

response of F-RAN can be achieved by employing the combination of Fog-computing and non-orthogonal multiple access (NOMA) technologies to improve performance of the F-RAN [38–40].

## 2.5 Fronthaul Interface Requirements

The interface between the RRH network (or radio unit (RU)) and the BBU pool (alternatively referred to as distributed unit (DU)) is called fronthaul interface (FHI). For over a decade, FHI has been defined by the CPRI as the basic interface for 4G LTE. The CPRI initiative focuses on the PHY layer and layer 2 and specifies a frame that includes radio signal digitization, synchronization, some control and management information from In-phase (I) and Quadrature (Q) samples [7]. Similarly, Open Base Station Architecture Initiative (OBSAI) specifications have been developed to allow multi-vendor inter-operation between RRHs and BBUs. Moreover, the OBSAI deals with clock/control, transport, baseband, and radio with interfaces and conformance test specifications. The interface defined by Open Radio Interface (ORI) builds on CPRI with a focus on developing an interface specification that allows inter-operation between the elements of BSs of mobile network devices. In a nutshell, the basic technical requirement for the fronthaul includes radio site configuration, data rate, latency and other timing parameters.

The CPRI bitrates are usually determined using the expression 2.2 [7]:

$$BitRate = M \times S_r \times N \times 2 \times (I/Q) \times C_w \times C \quad (2.2)$$

Where  $M$  is the number of antennas per sector,  $S_r$  is the sampling rate employed for digitization (sample/s/carrier),  $N$  is the sample width (bits/sample),  $2(I/Q)$  is a multiplication factor for in-phase (I) & quadrature-phase (Q) data,  $C_w$  stands for factor of CPRI control word, and  $C$  is a coding factor (either 10/8 for 8B/10B coding or 66/64 for 64B/66B coding).

As specified in CPRI, the bit error rate attributed to the fronthaul link must be less than  $10^{-12}$  [41]. Similarly, the error vector magnitude (EVM) is generally evaluated to optimize the radio performance at the output of RU. Typically, a maximum EVM of 17.5% is defined for QPSK modulation and 9% for 64 QAM [41]. To maintain a good QoS, CPRI specifies a maximum absolute round-trip delay,  $\tau$  (latency) of 5  $\mu s$  per connection for user plane data (IQ data) on the interface, excluding the group delay associated with the transmission medium [42]. It is worth noting that while the CPRI specification specifies minimum and maximum values for uplink and downlink IQ sample width, it also provides values for sampling rates suitable for different radio access technologies (RATs) and the associated channel bandwidths [7].

### The eCPRI

In the previous section, we noticed that using CPRI to support 5G use cases presents critical fundamental challenges. Therefore, it is expedient that the CPRI is redesigned not

only to improve efficiency and link capacity utilization, but also to serve as an interface that can support advanced networking and OAM features of legacy packet transport standards. Based on the aforementioned requirements, CPRI forum has developed an enhanced CPRI (eCPRI) that specifies a protocol for transferring information between enhanced radio equipment control (eREC) and enhanced radio equipment (eRE) at reduced data rate requirements compared to the CPRI as a result of radio base station decomposition. The eREC and the eRE are two basic blocks of a decomposed radio BS unit. The two blocks can be physically separated and interconnected via a transport network to carry eCPRI user plane data, control (C) & management (M) plane data, and synchronization plane [43]. The eREC consists of the PHY layer functions including the associated higher layer functions of the air interface, while the RE is usually located near the antenna and contains the PHY layer functions as well as analog radio frequency functions. The eREC and the eRE are included in the eNB/gNB, which is composed of the following functional components and protocol stacks: radio base station control & management, backhaul transport, RRC, PDCP, RLC, MAC, PHY, RF and measurements [43, 44].

The use of eCPRI is not limited to specific network and data layer protocols as long as the eCPRI requirements are met to ensure compliance with stringent requirements such as timing and frequency accuracy, bandwidth capacity, latency, packet loss, and others attributed to wireless technologies [44]. In addition, the design of eCPRI allows the use of existing legacy standard protocols and flexible functional decomposition without increasing the complexity of the eRE [44]. Therefore, the eCPRI functional decomposition comprises five inter-layer splits and three intra-PHY splits defined as Splits A, B, C, D, E,  $I_D$ ,  $I_U$ , and  $II_D$  [44], although any other split within the PHY layer can also be used with the eCPRI. While the data in Split  $I_D$  and  $II_D$  are bit-oriented, the data in Split  $I_U$  and  $II_D$  are IQ oriented. The functional splits are discussed in detail in section 2.6. Compared to classical CPRI, eCPRI brings a significant improvement in lowering the bit rate at the fronthaul interface, as can be seen in Table 2.1.

**Table 2.1:** CPRI and eCPRI compared

Feature	CPRI	eCPRI	Ref.
Supported Logical Connections	<ul style="list-style-type: none"> <li>Logical point to point (PtP) &amp; point to multipoint (PtMP) connections</li> </ul>	<ul style="list-style-type: none"> <li>Only PtMP is supported</li> </ul>	[43–45]
Ports Classification	<ul style="list-style-type: none"> <li>Slave and master ports with direct connection by optical fiber or electrical cable</li> </ul>	<ul style="list-style-type: none"> <li>Support for slave or master port categorization at the PHY layer is not required</li> </ul>	
Network Nodes	<ul style="list-style-type: none"> <li>Network nodes topologies rely on REC/RE functions</li> </ul>	<ul style="list-style-type: none"> <li>Include fronthaul network and other networking elements for timing &amp; network management functions</li> </ul>	
5G Appropriateness	<ul style="list-style-type: none"> <li>Not robust to support 5G use cases due to extreme bandwidth requirement on the fronthaul including latency and jitter limitations.</li> </ul>	<ul style="list-style-type: none"> <li>Ideal for 5G network due to the possibility for functional splits to achieve fronthaul with relaxed transport requirements, greater reliability and flexibility</li> </ul>	

---

## 2.6 Functional Splits

As mentioned in Section 2.5, C-RAN architecture pushes stringent requirements on the FH, especially when CPRI is used to transport baseband radio samples. Since the transmission of user data is achieved in the form of IQ-data block, large line bandwidth in gigabits per second (Gbps) is required and this scales with carrier bandwidth and the number of antenna elements, thus significantly limiting support for some 5G features [47]. Furthermore, the CPRI also necessitate tight latency and jitter requirements, for example an end-to-end latency of about  $250 \mu\text{s}$  is needed [48]. Meeting such critical requirements poses great challenges to support 5G services. Consequently, there have been tremendous efforts to address these limitations through various proposals for modification of RAN architecture to reduce fronthaul costs and support the demand for higher capacity while supporting lower delay services [49–52]. Functional split is considered by the industry and academia as a solution to relax the extreme bandwidth and latency requirements and engenders FH flexibility [53, 54].

Conceptually, the BBU-RRU functions of the C-RAN architecture are decomposed into functional subsets to provide a way to determine the functions to be processed locally at the antenna site and the functions to be processed centrally in the data center by high-performance processing facilities [55, 56]. To this end, a number of possible functional split options have been proposed and explored [2]. In the perspective of the NR framework, the radio processing and baseband functions of the 3GPP protocol stack are split into a central unit (CU), a DU and a RU. This defines new interfaces for the midhaul between a CU and a DU and the fronthaul between the DU and RU. With these interfaces, a possible split mapping could be achieved according to the proposed functional split options that are implemented at different layers, including the physical, data link and network layers, which are lower parts of the 3GPP protocol. The Figure 2.7 shows a representation of the functional split options proposed by 3GPP [56], open radio



## 2.6. Functional Splits

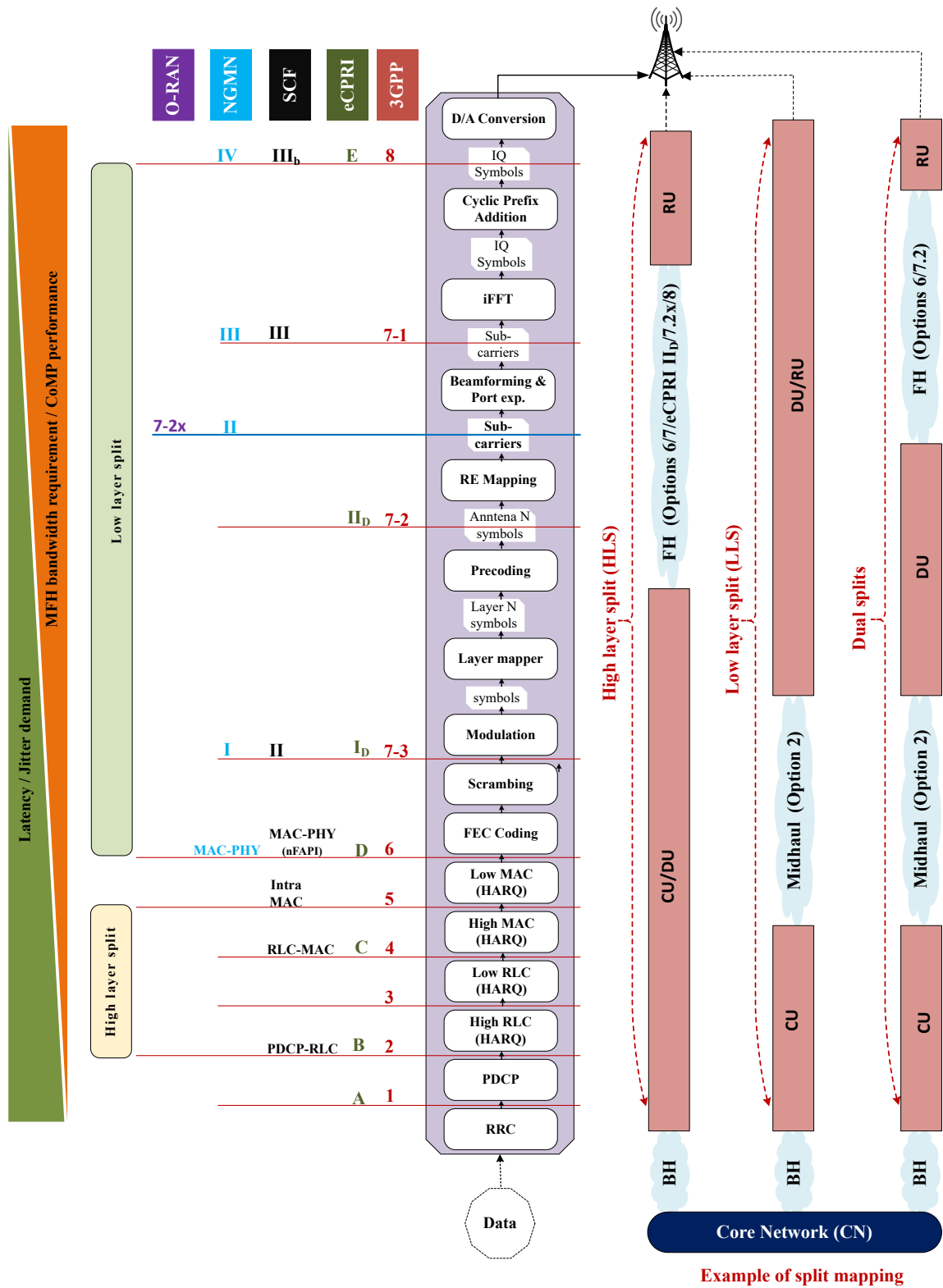


Figure 2.7: An overview of functional split options (Adapted from [46]).

access network (O-RAN) [57], small cell forum (SCF) [58], CPRI [43], and next generation mobile networks (NGMN) [59]. Eight functional split options were defined by 3GPP, one by O-RAN, seven by SCF, seven by CPRI for enhanced CPRI (eCPRI) implementation, seven by SCF, and five by NGMN.

The 3GPP proposed eight functional split options, from 8 at the PHY layer to 1 at the PDCP layer, as shown in Figure 2.7. With the subdivision presented by 3GPP, option 8 has a RU that processes digital-to-analog converter (DAC)/analog-to-digital converter (ADC) functions, while other baseband processing is performed in the combined CU/DU unit. The option 8 generally corresponds to fully centralized processing, such as that exhibited by the C-RAN with all its features. Furthermore, as an attempt to bring flexibility to the fronthaul of the modified C-RAN architecture, further subdivisions of option 7 are introduced by the 3GPP, comprising options 7-1, 7-2 and 7-3. With the inclusion of option 6 and the three variants of split 7, a low layer split (LLS) is defined, while split options 6 to 2 represent a high layer split (HLS). In option 7-1, the inverse Fast Fourier Transform (iFFT)/fast Fourier transform (FFT), cyclic prefix insertion/subtraction and DAC/ADC functions are performed by the RU near the antenna, while other higher layer functions up to PDCP are performed by the combined CU/DU. For downlink transmission, additional functions from the resource element mapping sub-layer and the modulation sub-layer are included in the RU functions for option 7-2 and 7-3, respectively. Similarly, option 6 features the MAC-PHY split with forward error correction, including the Cyclic Redundancy Check (CRC) encoding and decoding processing added to the RU functions along with other PHY processing, whereas the other MAC sub-layer and higher layers are processed in the CU /DU. Proceeding further with the 3GPP splits, functional option 5 is defined low MAC-high MAC split; option 4 is positioned the low MAC and the high RLC sub-layers; option 3 and 2 are defined for low RLC-high RLC split and high RLC-PDCP split respectively; while option 1 features all processing from the PDCP to the PHY at the RU.

Other functional splits proposed by O-RAN, CPRI, SCF, and NGMN follow a similar trend, as shown in Figure 2.7. For example, while split 7-2x of O-RAN corresponds to option II of NGMN, option E, II<sub>D</sub>, I<sub>D</sub>, D, C, B and A of eCPRI correspond to 8, 7-2, 7-3, 6, 4, 2 and 1 of 3GPP, respectively. Also, the option IV, III, I, MAC-PHY of the NGMN correspond to 8, 7-1, 7-3 and 6 of the 3GPP, respectively. Moreover, the SCF defined splits III<sub>b</sub>, MAC-PHY<sub>(nFAP)</sub>, intra-MAC, RLC-MAC, PDCP-RLC corresponding to Splits 8, 7-1, 7-3, 6, 4, and 2 of the 3GPP, respectively. In short, split options: LLS, HLS, and double-split mapping can be identified and defined for option 8 to 7-2, option 5 to 2, and splits 7-3 to 6, respectively. Table 2.2 compares the strengths and weaknesses of the three mapping categories of the functional splits.

### 2.6.1 RF/PHY Split

In this split option, the RF processing module including the digital/analog conversion is located in the RU, while the entire digital function is processed centrally in the DU /CU pool. This functional split corresponds to option 8. With this split, the RU is simple, cost effective and can support different RAT [2, 53, 54, 62]. The centralization of the

**Table 2.2:** Comparison of the three categories of functional split

Group	Split	Strength	Weakness	Ref.
LLS	8, 7-1, 7-2x,7-2, 7-3, 6	<ul style="list-style-type: none"> <li>• Support for a high degree of centralization and coordination involving the whole protocol stack</li> <li>• Ideal split for CoMP</li> <li>• Cost effective</li> <li>• Possible sharing of RF components as a result of RF-PHY separation</li> </ul>	<ul style="list-style-type: none"> <li>• Extremely high and constant fronthaul bitrate that scales with the antenna ports, especially for split option 8 &amp; 7-1</li> <li>• Very strict latency requirement due to centralised processing in the CU-pool</li> <li>• Extra effort might be required for CPRI compression at the DU &amp; CU</li> </ul>	[8] [2] [48] [56] [60]
		<ul style="list-style-type: none"> <li>• Significant reduction in fronthaul bitrate</li> <li>• Latency is tolerated for long distance transmission</li> <li>• RU processing is conditioned to support URLLC, since more functions are handled at the antenna edge</li> </ul>	<ul style="list-style-type: none"> <li>• Almost impossible or highly complex CoMP processing</li> <li>• Great complications arise from the implementation of HLS at the RU</li> <li>• Not cost effective</li> </ul>	[8] [2] [48] [53] [56] [60]
Double split	Both LLS & HLS. For example: split option 2 / 7-2 or 2 & 6	<ul style="list-style-type: none"> <li>• CU virtualization can be implemented</li> <li>• Good scalability</li> <li>• Lower implementation cost</li> <li>• Ideal for mobile and URLLC services</li> </ul>	<ul style="list-style-type: none"> <li>• The fronthaul is characterised by high bitrates and latency requirements, though lower than that of the LLS</li> </ul>	[8] [2] [56] [60] [61]

remaining functions of the RAN enables sharing and pooling of network resources, thus supporting CoMP, Joint Radio Resource Management (JRRM) [2, 8, 56]. The fronthaul is such that the raw IQ samples are transported between DU and CU in an encapsulated format defined by a protocol used at the interface, which may be CPRI, OBSAI or ORI. However, this split offers the highest fronthaul bitrate and most constrained latency and jitter requirements compared to other functional split options. For example, the maximum achievable distance between the RU and DU /CU is limited to 20 km due to latency constraints [56].

### 2.6.2 Low PHY Split

This functional split, which is also classified as a split option in the intra-PHY split group, is equivalent to option 7-1 and has the FFT/iFFT locally processed in the RU, while the exchange of I/Q samples in the frequency domain with the CU /DU unit is performed via the interface. The rest of the PHY processing and higher layer processing are located at the CU /DU. Compared to option 8, functional split option 7-1 has a relatively lower fronthaul bit rate, especially for the DL transmission, although it is constant since the resource element mapping is done in the CU /DU [2]. The rest of the tasks in the CU /DU exploits centralization and pooling gains such that, for example, distributed massive MIMO or CoMP can be facilitated without requiring disproportionate data exchange between nodes [8]. Transporting fronthaul traffic in the frequency domain enables a corresponding multiplexing gain resulting from the combination of multiple traffic-dependent streams [8]. Therefore, with this split, joint transmit and receive traffic processing is possible. On the downside, this split also has fronthaul bitrate that scales with the number of connected RUs. Apart from the fact that the latency is limited with this split, the timing for the connection between RU and CU /DU is very complicated [63].

### 2.6.3 Low PHY/High PHY Split

As with the Low PHY split, this split, which is also a variant of the Intra-PHY split group, beamforming resource element mapper is added to the DU or RU functions when CU and DU coexist as a unit. This split corresponds to option 7-2 of the 3GPP functional split. Since the FFT and resource element mapper with other PHY processing are handled by RU/DU, subframe symbols are transported over the fronthaul link, resulting in a slightly lower bit rate on the fronthaul link than in options 7-1 and 8. Therefore, in this split, the RU/DU is more complex while leaving fewer shared processing tasks for the CU. Downward from this split, a variable bit rate is possible on the fronthaul link. This split option also supports CoMP schemes without performance degradation [2, 48].

In addition, O-RAN has defined option 7-2x of the fronthaul specification between O-DU and O-RRU, which also belongs to the Low PHY/High PHY split group. Option 7-2x consists of two types: 7.2a and 7.2b, depending on the location of the precoding [58]. It is considered as split option 7.2a when precoding and resource element mapper are processed in the O-DU and beamforming is performed by the O-RU, whereas when precoding is added to the functions of the O-RU, the split is option 7.2b. Consequently, the implementation of option 7.2a requires a much simpler and less expensive RU than

option 7.2b, since more functions are assigned to the O-RU. As a result, the processing and memory requirements for the O-RU increase, while the fronthaul bandwidth requirements decrease, since a further increase of the fronthaul bandwidth is avoided by the DL precoding in the O-RU, e.g. when the number of MIMO streams exceeds the MIMO layers [60].

Considering the possibility of centralization with the split 7.2x options, multiplexing gains can be realized on the fronthaul link while enabling joint processing on multiple access nodes. However, support for multiple transmission and reception (mult-TRP), joint reception, multiple carrier aggregation, and the like comes at a tradeoff of low-latency transmission since high latency stringent requirement is imposed by the subframe-level timing activities of the intra-PHY layer interactions between CU and DUs [61]. The Split 7.2x is particularly suitable for use cases where multi-RAT and multi-connectivity are required for efficient resource utilization.

### 2.6.4 High PHY Split

This split corresponds to option 7-3 of the 3GPP functional split, option I<sub>D</sub> of the eCPRI specification, II of SCF split group, and option I defined by the NGMN. In this split, scrambling, modulation, and layer mapper reside in the DU /RU and has considerable reduction in bit rate on the fronthaul since processing of the modulation results to several bit are allocated to each symbol depending on the modulation format used. An in-band protocol is required for this split option to support modulation, multi-antenna processing, and physical resource block (PRB) allocation, since the demarcation point is at the high sub-layer of the PHY layers [2, 61].

Since the automatic repeat request (ARQ) is centrally processed in the the CU, this option may be more effective during mobility and non-ideal transmission conditions. While the FEC function is executed in the CU, codewords are transmitted on the fronthaul link between the DU and CU [2, 64]. In addition, the CoMP schemes, joint transmit and receive processing are possible with this split. The fronthaul bitrate is envisaged to lower than that of the other Option 7 splits but at the expense additional overhead from synchronization, scheduling control, including Ethernet framing function for Ethernet based fronthaul. Furthermore, this split is characterized with relatively high latency requirement due to complexity in the timing for RU and CU/DU connection, but it is more appropriate for a setup with constrained fronthaul fiber capacity.

### 2.6.5 PHY-MAC Split

In this split, the entire PHY layer stack and the RF are in the DU /RU, while the MAC, RLC and upper layers are in the CU. Through the interface between DU /RU and CU, the fronthaul link transmits data, configuration and scheduling-related information, including resource block allocation, antenna configuration, beamforming, layer mapping and MCS, and other information. This split is standardized by the Small Cell Forum.

It is worth noting that the sub-frame level timing interactions between DU /RU and CU are required because hybrid automatic repeat request (HARQ) timing and scheduling

result in a very tight fronthaul delay requirement [61]. However, these possible latencies over the fronthaul contribute to limiting the performance of the CoMP scheme [2]. Meanwhile, the fronthaul payload consists of transport blocks with a huge reduction in fronthaul link bandwidth compared to split 7.2x, while the centralized CU pooling gain offers efficient optimization and resource handling. Fronthaul bitrate suffers from the additional overhead due to scheduling control, synchronization, and Ethernet framing, which can compromise the benefits of shorter subframes and greater channel bandwidth.

To support modulation, multi-antenna processing, and PRB allocation, an in-band protocol is desirable because the MAC layer and the PHY layer are detached. This is beneficial when non-ideal transmission conditions are required due to centralized ARQ processing at CU and during mobility. Moreover, option 6 allows multiplexing gains for different UE densities, resulting in a significant reduction in the number of DUs, but provides lower cell-edge user throughput and average cell throughput performance compared to option 7.2x and other PHY splits [2, 65].

### 2.6.6 Intra-MAC Split

This functional split corresponds to 3GPP split option 5 and the Split MAC defined by SCF in which RF, the entire physical layer and the lower part of the MAC layer (low-MAC) are distributed, while the higher part of the MAC layer (high-MAC), RLC and PDCP functions are processed centrally in the CU. In this way, the multiple low-MAC sub-layers are controlled by the high-MAC sub-layer through high-level scheduling decisions. In addition, the inter-cell interference coordination in the high-MAC sub-layer is responsible for joint processing, coordinated scheduling/beamforming, and other interference coordination methods [58]. To reduce delay requirements on the fronthaul interface, time-critical functions in the Low-MAC sub-layer that include HARQ, radio channel, random access control, signal measurements from PHY, and also other functions related to latency are processed in the DU/RU [61]. By reducing the delay requirements on the fronthaul interface, longer distance to the CU-pool can be realized.

Although this split offers low bandwidth requirements, the interface between CU and DU is complex, scheduling operation is complicated, and CoMP performance is degraded. The implementation of option 5 is robust for scenarios that require a distance of more than 20 km between CU and DU. In addition, decentralization of the HARQ process and subsequent relaxation of latency requirements have been cited as advantages of the intra-MAC split in [66].

### 2.6.7 MAC-RLC Split

This split is similar to Option 4 of the 3GPP, also specified by the SCF, in which more functions of the protocol stack, including all PHY and all MAC processing, are moved to the DU, while the RLC, PDCP, and RRC are centralized in the CU. In this split, RLC protocol data units (PDUs) and MAC service data units (SDUs) are transferred in the DL and UL directions, respectively. In [2], the authors claimed that both memory and processor utilization can be improved by sharing resources through RLC virtualization.

The unique feature of this split is that RLC and MAC are tightly coupled, resulting in a scheduler on MAC that handles scheduling decisions for each transmission time interval (TTI) and RLC requests, requiring a low-latency fronthaul. This sharing provides low bandwidth requirements on the fronthaul link with the bit rates scaling with MIMO layers.

### 2.6.8 Intra-RLC Split

An intra-layer split is considered at the RLC layer, creating an interface between a low RLC and a high RLC sub-layer. In this split, the processing of the RRC, PDCP, and part of the RLC (high RLC) functions are centralized, while the remaining part of the RLC (low RLC), MAC, PHY including the RF are distributed. This split corresponds to option 3 of the 3GPP functional split and has two variants based on the splitting approaches for real-time/non-real-time functions [67].

In the first variant named option 3-1, the segmentation functions are performed by the low RLC in the distributed unit, while RLC acknowledged mode (AM) operation including all RLC functions are performed at the high RLC sublayer in the central unit. With option 3-1, the low RLC segments RLC PDU into the available MAC PDU resources, while the high RLC slices RLC PDU based on the status reports [56].

The second variant, option 3-2, has a Low RLC which may be composed of transmitting RLC unit in transparent mode (TM), the RLC unit in unacknowledged mode (UM), and the transmitting part of AM, including the routing function of a receiving side of AM related to downlink transmission. Also, the High RLC may consist of a receiving TM RLC entity, a receiving UM RLC entity and a receiving side of AM without receiving RLC status reports and routing function [56].

Option 3-2 uses flow control and has lower latency tolerance between CU and DU compared to the latency tolerance of option 3-1. This is because for option 3-2, no extra transmission delay of PDCP/RLC reestablishment procedures are required since the receiving RLC takes place in the CU [2]. Generally, option 3 is characterised with a very low bandwidth, low latency requirements, and a possible reduction in processing and buffer requirements. It is best suited for a low bit rate and latency tolerance implementation in less than ideal transport conditions [56].

### 2.6.9 RLC-PDCP Split

The decomposition of RLC and PDCP layers is also considered as a split option, corresponding to option 2 of the 3GPP functional split specification. In this split, the CU is assigned to handle PDCP and RRC functions while the RLC, MAC, PHY and RF functions are executed in the DU. The interface for this split has been standardized for coherent interworking between elements such as the 3C configuration in LTE Dual Connectivity [2, 58], which facilitate the transmission of a portion of the PDCP PDUs to the RLC of another cell [64].

As proposed, this split receives PDCP PDUs in the DL, while transmitting the RLC SDUs in the UL. In this way, multi-connectivity can be supported by splitting the traffic

into multiple streams for onward transmission to different access nodes. All real-time features are located in the DU, reducing the link requirements for this split [2, 58]. The design of an X2 related design may rely on this split option because the user plane is similar, though some functionality like the requests for new procedures for the control plane. However, the split may require beamforming schemes to compensate for limitation of coordinated scheduling associated with this split option [64].

As mentioned in [8], by centralizing PDCP function, this split can advantage of pooling gains from the CPU intensive header compression protocols like the Robust Header Compression, thus contributing to statistical multiplexing gains. Another advantage of this option is that it has relatively much relaxed latency requirements compared to split option 4 and above [8, 54, 68]. Considering the advantages offered by this split, it is most idea for high layer split between the CU and DU, and also for latency tolerance deployment requiring up to 40km distance between the CU and DU.

### 2.6.10 PDCP-RRC Split

This split is equivalent to option 1 of the 3GPP functional split option where the PDCP, RLC, MAC, PHY and RF are processed in the distributed unit, while the RRC is in the CU. Therefore, the entire user plane (UP) is moved to the DU, making user data close to the edge. Thus, this option capitalises on the benefits of RRC centralization in such a way that many functions are processed locally while the benefits of accelerated mobility management are seamlessly brought to users [58]. This split can also be referred to as the UP / control plane (CP) split, as the UP functions are performed by the PDCP and its subsequent layers, which are located in the DU, while the control plane functions are contained in the RRC.

While the simulations in [69] point to a possible advantage offered by UP/CP split in terms of low CP overhead that could positively contribute to mobility management and energy efficiency due to the implementation of virtualization for the PDCP and RRC sublayer functions, [70] shows that the use of CP /UP split with centralized CP functions is complex to implement. However, the PDCP-RRC split is suitable for low latency and edge computing use cases.

## 2.7 Flexible Functional Split

The challenges associated with the use of C-RAN have led to tremendous research efforts. One notable effort is the proposal for RAN-as-a-Service (RANaaS) by the iJOIN project of Interworking and JOINT Design of an Open Access and Backhaul Network Architecture for Small Cells based on Cloud Networks. RANaaS is based on the attempt to optimize latency, throughput, system complexity including energy and cost efficiency of mobile networks [8, 48, 71]. In principle, the proposed RANaaS is based on the premises on flexible functional split concept, where an intelligent splitting option is performed between the locally implemented conventional LTE technology composed of the whole protocol stack (from RF to Admission/ Congestion Control) functionality on the BS and the C-RAN with the radio front-end deployment [8]. While not all RAN functionality



is fully centralized according to the RANaaS framework, flexible centralization of a portion can be provided as a service. Nevertheless, RANaaS is designed to realize flexible centralization by aiming to simplify the management of RAN and support flexible small cell solutions, while enabling RAN functionality with cloud-based platforms. Moreover, the coexistence of access and backhaul network can be optimized by providing flexible centralization and backhaul for small cells. Some of the potential benefits offered by RANaaS are relaxed backhaul requirements and the use of a heterogeneous backhaul network. In addition, the use of RANaaS is expected to reduce complexity and cost due to flexible function assignments while enabling higher energy-efficiency [71].

A similar study of flexible functional split in [72] proposes an optimization model that exploits different functional splits to optimize the energy consumption of the CU pool and the number of handovers. The simulations in [73] provide an estimate of the time required for an ideal flexible functional split adaptation in response to the impact of user mobility in a 5G RAN. Similarly, in [74], a cooperation scheme based on SDN is proposed to manage adaptive flexible functional split in 5G networks depending on the available optical access network resources, with results showing that optimal optical resource allocation is guaranteed by wavelength and bandwidth management. Furthermore, an estimation of the available bandwidth and the associated real-time selection of the most suitable functional split option are investigated in [74].

Paper [75] reports on an experimental demonstration using software defined radio (SDR) and an open-source platform to flexibly configure, operate, and manage multiple nodes in a centralized and remote manner. In addition, Paper [76] investigates the flexible functional split functionality of 5G virtual RAN controllers in 5G networks through simulations that use frames at the controller as the basis for analyzing the trade-off between time at the controller and loss probability.

## 2.8 The 5G Radio Access Network

The inadequacy of C-RAN to support various 5G and beyond services leads to a rethinking of the RAN architecture to improve the network flexibility required for 5G and future networks. In this sense, the next generation radio access network (NG-RAN) architecture is designed to engender interoperability between new radio (NR) and LTE radio access, which could enable a smooth migration from LTE to 5G [77, 78]. To this end, a number of options for 5G deployment have been considered. These options are mapped from two main considerations, on having 5G NR access operating as an independent radio system, also referred to as a standalone (SA) mode, or that it coexists with the LTE access network employing multi-RAT-dual connectivity (MR-DC) in a non-standalone (NSA) mode [77, 79]. In this sense, the BS of a NG-RAN is either a next generation nodeB (gNB) that provides NR user plane and control plane services to the NR users; or an ng-eNB that provides LTE radio access to the users while providing E-UTRA control and user plane protocol signalling towards the user equipment side. The gNB that can connect to EPC and eNB is called en-gNB.

The architecture allows interconnection of gNBs and ng-eNBs through an Xn interface. The NG-RAN interfaces are defined based on the functional decomposition, the logical

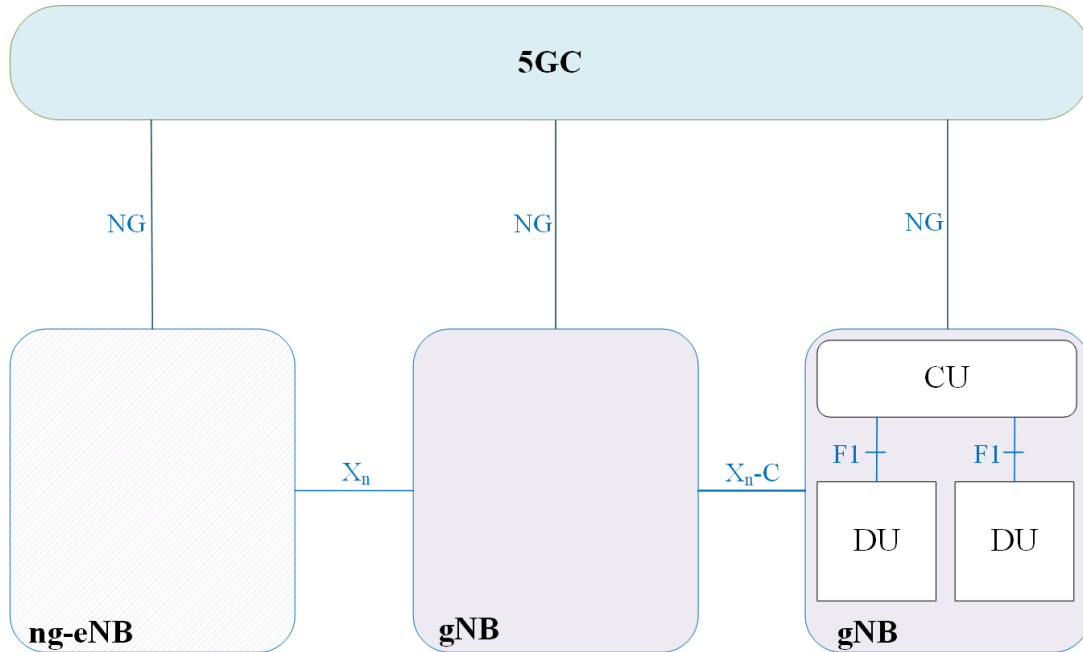


Figure 2.8: Overall architecture (Adapted from [77]).

model of the element controlled through the interface, and the network unit that can execute multiple logical nodes. As shown in Figure 2.8, the gNBs and ng-eNBs are connected to the 5G core (5GC) via the NG interfaces. In particular, the access and mobility management function (AMF) is accessed via the NG-C interface and the user plane function (UPF) through the NG-U interface. In view of the above, 3GPP release 15 [77] defined the NG-RAN architecture, which includes: a logical separation of data transport networks and signalling; a separation of transport functions from the NG-RAN and 5GC functions; fully controlled mobility for a RRC connection.

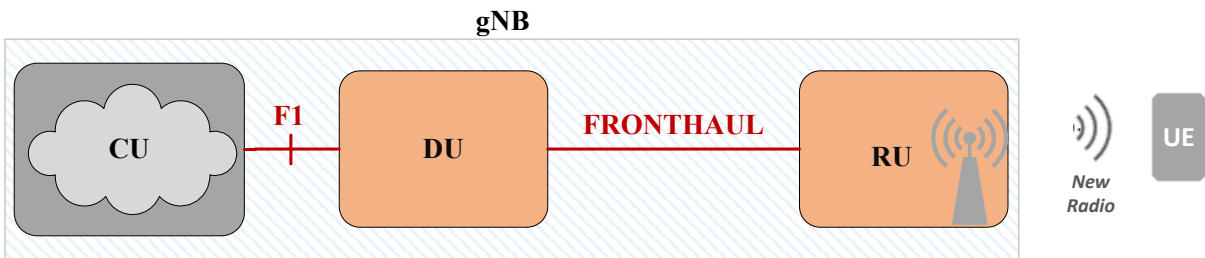


Figure 2.9: A generic structure of the gNB (Adapted from [77, 80, 81]).

## 2.9 5G NR Base station Architecture

In contrast to the 4G RAN architecture, which is based on a monolithic scheme of the eNB, the gNB (5G BS) is split into a central unit (CU) and at least one distributed unit (DU), as seen in Figure 2.8, or further comprises one or more radio units (RUs), as shown in Figure 2.9. The gNBs may be interconnected via the Xn interface, while the CU is connected to a DU through the F1 interface. Although a DU is intrinsically connected to a CU, it is possible to connect multiple CUs to a single DU by following proper implementation procedures for the purpose of failover.

As shown in Figure 2.9, the fronthaul network between RU and DU is established through the F1 interface, which could be an eCPRI compliant module. Moreover, the F1 interface enables a midhaul link between DU and CU. Furthermore, data transmission and signaling exchange, radio network layer and transport network layer separation, and interaction of UE-associated and non-UE-associated signaling are enabled through the F1 interface. Again, the F1 interface functions are divided into F1-U and F1-C functions for the user plane and the control plane, respectively. The F1-U functions include support for transferring user data between CU and DU as well as control of the downlink user data towards the DU. On the other hand, the F1-C functions include F1 Interface Management Functions, which includes F1 setup, CU and DU configuration update, F1 UE context management functions, which includes UE context setup and necessary corrections, RRC message transfer function, which includes RRC message exchange between CU and DU, system information management functions scheduling and broadcasting of system information including scheduling and broadcasting of system information by DU.

## 2.10 Architecture Options

Two basic deployment scenarios SA and NSA form the basis of the six identified architecture options as depicted in Figure 2.10. While SA provides the NR service over a single RAT, the NSA supports NR deployment by using the existing LTE systems. On this basis, it is straightforward to identify options 1, 2, and 5 as the SA group, while the NSA group includes options 3, 4, and 7. As can be seen in Figure 2.10, option 1 is required for NR deployment as it is a legacy LTE system where an E-UTRAN NodeB (eNB) is connected to an EPC, also referred to as 4G CN.

### option 2

This option is the ultimate goal of the 5G migration as only NR NSA is involved. In this option, the gNB is connected to the 5GC through the NG interface. This allows the gNB to communicate with UEs without support of a legacy network. Therefore, all 5G services including eMBB, mMTC, URLLC and network slicing are fully supported.

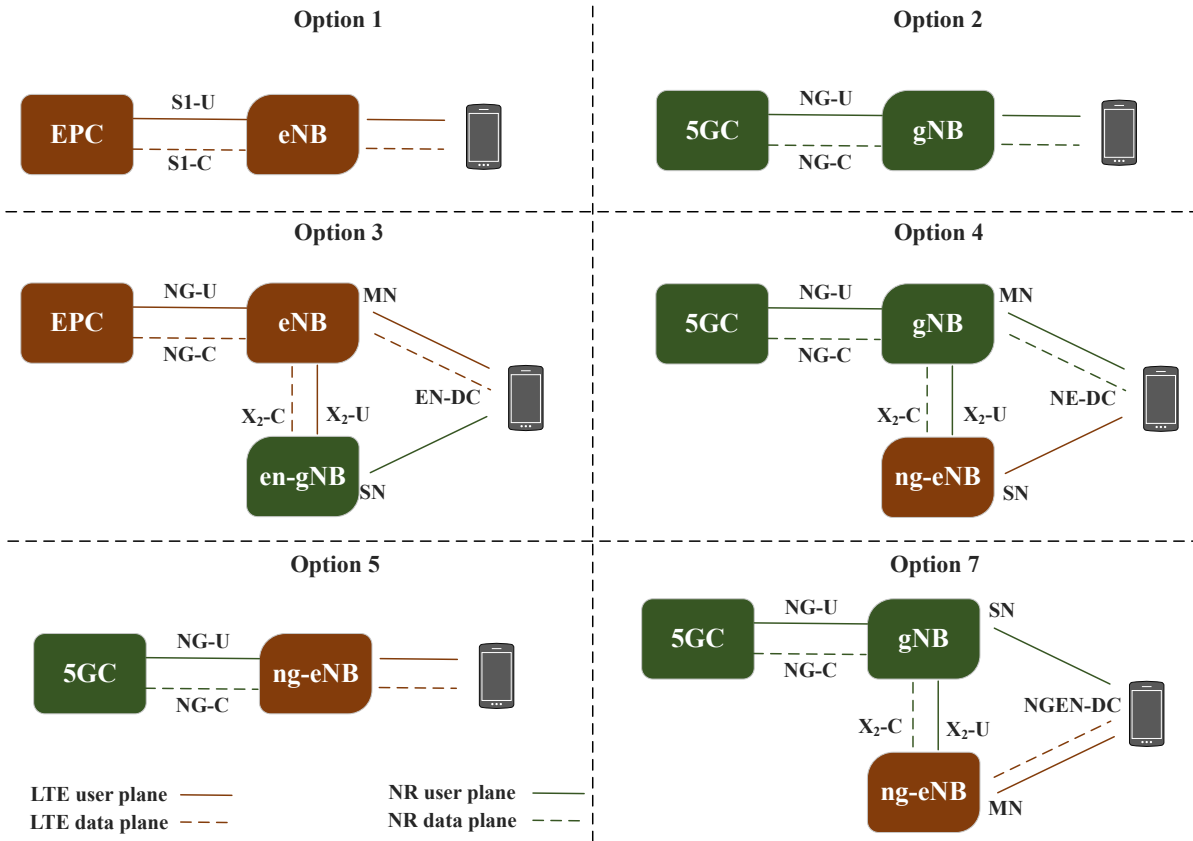


**Figure 2.10:** Baseline architecture options for NR deployment (Adapted from [78]).

### option 3

In this NSA option, which does not require 5GC, the en-gNB is deployed in the LTE network. As a result, 5G services are provided using the E-UTRAN new radio - dual connectivity (EN-DC) with LTE as the master node (MN) and NR as the slave node (SN). Although this option allows reuse of the existing LTE network for fast and seamless migration to 5G with minimal LTE upgrade. The scope of 5G services that can be supported depends on RAN capability due to the limitations of the legacy EPC. For example, URLLC or network slicing support is not possible with Option 3. For control plane signaling, the eNB is connected to the EPC and the en-gNB interacts with the eNB via the X2 interface. However, the user plane traffic is transmitted by the EPC either through the eNB and directly through the LTE air interface to the terminal or the en-gNB through the X2 interface to the terminal. In addition, it is possible to transmit UP traffic via both paths simultaneously.

### option 4

This falls into the family of NSA option where the gNB is connected to the 5GC while both gNB and ng-eNB are connected to each other. To interact with the 5GC or gNB, an upgrade of the eNB to ng-eNB is required [82]. Therefore, this option uses NR-EUTRA

Dual Connectivity (NE-DC) to aggregate NR and LTE traffic. For the control plane context, the gNB is connected to the 5GC and cooperates with the ng-eNB through the Xn interface. On the other hand, the gNB may transmit user plane traffic from the 5GC directly to the UE via the NR air interface or forward a portion of it indirectly via the Xn interface through the ng-eNB. Alternatively, the 5GC may receive and send user traffic to both the gNB and the ng-eNB.

### **option 5**

In this option, the ng-eNBs and 5GC are interconnected via the NG interface, while the ng-eNBs are interconnected via the Xn interface. This option belongs to the SA option family since dual connectivity with NR systems is not supported. In order for the interaction between eNB and 5GC to be established, the eNB request be upgraded. However, this option has a very limited use for 5G deployment, since 5g NR air interface like mmWave, multiple numerologies and a dynamic frame structure are required for 5G.

### **option 7**

This is another family of NSA option where the eNB is connected to the 5GC and both the eNB and the gNB are connected through the Xn interface. In this option, the upgrade of the eNB to the ng-eNB is essential to ensure interaction with the 5GC or gNB. Moreover, the aggregation of NR and LTE traffic in this option is achieved by using next generation-RAN E-UTRA-NR dual connectivity (NGEN-DC). Three possible configurations of traffic splitting can be achieved in this option, resulting in three variants. The control plane signaling is achieved through the master ng-eNB to 5GC link, and the ng-eNB operates with the gNB through the Xn interface. However, for the user plane, the traffic is split either at the ng-eNB or at 5GC. User plane traffic can be carried by the eng-eNB from the 5GC to the UE, either directly over the LTE air interface or route some of the UP traffic via the gNB through the Xn interface. Therefore, the user traffic from the 5GC can be delivered either by the ng-eNB or by the gNB.

## **2.11 Evolving Open RAN and Smart RAN**

The diversity of services and the ever-evolving innovative applications require continuous review of the RAN architecture. Therefore, efforts have been intensified to bring more flexibility and agility to the RAN. This is becoming more realistic with the advances in softwarization and virtualization technologies to enable possible replacement of physical BS and other network components with softwarized network functionality. To improve the flexibility of RAN, O-RAN is introducing a disaggregated radio access network (RAN) architecture with the launch of open initiatives driven by the O-RAN Alliance and the Linux Foundation [83]. The O-RAN builds on the ETSI NFV reference architecture, which includes commercial off-the-shelf hardware (COTS) as NFV infrastructure (NFVI).

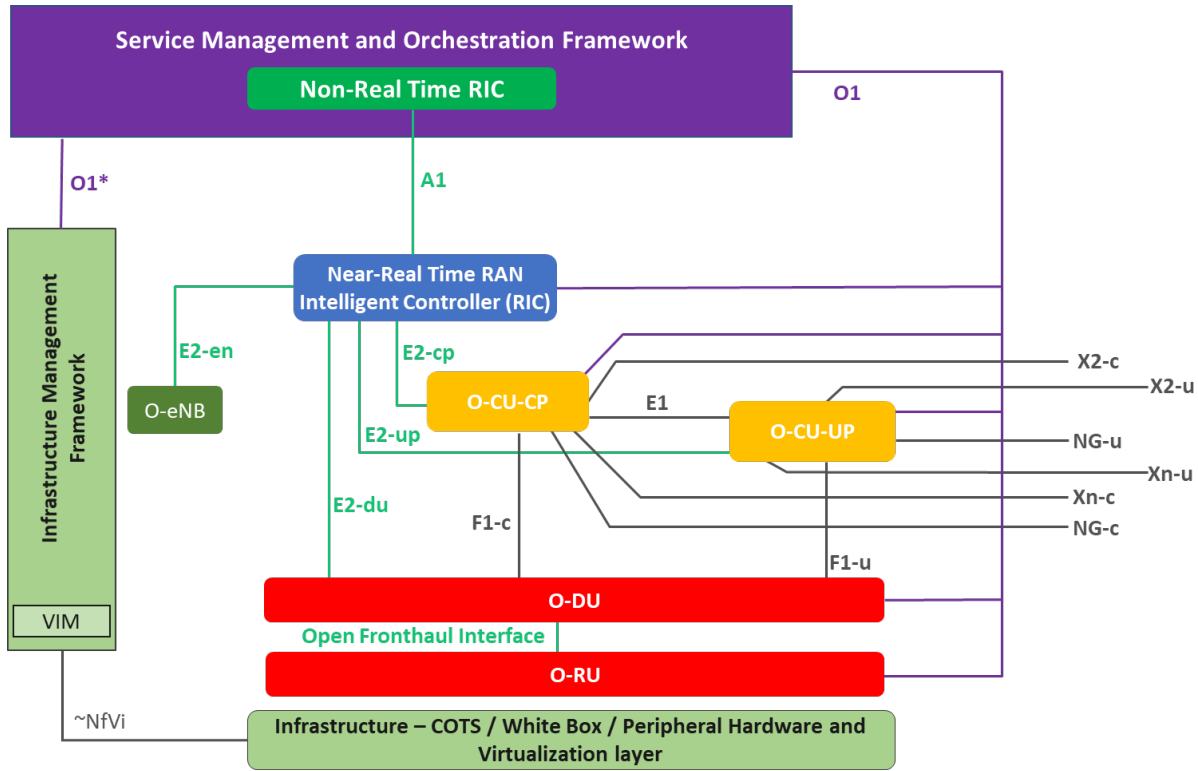


Figure 2.11: An O-RAN reference architecture [57].

In addition, O-RAN architecture relies on the RAN split to effectively decompose the RAN protocol stack so that individual components can be implemented separately. Thus, O-RAN enables the combination of open-source software and white-box hardware to develop an O-RAN architecture that implements baseband and radio unit components from the integration of a modular base station software stack on commodity hardware. In this way, embedded intelligence is introduced into each layer of the RAN architecture by using the 3GPP standard; and this ultimately leads not only to a reduction in total cost of ownership (TCO), but also an improvement in network efficiency and performance is possible [84]. To ensure openness, three vendor-independent layers are derived from the O-RAN decomposed hardware and software, and these include: the commercial off-the-shelf (COTS) processing devices, a hardware abstraction and application layer [57]; which support the execution of O-RAN network functions according to a set of requirements for realizing that is also referred to as O-RAN Cloud Platform.

As mentioned above, the effectiveness of virtualization technologies is extensively exploited to realize the cloudification of RAN, and this can be seen from the concept of the O-RAN reference architecture represented in the Figure 2.11 [57, 84, 85]. In addition to the 3GPP interfaces (X2, F1, Xn, W1, E1); open fronthaul, A1, O1 and E2 are introduced for the O-RAN as new interfaces to provide the necessary enhanced flexibility. As can be seen in the Figure, the reference architecture enables a separation of non-real-time (non-RT) and near-real-time (near-RT) functionalities, which are provided with the required

intelligence by RAN Intelligent Controller (RIC) [85–87]. The interaction between the non-RT and the near-RT is achieved through the A1 interface, which is located between the orchestration/network management system (NMS) layer comprising the RIC non-RT and the eNB/gNB including the near-RT RIC. The radio section includes near-RT RIC, O-RAN central unit - control plane (O-CU-CP), O-RAN central unit - user plane (O-CU-UP), O-RAN distributed unit (O-DU) and O-RAN radio unit (O-RU). The O-RAN is designed in such a way that the O-CU hosts the RRC, service data adaptation protocol (SDAP) and PDCP protocols, while O-DU serves as the logical node of the lower layer functional split and handles the processing of the RLC/MAC/High-PHY layers.

With the functional split at the O-DU, low-PHY layer and RF processing based on a lower layer functional split including FFT/ iFFT, physical random access channel (PRACH) extraction are performed by the O-RU which is a logical node corresponding to RRH of the 3GPP standard. For providing operation and management functions to the O-RAN managed elements by the management entities in the Service Management and Orchestration Framework (SMOF) through the O1 interface. Another interface to the SMOF is the O1\*, through which the Infrastructure Management Framework (IMF), including the Virtual Infrastructure Manager (VIM) as the control plane, manages the Network Functions Virtualization Infrastructure (NFVI). For lower layer splitting, the open fronthaul interface enables all necessary communication between the DU and RU, including real-time layer 2 functions, baseband processing, and radio frequency processing; while the CU-DU higher layer split is done via the F1 interface.

The functional split option defined by O-RAN underpins the effort to reduce the large bandwidth burden of the CPRI-based fronthaul that limits the use of cloud RAN architectures by supporting split option 7.2x with the open fronthaul interface (between O-DU and O-RU) and split option 6 with the F1 interface (between O-CU and O-DU) [85]. Other functional split options that have been considered are mentioned in the following section.

## 2.12 Summary

Mobile networks are evolving as a pragmatic response to the continuous revolutionary trends in information technology, which include innovative services with diverse traffic required by an increasing number of connected devices. The chapter discussed in detail the cloud radio access network (C-RAN) and its variants, focusing on the flexibility of the mobile fronthaul in line with the heterogeneity of the 5G and beyond network. Considering the widely reported limitations of C-RAN architecture, specifically on the fronthaul, we reviewed various functional split options that are proposed in the literature to relax the stringent requirements on the fronthaul. Lastly, smart RAN architecture based on open-source concept was discussed.

---

## References

- [1] J. Bartelt *et al.*, “5G transport network requirements for the next generation fronthaul interface,” *EURASIP Journal on Wireless Communications and Networking*, vol. 2017, no. 1, p. 89, 2017.
- [2] L. M. P. Larsen, A. Checko, and H. L. Christiansen, “A Survey of the Functional Splits Proposed for 5G Mobile Crosshaul Networks,” *IEEE Communications Surveys Tutorials*, vol. 21, no. 1, pp. 146–172, Firstquarter 2019.
- [3] NGMN Alliance, “Suggestions on Potential Solutions to C-RAN,” 2013.
- [4] M. A. Habibi, M. Nasimi, B. Han, and H. D. Schotten, “A Comprehensive Survey of RAN Architectures Toward 5G Mobile Communication System,” *IEEE Access*, vol. 7, pp. 70 371–70 421, 2019.
- [5] S. Jaffer, A. Hussain, M. Qureshi, and W. Khawaja, “Towards the shifting of 5g front haul traffic on passive optical network,” *Wireless Personal Communications*, vol. 112, 06 2020.
- [6] Alcatel-Lucent, “The LTE Network Architecture A comprehensive tutorial,” Tech. Rep.
- [7] P. P. Monteiro *et al.*, “Mobile fronthaul RoF transceivers for C-RAN applications,” *International Conference on Transparent Optical Networks*, vol. 2015-Augus, pp. 1–4, 2015.
- [8] I. A. Alimi, A. L. Teixeira, and P. P. Monteiro, “Toward an Efficient C-RAN Optical Fronthaul for the Future Networks: A Tutorial on Technologies, Requirements, Challenges, and Solutions,” *IEEE Communications Surveys Tutorials*, vol. 20, no. 1, pp. 708–769, Firstquarter 2018.
- [9] A. Checko *et al.*, “Cloud RAN for Mobile Networks - A Technology Overview,” *IEEE Communications Surveys and Tutorials*, vol. 17, no. 1, pp. 405–426, 2015.
- [10] X. Wang *et al.*, “Virtualized cloud radio access network for 5g transport,” *IEEE Communications Magazine*, vol. 55, no. 9, pp. 202–209, 2017.
- [11] H. H. Mahmoud, T. Ismail, and M. S. Darweesh, “Optimal function split via joint optimization of power consumption and bandwidth in v-ran,” in *2020 22nd International Conference on Transparent Optical Networks (ICTON)*, 2020, pp. 1–5.
- [12] J. Wang and Y. Hu, “Performance analysis of 5g nr vran platform and its implications on edge computing,” in *2020 IEEE International Symposium on Performance Analysis of Systems and Software (ISPASS)*, 2020, pp. 215–217.
- [13] S. Sezer *et al.*, “Are we ready for sdn? implementation challenges for software-defined networks,” *IEEE Communications Magazine*, vol. 51, no. 7, pp. 36–43, 2013.



- [14] G. Dandachi, T. Chahed, S. E. Elayoubi, N. C. Taher, and Z. Fawal, "Joint allocation strategies for radio and processing resources in virtual radio access networks (v-ran)," in *2017 IEEE 28th Annual International Symposium on Personal, Indoor, and Mobile Radio Communications (PIMRC)*, 2017, pp. 1–6.
- [15] D. Mishra, H. Gupta, B. R. Tamma, and A. A. Franklin, "Kora: A framework for dynamic consolidation relocation of control units in virtualized 5g ran," in *2018 IEEE International Conference on Communications (ICC)*, 2018, pp. 1–7.
- [16] D. Bhamare, A. Erbad, R. Jain, M. Zolanvari, and M. Samaka, "Efficient virtual network function placement strategies for cloud radio access networks," *Computer Communications*, vol. 127, pp. 50–60, 2018.
- [17] W. Ejaz *et al.*, "A comprehensive survey on resource allocation for cran in 5g and beyond networks," *Journal of Network and Computer Applications*, vol. 160, p. 102638, 2020.
- [18] G. Tseliou, F. Adelantado, and C. Verikoukis, "Scalable ran virtualization in multitenant lte-a heterogeneous networks," *IEEE Transactions on Vehicular Technology*, vol. 65, no. 8, pp. 6651–6664, 2016.
- [19] H. Claussen, D. Lopez-Perez, L. Ho, R. Razavi, and S. Kucera, *Small Cell Networks: Deployment, Management, and Optimization*, 10 2017.
- [20] T. D. Schneider, "Claude shannon: Biologist [information theory used in biology]," *IEEE Engineering in Medicine and Biology Magazine*, vol. 25, no. 1, pp. 30–33, 2006.
- [21] Y. Li, T. Jiang, K. Luo, and S. Mao, "Green heterogeneous cloud radio access networks: Potential techniques, performance trade-offs, and challenges," *IEEE Communications Magazine*, vol. 55, no. 11, pp. 33–39, 2017.
- [22] M. Mukherjee, L. Shu, and D. Wang, "Survey of fog computing: Fundamental, network applications, and research challenges," *IEEE Communications Surveys and Tutorials*, vol. 20, no. 3, pp. 1826–1857, 2018.
- [23] H. Li, G. Shou, Y. Hu, and Z. Guo, "Mobile Edge Computing: Progress and Challenges," in *2016 4th IEEE International Conference on Mobile Cloud Computing, Services, and Engineering (MobileCloud)*, 2016, pp. 83–84.
- [24] T. Taleb *et al.*, "On multi-access edge computing: A survey of the emerging 5g network edge cloud architecture and orchestration," *IEEE Communications Surveys and Tutorials*, vol. 19, no. 3, pp. 1657–1681, 2017.
- [25] K. Liang, L. Zhao, X. Chu, and H.-H. Chen, "An integrated architecture for software defined and virtualized radio access networks with fog computing," *IEEE Network*, vol. 31, no. 1, pp. 80–87, 2017.

- 
- [26] K. Liang, L. Zhao, X. Zhao, Y. Wang, and S. Ou, "Joint resource allocation and coordinated computation offloading for fog radio access networks," *China Communications*, vol. 13, no. Supplement2, pp. 131–139, 2016.
- [27] H. M. Abdel-Atty, R. S. Alhumaima, S. M. Abuelenin, and E. A. Anowr, "Performance analysis of fog-based radio access networks," *IEEE Access*, vol. 7, pp. 106 195–106 203, 2019.
- [28] P. Wiesner and L. Thamsen, "Leaf: Simulating large energy-aware fog computing environments," in *2021 IEEE 5th International Conference on Fog and Edge Computing (ICFEC)*, 2021, pp. 29–36.
- [29] D. Chen, H. Al-Shatri, T. Mahn, A. Klein, and V. Kuehn, "Energy efficient robust f-ran downlink design for hard and soft fronthauling," in *2018 IEEE 87th Vehicular Technology Conference (VTC Spring)*, 2018, pp. 1–5.
- [30] C.-H. Lin, W.-C. Chien, J.-Y. Chen, C.-F. Lai, and H.-C. Chao, "Energy efficient fog ran (f-ran) with flexible bbu resource assignment for latency aware mobile edge computing (mec) services," in *2019 IEEE 90th Vehicular Technology Conference (VTC2019-Fall)*, 2019, pp. 1–6.
- [31] Y. Zeng, A. Al-Quzweeni, T. E. H. El-Gorashi, and J. M. H. Elmirghani, "Energy efficient virtualization framework for 5g f-ran," in *2019 21st International Conference on Transparent Optical Networks (ICTON)*, 2019, pp. 1–4.
- [32] N. Khumalo, O. Oyerinde, and L. Mfupe, "Reinforcement learning-based computation resource allocation scheme for 5g fog-radio access network," in *2020 Fifth International Conference on Fog and Mobile Edge Computing (FMEC)*, 2020, pp. 353–355.
- [33] L. Chen, Z. Jiang, D. Yang, C. Wang, and T.-M.-T. Nguyen, "Fog radio access network optimization for 5g leveraging user mobility and traffic data," *Journal of Network and Computer Applications*, p. 103083, 2021.
- [34] Y.-Y. Shih, W.-H. Chung, A.-C. Pang, T.-C. Chiu, and H.-Y. Wei, "Enabling low-latency applications in fog-radio access networks," *IEEE Network*, vol. 31, no. 1, pp. 52–58, 2017.
- [35] H. Xiang, S. Yan, and M. Peng, "A realization of fog-ran slicing via deep reinforcement learning," *IEEE Transactions on Wireless Communications*, vol. 19, no. 4, pp. 2515–2527, 2020.
- [36] B. Guo, X. Zhang, Q. Sheng, and H. Yang, "Dueling deep-q-network based delay-aware cache update policy for mobile users in fog radio access networks," *IEEE Access*, vol. 8, pp. 7131–7141, 2020.
- [37] K. Guo, M. Sheng, T. Q. S. Quek, and Z. Qiu, "Task offloading and scheduling in fog ran: A parallel communication and computation perspective," *IEEE Wireless Communications Letters*, vol. 9, no. 2, pp. 215–218, 2020.
-

- [38] R. Rai, H. Zhu, and J. Wang, "Performance analysis of noma enabled fog radio access networks," *IEEE Transactions on Communications*, vol. 69, no. 1, pp. 382–397, 2021.
- [39] Y. Qiu, H. Zhang, K. Long, and V. C. Leung, "Noncooperative resource optimization for noma based fog radio access network," in *2020 IEEE 91st Vehicular Technology Conference (VTC2020-Spring)*, 2020, pp. 1–6.
- [40] B. Liu and M. Peng, "Joint resource block-power allocation for noma-enabled fog radio access networks," in *ICC 2019 - 2019 IEEE International Conference on Communications (ICC)*, 2019, pp. 1–6.
- [41] Common Public Radio Interface, "CPRI Specification V7.0," *Standard Document Specification*, vol. 0, p. 128, 2015.
- [42] Nokia, "Evolution to centralized RAN with mobile fronthaul," *Technical White Paper*, pp. 1–14, 2016.
- [43] Ericsson, "Common Public Radio Interface - eCPRI Presentation," [http://www.cpri.info/downloads/eCPRI\\_Presentation\\_for\\_CPRI\\_Server\\_2018\\_01\\_03.pdf](http://www.cpri.info/downloads/eCPRI_Presentation_for_CPRI_Server_2018_01_03.pdf), Tech. Rep., 2018, accessed: 2021-04-26.
- [44] G. Otero Pérez, D. Larrabeiti López, and J. A. Hernández, "5G New Radio Fronthaul Network Design for eCPRI-IEEE 802.1CM and Extreme Latency Percentiles," *IEEE Access*, vol. 7, pp. 82 218–82 230, 2019.
- [45] C. S. Shinde, "A pragmatic industrial road map for shifting the existing fronthaul from cpri to 5g compatible ecpr," in *2020 IEEE 3rd 5G World Forum (5GWF)*, 2020, pp. 297–302.
- [46] HUBER-SUHNER, "5G Fundamentals : Functional Split Overview," <https://www.hubersuhner.com/en/documents-repository/technologies/pdf/fiber-optics-documents/5g-fundamentals-functional-split-overview>, [Online; accessed 2020-10-10].
- [47] Microsemi, "White Paper - Timing for cRAN Fronthaul LTE," Microsemi Corporation, Tech. Rep., December 2017.
- [48] NGMN, "FURTHER STUDY ON CRITICAL C-RAN TECHNOLOGIES," Tech. Rep., 2015.
- [49] V. Ziegler *et al.*, "Stratification of 5g evolution and beyond 5g," in *2019 IEEE 2nd 5G World Forum (5GWF)*, 2019, pp. 329–334.
- [50] K. Miyamoto *et al.*, "Unified Design of LLR Quantization and Joint Reception for Mobile Fronthaul Bandwidth Reduction," in *IEEE Vehicular Technology Conference*, vol. 2017-June, 2017.

- 
- [51] A. Alabbasi and C. Cavdar, "Delay-aware green hybrid CRAN," *2017 15th International Symposium on Modeling and Optimization in Mobile, Ad Hoc, and Wireless Networks, WiOpt 2017*, no. Cc, pp. 1–7, 2017.
- [52] A. Maeder *et al.*, "Towards a flexible functional split for cloud-RAN networks," in *EuCNC 2014 - European Conference on Networks and Communications*, 2014.
- [53] C. Y. Chang, N. Nikaein, and T. Spyropoulos, "Impact of packetization and scheduling on C-RAN fronthaul performance," *2016 IEEE Global Communications Conference, GLOBECOM 2016 - Proceedings*, 2016.
- [54] A. Checko, A. P. Avramova, M. S. Berger, and H. L. Christiansen, "Evaluating C-RAN fronthaul functional splits in terms of network level energy and cost savings," *Journal of Communications and Networks*, vol. 18, no. 2, pp. 162–172, 2016.
- [55] C. Y. Chang, N. Nikaein, R. Knopp, T. Spyropoulos, and S. S. Kumar, "FlexCRAN: A flexible functional split framework over ethernet fronthaul in Cloud-RAN," *IEEE International Conference on Communications*, 2017.
- [56] 3GPP, "Technical specification group radio access network; study on cu-du lower layer split for nr; (release 15)," 3rd Generation Partnership Project, Tech. Rep., 2017.
- [57] O.-R. Alliance, "O-RAN Architecture Overview," <https://docs.o-ran-sc.org/en/latest/architecture/architecture.html>, 2019, [Online; accessed 2021-04-20].
- [58] SCF, "5G small cell architecture and product definitions," <https://www.smallcellforum.org/press-releases/scf-unveils-5g-small-cell-architecture-and-product-definitions/>, Tech. Rep. 238.10.01, 2020, accessed: 2021-04-26.
- [59] M. Gilson, R. Mackenzie, A. Sutton, and J. Huang, "NGMN Overview on 5G RAN Functional Decomposition by NGMN Alliance," [https://www.ngmn.org/wp-content/uploads/Publications/2018/180226\\_NGMN\\_RANFSX\\_D1\\_V20\\_Final.pdf](https://www.ngmn.org/wp-content/uploads/Publications/2018/180226_NGMN_RANFSX_D1_V20_Final.pdf), Tech. Rep., 2018, accessed: 2021-04-26.
- [60] V. Q. Rodriguez, F. Guillemin, A. Ferrieux, and L. Thomas, "Cloud-ran functional split for an efficient fronthaul network," in *2020 International Wireless Communications and Mobile Computing (IWCMC)*, 2020, pp. 245–250.
- [61] G. T. S. G. R. A. Network, "3GPP TR 38.801 (1 of 3) - Study on New Radio Access Technology: Radio access architecture and interfaces," <http://www.tech-invite.com/3m38/tinv-3gpp-38-801.html>, Tech. Rep., 2021, accessed: 2021-04-26.
- [62] A. De La Oliva, J. A. Hernandez, D. Larrabeiti, and A. Azcorra, "An overview of the CPRI specification and its application to C-RAN-based LTE scenarios," *IEEE Communications Magazine*, vol. 54, no. 2, pp. 152–159, 2016.

- [63] Parallel Wireless, “5G NR Logical Architecture and its Functional Splits,” <https://www.parallelwireless.com/wp-content/uploads/5GFunctionalSplits.pdf>, Parallel Wireless, Inc., Tech. Rep., 2019, accessed: 2021-04-26.
- [64] A. Tukmanov, “Fronthauling for 5g and beyond.”
- [65] K. Miyamoto, S. Kuwano, T. Shimizu, J. Terada, and A. Otaka, “Performance evaluation of ethernet-based mobile fronthaul and wireless comp in split-phy processing,” *IEEE/OSA Journal of Optical Communications and Networking*, vol. 9, no. 1, pp. A46–A54, 2017.
- [66] J. Bartelt *et al.*, “5G transport network requirements for the next generation fronthaul interface,” 2017, accessed: 2021-04-26.
- [67] 3GPP, “Technical specification group radio access network; cu-du split:refinement for annex a (transport network and ran internal functional split),” 3rd Generation Partnership Project, Tech. Rep. R3-162102, October 2016.
- [68] Telefonica ; Ericsson, “Cloud RAN Architecture for 5G Cloud,” *White Paper*, pp. 1–24, 2016.
- [69] L. Valcarenghi, K. Kondepu, F. Giannone, and P. Castoldi, “Requirements for 5g fronthaul,” in *2016 18th International Conference on Transparent Optical Networks (ICTON)*, 2016, pp. 1–5.
- [70] P. Arnold, N. Bayer, J. Belschner, and G. Zimmermann, “5g radio access network architecture based on flexible functional control / user plane splits,” in *2017 European Conference on Networks and Communications (EuCNC)*, 2017, pp. 1–5.
- [71] A. Maeder *et al.*, “Towards a flexible functional split for cloud-ran networks,” in *2014 European Conference on Networks and Communications (EuCNC)*, 2014, pp. 1–5.
- [72] H. Gupta, M. Sharma, A. Franklin A., and B. R. Tamma, “Apt-ran: A flexible split-based 5g ran to minimize energy consumption and handovers,” *IEEE Transactions on Network and Service Management*, vol. 17, no. 1, pp. 473–487, 2020.
- [73] A. M. Alba, S. Janardhanan, and W. Kellerer, “Dynamics of the flexible functional split selection in 5g networks,” in *GLOBECOM 2020 - 2020 IEEE Global Communications Conference*, 2020, pp. 1–6.
- [74] A. Marotta, D. Cassioli, K. Kondepu, C. Antonelli, and L. Valcarenghi, “Exploiting flexible functional split in converged software defined access networks,” *IEEE/OSA Journal of Optical Communications and Networking*, vol. 11, no. 11, pp. 536–546, 2019.
- [75] A. I. Salama and M. M. Elmesalawy, “Flexible and adaptive testbed for 5g experimentations,” in *2019 Novel Intelligent and Leading Emerging Sciences Conference (NILES)*, vol. 1, 2019, pp. 166–169.

- 
- [76] L. Diez, C. Hervella, and R. Agüero, “Understanding the performance of flexible functional split in 5g vran controllers: A markov chain-based model,” *IEEE Transactions on Network and Service Management*, vol. 18, no. 1, pp. 456–468, 2021.
- [77] TSGR, “TS 138 401 - V15.2.0 - 5G; NG-RAN; Architecture description (3GPP TS 38.401 version 15.2.0 Release 15),” Tech. Rep., 2018.
- [78] Samsung, “5G Standalone Architecture,” [https://images.samsung.com/is/content/samsung/p5/global/business/networks/insights/white-papers/0107\\_5g-standalone-architecture/5G\\_SA\\_Architecture\\_Technical\\_White\\_Paper\\_Public.pdf](https://images.samsung.com/is/content/samsung/p5/global/business/networks/insights/white-papers/0107_5g-standalone-architecture/5G_SA_Architecture_Technical_White_Paper_Public.pdf), Samsung, Tech. Rep. January, 2021.
- [79] J. F. Monserrat, F. Bouchmal, D. Martin-Sacristan, and O. Carrasco, “Multi-radio dual connectivity for 5g small cells interworking,” *IEEE Communications Standards Magazine*, vol. 4, no. 3, pp. 30–36, 2020.
- [80] “25G PON for 5G anyhaul.”
- [81] J. S. Wey and J. Zhang, “Passive Optical Networks for 5G Transport: Technology and Standards,” *Journal of Lightwave Technology*, pp. 1–1, 2018.
- [82] D. Telekom *et al.*, “Option 4 as a 5G SA complement-Option 4 for smooth 5G NSA-SA migration-by NGMN Alliance Project: 5G Architecture Option 4 Editor / Submitter: Contributors,” 2021.
- [83] ORAN Alliance, “Open & Intelligent Software for the Radio Access Networks,” <https://www.o-ran.org/software>, 2020, [Online; accessed 2021-04-20].
- [84] O-RAN, “O-RAN Use Cases and Deployment Scenarios Towards Open and Smart RAN,” <https://www.o-ran.org/resources>, Tech. Rep., 2020, [Online; accessed 2021-04-20].
- [85] W. Diego, “Evolution toward the next generation radio access network,” in *2020 IFIP Networking Conference (Networking)*, 2020, pp. 685–685.
- [86] A. Sadayuki, K. Toshiro, U. Anil, and M. Ryusuke, “O-RAN Alliance Standardization Trends,” *NTT DOCOMO Technical Journal*, vol. 21, no. 1, pp. 38–45, jul 2019.
- [87] S. K. Singh, R. Singh, and B. Kumbhani, “The evolution of radio access network towards open-ran: Challenges and opportunities,” in *2020 IEEE Wireless Communications and Networking Conference Workshops (WCNCW)*, 2020, pp. 1–6.

## Chapter 3

# Transport Solutions for the Evolving RAN

Driven by the increasing need to support the ever-evolving new requirements, stakeholders have been consistently alerted to the need to design and develop mobile networks to meet the new service requirements, e.g. augmented reality, virtual reality and other low-latency dependent services, while maintaining coexistence with existing network infrastructures, especially for some latency-insensitive or delay tolerant and low data rate services [1–3]. Consequently, 5G networks and beyond are envisaged to entail multiple RATs to support different services. Due to the requirements to support high data rates, low-latency and higher capacity as expected for 5G and beyond, high-speed transmission channels for the provision of backhaul and fronthaul networks [4, 5] and compatible transmission technologies for enabling air interface to user terminals are under intense investigation [6–8]. Therefore, new spectrum is desirable to achieve high-speed, increased capacities, and low-latency transmissions. In addition, high-band spectrum is obviously being considered as candidate spectrum to meet the requirements for 5G and Beyond-5G (B5G), as opposed to low-band and mid-band frequency spectrum used for 2G, 3G and 4G services [9].

It is important to note that the advent of 5G does not mean the abrupt end of the previous generation of mobile networks. However, with the transition to gigabit rates and tens of milliseconds latencies [10, 11], significant improvements are expected so that eMBB and critical services will not only be advanced, but will also tremendously promote widespread deployment of mMTC or heavy deployments of IoT and URLLC [12]. In order to support the above use cases, key enabling mobile transport technologies are continuously studied, especially to ensure the required flexibility and reliability of the mobile transport network [13]. To this end, transmission on mm-wave and terahertz (THz) are intensively studied and exploited for 5G and possibly B5G networks to realize the envisaged high data rate [14–17].

In this chapter, we provide an overview of the current state of the art, which reveals a promising direction for future mobile network transport in accordance with a set of requirements as envisioned for the ever-evolving mobile network generation. Particular attention is paid to the fronthaul networks of RAN for the current and next generation,

with a focus on optical transport solutions, optical-wireless communications and briefly ethernet technologies.

### 3.1 Millimeter-Wave and Terahertz Technologies

The use of mm-wave and THz technologies for mobile data traffic transmission will facilitate the realization of ultra-high data rates by effectively utilizing the huge bandwidths available. The mm-wave lies between microwaves and infrared waves and occupies a band of spectrum between 30 gigahertz (GHz) and 300 GHz, while the frequencies between 300 GHz and 3 THz are referred to as THz [16, 17]. Using the aforementioned frequency band also makes sense because the spectrum used for 4G is already crowded. As beneficial as transmissions at mm-wave and THz frequencies may be, they suffer from impairments arising from their propagation characteristics, including obstacles and diffraction, path loss, rain attenuation, phase noise (PN), atmospheric absorption, and foliage attenuation [18–20]. These impairments are even more pronounced for THz propagation than for mm-wave propagation, since the latter has shorter radiation wavelengths, because the wavelength of electromagnetic radiation is basically given by:  $\lambda = \frac{c}{f}$ , where  $c$  denotes the speed of light, which is  $3 \times 10^8$  m/s, and  $f$  is the frequency (in Hz).

Despite these challenges, the use of THz as mm-wave spectrum usable for 5G and B5G networks has been extensively investigated [21]. Although the sub-6 GHz band is currently designated as Frequency Range 1 (FR1) for the initial phase of 5G commercialization in accordance with the 3GPP R15 specifications, the spectrum beyond 52.6 GHz has been investigated by the RAN specification group, which has identified requirements for use of the mm-wave frequency band 52.6 GHz-114.25 GHz for 5G NR operations [22] with the goal of enhancing FR2 for 5G NR to include support for the 52.6 GHz-71 GHz frequency range [23]. As 5G matures, further improvements in high data rates, capacity, and other KPIs are expected. Therefore, THz communications would greatly enable the necessary drives to meet the requirements of future mobile networks.

#### Integrated Access and Backhaul

Taking advantage of the enormous available bandwidth of mm-wave spectrum for 5G, the potential of mm-wave communications can be tapped to achieve higher capacity by deploying densely populated small cells [24]. A promising solution to achieve improved coverage at low cost is an integrated access and backhaul (IAB) solution based on an approach that promotes the reuse of existing access links simultaneously for 5G backhaul and employs beamforming techniques to improve directional transmission. Since release 10 of the 3GPP standard, there have been consistent improvements in spectral efficiency, robustness and E2E latency performance up to release 17 of the standards.

In the IAB implementation, spectrum band flexibility is provided in accordance with the 3GPP 5G NR standard through the use of multiple bands and efficient spectrum utilization, as well as support for multiple network transitions when network coverage expansion is required, especially in complex, dense urban topographies. Moreover, the



IAB implementation considers the case of in-band and out-of-band IAB frequencies with support for sub-6 GHz and above-6 GHz mm-wave spectrum [25]. An in-band means full or partial overlap of access and backhaul in the frequency domain, while an out-of-band IAB means no overlap of access and backhaul. Therefore, the carrier frequency for the access and backhaul links may be configured the same (in-band) or different (out-of-band). Similarly, the IAB node is designed to be transparent to the UEs. The IAB architecture is in line with a fundamental evolution in 5G mobile networks according to the significant research efforts of the Technical Specification Group Radio Access Network Radio Access Network (TSGRAN) [25].

A basic framework for the IAB deployment scenario is shown in Figure 3.1, which supports IAB parent-child relationships since multi-hops are allowed due to the inherently short range of the mmWave access link. Backhaul links exist between an IAB parent node and an IAB child node, while access links exist between the access UE and an IAB node. The architectural design of IAB allows cascading of multiple IAB nodes according to the standards [26]. The DL/UL traffic scheduling for both access and backhaul links is performed in the parent IAB node, while the traffic scheduling to the UEs is performed in the IAB child node [27].

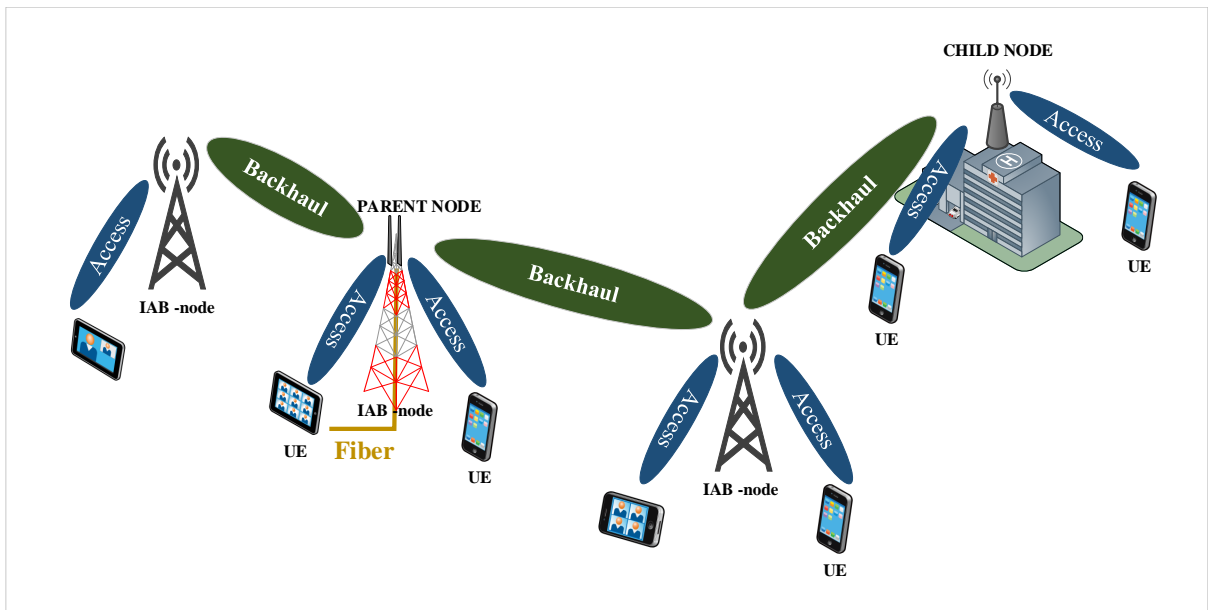


Figure 3.1: An illustration of IAB deployment (Adapted from [27]).

## 3.2 Radio over Fiber Techniques

The concept of radio-over-fiber (RoF) has evolved over the last two decades, converging radio frequencies and fiber optic communications by taking advantage of the best capabilities of both wireless and optical systems [28]. A basic RoF or fiber-wireless system is achieved by modulating photons by radio signals in a process where the modulated signal is transported over an optical fiber. This technique allows the transportation of microwave and mm-wave frequencies over optical fiber. The RoF technique is a promising solution for high data rates, considerably low delays and very low attenuation properties of optical fibers. Furthermore, by taking advantage of the enormous available bandwidth of the optical link (in the range of THz) and its low-loss wavelength (typically 0.3 dB/km at 1550 nm and 0.5 dB/km at 1310 nm), RoF is useful to extend the range of mm-wave signals that are susceptible to significant wireless transmission losses, atmospheric turbulence, and attenuation to achieve high capacity [29].

The transportation of analog and digitized radio over the optical links between BS and CO is achieved through the implementation of RoF techniques and these have attracted significant research interests [30] that continuously produce interesting results for a variety of applications. For the analog wireless transmission system over optical fiber, analog radio over fiber (ARoF) and intermediate frequency-over-fiber (IFoF) techniques are used, while the digitized wireless transmission system includes digitized radio over fiber (DRoF) and digitized intermediate frequency-over-fiber (DIFoF) techniques [31]. ARoF suffers performance degradation that limits the dynamic range of the optical link due to nonlinearity, chromatic dispersion, and noise [32, 33]. Conversely, DRoF can mitigate the inherent impairments of ARoF, but this technique requires high capacity optical links due to the use of ADC and DAC, which are also problematic due to aliasing, quantization, and jitter noise [34]. Another popular RoF transport scheme is baseband-over-fiber (BBoF). The performance of RoF schemes is experimentally studied and compared in [29]. In addition, RoF technologies have been used in [35] to address MFH for 5G and to develop transceivers that facilitate the transport of DRoF signals for C-RAN applications.

### 3.2.1 Basic Structure of RoF System

The figure 3.2 represents in simplified form a general concept of the RoF-system. The figure includes the electrical-to-optical (E-O) conversion among other basic functional blocks to provide a basic understanding of the differences between analog fiber links and digitized baseband fiber transport [36]. For simplicity, Figure 3.2 considers the radio over fiber from the base station to the remote antenna units, i.e., the downlink, for illustrative purposes only.

From the protocol processing at the higher layers down to the PHY layer, the baseband processing stage is passed to the RF up-conversion stage where the data is modulated onto a RF carrier signal. The optical carrier is modulated by radio frequency in the E-O conversion processing stage. To achieve high performance of RoF system, the optical-to-electrical (O-E) and electrical-to-optical (E-O) conversion processes must have low

loss and high linearity [37]. It should be noted that directly modulated lasers (DMLs), such as frequency-distributed feedback (DFB) laser diodes and vertical cavity surface emitting lasers (VCSELS), are preferred for low frequency signal transmission due to their lower cost, while external modulators, such as Mach-Zehnder Modulators (MZMs), are desirable for mm-wave frequencies and other higher frequency bands[36].

For digitized baseband fiber transport, the RF up-and down-conversion is not required because the baseband RF signals are directly optically modulated onto an optical carrier. Therefore, a simpler modulation scheme such as on-off keying can be used, resulting in better performance at the expense of a faster optoelectronic component and wider bandwidth [31]. Obviously, analog fiber links offer lower channel bandwidth, while digitized baseband fiber transport allows simpler modulation techniques.

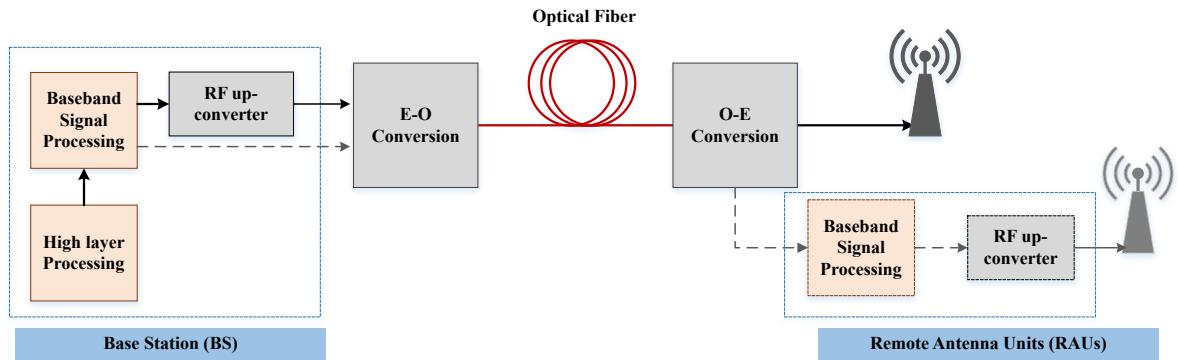


**Figure 3.2:** A simple illustration of RoF transport (Adapted from [38]).

### 3.2.2 Types of RoF Transport Schemes

As indicated in the previous section, wireless signals are generally distributed in a fiber-wireless system based on the following configurations: RF-over-fiber (RFoF), IF-over-fiber (IFoF), Baseband-over-fiber (BBoF), Digitized RF-over-fiber (DRFoF), and Digitized IF-over-fiber (DIFoF), as illustrated in Figure 3.3 and Figure 3.4. In the Figures, a C-RAN architecture is used to describe the RoF transport methods.

#### 3.2.2.1 Analog RoF Transport Schemes

In principle, analog radio signals could be transported over fiber by following the rudimentary configurations in Figure 3.3 showing a RF-over-fiber (RFoF) scheme in Figure 3.3(a) and a IF-over-fiber (IFoF) scheme in Figure 3.3(b). The analog RF-over-fiber transport is the simplest scheme for transmitting radio signals directly on a wireless carrier frequency without further frequency processing at the central office where the BBUs is located. In this configuration, the RF is modulated onto an optical carrier originating from a laser transmitter. Then the modulated signal is transported in analog form over the optical fiber and detected by a photodiode-enabled receiver. At the receiver in the RRU, the RF signal is appropriately filtered and amplified before being radiated

over the antenna for downlink transmission. For the uplink, the RF signal goes through a reverse process as shown in Figure 3.3(a).

In general, the simplicity of the base station design with the added benefits of centralized control, wireless signal transparency and multi-band wireless support, are some of the main advantages of using an analog RoF transport schemes. Nonetheless, the application of ARoF technique to microwave bands is challenging, which is one of the main drawbacks due to the complexity of matching the optical device speeds to those of the wireless carrier frequency [33]. Moreover, chromatic dispersion, which degrades the received RF power and limits the fiber transmission distance, affects the optically modulated wireless transmission through the fiber [39].

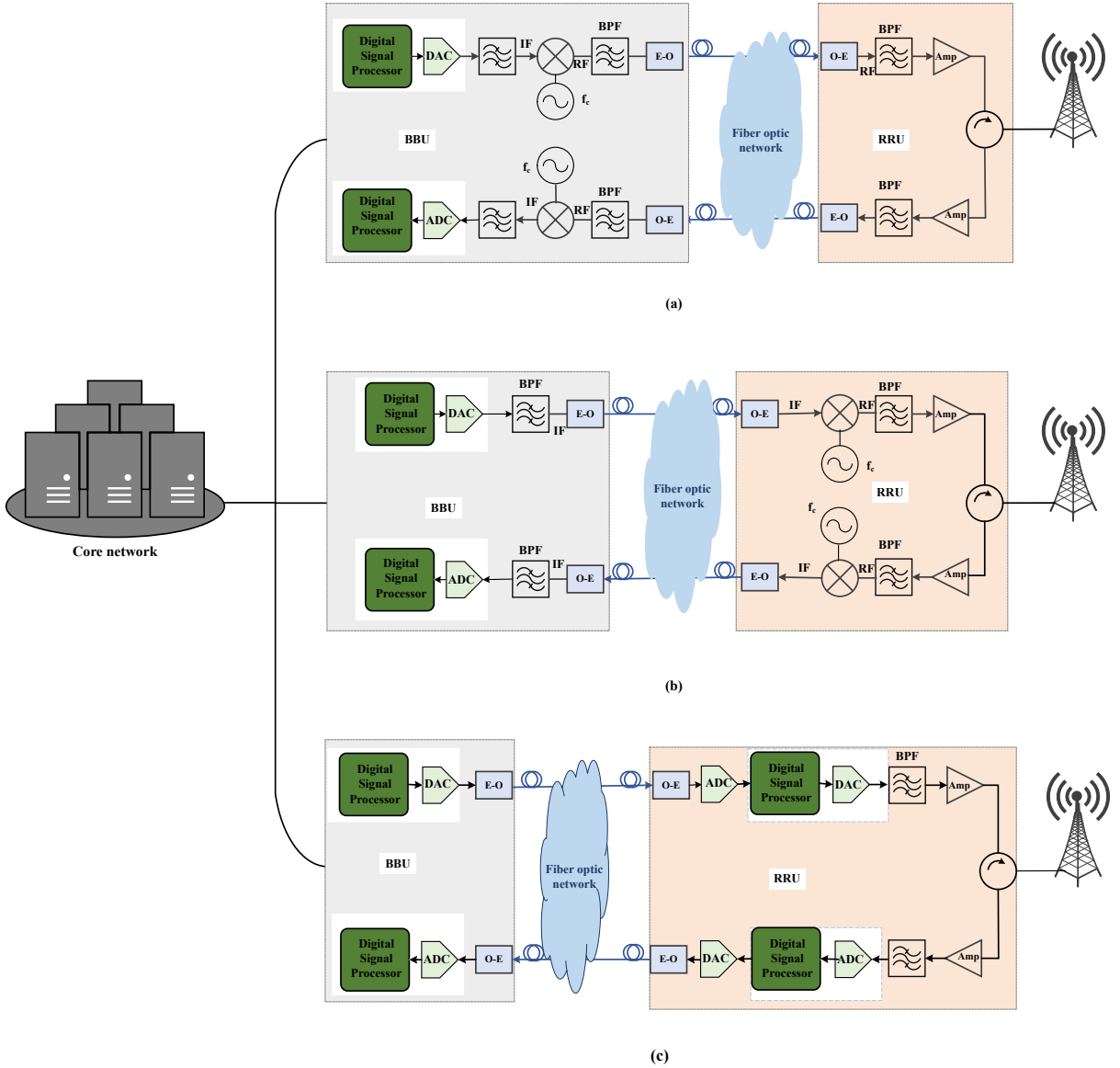
In the IF-over-fiber transport scheme in Figure 3.3(b), the wireless signals are transmitted at a lower intermediate frequency (IF) over an optical link, and this technique relaxes the requirements for high-speed optoelectronic hardware. Also, the effect of fiber chromatic dispersion is much less in this configuration, since the transmission of the IF-band signal is almost not affected by the effect of fiber dispersion because RF power fading depends on the carrier frequency [40]. However, a more complex antenna design is required, which requires a stable local oscillator (LO) and mixers with high conversion efficiency for frequency translation, as well as fast mixing components such as metal-semiconductor-metal photodetectors at the RRU [32, 39]. In addition, a simple configuration that supports high-frequency RF signals can be achieved by using external modulators such as electro-absorption modulator (EAM) in the RoF system design [32].

Figure 3.3(c) shows an architecture of DSP-ARoF. Like other analog systems, DSP-ARoF allows transmission of analog waveforms in the optical domain. Unlike other analog systems, DSP and a DAC/ADC are added in the RRU. On the one hand, seamless aggregation of traffic from different RRU is possible, and through this approach, integration of existing and future optical broadband networks for high-speed networks is possible [41].

### 3.2.2.2 Digitized RoF Transport Schemes

As an alternative to analog radio-over-fiber transport schemes, transmission of digitized RF signals over optical fiber is considered in favor of analog RoF transport schemes in some cases, depending on service requirements. In the optical links, the digital I and Q samples of the radio signal are transmitted to the remote radio units via the processes briefly illustrated in Figure 3.4, which consist of D/A converters, up-converters and amplifiers for the downlink direction, and A/D converters, down-converters and amplifiers for the uplink direction. The modulation functions take place at the central office, so the remote radio units are small and relatively simple [37, 38]. Housing the analog-to-digital and digital-to-analog converter functions in the base station allows digital implementation of functions within the receiver and transmitter modules.

Digitized RF-over-fiber (DRFoF) transport and digitized IF-over-fiber (DIFoF) transport are among the digitized wireless over optical fiber transport schemes. A basic digitized RF-over-fiber scheme is shown in Figure 3.4(a). The digitized wireless signal is generated by directly modulating the optical sources with a sampled digital data stream in a serial format. Interestingly, the dynamic range of the optical link is not only limited



**Figure 3.3:** A representation of analog RoF transport configurations: (a) RoF (b) IFoF (c) DSP-RoF (Adapted from [41]).

by the transmission distance of the optical fibers, provided that the received signal is within the link sensitivity but also subject to fiber dispersion. Moreover, the complex signal processing for the DRFoF transport scheme is handled in the central unit, while the functionality of the front-end components in the antenna at the RRU block is limited to analog-to-digital (ADC) and digital-to-analog conversion (DAC) [31]. In this way, transparency is preserved since full processing of the radio signals in the RRU is not required. However, to realize the digitization of the radio signals, the analog bandwidth of the ADC must be larger than the carrier frequency of the radio signal with sufficient sampling rate and resolution [42, 43].

As mentioned earlier, this requirement is particularly stringent for radio signals

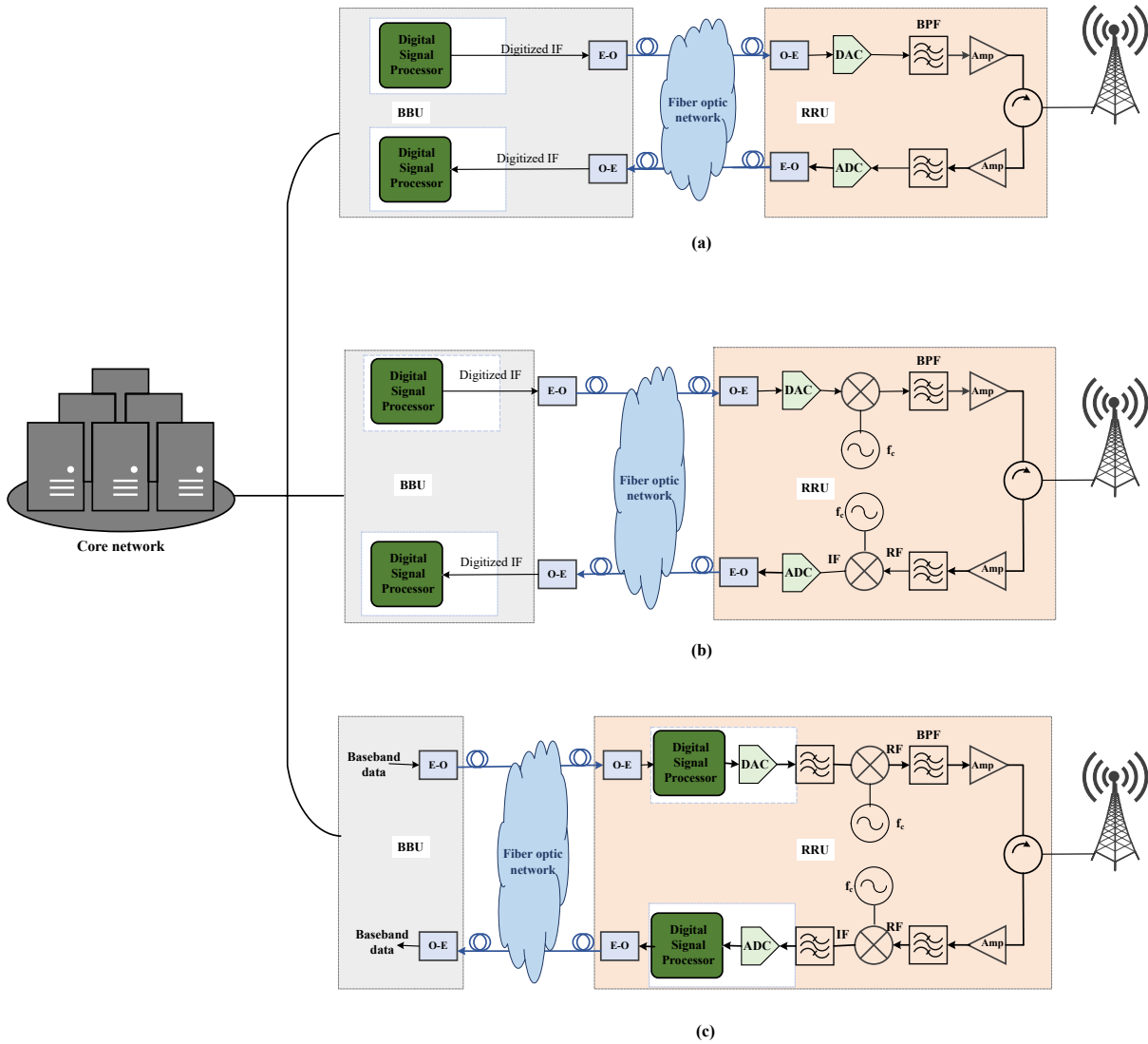


**Figure 3.4:** A representation of digital RoF transport configurations: (a) DRoF (b) DIFoF (c) BBoF (Adapted from [41]).

beyond the microwave bands. To overcome this limitation, the digitized IF-over-fiber technique is introduced, where the radio signal is first down-converted to a IF frequency to accommodate the limitations of the current ADC technology [31, 37, 43]. A IF-over-fiber transport scheme is shown in Figure 3.4(b). Instead of direct sampling, which requires the use of ADC technology, the use of bandpass sampling technique achieves the complexity of ADC conversion. Thus, with the bandpass sampling technique, frequency conversion is achieved without LO and mixers, while a suitable bandpass filter can also be used to recover the radio signal [41, 44]. This technique minimizes the digital memory required to acquire a radio signal at a given time, since the information bandwidth is only a small percentage of the wireless carrier frequency [41, 45]

An architecture for baseband over fiber transport is shown in Figure 3.3(c), where the radio signal is transmitted optically as baseband data and the wireless signal is

processed entirely at the antenna BS. This transport scheme is similar to existing optical networks where data is transmitted in a digital environment, typically for long-range scenarios. The challenge with BBoF is that a complex remote antenna unit (RAU) configuration is required for frequency conversion, data modulation, and demodulation, and these additional tasks result in higher power consumption [45, 46]. Consequently, the implementation based on BBoF is expensive because a large number of RAUs is required, as expected for distributed antenna system (DAS). In the BBoF technique, the link transparency decreases while the complexity of BS increases significantly. To overcome the challenges associated with the BBoF transport scheme, the digitization of wireless signals by using the transport scheme for the fiber-wireless applications has been considered to achieve advanced digital optical links while simplifying BS design of the RRU Block [41].

## 3.3 Optical-Wireless Communication Based Mobile Transport Solutions

As a result of increasing spectrum utilization and gradual congestion of RF allocations, coupled with the drive for seamless high data rate communications, attention is being drawn to the adoption of optical-wireless communications (OWC) as an alternative or backup link to wireless communications. In addition, the propensity to support high bit rates and full duplex transmission, ease of deployment, license-free operation, and secured transmission with resistance to electromagnetic interference are some of the tremendous advantages of OWC links [47–50]. These advantages arise from the properties of optical fibers. In short, both OWC and fiber optic transmission are similar except that in the case of OWC, unguided channels are involved for the transmission of modulated signals.

OWC operates in the spectrum from 350 nm to 1550 nm and can be categorised into two main classes, indoor and outdoor in terms of deployment scenarios. The former deals with indoor communications and includes generic configurations such as directed line-of-sight (LOS), non-directed LOS, diffused and tracked; while the latter, also referred to as Free Space Optics (FSO) is for building-to-building, satellite-to-satellite, satellite-to-ground, ground-to-satellite, satellite-to-airborne platforms [47]. OWC can also be classified into three categories based on spectrum, namely infrared, visible light and ultraviolet. In addition, FSO communication systems typically use the near-IR (NIR) spectrum for PtP operation, including ultra-short (750 nm to 1450 nm), short (1400 nm to 3000 nm), medium (3000 nm to 8000 nm), long (8000 nm to 15000 nm), and ultra-long (15000 nm to 1 mm). For long range FSO links, ultra-short IR and short IR optical spectra are used, while the long IR and medium IR are used for thermal imaging and military applications, respectively [51].

As promising as OWC links are, their reliability depends on the requirement of a strict line of sight (LoS), obstruction of signal propagation by objects within the LoS, the large influence of weather conditions, and reliance on a very narrow beamwidth to maximize gain. FSO is particularly affected by background illumination and the sun, leading to noise in the photodetector [52].

### 3.3.1 Free-space optical communication system

As a promising wireless communication system, FSO communication systems are tremendously investigated in wide areas for providing high-speed and reliable communication for various applications. FSO uses LoS for data transmission through free space between transmitter and receiver instead of optical fibers or wireless RF links. Consequently, FSO links can serve as an alternative to wireless RF to achieve high data rate transmission comparable to fiber optic communication. However, unlike fiber optic transmission, a unique feature of the FSO communication system is that the FSO output signal is collimated and transmitted through the atmosphere with a modulated narrow optical laser beam and then processed at the receiver. Generally, eye-safe invisible light beams are transmitted from the transmitter to the receiver by using low-power infrared lasers, especially in the terahertz spectrum.

Although optical fiber offers a very reliable and high data rate transmission, its deployment involves high capital expenditure (CAPEX). Therefore, optical fiber cable can be replaced with FSO systems, especially in topographical location where the installation of optical fiber cables is impractical or there is paucity of fiber infrastructure [53]. Aside from the ability of the FSO link to deliver high bandwidth transmission, the optical frequency yields high antenna gain with comparatively small size of the antenna [48]. In this case, additional benefits of smaller size, low mass, and lower power consumption can be attributed to FSO links as opposed to the RF channels. It is thus possible to operate an FSO link with an optical antenna whose diameter is about a factor of 13 smaller than that of the RF [41, 48, 54].

Considering the various benefits attributed to FSO technology, it is being used to provide transport solutions for broadband access technology to meet the bandwidth requirements of various services and application that could be supported by 5G and beyond networks [41, 55], taking into account the atmospheric absorption and other propagation-hindrance effects including weather conditions such as turbulence, rain, fog, haze and dust [48, 56], pointing instability arising from spatial and temporal variation in the refractive index of the atmosphere [49]. However, to mitigate propagation losses due to atmospheric absorption, transmittance wavelength are carefully selected since atmospheric absorption is an upshot of the wavelength employed for the transmission. Normally, unlicensed band of 780 nm - 850 nm and 1520 nm - 1600 nm wavelengths are use because of their approximately minimal absorption effects and resistant to electromagnetic interference [56, 57]. Furthermore, it is therefore essential that FSO communication system is intensively studied with respect to the above constraints to ensure reliable and robust transmission and reception.

### 3.3.2 Basic Structure of a FSO System

Basically in its simplest form, an FSO system consists of a transmitter, the free space channel and a receiver. The conversion of the digital data stream into analog optical signal at the transmitter by modulating the laser beam, which is then propagated to the receiver via an optical channel. In simplified form, a FSO transmitter includes an optical laser source, a laser modulator, a driver, and a transmitting telescope for focusing the



optical radiation toward the receiver, since LoS is essential for establishing communication between the transmitter and receiver [56]. The requirement for LoS is due to the fact that the propagated optical beams radiate linearly through the Fresnel zone [58]. As the optical signal travels through space, it is attenuated in the atmosphere by absorption, scattering, scintillation, propagation geometric and other phenomena. Therefore, the total radiation attenuation (in  $dB/km$ ) can be expressed as [59]:

$$A(\lambda) \approx \alpha_{fog}(\lambda) + \alpha_{snow}(\lambda) + \alpha_{rain}(\lambda) + \alpha_{scattering}(\lambda) \quad (3.1)$$

Where  $\alpha_x(\lambda)$  represents attenuation subject to aforementioned weather conditions and  $\lambda$  is the operational wavelength.

Direct modulation and external modulation techniques are commonly employed to convert the data streams into the analog optical signal. In the case of the direct modulation technique, the modulation takes place inside the laser resonator and depends on the variation resulting from the add-on input components which produce a corresponding laser beam intensity, while the modulation process takes place outside the laser resonator and depends on both the polarization and the refractive dualism polarity phenomenon [56, 60]. In addition to the modulator, a driver circuit is used to vary the current flow through the light source, specifically a laser diode (LD) such as the fabry-perot (FP), distributed-feedback laser (DF), and vertical cavity surface emitting laser (VCSEL).

The incoming signal from the FSO link is received and processed by the optical receiver. An optical receiver consists of a receiving telescope, a filter, an amplifier, a detector, and a demodulator. The telescope collects and focuses the incoming optical light signal onto the photodetector (PD), which is either a pin photodiode (PIN) or an avalanche photodiode (APD) for converting the collected optical into an electrical signal. Due to the attenuation effect on the optical signal, an optical preamplifier may be required to amplify the signal. Finally, the recovery of the original signal in the demodulator is done by comparing the phase of the received signal with that of the reference signal. Maximum likelihood sequence detection (MLSD), error control coding including interleaving, and adaptive optics are used to minimize the bit error rate (BER) and mitigate turbulence-induced fading [41, 56].

### 3.3.3 Free Space Optics (FSO) Transport Schemes

The benefits of FSO communication are consistently motivating its adoption in diverse areas. However, the reliability of FSO links poses a critical challenge to the use of FSO links for mobile backhaul or fronthaul solutions due to the adverse effects of atmospheric conditions. Therefore, to improve the performance of FSO links to support the delivery of 5G and beyond services, FSO technology is used in conjunction with other technologies. Possible concepts that are widely used are hybrid RF/FSO and relay-based transmission technologies [41].

### 3.3.3.1 Hybrid RF/FSO System

Considering the strengths and weaknesses of FSO communication mentioned in the previous section, it is desirable to combine FSO links with other technologies that have complementary properties to improve robustness of the transmission channel. An outstanding solution is the hybrid RF/FSO-based transmission, which is an attractive scheme to effectively realize mobile transport with a certain degree of resilience and robustness required to support cellular services by simultaneously suppressing the weaknesses of both technologies and bolstering their advantages.

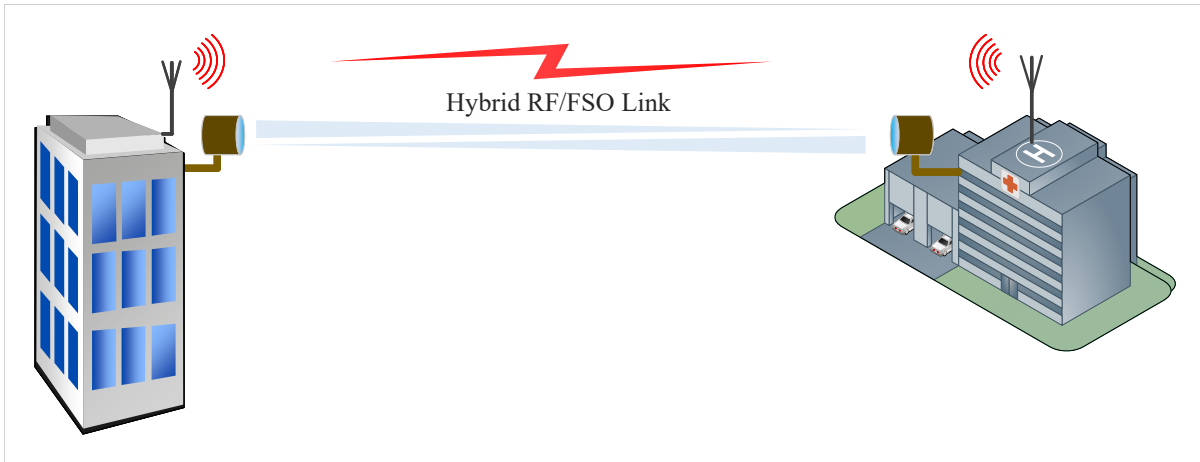


**Figure 3.5:** A basic schematic to illustrate hybrid RF/FSO transmission (Adapted from [41]).

A representation of the hybrid RF /FSO is shown in Figure 3.5, where both links are capable of transmitting data simultaneously. The communication can be designed and configured according to weather conditions and electromagnetic interference levels. Following a similar concept, a hybrid FSO/RF communication system based on adaptive combining is presented in [61], where the transmission is prioritized based on the comparative instantaneous signal-to-noise ratio (SNR) at the FSO receiver, such that the FSO link is active when its SNR is above the threshold level.

The prioritization of RF-FSO transmission links as a function of signal quality has been extensively studied [62–66]. In [62], the authors use a gamma-gamma channel and PSK modulation for a dualhop hybrid RF/FSO with decode-and-forward (DF) relaying to improve the performance of the transmission system. Similarly, in [63], the authors consider the outage probability and average symbol error rate (SER) for a selective DF relay network based on maximum ratio combining (MRC) assumption to enable RF/FSO switching based on an optimal threshold SNR. In [64], a cascaded RF and hybrid RF/FSO system is considered in which multiple users transmit data over a single RF link to a relay node, which then forwards the information to the destination over a hybrid RF/FSO backhaul link. Transmission time is allocated to RF links based on optimal fixed and adaptive link allocation strategies derived for both delay-limited and delay-tolerant links, as described in this paper. Paper [65] investigates adaptive transmission schemes over a hybrid RF/FSO backhaul network to a macrocell base station. The authors further claim

that the adaptive transmission scheme has better performance than the conventional RF/FSO switching scheme.

In [67], a practical demonstration of a hybrid RF/FSO transmission system is presented, where the RF link transmits 300 Mbps pseudo random digital signals, while 10 Gbps pseudorandom digital signals are transmitted on the FSO link. Also, in [68], the joint optimization of fronthaul compression and RF time allocation in uplink C-RAN with hybrid RF/FSO fronthauling is investigated, and the authors concluded that hybrid RF/FSO fronthauling has better performance compared to pure FSO fronthauling. Furthermore, the problem of inband full-duplex (IBFD) hybrid RF/FSO that supports self-backhauling in a C-RAN architecture with many RUs and users is investigated in [69]. Unlike the traditional time-division hybrid RF/FSO approach, the authors employ an alternating convex optimization to solve the problem of resource and link allocations and establish a lower-bound for the user's sum-rate for solvable problems.

#### 3.3.3.2 Relay-assisted FSO Transmission System

Another technique that has been extensively studied to improve the reliability of FSO links by integrating RF and FSO is relay-assisted FSO transmission. In addition, the use of this technique enables the effective use of a single high-speed FSO link as a trunk for traffic from multiple users with RF capabilities, thereby leveraging optical capacity [70]. An interesting feature of relay-assisted FSO transmission is that RF and FSO operate on completely different frequency bands, so the problem of interference between the two is not relevant, which contributes to the robustness of this model compared to conventional RF-RF relay transmission. The concept of dual-hop communication has been used extensively as a technique to facilitate simplified spatial diversity. Moreover, this technique is robust to extend the coverage area of the cellular network and improve the signal quality at the receiver side [71, 72].

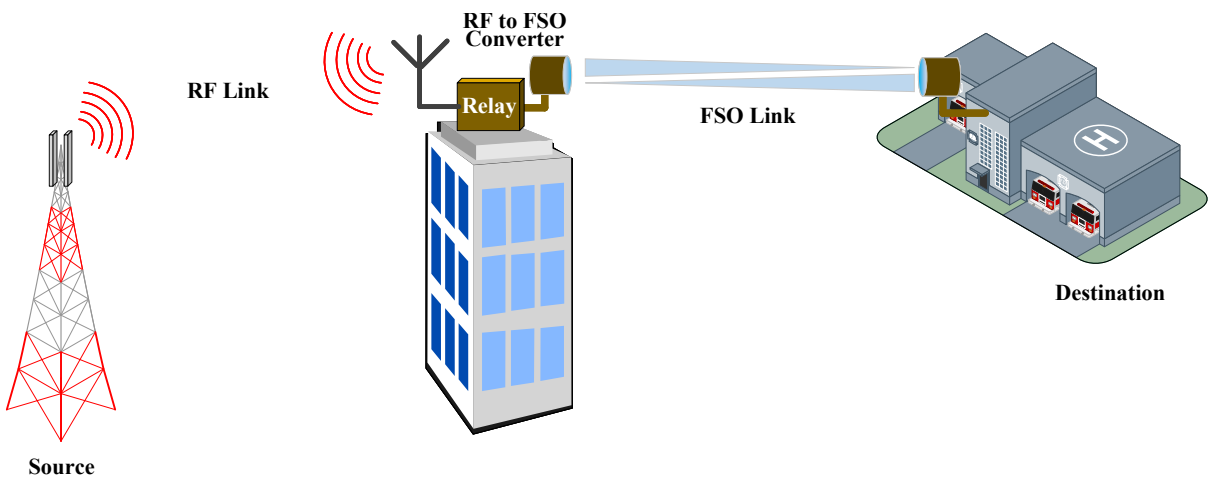


**Figure 3.6:** An illustration of relay-assisted FSO transmission (Adapted from [41]).

In contrast to RF dual-hop, relay-assisted FSO transmission is a mixed RF/FSO dual-hop model that exploits the properties of both RF and FSO communications to transmit

traffic from source to destination, as shown in Figure 3.6, and provides the ability to create a system with multiple apertures to achieve MIMO transmission between the source and relay to mitigate the limitations due to multipath fading and atmospheric turbulence [73]. In this model, one hop is used for RF links from the source, while the other hop is used for FSO links to relay the traffic to the destination [74].

A unique feature of the relay-based FSO transmission model is the relay-functional RF to FSO converter, which is generally located on a high platform and connects the source and destination [75]. At the RF to FSO conversion stage, RF signals are received at a relay's receive antenna, while optical signals are transmitted at a separate transmit aperture [41, 75]. As a result, RF users can connect to the backbone network via FSO links.

## 3.4 Optical Access Transport Solution

Telecom network usually consists of the access network, the metropolitan (or regional) network, and the backbone network. The first two may be combined as the access network in some cases, as the metropolitan network disappears due to the reach of the access network. The most commonly deployed optical access networks are active optical networks (AON) and passive optical networks (PON), which are deployed in either on a PtP and PtMP topology. Meanwhile, the AON usually include fiber-to-the-home (FTTH) or fiber-to-the-building (FTTB) with active remote nodes (RN) connected to the CO, and multiple users. In the network, the traffic of a group of nodes is bundled via an Ethernet switch connected to another switch at the CO. However, to support optical broadband services to multiple users, passive optical networks (PONs) are popular choices because of their relative cost-effectiveness.

PON, a set of technologies standardized by International Telecommunications Union – Telecommunications Sector (ITU-T) and Institute of Electrical and Electronics Engineers (IEEE), is a conglomerate of infrastructure with the ability to carry multiple services. A PON system is composed of an optical line terminal (OLT) which is at the central office (CO), optical distribution network (ODN) consisting of passive power or wavelength splitters, and optical network units (ONUs) located at the subscribers' premise [76, 77]. PON is widely adopted in access networks because of its infrastructural simplicity and propensity to deliver improved capacity and higher data rate. The employment of PON system allows efficient use of the existing fiber infrastructures, thus reducing site space and significantly improving the power conservation of base stations. [77].

### 3.4.1 Passive Optical Network

Evolution of the fifth-generation mobile communications system (5G) network surely brings about paradigm shift from conventional network architecture to achieve the requirement of 5G and beyond network. Also, the passive optical network (PON) is evolving from generation to generation in conformity with a set of requirements to support mobile network for improved services delivery. Provisioning of access network requiring high bandwidth and low latency has attracted significant researches to enable

a single optical distribution network (ODN) provide broadband services to mobile, residential, and business services. Majority of these works focus on multi-wavelength based PON and typically time and wavelength division multiplexing PON (TWDM-PON) which is a hybrid of traditional TDM/TDMA and wavelength division multiplexing (WDM) technologies and this is adopted by 2nd next-generation PON (NGPON2) [78]. NGPON2 enables stacking of four wavelengths in a single fiber to achieve a 10 Gb/s per wavelength. However, higher capacity can be delivered by adopting channel bonding in a NGPON2. Also, 10 Gigabit Ethernet PON (10G-EPON), 10 Gigabit PON (XG-PON), and 10 Gigabit capable symmetric PON (XGS-PON) have been standardized by the International Telecommunication Union - Telecommunication Standardization Sector (ITU-T) [79].

To achieve the requirements for capacity enhancement and improved network coverage, ultra-dense small cells deployment is envisaged for 5G and B5G. Therefore, mobile transportation is posed with the challenges to support diverse use cases, especially mission-critical applications, increased video streaming capabilities and the likes, that could be affected by more stringent end-end latency requirements [12, 80, 81]. Although 5G backhaul entails both wired and wireless backhaul solutions, fiber optic link is readily considered as a good choice, especially when an ultra-low end-end latency is desirable [82]. Apparently, PHY PtP based fiber deployment could be used, but it is not cost-effective transport solution for 5G because of the envisaged explosion of small cells arising from heavy exploitation of mm-wave spectrum and MIMO technology. Conversely, PtMP topology is widely acknowledged for 5G backhaul to support billions of interconnected smart devices. Consequently, there are several research efforts aiming at providing low cost solutions while meeting the requirements of 5G mobile network.

#### 3.4.2 PON Based Mobile Transport Solution

There are several options for mobile transportation, classified as either active or passive. In an active solution, a power supply is required at the cell sites to carry the CPRI traffic, which is encapsulated using either an optical transport network (OTN) or other protocols and multiplexed over the fronthaul. In the passive solution, on the other hand, CPRI traffic is multiplexed and de-multiplexed and no power supply is required at the radio cell demarcation points.

In addition, as 5G matures into 3GPP Release 16 and beyond, integrated access and backhaul (IAB) is seen as a key enabler for delivering fast and cost-effective deployments, mainly targeting dense outdoor mm-wave deployments, especially where fiber is extremely expensive or difficult to install. Considering the advantages of fiber optic transport solutions (FOTs), one of the promising solutions is the reuse of existing fiber optic network infrastructures for the deployment of passive optical networks. In this way, the PON system could be used as backhaul and fronthaul transport solutions as illustrated in Figure 3.7 and 3.8. This could be a promising backhaul solution for capacity expansion, but the problem of latency with PON poses a challenge for the deployment of PON systems for mobile fronthaul.

Considering the diverse 5G use cases, there is no single MFH solution that dominates

for all services. In fact, the choice of 5G MFH network depends on the deployment area and user traffic [12, 83]. To support the 5G use cases mentioned in the previous section, it is necessary that the transport solution meets the requirements of the traffic characteristics that are expected for various 5G use cases. As 5G and future network are expected to involve heterogeneous architectures enabled by combination of technologies, several backhaul transport solutions have been investigated. Therefore, there is no generic solution for backhaul since it depends on the technology employed and envisaged services to be supported. The 3GPP and ITU-T have some recommendations, some of which contained the technique for relaxing the stringent conditions imposed on midhaul and fronthaul by employing functional split options [80, 81, 83] .

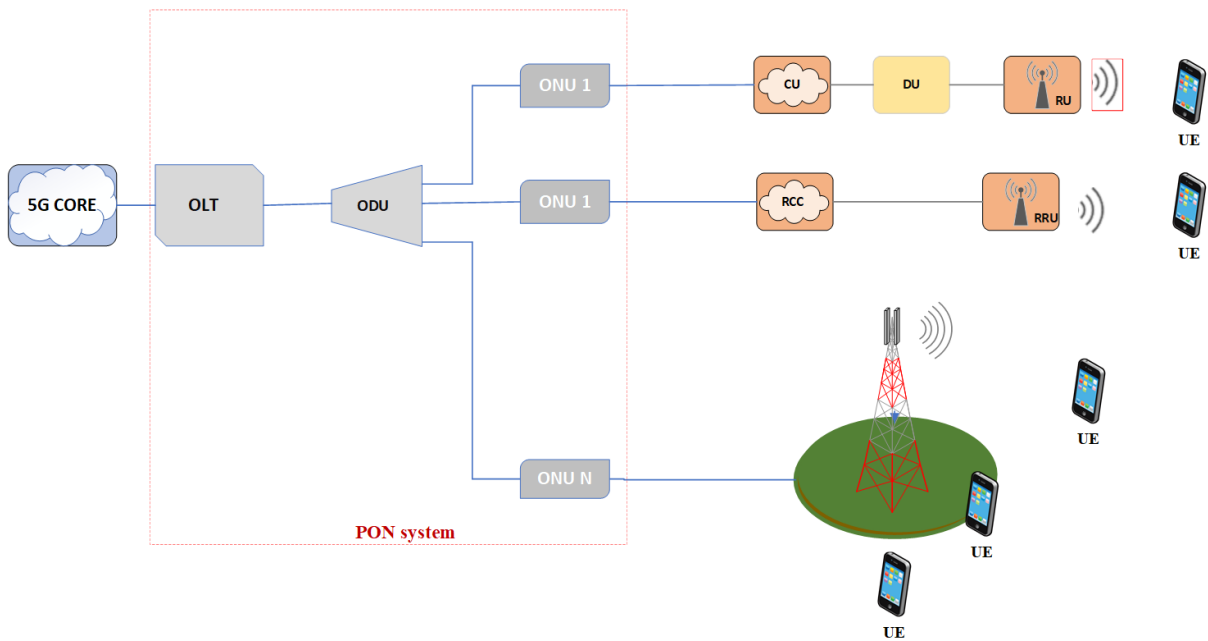


**Figure 3.7:** A simple representation of a PON based backhaul scheme.

### WDM Technology Based Approach

Wavelength-division multiplexing (WDM) based PON systems require less complexities to achieve low latency unlike the time division multiplexing (TDM) based PON and thus much suitable for 5G ULLC, because of the capability of WDM-PON to support several ONUs by one optical splitter and one fiber using different wavelengths. Further enhancement could be introduced by an auxiliary management and control channel (AMCC) aids to attain needed high bandwidth by enable loading a management channel onto each wavelength while also guaranteeing low latency traffic [84]. Moreover, it is important that the system framing scheme of logical PtP WDM PON must not induce unnecessary delay and jitter in compliance with the IEEE 802.1 CM Time-Sensitive Networking for fronthaul [85]. In [86], a simple delay and differentiation method has been reported to yield much reduction in the reflective crosstalk for self-seeded reflective

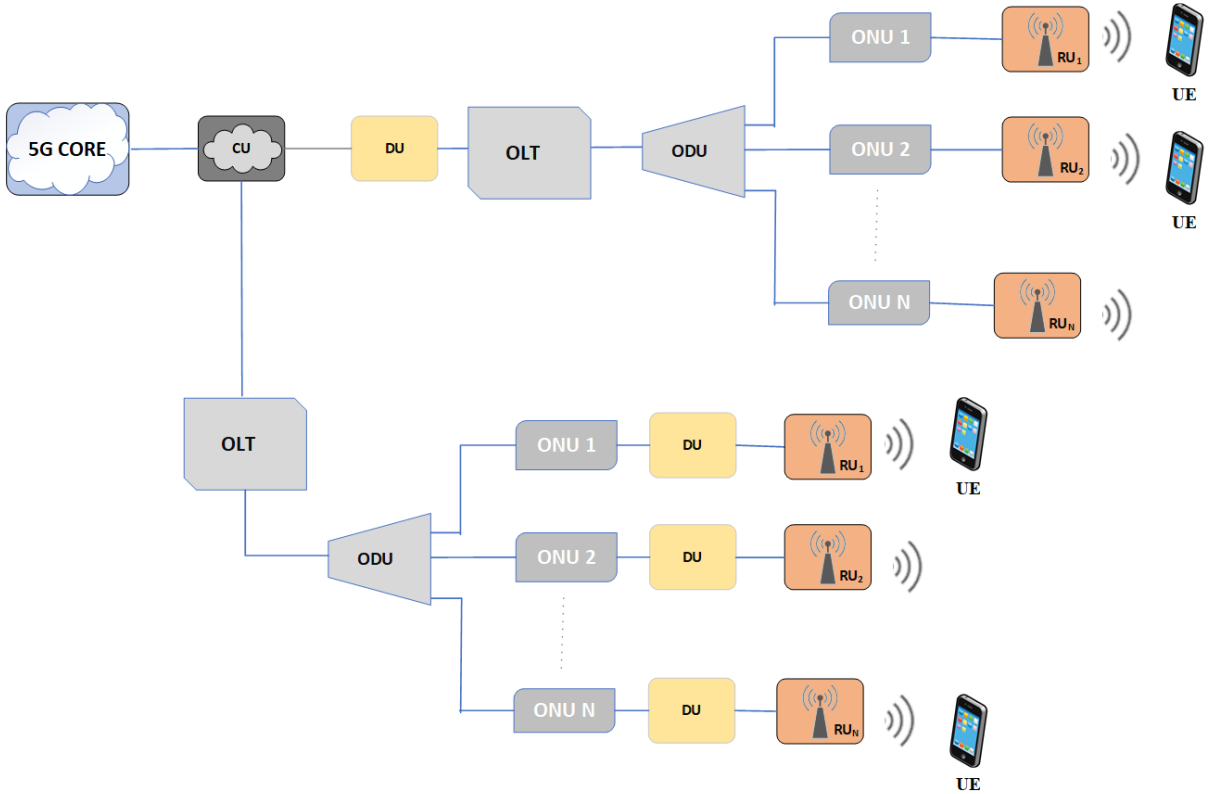


**Figure 3.8:** A simple representation of a PON based fronthaul scheme.

semiconductor optical amplifier (RSOA) when used to offer large capacity and low latency as a low-cost solution.

### TDM Technology Based Approach

For 5G, one-way end-end latency at the service layer could be 1 ms, for example. It is rather impossible for a basic TDM-PON to support such service. Therefore, to offer low latency service, one technique is to use lower latency dynamic bandwidth allocation (DBA) to reduce the delay. There are several approaches towards achieving this. One method is by utilizing fixed bandwidth allocation (FBA) for the US per UN at regular interval [84, 87]. While FBA offers low latency, it has low bandwidth utilization. Conversely, DBA yield good bandwidth utilization but with relatively poor latency. It is interesting to know that there exists a trade-off performance relation between FDA and DBA and careful measure should be taken to implement in the OLT engine for optimal use of the two bandwidth allocation techniques while avoiding detrimental effect on the latency. Other techniques being used to reduce DBA associated delay include online DBA algorithm based on interleaved polling with adaptive cycle time (IPACT), fast class-of-service oriented packet scheduling (FCOPS), latency-oriented packet scheduling (LOPS) based DB. In a TMD-PON system, DBA associated latency also depends on grant processing time (GPT) and handshake between the OLT and ONUs. Therefore, 5G requirements can be met by devising means to lower the GPT and reduce the complexities

involved in the handshake processing. This method is exploited and investigated in [88, 89] to relax the DBA cycle length and latency.

Furthermore, the benefits of artificial neural network could be tapped and adopted for based TDM-PON, if the DBA engine is manipulated to allow reduction of the upstream (US) delay by making the OLT pre-allocates the scheduling grant to the ONUs in advance based on ONU logs from ONUs transmission containers (T-CONTs) using deep-Learning algorithm [90]. In addition to the above, to boost timing response for 50G-PON to 5G latency-sensitive service, cyclic-based low latency oriented packet scheduling (LOPS) DBA is demonstrated in [91], providing bandwidth allocation for 4 service classes to each ONU based on multiple user link identifiers (ULIDs). Also, an improved low latency DBA scheme for NG-PON2 is proposed in [92] to reduce the 5G fronthaul delay while ensuring maximum attainable throughput to the active ONUs. While in [93], the authors proposes and analysis through simulation a hybrid fixed-elastic DBA for XG(S)-PONS by enabling regular fixed-size TDM allocations to guarantee enough bandwidth, thereby lowering latency and jitter to the ONU. Another method that is proposed to address latency issue in PON is the so-called “cooperative DBA” (CO-DBA) with which the ONU scheduling process tells the OLT precisely when exactly it needs resources [94]

**Table 3.1:** Comparison of PON baseline systems

System	Multiplexing Technique	Pros	Cons	Ref
WDM-PON	WDM on logical PtP	isolated channels and independent wavelength route, scalable, dynamic, adaptive resource allocation, low latency capability	insufficient power budget, limited rate per wavelength, management and monitor, difficulty of eCPRI signal, relatively expensive	[95] [76] [96] [97] [98] [99]
TWDM-PON	TDM on Physical PtM	relatively cost effective 5G transport, multiple wavelengths to one power splitter	dynamic bandwidth allocation (DBA) associated latency on the US, stringent timing requirements, stiff architecture, complex dynamic adaptability and scalability, limits resource pooling.	[95] [96] [97] [98]
OFDMA-PON	OFDM using logical PtP	large capacity, high spectral efficiency, refined bandwidth resource, multi-carrier transmission	low bandwidth optical sub-channels, high peak-to-average power ratio (PAPR), frequency offset limitation, and disturbs by phase noise	[97] [99] [100]



### 3.4.3 Low latency PON Based Solution

Essentially, for PON to support 5G transport, it should meet the synchronization timing error requirements which depend on fiber propagation delay which is derived from different upstream and downstream wavelengths causing systematic error when transmitting, equalization delay (EqD) accuracy, internal timing correction including logical computation within the OLT and ONU, system hardware internal error; PON-wireless interface coordination. The internal requirements of PON system comprises timing ascribe to OLT and ONU, channel management and monitoring; support for operations, administration and maintenance (OAM) functions vis-à-vis the ONT management and control interface (OMCI) in the case of TDM based PON systems, and auxiliary management and control channel (AMCC) scheme supports per-wavelength monitoring for WDM-PON system [82, 101, 102]. A comparison of basic PON system is presented in Table 3.1 to showcase the justification for integrating combination of the features of these PON systems for performance improvement. In particular, NG-PON2 has been widely investigated as a promising candidate for mobile fronthaul and backhaul to drive the 5G traffic. This motivation emanates from the fact that NG-PON2 system coexists with legacy PON systems and combines the features of logical PtP WDM and TWDM.

As promising as the NG-PON2 system is, it is characterized with delays emanating from heavy dependant on DBA. Consequently, the quest to improve overall capacity offer by PON system while offering higher data rate and realistic reduction in delay is triggering evolution of PON architecture and functionality. The dynamic nature of unceasingly increasing characteristics of 5G and beyond services requires proactive design of a reliable transport solution that evolves with the mobile network generation. In line with this, higher speed PON (HSP) series are proposed to include a single wavelength 50 Gbps TDM-PON, an x50G TWDM-PON, and PtP WDM overlay by ITU-T working group [103].

## 3.5 Ethernet Based Mobile Fronthaul

Considering these conspicuous challenges of the Ethernet, its adoption as mobile fronthaul has attracted tremendous research studies. The IEEE Standard Association 1914 working group through the IEEE 1914.3 task force is investigating ways of transferring IQ user-plane data, vendor-specific data, and control and management (CM) information channels over an Ethernet-based packet-switched network. time-sensitive network (TSN) Ethernet techniques are also being considered for carrying fronthaul data [104]. An attempt is made in [105] to improve the performance of Ethernet-based fronthaul regarding delay and jitter by employing Frame Preemption and Scheduled Traffic mechanism to reduce jitter. The study also observed that a time-based encapsulation of CPRI into Ethernet frames produces constant encapsulation delay and avoid jitter. Ref [106] presented an overview of merits and demerits of fronthaul re-configurability together with the benefits and drawbacks of an Ethernet-based fronthaul. An estimation of delay overhead corresponding distances supported

by Ethernet-based fronthaul was obtained through an FPGA-based Verilog simulation on Ethernet encapsulation of CPRI data. Dynamic fronthaul reconfiguration can also be achieved by the encapsulation of CPRI on Ethernet frames. [107] proposed an NS3 based Zero-jitter which combines SDN technology with the new IEEE time sensitive networking to minimize jitter in the fronthaul network at the cost of extra delay.

### **3.6 Time-Sensitive Network (TSN)**

With the trend turning towards implementation of diverse functional split Options to realize the flexible fronthaul network, splitting of RAN functions across PHY layers could yield two extremes points: High-end transport profile which will involve antenna/RF and some parts of Layer 1 processing at the cell premises while others are handled at the centralized Unit; and Lower-end transport/fronthaul profile in which case all Layer 1-3 including antenna/RF processing are carried out on the cell premises. All these processes are deterministic and as such require deterministic mechanism. On the contrary, Ethernet is fundamentally probabilistic. Therefore, present Ethernet technology needs enhancement to be able to carry I/Q sample signals. One key solution is adopting TSN. TSN is defined to provide deterministic communication on standard Ethernet. It is a layer 2 technology that is centrally managed with support for guarantees of delivery and reduced jitter using time scheduling for those real-time signaling like I/O data streams. In addition, TSN allows successful convergence of critical control, non-critical control, and data streams on a single network.

Enormous works are ongoing in providing enhancement to Ethernet technologies for fronthaul implementations. With the active involvement of the IEEE work group and the specific task force, some of the standards have been published, some undergoing amendments and reviews. Some of these TSN standards are listed in 3.2. Likewise, while these efforts are going on, researches are simultaneously going to validate and investigate these technologies based on Next Generation Fronthaul Interface (NGFI) requirements. [105] demonstrated CPRI over ethernet (CoE) using preemption mechanism to satisfy the delay requirements based on few scenarios tests. To minimize the influence from lower-priority traffic and thus improving the cumulative high-priority queuing delay within a limited-capacity network, packet preemption discipline is predominantly employed [108]. Evaluating packet preemption in [108], the authors reported that the waiting time for higher-priority packets does not depend on the density of low-priority packets. The suitability of CoE to meet delay and jitter requirements is reported in [104] by using FPGA-based Verilog experiments and simulations, which employs a proposed comb-fitting (C-FIT) algorithm that schedules flows in Ethernet to reduce jitter. According to the author, using appropriate scheduling could significantly reduce the jitter effect of the Ethernet fronthaul.

For future RAN deployments, it is envisaged that there might be transmission and processing instabilities since functionalities will be distributed in generic platforms with virtualization techniques. This can lead to frame bursting in the fronthaul and hence resulting in contention-induced delays and delay variation [108], [109]. Consequently, time-aware shaper design is presented in [107], [109] to address this issue and the authors

### 3.6. Time-Sensitive Network

**Table 3.2:** Summary of IEEE standards for Ethernet Fronthauls

Standard	Title	Brief Description	Status
802.1Qbu	Bridges and Bridged Networks - Amendment 26: Frame Pre-emption.	Allows a Bridge Port to hold the transmission of non-time critical frames while any available time-critical frames are transmitted.	project authorization request (PAR) approved 15th May 2012. Standard approved Dec 5th, 2015. Published Mar 18th, 2016.
802.1Qbv	Bridges and Bridged Networks - Amendment 25: Enhancements for Scheduled Traffic.	Defines time aware queue draining to schedule the transmission of frames according to a known time scale	Published, 2015.
802.1Qca	Bridges and Bridged Networks - Amendment 24: Path Control and Reservation.	Provides explicit trees for data traffic by extending the application of Intermediate System to Intermediate System (IS-IS) to bridged networks.	Published, 2015.
802.1AS-Rev	Timing and Synchronization	Enables timing and synchronization for Time-Sensitive for most strict requirement of some applications, allowing Synchronization to an externally provided timing signal e.g. UTC	PAR approved Feb 16, 2015
802.1CB	Frame Replication and Elimination for Reliability	Identification and replication of frames, for redundant transmission, while also allowing Identification and Elimination of duplicate frames.	PAR approved Jun 2013
802.1Qcc	stream reservation protocol (SRP) Enhancements and Performance Improvements	Support for more streams, Configurable stream reservation classes and streams, Layer 3 streaming, and allows deterministic stream reservation convergence, UNI (User Network Interface)	PAR approved Oct 21, 2013
802.1Qch	Cyclic Queuing and Forwarding	provides algorithm that allows deterministic delays through a bridged network to be easily calculated regardless of network topology	PAR approved Feb 16, 2015. Standard approved May 18th, 2017
802.1Qci	Per-Stream Filtering and Policing	for frame counting, filtering, policing, and service class selection for a frame based on the data stream class and synchronized cyclic time schedule.	PAR approved Jun 11, 2015. Standard approved Feb 14th, 2017.
802.1Qcj	Automatic Attachment to Provider Backbone Bridging (PBB) services	auto-attachment of network devices to Provider Backbone service instances by using Type, Length, Value (TLVs) within the Link Layer Discovery Protocol (LLDP). Also simplifies deployment and administration of PBB networks.	PAR approved Jun 11, 2015.
802.1CM	TSN for Fronthaul	enables the transport of time sensitive fronthaul streams in Ethernet bridged networks	PAR approved 3 Sep 2015. Editor's draft.
802.1Qcp	YANG Data Model	specifies a Unified Modelling Language (UML) and a YANG data model for bridges and bridge components	PAR approved Sep 3, 2015.
802.1Qcr	Asynchronous Traffic Shaping	defines asynchronous traffic shaping over full-duplex links with constant bit data rates and specifies mechanisms that do not require synchronous communication.	PAR approved Jun 30, 2016.

demonstrated how different traffic flows affects the fronthaul-induced processing delays.

## 3.7 Summary

The transport network segment of the radio access network plays an important role in providing the mobile data traffic required to support the various 5G and beyond services. In this chapter, we have studied the optical communication based transport techniques for achieving high data rates transmission and enabling high capacity, especially for realizing enhanced mobile broadband communications. The basic concept of a radio-over-fiber (RoF) system, including the categories of RoF schemes, is discussed with respect to the 5G NR architecture. In addition, FSO and PON-based mobile transport solutions were also discussed, highlighting their strengths and challenges. Moreover, as networks with multiple radio access technologies are prevalent for 5G and beyond, hybrid transport networks were discussed in detail.

## References

- [1] A. Lometti and V. Sestito, “Fronthaul in 5G Transport Networks: IEEE1914.1 Architecture and Requirements,” in *2020 22nd International Conference on Transparent Optical Networks (ICTON)*, 2020, pp. 1–4.
- [2] G. Liu, Y. Huang, F. Wang, J. Liu, and Q. Wang, “5G features from operation perspective and fundamental performance validation by field trial,” *China Communications*, vol. 15, no. 11, pp. 33–50, Nov 2018.
- [3] M. Asad, A. Basit, S. Qaisar, and M. Ali, “Beyond 5g: Hybrid end-to-end quality of service provisioning in heterogeneous iot networks,” *IEEE Access*, vol. 8, pp. 192 320–192 338, 2020.
- [4] F. J. Effenberger, “Mobile backhaul and fronthaul systems,” in *2016 21st OptoElectronics and Communications Conference (OECC) held jointly with 2016 International Conference on Photonics in Switching (PS)*, 2016, pp. 1–3.
- [5] K. M. S. Huq and J. Rodriguez, *Backhauling 5G Small Cells with Massive-MIMO-Enabled mmWave Communication*, 2016, pp. 29–53.
- [6] G. Thirunavukkarasu and G. Murugesan, “A comprehensive survey on air-interfaces for 5g and beyond,” in *2019 10th International Conference on Computing, Communication and Networking Technologies (ICCCNT)*, 2019, pp. 1–7.
- [7] T. Poornima, K. Dhinesh, and R. Sudhakar, “Waveform candidates for 5g mobile communications,” in *2017 2nd IEEE International Conference on Recent Trends in Electronics, Information Communication Technology (RTEICT)*, 2017, pp. 856–860.
- [8] J. Vihriälä *et al.*, “Numerology and frame structure for 5g radio access,” in *2016 IEEE 27th Annual International Symposium on Personal, Indoor, and Mobile Radio Communications (PIMRC)*, 2016, pp. 1–5.

- [9] V. Tikhvinskiy, E. Deviatkin, A. Aitmagambetov, and A. Kulakaeva, "Provision of iot services for co-located 4g/5g networks utilisation with dynamic frequency sharing," in *2020 International Conference on Engineering Management of Communication and Technology (EMCTECH)*, 2020, pp. 1–4.
- [10] I. Parvez, A. Rahmati, I. Guvenc, A. I. Sarwat, and H. Dai, "A survey on low latency towards 5g: Ran, core network and caching solutions," *IEEE Communications Surveys Tutorials*, vol. 20, no. 4, pp. 3098–3130, 2018.
- [11] G. J. Sutton *et al.*, "Enabling technologies for ultra-reliable and low latency communications: From phy and mac layer perspectives," *IEEE Communications Surveys Tutorials*, vol. 21, no. 3, pp. 2488–2524, 2019.
- [12] A. Ghosh, A. Maeder, M. Baker, and D. Chandramouli, "5G Evolution: A View on 5G Cellular Technology Beyond 3GPP Release 15," *IEEE Access*, vol. PP, pp. 1–1, 09 2019.
- [13] V. Ziegler *et al.*, "Stratification of 5g evolution and beyond 5g," in *2019 IEEE 2nd 5G World Forum (5GWF)*, 2019, pp. 329–334.
- [14] R. G. Stephen and R. Zhang, "Joint Millimeter-Wave Fronthaul and OFDMA Resource Allocation in Ultra-Dense CRAN," *IEEE Transactions on Communications*, vol. 65, no. 3, pp. 1411–1423, March 2017.
- [15] Y. Huo, X. Dong, W. Xu, and M. Yuen, "Cellular and WiFi Co-design for 5G User Equipment," in *2018 IEEE 5G World Forum (5GWF)*, 2018, pp. 256–261.
- [16] M. Xiao *et al.*, "Millimeter wave communications for future mobile networks," *IEEE Journal on Selected Areas in Communications*, vol. 35, no. 9, pp. 1909–1935, 2017.
- [17] T. S. Rappaport *et al.*, "Wireless communications and applications above 100 ghz: Opportunities and challenges for 6g and beyond," *IEEE Access*, vol. 7, pp. 78 729–78 757, 2019.
- [18] D. Solomitckii, A. Orsino, S. Andreev, Y. Koucheryavy, and M. Valkama, "Characterization of mmwave channel properties at 28 and 60 ghz in factory automation deployments," in *2018 IEEE Wireless Communications and Networking Conference (WCNC)*, 2018, pp. 1–6.
- [19] Y. Zhang *et al.*, "Propagation Modeling Through Foliage in a Coniferous Forest at 28 GHz," 2018.
- [20] H. M. Rahim, C. Y. Leow, and T. A. Rahman, "Millimeter wave propagation through foliage: Comparison of models," in *2015 IEEE 12th Malaysia International Conference on Communications (MICC)*, 2015, pp. 236–240.
- [21] S. A. Busari, K. M. S. Huq, S. Mumtaz, and J. Rodriguez, "Terahertz massive mimo for beyond-5g wireless communication," in *ICC 2019 - 2019 IEEE International Conference on Communications (ICC)*, 2019, pp. 1–6.

- 
- [22] Tech. Spec. Group Radio Access Network Rel. 16, “Study on NR beyond 52.6 GHz,” vol. 0, no. Release 16, 2019.
- [23] O. Tervo *et al.*, “5g new radio evolution towards sub-thz communications,” in *2020 2nd 6G Wireless Summit (6G SUMMIT)*, 2020, pp. 1–6.
- [24] Small Cell Forum, “5G nFAPI Specifications,” no. September, 2020.
- [25] 3GPP TSG-RAN, “Integrated Access and Backhaul for NR,” Tech. Rep., 2019.
- [26] 3GPP TSGRAN, “Study on Integrated Access and Backhaul (Release 16),” vol. 0, no. Release 16, 2018.
- [27] 5G Americas, “Innovations in 5G Backhaul Technologies,” Tech. Rep., 2019.
- [28] R. E. Schuh, D. Wake, B. Verri, and M. Mateescu, “Hybrid Fibre Radio Access: A Network Operators Approach and Requirements,” Tech. Rep.
- [29] D. Novak *et al.*, “Radio-Over-Fiber Technologies for Emerging Wireless Systems,” *IEEE Journal of Quantum Electronics*, vol. 52, no. 1, pp. 1–11, 2016.
- [30] M. Noweir *et al.*, “Digitally linearized radio-over fiber transmitter architecture for cloud radio access network’s downlink,” *IEEE Transactions on Microwave Theory and Techniques*, vol. 66, no. 7, pp. 3564–3574, July 2018.
- [31] C. Lim, Y. Yang, and A. Nirmalathas, “Transport schemes for fiber-wireless technology: Transmission performance and energy efficiency,” *Photonics*, vol. 1, pp. 67–83, 06 2014.
- [32] V. Sharma, A. Singh, and A. K. Sharma, “Challenges to radio over fiber (rof) technology and its mitigation schemes – a review,” *Optik*, vol. 123, no. 4, pp. 338–342, 2012.
- [33] M. C. R. Medeiros *et al.*, “RoFnet – Reconfigurable Radio over Fiber Network Architecture Overview,” *Journal of Telecommunications and Information Technology*, vol. 2009, no. 1, 2009.
- [34] S. Kaur, M. Srivastava, and K. S. Bhatia, “Radio over Fiber Technology – A Review,” *International Conference of Technology, Management & Social Sciences (ICTMS-15)*, vol. 6913, no. December, pp. 85–89, 2015.
- [35] P. P. Monteiro *et al.*, “Mobile fronthaul RoF transceivers for C-RAN applications,” *International Conference on Transparent Optical Networks*, vol. 2015-Augus, pp. 1–4, 2015.
- [36] S. Rajpal and R. Goyal, “A Review on Radio-Over-Fiber Technology-Based Integrated (Optical/Wireless) Networks,” *Journal of Optical Communications*, vol. 38, no. 1, pp. 19–25, 2017.

- [37] D. Novak *et al.*, “Radio-Over-Fiber Technologies for Emerging Wireless Systems,” *IEEE Journal of Quantum Electronics*, vol. 52, no. 1, pp. 1–11, Jan 2016.
- [38] D. Wake, A. Nkansah, and N. J. Gomes, “Radio over fiber link design for next generation wireless systems,” *Journal of Lightwave Technology*, vol. 28, no. 16, pp. 2456–2464, 2010.
- [39] D. F. Paredes-Páliz, G. Royo, F. Aznar, C. Aldea, and S. Celma, “Radio over fiber: An alternative broadband network technology for iot,” *Electronics*, vol. 9, no. 11, 2020.
- [40] F. Ujang, T. Firmansyah, P. S. Priambodo, and G. Wibisono, “Irregular shifting of RF driving signal phase to overcome dispersion power fading,” *Photonics*, vol. 6, no. 4, 2019.
- [41] I. A. Alimi, A. L. Teixeira, and P. P. Monteiro, “Toward an Efficient C-RAN Optical Fronthaul for the Future Networks: A Tutorial on Technologies, Requirements, Challenges, and Solutions,” *IEEE Communications Surveys Tutorials*, vol. 20, no. 1, pp. 708–769, Firstquarter 2018.
- [42] S. Rommel *et al.*, “High-Capacity 5G Fronthaul Networks Based on Optical Space Division Multiplexing,” *IEEE Transactions on Broadcasting*, vol. 65, no. 2, pp. 434–443, June 2019.
- [43] A. Nirmalathas, P. A. Gamage, C. Lim, D. Novak, and R. Waterhouse, “Digitized radio-over-fiber technologies for converged optical wireless access network,” *Journal of Lightwave Technology*, vol. 28, no. 16, pp. 2366–2375, 2010.
- [44] Junghwa Bae and Jinwoo Park, “An efficient algorithm for bandpass sampling of multiple rf signals,” *IEEE Signal Processing Letters*, vol. 13, no. 4, pp. 193–196, 2006.
- [45] S. I., *Understanding Digital Signal Processing (2nd Edition)*. USA: Prentice Hall PTR, 2004.
- [46] Xiaoxiong Song *et al.*, “Integrating baseband-over-fiber and six-port direct modulation for high-speed high-frequency wireless communications,” in *2016 IEEE MTT-S International Microwave Symposium (IMS)*, 2016, pp. 1–4.
- [47] Z. Ghassemlooy, S. Zvanovec, M.-A. Khalighi, W. O. Popoola, and J. Perez, “Optical wireless communication systems,” *Optik*, vol. 151, pp. 1–6, dec 2017.
- [48] A. Mansour, R. Mesleh, and M. Abaza, “New challenges in wireless and free space optical communications,” *Optics and Lasers in Engineering*, vol. 89, pp. 95 – 108, 2017, 3DIM-DS 2015: Optical Image Processing in the context of 3D Imaging, Metrology, and Data Security.

- 
- [49] H. Kaushal and G. Kaddoum, "Optical Communication in Space: Challenges and Mitigation Techniques," *IEEE Communications Surveys Tutorials*, vol. 19, no. 1, pp. 57–96, Firstquarter 2017.
- [50] K. Anbarasi, C. Hemanth, and R. G. Sangeetha, "A review on channel models in free space optical communication systems," *Optics & Laser Technology*, vol. 97, pp. 161–171, dec 2017.
- [51] A. Jahid, M. H. Alsharif, and T. J. Hall, "A contemporary survey on free space optical communication: Potential, technical challenges, recent advances and research direction," *CoRR*, vol. abs/2012.00155, 2020.
- [52] I. K. Son and S. Mao, "A survey of free space optical networks," *Digital Communications and Networks*, vol. 3, no. 2, pp. 67–77, may 2017.
- [53] I. Alimi *et al.*, "Challenges and Opportunities of Optical Wireless Communication Technologies," in *Optical Communication Technology*. InTech, aug 2017.
- [54] M. Toyoshima, "Trends in satellite communications and the role of optical free-space communications  
*invited*  
," *J. Opt. Netw.*, vol. 4, no. 6, pp. 300–311, Jun 2005.
- [55] I. Alimi *et al.*, "Channel characterization and empirical model for ergodic capacity of free-space optical communication link," *Optics Communications*, vol. 390, pp. 123–129, 2017.
- [56] S. A. Al-Gailani *et al.*, "A survey of free space optics (fso) communication systems, links, and networks," *IEEE Access*, vol. 9, pp. 7353–7373, 2021.
- [57] Z. Ghassemlooy, S. Arnon, M. Uysal, Z. Xu, and J. Cheng, "Emerging optical wireless communications—advances and challenges," *IEEE Journal on Selected Areas in Communications*, vol. 33, no. 9, pp. 1738–1749, 2015.
- [58] A. Hamza, J. Deogun, and D. Alexander, "Classification framework for free space optical communication links and systems," *IEEE Communications Surveys & Tutorials*, vol. PP, pp. 1–1, 10 2018.
- [59] J. Mikolajczyk *et al.*, "Analysis of free-space optics development," *Metrology and Measurement Systems*, vol. 24, 12 2017.
- [60] J. Singh and N. Kumar, "Performance analysis of different modulation format on free space optical communication system," *Optik*, vol. 124, no. 20, pp. 4651–4654, 2013.
- [61] T. Rakia, H.-C. Yang, M.-S. Alouini, and F. Gebali, "Outage analysis of practical fso/rf hybrid system with adaptive combining," *IEEE Communications Letters*, vol. 19, no. 8, pp. 1366–1369, 2015.



- [62] H. Saidi, K. Tourki, and N. Hamdi, "Performance analysis of psk modulation in df dual-hop hybrid rf/fso system over gamma gamma channel," in *2016 International Symposium on Signal, Image, Video and Communications (ISIVC)*, 2016, pp. 213–216.
- [63] S. Sharma, A. S. Madhukumar, and R. Swaminathan, "Switching-based cooperative decode-and-forward relaying for hybrid fso/rf networks," *IEEE/OSA Journal of Optical Communications and Networking*, vol. 11, no. 6, pp. 267–281, 2019.
- [64] V. Jamali, D. S. Michalopoulos, M. Uysal, and R. Schober, "Link allocation for multiuser systems with hybrid rf/fso backhaul: Delay-limited and delay-tolerant designs," *IEEE Transactions on Wireless Communications*, vol. 15, no. 5, pp. 3281–3295, 2016.
- [65] M. Z. Hassan, M. J. Hossain, J. Cheng, and V. C. M. Leung, "Hybrid rf/fso backhaul networks with statistical-qos-aware buffer-aided relaying," *IEEE Transactions on Wireless Communications*, vol. 19, no. 3, pp. 1464–1483, 2020.
- [66] Y. F. Al-Eryani, A. M. Salhab, S. A. Zummo, and M.-S. Alouini, "Protocol design and performance analysis of multiuser mixed rf and hybrid fso/rf relaying with buffers," *IEEE/OSA Journal of Optical Communications and Networking*, vol. 10, no. 4, pp. 309–321, 2018.
- [67] Z. Jiang *et al.*, "An experimental hybrid rf/fso system using optical heterodyne method," in *2018 10th International Conference on Advanced Infocomm Technology (ICAIT)*, 2018, pp. 83–87.
- [68] M. Najafi, V. Jamali, D. W. K. Ng, and R. Schober, "C-ran with hybrid rf/fso fronthaul links: Joint optimization of fronthaul compression and rf time allocation," *IEEE Transactions on Communications*, vol. 67, no. 12, pp. 8678–8695, 2019.
- [69] S. Bayati, M. Darabi, A. Mostafa, and L. Lampe, "Resource allocation in c-ran with hybrid rf/fso and full-duplex self-backhauling radio units," in *ICC 2021 - IEEE International Conference on Communications*, 2021, pp. 1–7.
- [70] C. Abou-Rjeily, "Performance analysis of fso communications with diversity methods: Add more relays or more apertures?" *IEEE Journal on Selected Areas in Communications*, vol. 33, no. 9, pp. 1890–1902, 2015.
- [71] A. Al-Hourani, S. Kandeepan, and E. Hossain, "Relay-assisted device-to-device communication: A stochastic analysis of energy saving," *IEEE Transactions on Mobile Computing*, vol. 15, no. 12, pp. 3129–3141, 2016.
- [72] B. Bag *et al.*, "Performance Analysis of Hybrid FSO Systems Using FSO/RF-FSO Link Adaptation," *IEEE Photonics Journal*, vol. 10, no. 3, pp. 1–17, June 2018.
- [73] B. Asharafzadeh, E. Soleimani-Nasab, and M. Kamandar, "Outage analysis of mixed rf/fso cooperative systems with multiple antennas and apertures," in *2016 24th Telecommunications Forum (TELFOR)*, 2016, pp. 1–4.

- 
- [74] J. Zhang, L. Dai, Y. Zhang, and Z. Wang, “Unified performance analysis of mixed radio frequency/free-space optical dual-hop transmission systems,” *Journal of Lightwave Technology*, vol. 33, no. 11, pp. 2286–2293, 2015.
- [75] X. Pan, H. Ran, G. Pan, Y. Xie, and J. Zhang, “On secrecy analysis of df based dual hop mixed rf-fso systems,” *IEEE Access*, vol. 7, pp. 66 725–66 730, 2019.
- [76] R. Koma, J. I. Kani, K. Asaka, and K. I. Suzuki, “Standardization trends for future high-speed passive optical networks,” *NTT Technical Review*, vol. 15, no. 10, 2017.
- [77] I. A. Alimi *et al.*, “Enabling optical wired and wireless technologies for 5g and beyond networks,” in *Telecommunication Systems*, I. A. Alimi, P. P. Monteiro, and A. L. Teixeira, Eds. Rijeka: IntechOpen, 2019, ch. 8.
- [78] M. Kumari, R. Sharma, and A. Sheetal, “Passive Optical Network Evolution to Next Generation Passive Optical Network: A Review,” in *2018 6th Edition of International Conference on Wireless Networks Embedded Systems (WECON)*, 2018, pp. 102–107.
- [79] ITU-T, “5G wireless fronthaul requirements in a passive optical network context,” in *SERIES G: TRANSMISSION SYSTEMS AND MEDIA, DIGITAL SYSTEMS AND NETWORKS*, 2018.
- [80] M. Jaber, M. A. Imran, R. Tafazolli, and A. Tukmanov, “5G Backhaul Challenges and Emerging Research Directions: A Survey,” *IEEE Access*, vol. 4, pp. 1743–1766, 2016.
- [81] Galvan *et al.*, “5G Backhaul: Requirements, Challenges, and Emerging Technologies,” in *Intech*, 2016, vol. i, no. tourism, ch. 4, p. 13.
- [82] C. Browning *et al.*, “5G wireless and wired convergence in a passive optical network using UF-OFDM and GFDM,” in *2017 IEEE International Conference on Communications Workshops (ICC Workshops)*, 2017, pp. 386–392.
- [83] 3GPP, “Revised Work Item Description: Integrated access and backhaul for NR,” *document RP-190712, Shenzhen, China*, Mar. 2019.
- [84] J. Terada, “Optical Access Technologies for 5G and Beyond,” in *2019 24th OptoElectronics and Communications Conference (OECC) and 2019 International Conference on Photonics in Switching and Computing (PSC)*, 2019, pp. 1–3.
- [85] G. Otero Pérez, D. Larrabeiti López, and J. A. Hernández, “5G New Radio Fronthaul Network Design for eCPRI-IEEE 802.1CM and Extreme Latency Percentiles,” *IEEE Access*, vol. 7, pp. 82 218–82 230, 2019.
- [86] N. Cheng, L. Zhou, X. Liu, and F. J. Effenberger, “Reflective Crosstalk Cancellation in Self-Seeded WDM PON for Mobile Fronthaul/Backhaul,” *Journal of Lightwave Technology*, vol. 34, no. 8, pp. 2056–2063, 2016.
-

- [87] K. Kim *et al.*, “High Speed and Low Latency Passive Optical Network for 5G Wireless Systems,” *Journal of Lightwave Technology*, vol. 37, no. 12, pp. 2873–2882, 2019.
- [88] S. Hatta, N. Tanaka, and T. Sakamoto, “Feasibility demonstration of low latency DBA method with high bandwidth-efficiency for TDM-PON,” in *2017 Optical Fiber Communications Conference and Exhibition (OFC)*, 2017, pp. 1–3.
- [89] A. M. Mikaeil, W. Hu, and S. B. Hussain, “A Low-Latency Traffic Estimation Based TDM-PON Mobile Front-Haul for Small Cell Cloud-RAN Employing Feed-Forward Artificial Neural Network,” in *2018 20th International Conference on Transparent Optical Networks (ICTON)*, 2018, pp. 1–4.
- [90] R. Bera, S. Bera, S. Shome, and S. N. Sur, “5G NR Test Bed Integrated with Pathways and Gateways for Access to the Cloud Towards Smart City Communication Applications,” in *2019 URSI Asia-Pacific Radio Science Conference (AP-RASC)*, 2019, pp. 1–4.
- [91] K. O. Kim, K. H. Doo, and H. S. Chung, “Low Latency DBA Scheme for 5G Mobile Service in Multilane-Based 50G-EPON,” in *2019 Asia Communications and Photonics Conference (ACP)*, 2019, pp. 1–3.
- [92] A. Zaouga, A. de Sousa, M. Najja, and P. Monteiro, “Low Latency Dynamic Bandwidth Allocation Algorithms for NG-PON2 to Support 5G Fronthaul and Data Services,” in *2019 21st International Conference on Transparent Optical Networks (ICTON)*, 2019, pp. 1–4.
- [93] D. Eugui and J. A. Hernández, “Low-Latency Transmission of Fronthaul Traffic Over XG(S)-PON with Fixed-Elastic Bandwidth Reservations,” in *2019 Optical Fiber Communications Conference and Exhibition (OFC)*, 2019, pp. 1–3.
- [94] E. Harstead, D. van Veen, V. Houtsma, and P. Dom, “Technology Roadmap for Time-Division Multiplexed Passive Optical Networks (TDM PONs),” *Journal of Lightwave Technology*, vol. 37, no. 2, pp. 657–664, 2019.
- [95] H. S. Chung, “Low Latency PON and RoF for 5G Wireless Systems,” in *2018 IEEE Photonics Conference (IPC)*, 2018, pp. 1–2.
- [96] D. Larrabeiti, M. Umar, R. Sanchez, and J. A. Hernandez, “Heuristics for PON-based 5G backhaul design,” in *2014 16th International Conference on Transparent Optical Networks (ICTON)*, 2014, pp. 1–2.
- [97] Y. Liu and L. Guo, “Planning of Resilient OFDM-PON in Support of 5G Backhaul,” in *2018 20th International Conference on Transparent Optical Networks (ICTON)*, 2018, pp. 1–4.
- [98] J. Li and J. Chen, “Passive optical network based mobile backhaul enabling ultra-low latency for communications among base stations,” *IEEE/OSA Journal of Optical Communications and Networking*, vol. 9, no. 10, pp. 855–863, 2017.

- 
- [99] M. Kumari, R. Sharma, and A. Sheetal, "Passive Optical Network Evolution to Next Generation Passive Optical Network: A Review," in *2018 6th Edition of International Conference on Wireless Networks Embedded Systems (WECON)*, 2018, pp. 102–107.
- [100] M. Ghanbarisabagh and E. Giacomidis, "A Survey on High-Capacity OFDM-based Passive Optical Networks A Survey on High-Capacity OFDM-based Passive Optical Networks," no. July, pp. 1–27, 2018.
- [101] ITU-T, "Supplement 66 SERIES G: TRANSMISSION SYSTEMS AND MEDIA, DIGITAL SYSTEMS AND NETWORKS 5G wireless fronthaul requirements in a passive optical network context," vol. 66, 2019.
- [102] X. Liu *et al.*, "Enabling Technologies for 5G-Oriented Optical Networks," in *2019 Optical Fiber Communications Conference and Exhibition (OFC)*, 2019, pp. 1–3.
- [103] S. Garg, M. Aggarwal, and A. Dixit, "Power, Cost and Reach Based Evaluation of Next Generation Passive Optical Networks Architectures," in *2018 IEEE International Conference on Advanced Networks and Telecommunications Systems (ANTS)*, 2018, pp. 1–6.
- [104] D. Chitimalla, K. Kondepu, L. Valcarengi, M. Tornatore, and B. Mukherjee, "5G Fronthaul–Latency and Jitter Studies of CPRI Over Ethernet," *Journal of Optical Communications and Networking*, vol. 9, no. 2, p. 172, 2017.
- [105] T. Wan and P. Ashwood, "A Performance Study of CPRI over Ethernet with IEEE 802.1Qbu and 802.1Qbv Enhancements," pp. 1–12, 2015.
- [106] D. Chitimalla, "Joint resource allocation for combined fronthaul / midhaul / backhaul using Ethernet Motivation for using shared resources in fronthaul / midhaul / backhaul," pp. 1–14, 2016.
- [107] T. Wan, B. McCormick, Y. Wang, and P. Ashwood-Smith, "ZeroJitter: An SDN based scheduling for CPRI over Ethernet," *2016 IEEE Global Communications Conference, GLOBECOM 2016 - Proceedings*, 2016.
- [108] Z. Zifan Zhou, Ying Yan, S. Ruepp, and M. Berger, "Analysis and implementation of packet preemption for Time Sensitive Networks," *2017 IEEE 18th International Conference on High Performance Switching and Routing (HPSR)*, vol. 2017-June, pp. 1–6, 2017.
- [109] P. Assimakopoulos, G. S. Birring, M. K. Al-hares, and N. J. Gomes, "Ethernet-Based Fronthauling for Cloud-Radio Access Networks," pp. 2–5, 2017.

## Chapter 4

# Open-Source enabled Real-time RAN with a PON Based Fronthaul

**R**obust transport solutions are critical to delivering mobile data traffic required for the various use cases of 5G and beyond. To achieve improved network capacity, especially required for enhanced mobile broadband (eMMB) communications, the deployment of optical access technologies is being closely studied by the research community to provide connectivity at low-cost derived from the reuse of existing infrastructure for passive optical networks (PON) [1]. Moreover, the densification of wireless networks, which include numerous small cells in addition to macrocells, is essential for eMMB communication. Therefore, this heterogeneous architecture scenario requires effective backhaul and fronthaul (x-haul) transport to provide the desired connectivity.

Due to the above advantages, preponderance of research works focus on the theoretical modeling of the PON-based transport system for RAN [1–7], while few enunciate experimental demonstration of the PON integrated RAN for performance evaluation of the PON-based fronthaul in a real-time scenario. Obviously, due to the complexity, researchers have difficulty using a real cellular infrastructure to test and validate the transport technology. Therefore, we take advantage of an open-source platform and a software-defined radio utility to develop a testbed based on a modified C-RAN architecture to validate a PON-based fronthaul. We reported this research work in our paper [8].

Therefore, this chapter presents the development of prototype mobile network testbeds to facilitate the study of real-time mobile traffic over a transport system. In the context, this chapter include:

- a review of softwarization and virtualization techniques as key enablers for realizing cloud radio access networks. In addition, OAI software implementation is mentioned.
- a presentation of an open-source software platform and software-defined radio (SDR) to develop a C-RAN testbed that can be easily configured with a flexible mobile fronthaul based on functional split options.

- a demonstration of real-time radio over a passive optical network (PON) based fronthaul transmission.

In addition, this chapter presents our contributions to the realization of testbeds for the ORCIP (Optical Radio Convergence Infrastructure for Communications and Power Delivering) project and for the Mobilizador 5G project, in particular the PPS1 (Products and Services for Network Edge) component. Finally, the main conclusions of this chapter are presented in section 4.8.

## 4.1 An overview of the ORCIP Project

The ORCIP project is an open infrastructure targeted at providing enabling research facilities to the scientific community and industry for testing, measuring and certifying advanced optical and radio systems. Also, in an attempt to ease the complexities involve in system characterization of present and even upcoming optical-radio access systems making field trials cumbersome and extremely expensive, ORCIP offers hybrid fiber-radio research infrastructures with embedded simulators and physical testbeds to facilitate research collaboration between the industries and Universities [9]

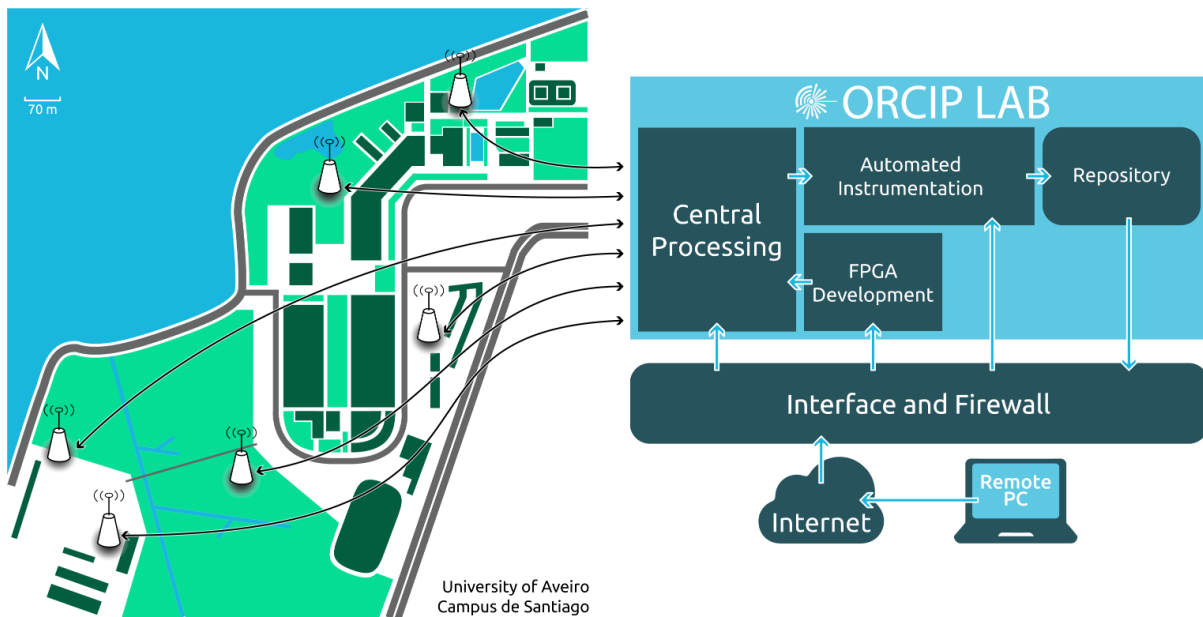


Figure 4.1: Schematic representation of ORCIP research infrastructure [10].

### ORCIP Testbed Architecture

The architecture consists of indoor (in-lab) and outdoor (in-campus) deployments, as shown in Figure 4.1, while serving as a hybrid platform to emulate the 5G standardization and open multi-tenancy scenario. The hybrid in-campus/in-lab allows testing of different state-of-the-art transmission technologies and protocols while investigating the functional

separation between BBU and RRH. A complementary approach is the use of Field Programmable Gate Arrays (FPGA)-based testbed using in-house hardware development and custom design of MFH transport protocols and a universal software radio peripheral (USRP)-based testbed with commercial off-the-shelf USRPs that provide a lower-cost SDR with MIMO interface that can be adapted to the new generation fronthaul interface. The developed testbed interface can be used to study MFH transport networks and heterogeneous protocols based on fiber, wireless, optical wireless and hybrid fiber-wireless access solutions.

It is worth mentioning that for the in-campus project, outdoor antennas will be placed on the campus of the University of Aveiro and connected to the ORCIP LAB, a central laboratory located on the premises of the Instituto de Telecomunicações. Within the conceptual framework of the ORCIP project, we discuss the development of the SDR-based testbed and present some of its applications.

## 4.2 Softwarization and Virtualization of RAN

As the technology evolves towards 5G and possibly beyond, there is a growing interest in flexibility and rapid reconfiguration of mobile networks resulting from the openness and programmability of the individual network components. To achieve this, the concepts of virtualization and softwarization of mobile networks are of great importance. Therefore, in this section, the concepts of virtualization and softwarization are discussed with respect to RAN. In addition, some of the open-source software platforms and virtualization techniques to achieve the flexibility of mobile networks are presented.

The success of softwarization and virtualization in cloud and edge computing, including NFV, is driving the adoption of these technologies for 5G and B5G to achieve unprecedented flexibility while supporting various services resulting from the increasing densification of mobile networks and users. Basically, softwarization refers to the concept of running a particular functionality in a software platform rather than the usual hardware platform, while virtualization is a process of creating a virtual instance or software-based abstraction of actual hardware and a virtual hardware platform, storage devices, computer network resources, and operating systems. In addition, the move towards open-source and programable networks is bringing an improvement in operational efficiency and optimization of network configuration, which in turn contributes to a reduction in total cost of ownership [11].

The paradigms of softwarization are leading to revolutionary advances in the telecommunications industry, enabling greater flexibility, scalability and programmability, and also enhancing the security of mobile networks [12, 13]. The combined adoption of SDN and NFV in the softwarization of mobile networks with the support of virtualization calls for software defined mobile network (SDMN) to achieve cloud processing of network functionalities and services [14–18]. The SDN approach achieves the separation of control plane and data plane by using a well-defined application programming interface (API) between the data infrastructures and the software based SDN.

### 4.3 Virtualization Paradigm

Certainly the concept of virtualization has come into play as its application is widespread and increasingly relevant to, among other things, the development, deployment and operation of mobile networks, particularly 5G and the upcoming 6G. Virtualization already has its roots in networking as a precursor to cloud computing with the development of virtual local area networks (VLAN), virtual network interface card (NIC), virtual private networks (VPN), to name a few. As the mobile network is evolving towards softwarization, the adoption of virtualization not only helps to reduce capital expenditures (CAPEX) and operational expenditure (OPEX), but would also significantly promote the mobile network ecosystem.

Considering the involvement of multiple RAT to drive 5G and beyond networks, virtualization is therefore desirable to reduce critical functional and architectural complexity and thus bring elasticity and flexibility to mobile networks in a manner for realizing a flexible RAN. In addition, a fully virtualized and cloud-based RAN architecture is evolving with the ability to enable virtualized baseband units (vBBU), remote radio units (RRUs), and dynamic fronthaul. Virtual RAN (vRAN) is becoming increasingly important as virtualization tools enable better abstraction of hardware units.

In the context of networks, virtualization is used to arrive at the concept of network function virtualization (NFV) proposed by European Telecommunications Standards Institute (ETSI) in 2012 [19]. In addition, the use of NFV reduces the traditionally heavy reliance on single-purpose infrastructures by using hardware-integrated functions in software hosted on COTS systems to provide network services in virtual machines called Virtual Network Functions (VNFs). An NFV architecture consists of multiple VNFs, each of which is tasked with different operations. While each VNF consists of several sub-functions called VNF components (VNFCs), the monitoring of VNFs is done by element-management-systems (EMSs). Moreover, all the software and hardware needed for the deployment, functioning and monitoring of the VNFs are grouped together as the NFV infrastructure (NFVI), where the virtualization layer is located for the necessary abstraction of hardware resources [20]. As a typical example, the virtualization layer may contain servers with hypervisors or containers. The management and control of the interaction of VNFs with hardware resources is performed by the Virtualized Infrastructure Manager (VIM), the VNF lifecycle is managed by the VNF Manager (VNFM), and the NFV Orchestrator (NFVO) performs the task of realizing network services on NFVI [21]. Consequently, the three aforementioned components VIM, VNFM and NFVO are grouped together as NFV Management and Orchestration (MANO). Another component of the NFV framework is the Operations Support Systems and Business Support Systems (OSS/BSS) element, which acts as a legacy management system and assists MANO in implementing network policies.

#### Basic Virtualization Approaches

Hypervisor-based and container-based methods, as illustrated in Figure 4.2, are two prominent approaches to implementing virtualization, both of which have different tradeoffs [22]. In the hypervisor-based approach, the virtualization setup depends on the



software platform, often referred to as the hypervisor or virtual machine monitor (VMM). Depending on the type of hypervisor-based virtualization, the hypervisor can be deployed directly on a piece of hardware (*bare-metal*) called a host that runs the hypervisor, while the emulated hardware within a host is called a guest. After enabling the creation of virtual hardware or machines that have an emulated version of real hardware resources, the hypervisor facilitates the interaction between the virtual environment and real hardware by intercepting the virtual machine system calls. This type of hypervisor-based approach, which includes *bare-metal*, is often referred to as paravirtualization (PV) [23]. The second hypervisor-based approach, referred to as Type 2, is also called full virtualization, as shown in Figure 4.2a. In Type 2, the hypervisor runs on the OS of the host instead of the *bare-metal*. Hypervisor-based virtualization provides strong isolation, even though each virtual machine has logical separation between its peers, which contributes to the time overhead typically associated with this virtualization approach. Commonly used hypervisors are listed in Table 4.1.

On the other hand, container-based virtualization uses the kernel features of the host's operating system (OS) to create an isolated environment for multiple guest instances, called containers. A graphical description of container-based virtualization is shown in Figure 4.2b. The resulting isolation allows each container to have its own root file system, process, and network stack. Unlike hypervisor-based virtualization, containers use the host's hardware and do not require individual hardware emulation, which reduces application process complexity while supporting virtualization system scalability and agility [24, 25]. Moreover, unlike hypervisor-based virtualization, container-based virtualization appears to be more efficient, faster, and more powerful because hardware emulation is not required for each container individually [24–26]. Table 4.1 lists examples of commonly used container-based solutions. Considering the performance of container-based virtualization, it is often used for time-critical deployments, making it a promising candidate for mobile network virtualization [27–29]. For this reason, we use Docker, a container-based virtualization, for our experimental setup, which is described in Section 4.5

## 4.4 Software-Enabled RAN

The effectiveness of SDN and NFV to achieve the softwarization of mobile networks was mentioned in the previous section. Also, the service-based architecture (SBA) of 3GPP R15 promotes the adoption of SDN and NFV for 5G networks as it supports the modularization of network functions while realizing the agility and flexibility of network functions. Moreover, as complementary technologies, SDN and NFV lead to less dependence on traditional hardware components, thereby reducing the cost of deploying mobile networks [20]. Considering the ability of SDN/NFV approach to enhance the open source integration of mobile networks, significant research efforts are directed towards the use of these technologies to realize the softwarization of networks as an essential aspect in the advancement of 5G and B5G networks [39, 40].

Open source platforms that support the ecosystem are becoming increasingly popular among telecom operators and researchers for implementing software standards for mobile

**Table 4.1:** Summary of some virtualization solutions

Solution	Technology	Brief description
Hyper-V [30]	Type 2, Hypervisor-based	A virtualization tool that is embedded in Microsoft windows operating system.
KVM (Kernel-based Virtual Machine) [31]	Type 1, Hypervisor-based	It allows conversion of Linux into a type-1 (bare-metal) hypervisor.
QEMU [32]	Type 2, Hypervisor-based	An open source and generic for emulating hardware resource.
Virtual Box [33]	Type 2, Hypervisor-based	A platform independent and free virtualization utility developed by Oracle
VMware Workstation [34]	Type 2, Hypervisor-based	A commercially available proprietary virtualization solution from VMware.
Xen [35]	Type 1, Hypervisor-based	A freely available <i>bare-metal</i> virtualization solution developed by Xen Project.
Docker [36]	Container-based	A command line tool for creating and managing containers to perform operating-system-level virtualization. Though it requires commercial license, it allow registered users within its community to use it freely for small-scale virtualization.
LXC (Linux containers) [37]	Container-based	LXC are lightweight virtualization technology and aims at creating an environment (container) that is closer to a standard Linux installation without requiring a separate kernel.
Google Kubernetes Engine [38]	Container-based	An open-source system from Google for managing and scaling containers.

---

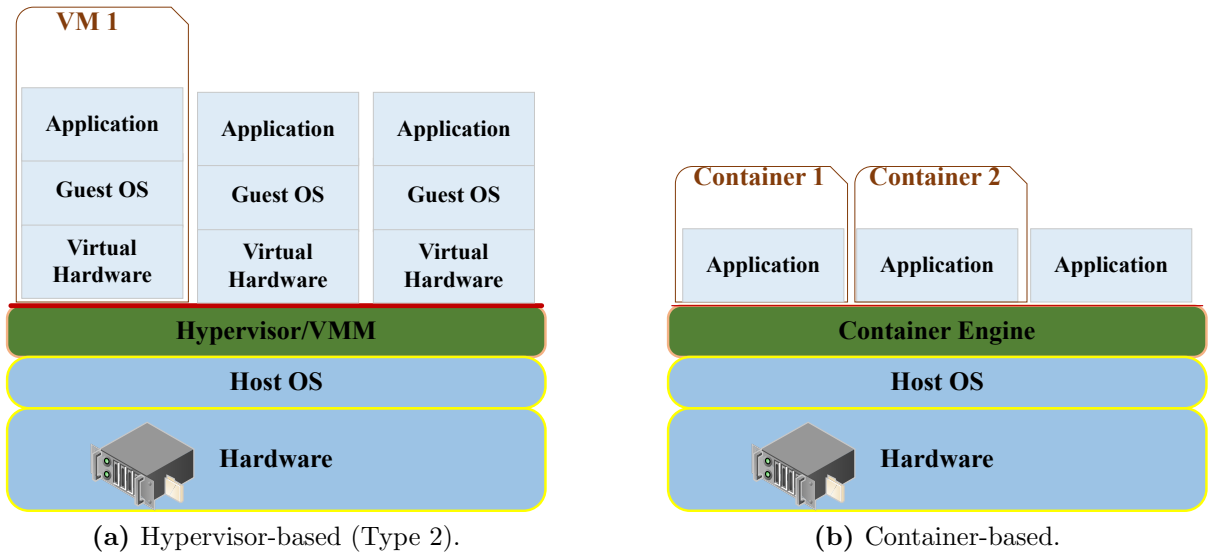


**Figure 4.2:** Virtualization approach (Adapted from [24, 25]).

networks. For example, the open source project [41] has evolved, and recently a collaboration between the O-RAN Alliance and Linux Foundation emerged as the O-RAN software community to develop software for the Radio Access Network [42]. Similar efforts are made by OpenAirInterface Software Alliance (OSA) [43] in applying open source to the 5G system architecture in accordance with the 3GPP Release 15 standard [44]. Although there are other counterpart open source software for RAN prototyping, including software radio system long term evolution (srsLTE), OpenLTE, NextEPC Open Source and LTE sidelink, only OAI and srsLTE are considered for real-time mobile network emulation in this work due to their robustness. Starting from 4G, OAI implements a complete communication stack shown in Figure 4.4 and consistent work has been done to update the software to implement the 5G stack [43].

The following sections describe the development of a laboratory prototype of a real-time cellular network based on an open-source software platform and corresponding hardware resources, and demonstrate the transmission of real-time RF over selected mobile transport solutions.

#### 4.4.1 srsLTE Implementation

srsLTE is another free and open-source project written in the American National Standards Institute (ANSI) C programming language to build a real 4G LTE mobile network using its library for the PHY layer of LTE Release 8. The library provides a set of tools to create a complete eNodeB, EPC, UE, and network performance analyser or LTE sniffer. srsLTE supports FDD configuration with transmission modes 1 and 2 for single antenna and transmit diversity, respectively. srsLTE works with channel bandwidths of 1.4, 3, 5, 10, and 20 MHz. The current library also supports UE synchronization procedure and cell search; DL channels/signals including synchronization signals (primary synchronization signal (PSS) and secondary synchronization signal (SSS)), physical

broadcast channel (PBCH), physical control format indicator channel (PCFICH), physical hybrid ARQ indicator channel (PHICH), physical downlink control channel (PDCCH) and physical downlink shared channel (PDSCH); total UL channels/signals consisting of PRACH, physical uplink shared channel (PUSCH), physical uplink control channel (PUCCH) and sounding reference signal (SRS); optimized turbo decoder. In addition, the srsLTE software uses single instruction multiple data (SIMD) operations in the code for performance enhancement.

Like OAI, srsLTE also has a set of recommended compatible hardware, including RF lab devices such as National Instruments/Ettus USRP and other SDR devices. However, using the same hardware, srsLTE provides a relatively stable solution for LTE implementation as OAI, especially when dealing with monolithic processing, according to the general experience of the user community. Similarly, the srsLTE suite runs on Linux on general purpose processor (GPP) machine to implement a fully functional mobile network based on commercial SDR devices. The suite includes srsUE, srsENB and srsEPC. The srsUE is an instantiation of the LTE UE, the srsENB runs the LTE eNodeB application, while the srsEPC implements mobile management entity (MME), home subscriber services (HSS), packet data network gateway (PGW) and serving gateway (SGW). Both the srsENB and the srsEPC are deployed on a single computer, as shown in Figure 4.3.

#### 4.4.2 SDR based srsUE

A full software implementation of LTE UE is enabled by srsUE as an application of a Linux-based operating system to connect not only to a srsLTE network, but to any other LTE network. The transmission of radio signals over the air is achieved using an SDR device such as the Ettus Research USRP. Like the OAI UE, srsUE handles layer 1, 2, and 3 functions as shown in Figure 4.4, supporting full LTE bandwidths, TDD and FDD configurations, manual configuration of DL/UL carrier frequencies.

To implement srsUE, a PC with Linux-based operating system and an SDR as RF front-end are required. The SDR used in our setup is an Ettus Research USRP B210 connected to the PC via USB to process the RF signal. The source code is downloaded from the srsLTE repository [45]. After successful installation of the srsUE application, administrator privileges are required to create high priority threads and a network tunnel (TUN) that simulates a network layer device for carrying IP packets when the UE is successfully connected to the network. Then, the UE is authenticated by the core network with the unique identity, which includes international mobile subscriber identity (IMSI), authentication key (K), operator code (OP), and phone number. The XOR [46] and Milenage [47] authentication algorithms are supported by srsLTE for both soft and hard UMTS subscriber identity module (USIM) authentication. However, hard USIM requires a physical SIM card that is programmed with user parameters via a smart card reader or programmer. In our experimental setup, both hard and soft USIM are used for the UE.

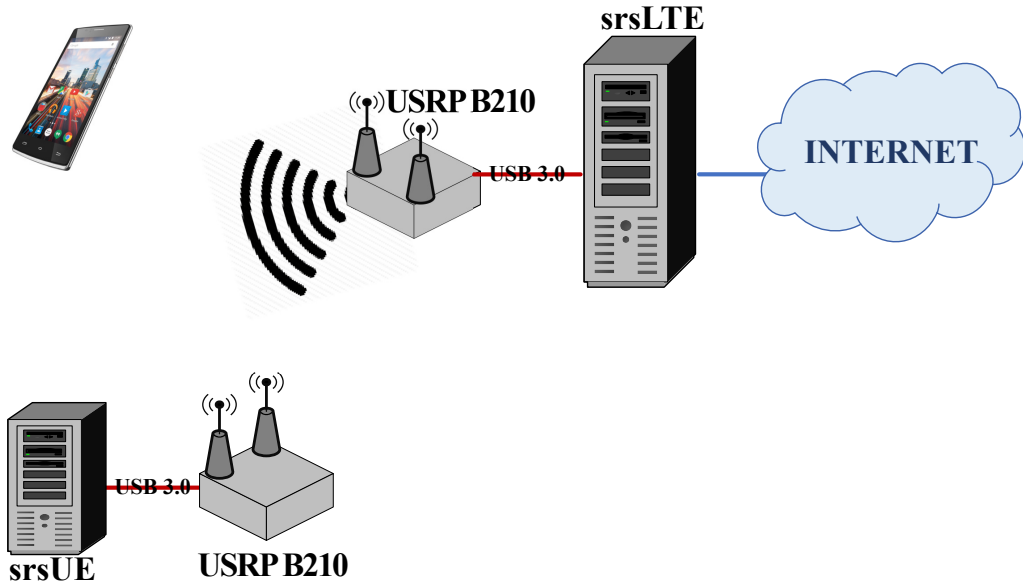


**Figure 4.3:** A Simple Representation of srsLTE Based Testbed exemplifying Monolithic Baseband processing

### 4.4.3 OpenAirInterface Enabled Network Realization

Although a variety of network simulation software exists and continues to evolve, its ability to fully capture real-world phenomena remains a challenge for now. Regardless, having a real-time replica of a real mobile network in the lab is essential for advancing research and education, and OpenAirInterface (OAI) is making strides to make this a reality. The combination of open software solutions and COTS equipment is increasingly making practical experiments with mobile networks are becoming increasingly available and less difficult to access for research purposes. Unlike in the past, the high cost of equipment and radio spectrum licensing requirements limited the extent to which practical experiments with real cellular networks could be conducted. With this in mind, in this section we use the OAI stack to build an E2E mobile network for real-world experiments, following the 3GPP specification. We start with the development of 4G LTE testbed and later implement 5G NR architecture testbed.

#### An OAI Based Testbed Development

OAI is open-source software written in the C language and made available to the public under Public License version 2 for providing real-time functionality with the implementation of the 3GPP protocol stack, which includes the RAN and the core network. However, the source code is regularly updated and evolved, starting with the support for LTE Release 8, then LTE-Advanced (Releases 10 to 12), LTE-Advanced-Pro (Releases 13 and 14) and currently developing the 5G (Release 15) functions. OAI is always structured along these two subsystems to develop a full-fledged E2E emulation with features of the real mobile networks. This section focuses on the 4G LTE development as a fundamental step towards prototyping 5G networks.

OAI is able to emulate and simulate the functionalities of RAN and core network. Meanwhile, the deployment of OAI software, especially OAI-RAN, depends on the available computing power of PC to run the OAI commands and USRP hardware driver (UHD) software of SDR. In other words, the deployment of OAI software requires adequate processing resources to support the extensive digital signal processing required for baseband processing and other layers of the protocol stack. Therefore, the need for supporting hardware depends on the network implementation to be achieved.

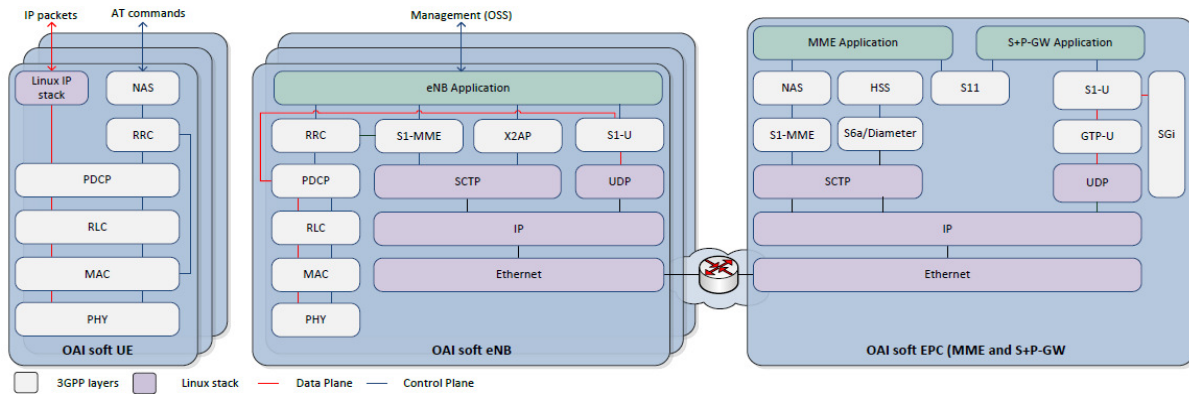


Figure 4.4: OAI Communication Stack [48].

The scheme shown in Figure 4.4 represents the full protocol stack of the 3GPP standard in both the evolved universal terrestrial access network (E-UTRAN) and the evolved packet core (EPC) and consists of OAI soft UE, OAI soft eNB and OAI soft EPC. The OAI platform, operating in a Linux environment, enables the processing of protocol layers including physical layer (PHY), media access control (MAC), radio link control (RLC), packet data convergence protocol (PDCP), radio resource control (RRC), and non-access stratum (NAS). In addition, the E-UTRAN protocol stack provides standard S1AP and GTP-U interfaces to Core Network, Internet Protocol (IP) version 4 and 6 support, a priority-based MAC scheduler with dynamic modulation and coding scheme (MCS) selection, integrity checking, and encryption; while the EPC features mobility management entity (MME), serving gateways (SGW), packet data network gateway (PGW) and home subscriber server (HSS) implementations, UE procedures handling (e.g., attachment, authentication, service access, and radio bearer setup), NAS integrity and encryption, direct access to the IP network, and IPv4 and v6 support [43].

The experimental setup shown in Figure 4.5a was implemented to realize an LTE network by deploying the OAI codes on general-purpose x86 computer hardware. In order to generate real-time mobile traffic and investigate the properties of an end-to-end cellular network, we start by implementing the basic setup shown in Figure 4.5a. Virtualization techniques are then used to practically demonstrate the possibility of cloud processing of mobile network-specific traffic in the lab, as shown in Figure 4.8, while optimally utilizing the computational power of the high-end system PC used. The application of the virtualization approach for the generation of mixed mobile data streams is demonstrated in Section 4.5.

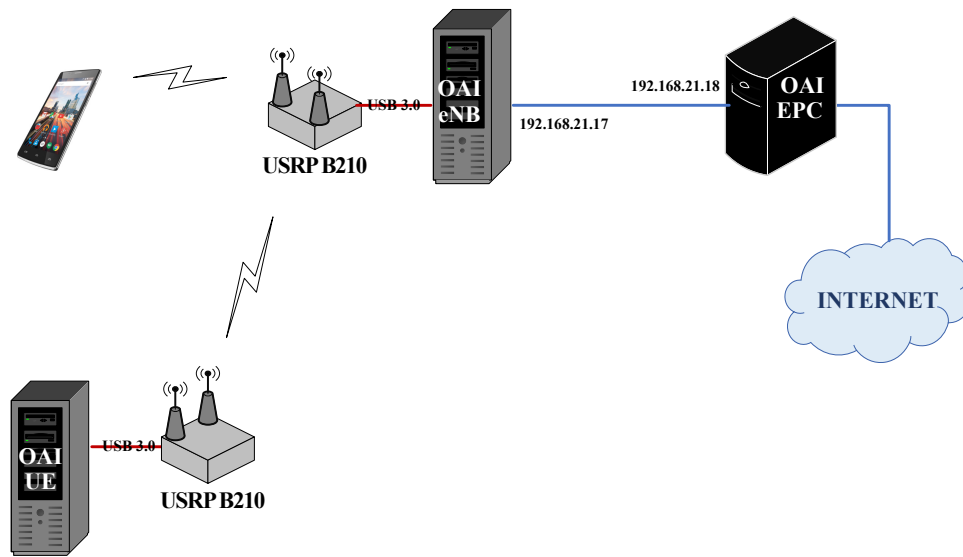
#### 4.4.4 OAI-Based Baseband Processing

To implement the eNB, the OAI source code is installed on a microcomputer system by following the instructions on the tutorial page of the OpenAirInterface Software Alliance website [43]. For successful deployment, the OAI software runs on a compatible Linux operating system (OS), usually Ubuntu 14.04, 16.04, and more recently 18.04. In the experimental setup shown in Figure 4.5, all baseband processing is performed by the computer system, with an SDR connected as the RF front-end to perform RF processing, including analog-to-digital conversion.

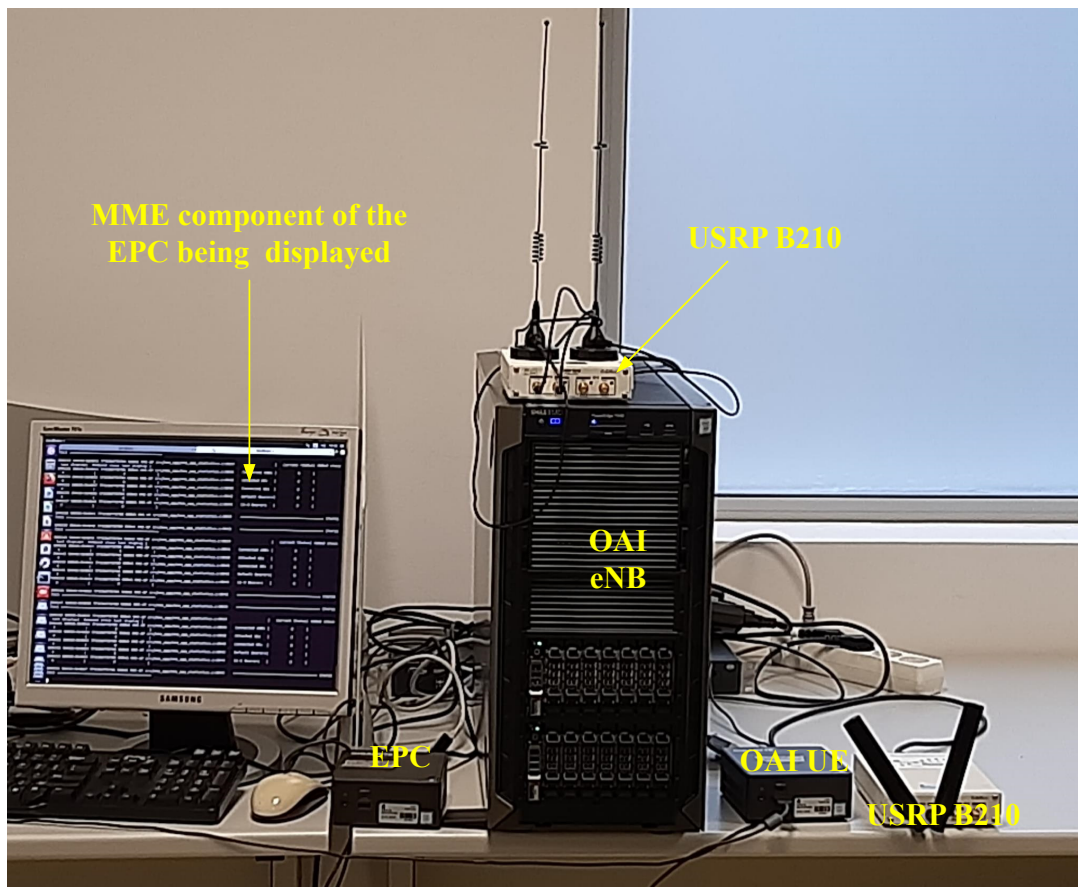
According to the 3GPP standard, the eNB can operate at 5, 10 and 20 MHz channel bandwidth with FDD and TDD configurations. The experimental setups shown in Figure 4.5 are configured to operate in FDD mode. In addition, OAI provides both downlink (DL) and uplink (UL) processing chain with OFDMA and SC-FDMA for FDD configuration. Transmission modes supported by the OAI-RAN include transmit diversity, SISO, 2 x 2 MIMO, closed-loop spatial multiplexing, multi-user multiple input, multiple output (MU-MIMO) and other LTE MIMO modes. The eNB also handles media access Control (MAC), radio link control (RLC), packet data convergence protocol (PDCP), radio resource control (RRC), and non access stratum (NAS) drivers that enable connection to the OAI-evolved packet core (OAI-EPC) or IP network over IPv4/IPv6 connectivity [49]. A maximum of 64 QAM and 16 QAM are supported for the transmission of DL and UL, respectively, including QPSK corresponding to 27, 16 and 9 MCS, which depends on the quality of the radio link and indicates the useful bits that can be transmitted per resource element (RE).

In UL transmission, the channels carrying reference signals such as the sounding reference signal (SRS) and the discovery reference signal (DRS) over the physical random access channel (PRACH) enable the UE to request the UL allocation from the eNB. While the data is transmitted over the physical (PHY) UL shared channel (PUSCH) from the UE to the eNB, the UL control information is transmitted over a physical UL control channel (PUCCH). On DL, a primary synchronization signal (PSS) and a secondary synchronization signal (SSS) are used by the UE to achieve symbol frequency synchronization, while the physical broadcast channel (PBCH) and the physical control format indicator channel (PCFICH) carrying DL control information and scheduling assignments of the UEs are implemented by the eNB on the physical downlink control channel (PDCCH). In addition, the data is transported from the eNB to the specific UEs via the Physical Downlink Shared Channel (PDSCH), while the acknowledgements (ACKs) or negative acknowledgements (NACKs) for the data are transmitted via the physical hybrid automatic repeat request (HARQ) indicator channel. In addition, the physical multicast channel (PMCH) provides broadcast and multicast services.

The OAI-EPC is implemented by using an open-core network (OAI-CN) on a commodity computer system. Unlike OAI-RAN, the openair-cn consumes less computational resources and can therefore be used on low-end computer systems. Table 4.2 lists the hardware, software and system configuration for the experimental setup shown in Figure 4.5a. As an implementation of the 3GPP specifications, the OAI-EPC contains the following network elements: MME, HSS, SGW and PGW. The functionality of Packet Data Network Gateway (PGW) and Serving Gateway (SGW) is implemented in



(a) Block diagram



(b) Laboratory Experimental setup

Figure 4.5: Monolithic OAI-LTE RAN



one module, SGW with the support of the general packet radio service (GPRS) tunneling protocol (GTP) Linux kernel module for the successful operation of SGW.

Apart from OAI-EPC, OAI-eNB is compatible with both commercial and open source EPCs such as Open5GS and srsEPC. However, our setup uses OAI-EPC to provide LTE core network functionalities. The air interface is provided by using OAI-compatible SDR including USRP's [50], as recommended by OSA for the implementation of eNB and UE. However, the majority of OAI community members have reported that the X-series USRPs have some instability issues when running OAI RAN applications, and this issue occurred during the development of the testbeds. Therefore, we rely on USRP B210 to achieve OAI-eNB and OAI-UE. Moreover, for this work, the COTS smartphone is used as UE to avoid connectivity problems that often occur between OAI-eNB and OAI-UE. Despite the tremendous use of OAI to achieve RAN emulation, complications due to hardware compatibility and high cost can often be a challenge. Therefore, an alternative solution is OAI Simulation (OASIM), which provides a simulation environment, without requiring a SDR device to realize only layer 3 (RRC, non access stratum (NAS), and internet protocol (IP)) and layer 2 (PDCP, RLC, and MAC) operations, while making the PHY layer transparent. For this reason, OASIM could be useful for studying upper layer algorithms and protocols. However, since this work focuses on characterizing the real-time signal from the emulated RAN via PHY fronthaul, OASIM is not considered for this work.

**Table 4.2:** System parameter and configuration of the developed E2E OAI-LTE testbed

Network Element	Component	Description
OAI-eNB Operating Bands: 7 (2500 MHz – 2570 MHz) (2620 MHz – 2690 MHz) Channel Bandwidth: 5, 10 and 20 MHz; FDD	Hardware:	PC: Intel® Core i7 (4 cores), 4.3 GHz, 16GB DDR SDR: Ettus/NI USRP B210; 70 MHz - 6 GHz frequency, 2x2 MIMO capability, 56 MHz real-time bandwidth, 61.44 MS/s.
	Software:	OAI-RAN, master branch tag ae0494b
OAI-EPC	Hardware: Software:	PC: Intel® Core i7 (2 cores), 2.7 GHz, 8 GB DDR OAI-CN, develop branch, version tag 0.5.0
OAI-UE	Hardware:	PC: Intel® Core i7 (2 cores), 2.7 GHz, 8 GB DDR SDR: Ettus/NI USRP B210; 70 MHz - 6 GHz frequency, 2x2 MIMO capability, 56 MHz real-time bandwidth, 61.44 MS/s.
	Software:	OAI-RAN, master branch tag ae0494b

### 4.4.5 Prototyping of a Non-Monolithic RAN

The motivation for decomposing the baseband processing of the centralized BS functionality has been discussed in Chapter 2. Using the freely available open-source software, it is therefore interesting to explore the possibility of emulating a real-time mobile network in order to evaluate the impact of functional splitting on the fronthaul. To this end, we develop a laboratory prototype based on functional split option 7 using the OAI source code and compare the performance of the supported functional split option with the monolithic type BS.

### 4.4.6 Functional Split Based Architecture

The OAI attempts to implement function splitting of the fronthaul started with the development of the Next-Generation Fronthaul Interface (NGFI) architecture source code and was later updated to include the 3GPP 5G NR. The NGFI OAI version includes applications for remote cloud center (RCC) and remote radio units (RRU) installed on different host machines. For Ethernet technology, the RCC is connected to the RRU via an Ethernet cable (minimum category 5e) through a Gigabit/s NIC of each host machine, as shown in Figure 4.6. In the same framework, OAI has been updated to comply with the 5G NR architecture paradigm with inclusion codes for CU and DU, starting with the master branch tag v1.1.0. In compliance with the 3GPP specification, OAI uses a split F1 interface between CU and DU, which is implemented with a soft LTE modem like other OAI implementations. In this case, CU performs processing including PDCP, RRC and SDAP, while DU processes RLC, MAC and PHY. However, OAI currently only allows DU mapping to a single CU functionality.

The separation of control plane and data plane is achieved via F1-C and F1-U logical interfaces respectively. For a successful implementation of the control plane via the F1-C interface, *F1 setup request* and *F1 setup response* are enabled [51]. In addition, the current OAI support for CU-DU implementation is the initial UL RRC message transmission, the UL/DL RRC message transmission, and the release request, command, or completion of the F1 UE context. In addition, the OAI code uses Google protocol buffers to encapsulate RLC packets, also called SDU, for transport over user datagram protocol (UDP) tunnels. With this setting, a stable user data rate of 70 Mbps can be achieved for a single CU-DU connection with 100 PRBs in TM1 mode configuration over a wireless channel to the UE.

In our setup shown in Figure 4.6 and its lab setup in Figure 4.7, the logical F1 interfacing is achieved via a physical link by using a standard single-mode optical fiber (SMF) terminated with a 10Gb SFP+ at each end to a 10 Gb small form-factor pluggable (SFP)+ and connected to an Ethernet NIC of each host computer. Also connected to the DU is the USRP B210, a RF frontend that provides an air interface to the COTS UE used for this facility. The connection to the OAI-EPC is made over a 1 Gigabits Ethernet link to establish a E2E mobile system.

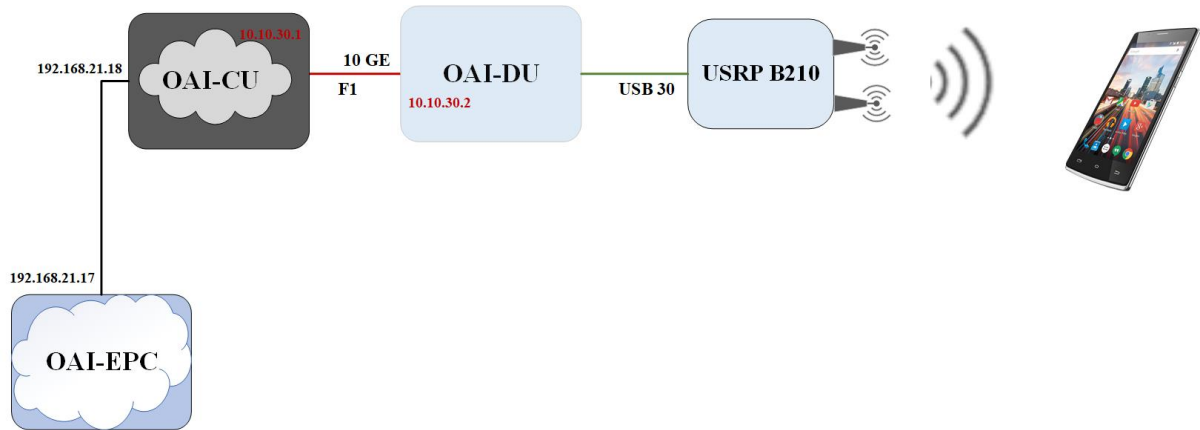


Figure 4.6: Basic representation of OAI based functional split architecture

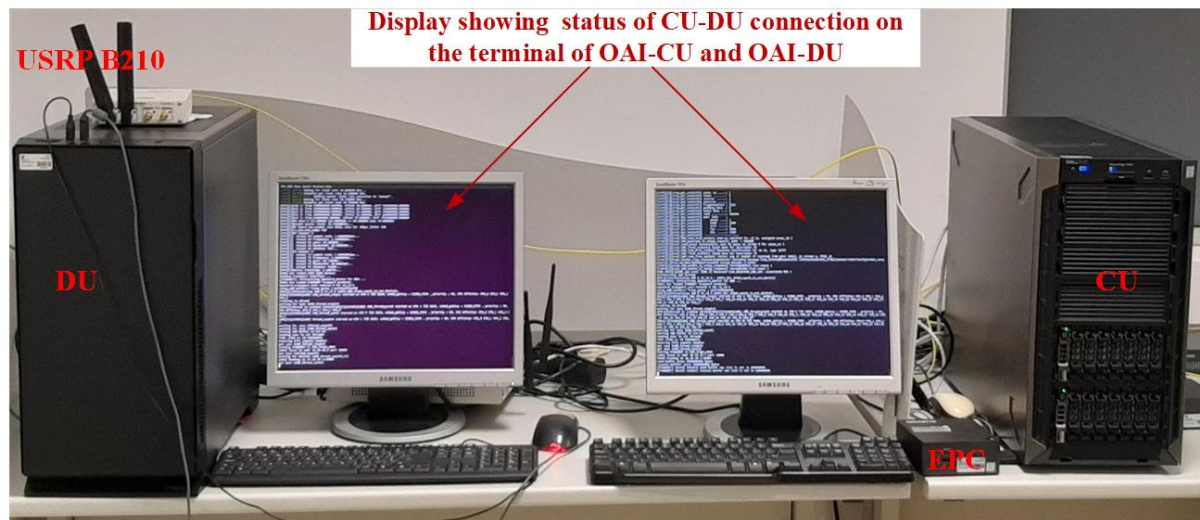


Figure 4.7: Laboratory Setup for OAI based functional split architecture

#### 4.4.7 Building and Operating the Functional Split Setup

EPC, CU and DU are realised by deploying the respective OAI software application for each network unit on the host's Ubuntu terminal PC. To make the system operational, the EPC must first be initiated. Sequentially, the *build\_oai* script command is executed to compile the source code for CU and DU (or radio cloud center (RCC) and RRU in the case of the NGFI architecture). The channel configuration parameters are specified in the configuration files for CU and DU. The system parameters are listed in Table 4.3. The PHY parameters including bandwidth, band, frequency are configured for the CU, while MAC, address and ports are set for the DU to enable the F1 interface locate the CU on control and data plane. Examples of the configuration files CU and DU can be found in Appendix C.2 and C.3 respectively. Then, the *sudo -E ./lte-softmodem* command is run in conjunction with the appropriate configuration file to launch the OAI CU application and then the OAI DU application. An example is shown below:

```
sudo -E ./lte-softmodem -O CONFIG_FILES_LOCATION/enb.band7.tm1.usrpX310.conf
```

**Table 4.3:** System parameter and configuration for functional split testbed

Network Element	Component	Description
<b>OAI-DU</b> Operating Bands: 7 (2500 MHz–2570 MHz) UL (2620 MHz–2690 MHz) DL Channel Bandwidth: 5, 10 and 20 MHz; FDD IP: 10.10.30.2 (F1)	Hardware:	PC: Intel® Core i7 (4 cores), 4.3 GHz, 16GB DDR SDR: Ettus/Ni USRP B210; Frequency range: 70 MHz - 6 GHz, 2x2 MIMO capability, Max. instantaneous real-time bandwidth: 56 MHz. Max. I/Q sample rate: 61.44 MS/s. Optional SDR: NI USRP 2953R or Ettus USRP X310 ; Frequency range: 1.2 GHz to 6 GHz, 2x2 MIMO capability, Max. instantaneous real-time bandwidth: 120 MHz , Max. I/Q sample rate: 200 MS/s.
	Software:	OAI-RAN, master branch: tag v1.1.0 upward
<b>OAI-CU</b> IP: 10.10.30.1 (F1), 192.168.21.18 (S1)	Hardware:	Dell PowerEdge T440, Intel® Xeon® Gold 5120 2.2 GHz, 28 cores, 16Gb
	Software:	OAI-RAN, master branch: tag v1.1.0 upward
<b>OAI-EPC</b> IP: 192.168.21.17	Hardware:	PC: Intel® Core i7 (2 cores), 2.7 GHz, 8 GB DDR
	Software:	OAI-CN, develop branch, version tag 0.5.0
<b>COTS UE</b>		Samsung Galaxy Note 4

#### 4.4.8 OAI based 5G NR Experimental Demonstration

Following the development of the specifications for the 5G new radio (5G-NR) according to 3GPP R15, evolved universal terrestrial radio access (EUTRA) with dual connectivity (EN-DC) is considered by 3GPP as an option for initial deployment. Therefore, non-standalone (NSA) configuration architecture is adopted by OAI for the emulation of the 5G-NR network [51]. The NSA configuration enables the orchestration of multiple radio access technologies, supporting the reuse of the EPC of the 4G network as CN by both eNB and gNodeB (gNB). All cyclic prefix (CP) functions are handled by the eNB, while the gNB is only responsible for user plane traffic. To ensure interoperability between eNB and gNB, OAI has upgraded the eNB implementation of RRC to be compliant with the R15 standards, and adopted the 5G Functional Application Platform Interface (FAPI) between PHY and MAC specified by the Small Cell Forum (SCF) [51, 52]. However, the OAI is subject to a rapid development process.

The OAI 5G-NR setup uses the FR1 band (410 - 7125 MHz), specifically the n78 band (3.5 GHz) frequency. Two SDR devices, each USRP B210 for eNB and gNB, are required to establish the initial control plane between UE and eNB and the user plane

between UE and gNB, respectively. The configured channel bandwidth is 40 MHz in TDD mode. At the time of writing, only the SISO antenna scheme is supported by the OAI 5G-NR setup solution. However, it should be noted that synchronization is required between the eNB and gNB as they have different frequency offsets and timings, especially because OFDM is very susceptible to frequency offsets.

### 4.4.9 Building gNodeB

The procedure for building OAI-gNB is similar to that of OAI-eNB, as mentioned in the previous section. Starting with obtaining the OAI-RAN source codes from the OpenAirInterface repository, the usual *build\_oai* is performed with the gNB component as follows to compile and build the OAI-gNB application:

```
./buildoai-I-USRP--gNB
```

The *I* and *USRP* switches are required to install the necessary software dependencies for the OAI software and UHD driver support for the USRP radio head, respectively.

With the execution of the *build\_oai* script, a soft-link to the real hardware is created and ready to use at runtime, generating the *nr-softmodem* command, which is then combined with a specific configuration script containing a set of system parameters specified in Table 4.3. An example of a typical configuration file is shown in Appendix C.4.

## 4.5 The Overall Setup Description

All the testbeds described above are composed as shown in Figure 4.8. For the srsLTE-based 4G and OAI-based 5G NR setups as well as the functional split RAN setups, the baseband processing functions reside in a high-end microprocessor-based server. To implement the setup shown in the figure, we use the virtualization technique that supports multiple processing by sharing expensive hardware resources. Docker software is used to deploy a virtual environment, creating the required logically isolated containers for OAI-CU, OAI-gNB and srsLTE. Then, OAI and srsLTE open source software are deployed following the procedure described in the previous sections. For the functional split setup, the OAI-based core network entity is connected to the OAI-CU container through a logical interface with IP address on the same subnet mask, as indicated in the Figure 4.8, while a E2E is realized through the fronthaul connection to the OAI-DU connected to USRP B210 as RF front-end. Similarly, another USRP B210 is connected to the gNB container. Moreover, a USRP B210 is connected to the srsLTE container, which handles both BBU and EPC functions. Each emulated mobile network is configured to operate with a channel bandwidth of 5 MHz, 10 MHz and 20 MHz.

The functional split based E2E network shown in the figure above allows easy integration of fiber, OWC, and PON as fronthaul links for experimental demonstrations. In the next section, we present a use case involving the demonstration of real-time transmission of RF over the PON system as a fronthaul.

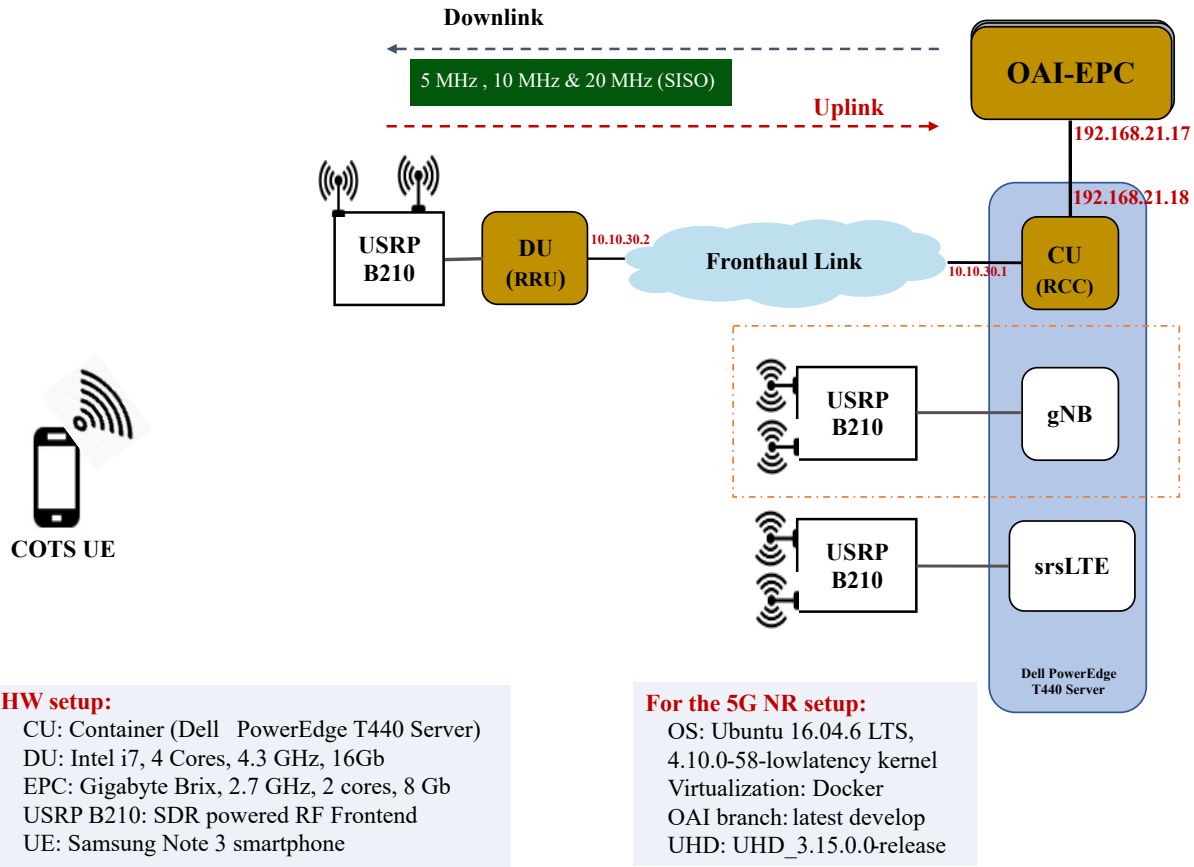


Figure 4.8: Overall Setup showcasing virtualization approach

## 4.6 Real-time Transmission over PON

In this section, we present an experimental demonstration of RF transmission over the PON system as a fronthaul. Using the setup in Figure 4.8, in particular the functional split setup component, an XG-PON system is integrated as a link between CU and DU. The OLT is connected to the CU via a 10G SFP+ interface and to a 10G SFP+ of the ONU via a single-mode fiber (SMF). Similarly, the other interface of the OLT is connected to the ONU, which in turn is connected to the DU to establish a E2E real-time mobile network with a PON system as MFH.

Using a functional split option 7.1 for the fronthaul configuration, the system parameters in Table 4.3, which include the LTE channel bandwidth of 5 MHz, 10 MHz and 20 MHz, are configured for the emulated mobile network. Furthermore, connectivity from CU to DU is achieved through basic transmission control protocol (TCP)/IP configurations with the specified IP addresses, as shown in Figure 4.8. The network is operated sequentially, starting with 5 MHz channel bandwidth, then 10 MHz and 20 MHz. As a preliminary step to running the network, a throughput test is performed on the NG-PON2 system using the *iperf* tool, and the line rate of NG-PON2 is measured as 5.36 Gbps and 8.16 Gbps for the US and downstream (DS) traffic, respectively. A similar measurement is performed for maximum transmission unit (MTU) with 3424

#### 4.6. Real-time Transmission over PON

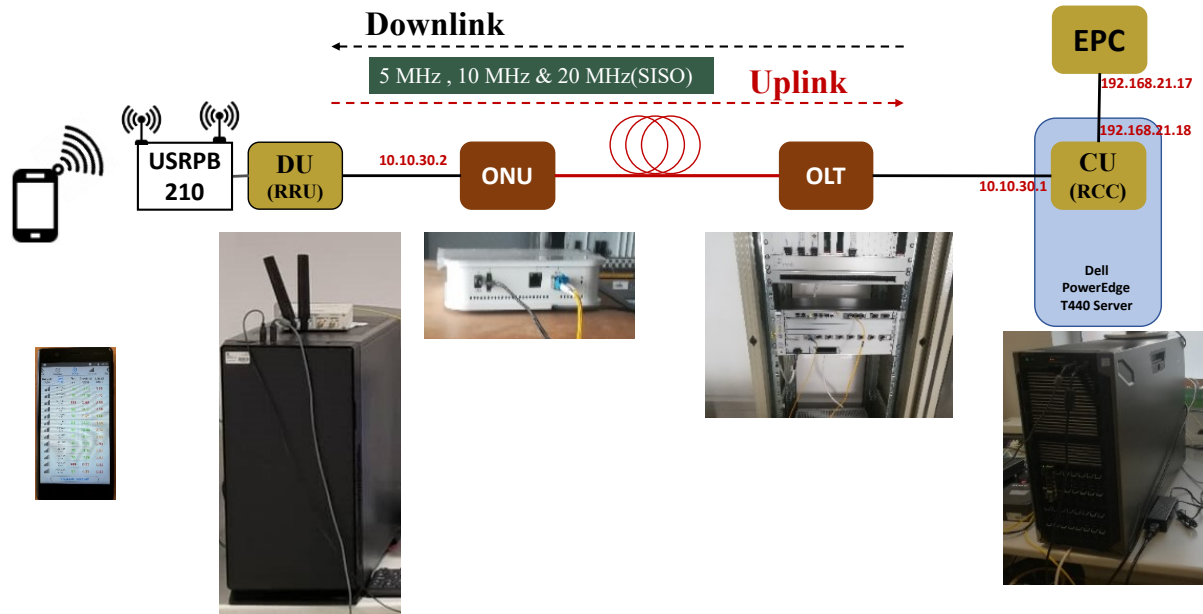


**Figure 4.9:** Demonstration of real-time transmission over PON.

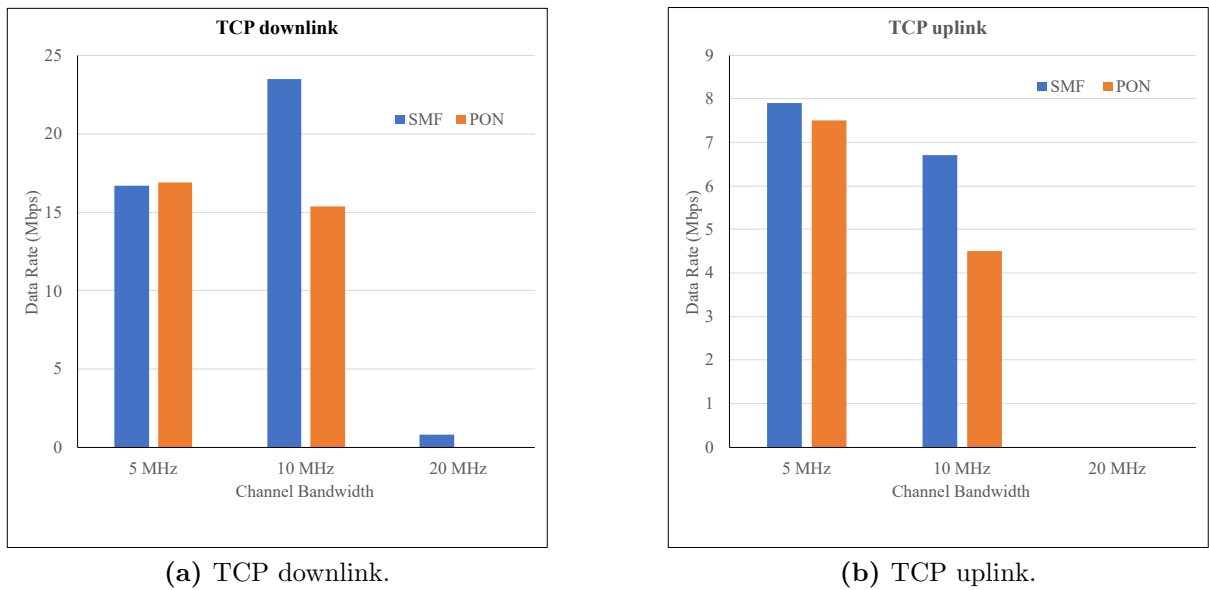


**Figure 4.10:** Measured data rate for TCP traffic.

bytes.

Then, the network is operated at each configured channel bandwidth and a successful connection is established between UE and EPC while measuring the downlink and uplink throughput for each channel bandwidth for both TCP and UDP traffic, as shown in Figures 4.10 and 4.11, respectively. It should be noted that the PON system is used as an MFH system to check for possible limitations due to timing delays normally associated with PON systems. This is therefore reflected in the results shown in Figure 4.11 and

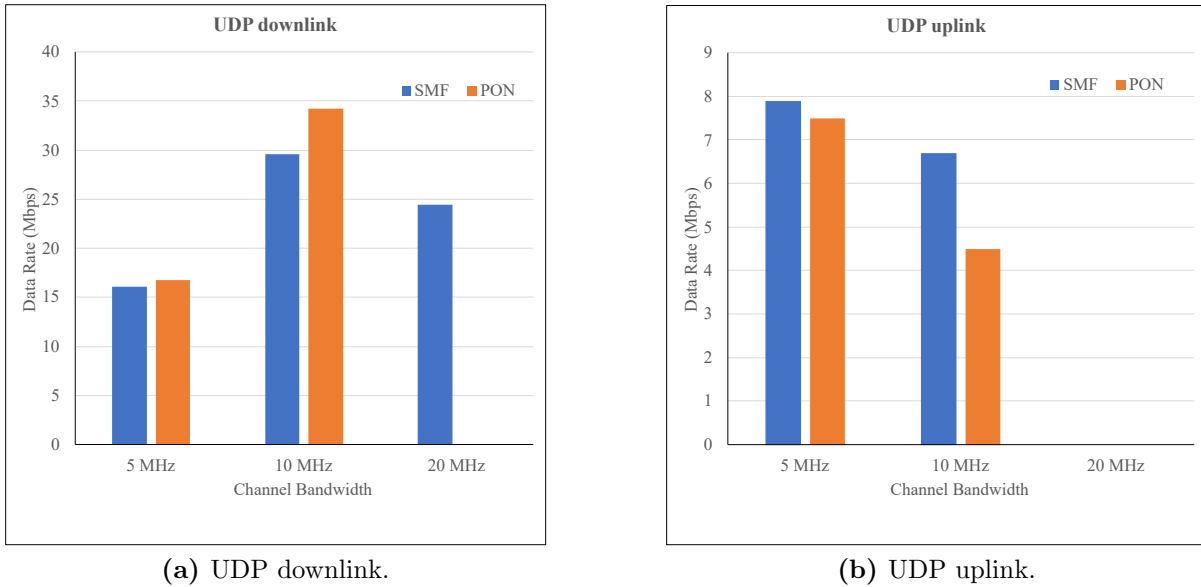


**Figure 4.11:** Measured data rate for UDP traffic.

discussed in the following section. In addition, to investigate the quality of the signal received from the UE, a Keysight N9041B vector signal analyzer (VSA) is used to obtain the constellation, waveform, and EVM as shown in Figure 4.12.

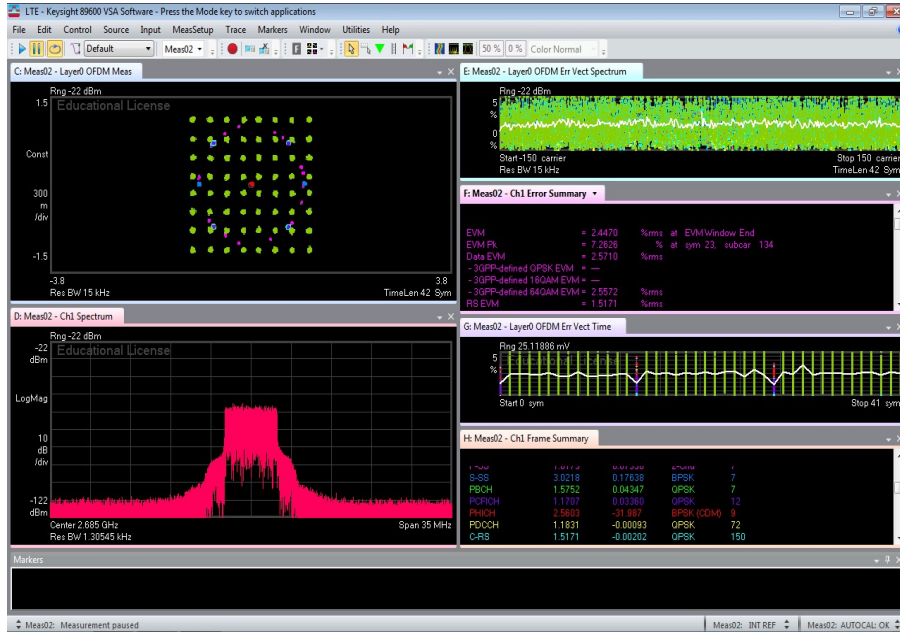
## 4.7 Results and Discussions

While establishing E2E connectivity using NG-PON2 as MBF between CU and DU, successful transmission is achieved for both DL and UL at 5 MHz and 10 MHz LTE channel bandwidth. However, when transmitting at 20 MHz, signal degradation occurs due to insufficient computational resources required for extensive digital signal processing and the inherent delay overhead of the PON system. Considering this limitation, data rates are measured at higher levels as shown in Figure 4.10 and Figure 4.11. For comparative performance analysis, a fiber MFH in the same configuration is used and the measurement was repeated sequentially. UDP and TCP throughput tests are performed to investigate the capability of MFH to transmit real-time signals.

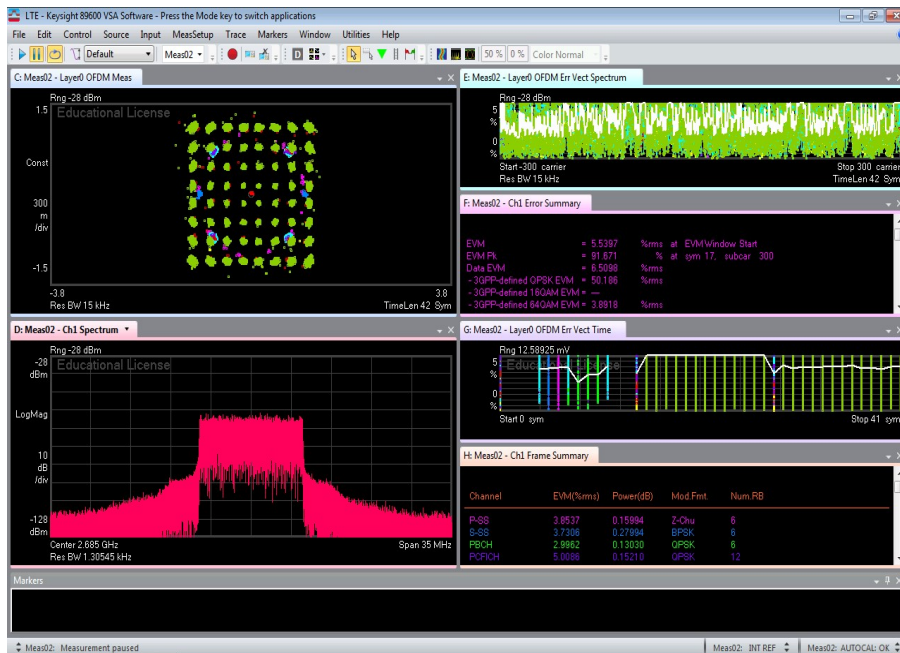
On one hand, for the TCP test, data is transmitted on connection-oriented (bidirectional) protocol that provides error-checking, delivery guaranteed, packets order preservation, and retransmission (in case of lost packets). On the other hand, the UDP test is faster than TCP because error-checking and data recovery are not required while measuring the data rate, thus revealing the maximum achievable data rate of the channel. This is justified by the measurements reported in Figure 4.11, in particular in Figure 4.11a, which show about 25 Mbps on the DL, but none on the UL for the 20 MHz channel bandwidth when using fiber-based MFH, while no successful transmission is recorded at 20 MHz bandwidth for PON-based MFH. However, the data rate measured with fiber-based MFH and PON-based MFH links show approximately similar trends



## 4.7. Results and Discussions



(a) 5 MHz Channel Bandwidth.



(b) 10 MHz Channel Bandwidth

**Figure 4.12:** Over-the-Air signal capture by the VSA, showing modulation constellation points, signal waveform and EVM while data traffic is being transmitted.

for 5 MHz and 10 MHz channel bandwidth. In view of the above, the modulation constellation is investigated and the EVM is measured with a VSA when the real-time signal is transmitted over PON based MFH; an example is shown in Figure 4.12. As expected, 5 MHz shows a clearer constellation than 10 MHz, indicating 2.5% and 6.5%

EVM, respectively, which are within the tolerable EVM range for 256 QAM modulation as recommended by 3GPP [53].

The results presented in this work demonstrate the feasibility of a full 4G deployment enabled by virtualized C-RAN setup implemented in mid-range commercial CPU. Seamless and robust support has been demonstrated for 5 and 10 MHz, while higher bandwidths (20 MHz and above) may require increased computational power provided by more powerful CPUs [43]. Recent advances by the OAI research community in the development of the 5G stack also rely on the use of co-simulations with dedicated hardware platforms such as FPGAs to accelerate processing and enable real-time operation at higher bandwidths [54]. Furthermore, the results presented in this work demonstrate the compatibility of PON-based fronthauling with virtualized C-RAN architectures, enabling efficient management of network resources and helping to reduce the CAPEX and OPEX of future mobile fronthaul networks.

## 4.8 Summary

In this chapter, we have provided an overview of the basic technologies for realizing an emulation of a real cellular network by taking advantage of an open-source platform to develop testbeds that serve as a contribution to the research infrastructure and ultimately enable testing and validation of wireless and optical transport systems. Taking advantage of the flexibility and centralized processing benefits of C-RAN, we have demonstrated the use of OAI and SDR to develop a C-RAN testbed. In addition, two functional split options of the C-RAN fronthaul were experimentally explored within the constraints of the available open-source software and hardware resources.

The developed C-RAN testbed not only demonstrates the practicality of RAN softwarization but also provides a platform on which various mobile transport solutions can be tested. Consequently, a NG-PON based fronthaul has been experimentally validated to investigate the transmission of real-time radio streams over PON. Preliminary results show successful transmission over the PON fronthaul. However, we found that in order to improve the performance of the whole setup, a further enhancement mechanism is required to minimize the impact of delay overhead due to the processing of PON.

## References

- [1] J. S. Wey, Y. Luo, and T. Pfeiffer, "5g wireless transport in a pon context: An overview," *IEEE Communications Standards Magazine*, vol. 4, no. 1, pp. 50–56, 2020.
- [2] X. Liu *et al.*, "Enabling Technologies for 5G-Oriented Optical Networks," in *2019 Optical Fiber Communications Conference and Exhibition (OFC)*, 2019, pp. 1–3.
- [3] H. Khalili *et al.*, "Design Considerations for an Energy-Aware SDN-Based Architecture in 5G EPON Nodes," in *2018 20th International Conference on Transparent Optical Networks (ICTON)*, 2018, pp. 1–4.
- [4] H. S. Chung, "Low Latency PON and RoF for 5G Wireless Systems," in *2018 IEEE Photonics Conference (IPC)*, 2018, pp. 1–2.
- [5] E. Harstead, D. van Veen, V. Houtsma, and P. Dom, "Technology Roadmap for Time-Division Multiplexed Passive Optical Networks (TDM PONs)," *Journal of Lightwave Technology*, vol. 37, no. 2, pp. 657–664, 2019.
- [6] M. M. Mowla, I. Ahmad, D. Habibi, and Q. V. Phung, "Energy Efficient Backhauling for 5G Small Cell Networks," *IEEE Transactions on Sustainable Computing*, vol. 4, no. 3, pp. 279–292, 2019.
- [7] K. Kim *et al.*, "High Speed and Low Latency Passive Optical Network for 5G Wireless Systems," *Journal of Lightwave Technology*, vol. 37, no. 12, pp. 2873–2882, 2019.
- [8] A. O. Mufutau, F. P. Guiomar, A. Oliveira, and P. P. Monteiro, "Software-defined radio enabled cloud radio access network implementation using openairinterface," *Wireless Personal Communications*, Sep 2021.
- [9] P. P. Monteiro *et al.*, "Flexible optical and wireless testbed for 5g and beyond communication systems," in *OSA Advanced Photonics Congress (AP) 2019 (IPR, Networks, NOMA, SPPCom, PVLED)*. Optical Society of America, 2019, p. JT4A.15.
- [10] P. P. Monteiro, A. Gameiro, and N. B. Carvalho, "Optical radio convergence infrastructure for communications and power delivering (ORCIP)," in *2016 18th International Conference on Transparent Optical Networks (ICTON)*, 2016, pp. 1–3.
- [11] A. Y. Ding, J. Crowcroft, S. Tarkoma, and H. Flinck, "Software defined networking for security enhancement in wireless mobile networks," *Computer Networks*, vol. 66, pp. 94 – 101, 2014, n Leonard Kleinrock Tribute Issue: A Collection of Papers by his Students.
- [12] M. Liyanage, A. Braeken, A. D. Jurcut, M. Ylianttila, and A. Gurtov, "Secure communication channel architecture for software defined mobile networks," *Computer Networks*, vol. 114, pp. 32 – 50, 2017.

- 
- [13] F. Zanferrari Morais, C. André da Costa, A. M. Alberti, C. Bonato Both, and R. da Rosa Righi, “When sdn meets c-ran: A survey exploring multi-point coordination, interference, and performance,” *Journal of Network and Computer Applications*, vol. 162, p. 102655, 2020.
- [14] T. Chen, M. Matinmikko, X. Chen, X. Zhou, and P. Ahokangas, “Software defined mobile networks: concept, survey, and research directions,” *IEEE Communications Magazine*, vol. 53, no. 11, pp. 126–133, 2015.
- [15] E. Benkhelifa, T. Welsh, L. Tawalbeh, Y. Jararweh, and M. Al-Ayyoub, “Leveraging Software-Defined-Networking for Energy Optimisation in Mobile-Cloud-Computing,” *Procedia Computer Science*, vol. 94, pp. 479 – 484, 2016, the 11th International Conference on Future Networks and Communications (FNC 2016) / The 13th International Conference on Mobile Systems and Pervasive Computing (MobiSPC 2016) / Affiliated Workshops.
- [16] S. Khan Tayyaba and M. A. Shah, “5G cellular network integration with SDN: Challenges, issues and beyond,” in *2017 International Conference on Communication, Computing and Digital Systems (C-CODE)*, 2017, pp. 48–53.
- [17] O. Narmanlioglu and E. Zeydan, “Software-defined networking based network virtualization for mobile operators,” *Computers & Electrical Engineering*, vol. 57, pp. 134 – 146, 2017.
- [18] B. Özbek, Y. Aydoğmuş, A. Ulaş, and B. Görkemli, “Joint routing and resource allocation for software defined mobile networks,” in *2019 IEEE 30th Annual International Symposium on Personal, Indoor and Mobile Radio Communications (PIMRC)*, 2019, pp. 1–6.
- [19] G. Craik, “Network Transformation; (Orchestration, Network and Service Management Framework) Network Transformation; (Orchestration, Network and Service Management Framework) 3,” [https://www.etsi.org/images/files/ETSIWhitePapers/ETSI\\_White\\_Paper\\_Network\\_Transformation\\_2019\\_N32.pdf](https://www.etsi.org/images/files/ETSIWhitePapers/ETSI_White_Paper_Network_Transformation_2019_N32.pdf), Tech. Rep., [Online; accessed 2021-01-05].
- [20] R. Martínez *et al.*, “Integrated sdn/nfv orchestration for the dynamic deployment of mobile virtual backhaul networks over a multilayer (packet/optical) aggregation infrastructure,” *J. Opt. Commun. Netw.*, vol. 9, no. 2, pp. A135–A142, Feb 2017.
- [21] M. S. Bonfim, K. L. Dias, and S. F. L. Fernandes, “Integrated nfv/sdn architectures: A systematic literature review,” *ACM Comput. Surv.*, vol. 51, no. 6, Feb. 2019.
- [22] L. Bouali, E. Abd-Elrahman, H. Afifi, S. Bouzefrane, and M. Daoui, “Virtualization techniques: Challenges and opportunities,” vol. 10026, 06 2016, pp. 49–62.
- [23] D. Ageyev, O. Bondarenko, T. Radivilova, and W. Alfroukh, “Classification of existing virtualization methods used in telecommunication networks,” 05 2018, pp. 83–86.

- [24] I. Mavridis and H. Karatza, “Lightweight virtualization approaches for software-defined systems and cloud computing: An evaluation of unikernels and containers,” in *2019 Sixth International Conference on Software Defined Systems (SDS)*, 2019, pp. 171–178.
- [25] M. Plauth, L. Feinbube, and A. Polze, “A performance survey of lightweight virtualization techniques,” 09 2017, pp. 34–48.
- [26] T. V. Doan *et al.*, “Containers vs virtual machines: Choosing the right virtualization technology for mobile edge cloud,” in *2019 IEEE 2nd 5G World Forum (5GWF)*, 2019, pp. 46–52.
- [27] A. Gopalasingham, D. G. Herculea, C. S. Chen, and L. Roulet, “Virtualization of radio access network by virtual machine and docker: Practice and performance analysis,” in *2017 IFIP/IEEE Symposium on Integrated Network and Service Management (IM)*, 2017, pp. 680–685.
- [28] R. Behraves, E. Coronado, and R. Riggio, “Performance evaluation on virtualization technologies for nfv deployment in 5g networks,” in *2019 IEEE Conference on Network Softwarization (NetSoft)*, 2019, pp. 24–29.
- [29] A. M. Potdar, N. D G, S. Kengond, and M. M. Mulla, “Performance evaluation of docker container and virtual machine,” *Procedia Computer Science*, vol. 171, pp. 1419–1428, 2020, third International Conference on Computing and Network Communications (CoCoNet’19).
- [30] “Hyper-v on windows server,” <https://docs.microsoft.com/en-us/windows-server/virtualization/hyper-v/hyper-v-on-windows-server>, [Online; accessed 2021-01-05].
- [31] “KVMproject homepage,” [https://www.linux-kvm.org/page/Main\\_Page](https://www.linux-kvm.org/page/Main_Page), [Online; accessed 2021-01-05].
- [32] “QEMUproject homepage,” <https://www.qemu.org/>, [Online; accessed 2021-01-05].
- [33] “VirtualBox project homepage,” <https://www.virtualbox.org/>, [Online; accessed 2021-01-05].
- [34] “Vmware homepage,” <http://www.vmware.com/>, [Online; accessed 2021-01-05].
- [35] “XEN project homepage,” <https://www.virtualbox.org/>, [Online; accessed 2021-01-05].
- [36] “Docker homepage,” <https://www.docker.com/>, [Online; accessed 2021-01-05].
- [37] “LXC homepage,” <https://linuxcontainers.org/>, [Online; accessed 2021-01-05].
- [38] “kub homepage,” <https://kubernetes.io/>, [Online; accessed 2021-01-05].

- 
- [39] I. Afolabi, T. Taleb, K. Samdanis, A. Ksentini, and H. Flinck, “Network slicing and softwarization: A survey on principles, enabling technologies, and solutions,” *IEEE Communications Surveys Tutorials*, vol. 20, no. 3, pp. 2429–2453, 2018.
- [40] A. Rostami *et al.*, “Orchestration of ran and transport networks for 5g: An sdn approach,” *IEEE Communications Magazine*, vol. 55, no. 4, pp. 64–70, 2017.
- [41] L. Bertz and B. Pankajakshan, “The Status of Open Source for 5G,” 5G Americas, Tech. Rep.
- [42] ORAN Alliance, “Open & Intelligent Software for the Radio Access Networks,” <https://www.o-ran.org/software>, 2020, [Online; accessed 2021-04-20].
- [43] OAISA, “The open-air-interface project,” <https://gitlab.eurecom.fr/oai/openairinterface5g/-/wikis/home>, OpenAirInterface Software Alliance, 2020, accessed: 2021-04-26.
- [44] 3GPP Technical Specifications Groups, “Submission of initial 5G description for IMT-2020.”
- [45] Software Radio Systems Ltd, “srsLTE 20.10 Documentation — srsLTE 20.10 documentation.”
- [46] 3GPP, “3G Security; Cryptographic Algorithm Requirements,” 3rd Generation Partnership Project (3GPP), Technical Specification (TS) 33.105, 7 2020, version 16.0.0,” vol. 0, no. Release 16, 2020.
- [47] —, “3G Security; Specification of the MILENAGE algorithm set: An example algorithm set for the 3GPP authentication and key generation functions f1, f1\*, f2, f3, f4, f5 and f5\*,” Document 2: Algorithm specification,” vol. 0, no. Release 16, 2020.
- [48] OpenAirInterface Software Alliance (OSA), “OpenAirInterface: 5G Software Alliance for Democratising Wireless Innovation,” <https://openairinterface.org/getting-started/openairinterface-an-open-cellular-ecosystem/>, [Online; accessed 2021-10-06].
- [49] L. Bonati, M. Polese, S. D’oro, S. Basagni, and T. Melodia, “Open, Programmable, and Virtualized 5G Networks: State-of-the-Art and the Road Ahead,” Tech. Rep.
- [50] “USRP Software Defined Radio (SDR) online catalog - Ettus Research — Ettus Research, a National Instruments Brand — The leader in Software Defined Radio (SDR).”
- [51] F. Kaltenberger, A. P. Silva, A. Gosain, L. Wang, and T. T. Nguyen, “OpenAirInterface: Democratizing innovation in the 5G Era,” *Computer Networks*, vol. 176, p. 107284, July 2020.
- [52] Small Cell Forum, “5G nFAPI Specifications,” no. September, 2020.

## References

---

- [53] TSGR, “TS 138 104 - V15.3.0 - 5G; NR; Base Station (BS) radio transmission and reception (3GPP TS 38.104 version 15.3.0 Release 15),” Tech. Rep.
- [54] F. Kaltenberger, A. P. Silva, A. Gosain, L. Wang, and T. T. Nguyen, “OpenAirInterface: Democratizing innovation in the 5G Era,” *Computer Networks*, vol. 176, p. 107284, July 2020.





## Chapter 5

# Hybrid Optical Fiber–Wireless 5G and 4G fronthaul coexistence

As the next era of mobile network generation is fast approaching going by the recent pace of commercial deployment of the first 5G networks, coexistence with current 4G networks is expected to be prevalent over a transitional period, before full fledged E2E 5G network infrastructures and services take precedence [1–3]. Moreover, with the plethora of services envisaged to be supported by 5G, the development of a RAN infrastructure is essential to support a variety of user-demanded mobile services required by diverse traffic scenarios. Likewise, the growing demand for high capacity and ultra-low latency in access networks are being addressed by massive deployment of pico and femtocells, in addition to ultra-high-capacity macro base stations equipped with M-MIMO antennas [4]. Therefore, with the prevalence of these ultra-dense networks being massively deployed, it is pertinent to consider heterogeneous transport solutions on the RAN fronthaul and/or backhaul to convey mobile traffic within the requirements of the network service. However, while allowing ease of deployment and minimizing cost of implementation, among other criteria; it is essential to avoid compromising retro-compatibility with legacy communications.

In this chapter, we present our work published in [5] which addresses the development and experimental assessment of novel low-latency and bandwidth-efficient transmission techniques for 5G and B5G access networks. Also, we propose the use of minimal latency and bandwidth-efficient ARoF transmission, in order to tackle the fronthaul transmission challenges for 5G while evaluating its coexistence with legacy E2E 4G LTE networks having different functional splits that are supported by Ethernet-based fronthauling. Sequentially, a hybrid fiber–FSO system with real-time RAN traffic from OAI-enabled processors is realized to emulate a real 4G LTE RAN, which is jointly transmitted with 5G traffic over an integrated fiber optic and 55 m FSO link. To the best of our knowledge, our paper [5] is the first to experimentally demonstrate an integrated heterogeneous network supporting 4G and 5G traffic, together with digital and analog transmission over a hybrid fiber–FSO fronthaul.

The rest of this chapter is organized as follows. Optical fiber–wireless fronthaul for E2E Mobile Network is presented and described in Section 4.1 as a prelude to subsequent

sections. In Section 4.2, we present the experimental setup and provide a detailed description of its components. Experimental results are discussed in Section 4.3. Finally, section 4.4 concludes this chapter by summarising the most salient contributions.

## 5.1 4G-5G Combined Transmission over Optical Fiber–Wireless Fronthaul

Following the 3rd Generation Partnership Project (3GPP) [6] release 15 specification, it has been agreed that the initial 5G deployments will be based on a non-standalone (NSA) architecture, which partially reuses the legacy 4G LTE infrastructure. This development therefore provides challenges for the development of heterogeneous transport solutions for allowing coexistence of 5G with previous network generation, most importantly, the 4G LTE. Furthermore, infrastructural support for network slicing technology could also be harnessed to achieve a dynamic and flexible slice configuration which could provide specific support to 5G use-cases [7–9]. For instance, massive machine-type communications (mMTC), defined for some non-delay-sensitive data exchange among massive interconnection of low-powered devices, could be supported by a specific slice of the overall network [10]. Similarly, considering service requirement, technique for joint transmission over OWC fronthaul could support ultra-reliable and low latency communications (URLLC) and enhanced mobile broadband (eMBB) 5G use-cases [11].

In addition, the delivery of B5G network services is strongly influenced by the transport solution existing between the CU and DU. Therefore, to achieve high-speed signal delivery in an accurately-synchronized form (either as digital or analog), optical fiber is often considered for the fronthaul network [12, 13]. However, the benefits of implementing digital radio over fiber (DRoF) using the legacy CPRI are hindered by the stringent requirements of high bit rate, latency and jitter that CPRI imposes on the fronthaul [14, 15]. Thus, it is imperative to investigate other transport solutions that negate the use of CPRI. In this context, a rethink of CPRI has led to the development of evolved CPRI (eCPRI) [16]. The eCPRI interface facilitates flexible and efficient transmission of radio signals through Ethernet-based fronthaul networks, thereby allowing functional splitting within the physical layer [17, 18]. In addition, it provides compatibility with legacy Ethernet infrastructures and network components, while enabling a significant reduction of required bandwidth [19]. However, Ethernet is characterized with inherent delays and incessant bursts that could impair delivery of latency-sensitive services, especially URLLC use case.

Therefore, to minimize latency while maximizing spectral efficiency, analog RoF transmission, discussed in chapter 2, has recently been revisited as a potential candidate for high-performance 5G transport [12, 20]. In addition to the aforementioned advantages, ARoF also provides higher cost-effectiveness compared to its digital equivalent, better flexibility and transparency, lower complexity and lower power consumption in the RRU [20]. Recently, efforts are being made to tap on the strength of both DRoF and ARoF by considering hybrid RoF whereby each is designed to support specific applications [21–23]. For instance, DRoF could support Mobile macro-cell deployment, while transmission for

small cell (femtocells, picocells, and microcells) could be provided ARoF [24].

## 5.2 FSO Fronthaul Integration

Developing a novel high-capacity wireless transport solution is necessary to support 5G and B5G services. As mentioned in Chapter 1, higher carrier frequencies in the region of the mm-wave and THz-wave frequency bands are considered vital enablers for achieving high-speed communications because of their enormous available bandwidth [25, 26]. However, adoption of these new transmission paradigms depend on cost and complexity of deployment. For example, THz-wave requires ultra-high-bandwidth low-noise amplifiers, RF mixers and antennas, which culminate to very high costs. Interestingly, line-of-sight (LOS) high-capacity wireless transmission technology, infrared free-space optics (FSO) communications have been recently proposed [27] as an alternative technology because of its cost-effectiveness. Thus, unprecedented high bit rates could be yielded when operating at extremely high carrier frequencies (typically in the range of 192 THz). In addition, FSO also possesses extra benefits [28], which include: license-free spectrum usage; item less expensive and simple operation; support to full-duplex transmission; resistance to electromagnetic interference; eye safety operation; high transmission security.

Furthermore, FSO is a promising technology for providing a wideband and low-cost fronthaul alternative in regions where fiber cannot be deployed (mountainous terrain, natural disasters, licensing issues). However, without prejudice to performance dependency on atmospheric condition [29, 30], FSO communications have received tremendous attentions for variety of applications. Particularly, radio-over-Free Space Optics (RoFSO) transmission for mobile fronthaul / backhaul solution is increasingly being adopted [31, 32]. When applied in combination with a backup RF link, ultra-reliable FSO communications have been reported in [33]. The transmission of 5G signals over hybrid FSO-RF links comprising a 6.5 m FSO link was demonstrated in [33]. Similarly, the huge bandwidth potential of these FSO systems has been recently demonstrated in [34], where 200 Gbps transmission was achieved using standard lasers and photodiodes. Also in [35], a bi-directional mobile fronthaul based on the joint use of mm-wave and FSO technologies was demonstrated for 5G networks.

## 5.3 Experimental Setup

In this section, we present our experimental setup that is propose to realize a converged optical–wireless techniques for mobile fronthaul. Our experimental setup consists of two integrated parts as simplified in Fig. 5.2. The first part deals with generation of mobile traffic both in the real-time from the 4G E2E network and offline for 5G setup, while the second is about the proposed integration of optical-wireless transport solution with RAN to convey the mobile traffic to the user equipment; for instance. In subsequent sections, we explain in detail, the experimental setup with its individual components.

### 5.3.1 Open-source Based RAN

In Chapter 4, we established the possibility of emulating, in real-time, an E2E mobile network with the support of OAI for generating 4G LTE traffics according to the 3GPP specification [17]. In the light of this, OAI and SDR concepts are extensively exploited in this section. Therefore, to realize the RAN architecture in the experimental setup, we adopt the traditional C-RAN configuration, which enables whole baseband processing functions in the CU, while only RF functionalities are done by the DU near the user [36]. This monolithic processing also corresponds to Split 8 of the functional split options [18, 37]. Furthermore, to offer CPRI alternative fronthaul, decomposition of the CU functions is an obvious solution. With this technique, extra processing functions is allocated to the DU. Hence, options 8 and 7.1 for 4G LTE, which are illustrated in Fig. 5.1, are considered for emulating a realistic RAN that corresponds to their respective open-source OAI implementations.

Furthermore, OAI source code release v0.6.1 [38] is extensively employed to build OAI-RAN and OAI core network (OAI-CN) to realize the DU/CU functionalities and EPC respectively. Also, access to the core network is facilitated by the EPC to the CU through 1 Gigabit Ethernet (GbE) interface. RF front-ends are provided by two software-defined radio (SDR) devices, precisely USRP B210 and USRP 2953R, from National Instruments for transmitting radio signals to the User Equipment (UE) through the air-interface. Meanwhile, a COTS mobile terminal, specifically Samsung Galaxy Note4, is used as the UE for this work. Table 5.1 provides a list of hardware components employed to implement the CU, DU and EPC building blocks. Full centralization is offered by

**Table 5.1:** Hardware component for the setup

Component	Description
RRU	Intel® Core i7 (4 cores), 4.3 GHz, 16GB DDR.
RCC	Intel® Xeon® Gold 5120 2.2 GHz 28 cores, 16Gb DDR.
EPC	Low-power PC, Intel Atom 1.8 GHz, 4 GB LPDDR4
SDR 1 (for Split 7.1)	Ettus USRP B210; 70 MHz - 6 GHz, frequency, 2x2 MIMO capability, 56 MHz of real-time bandwidth, 61.44MS/s.
SDR 2 (for Split 8)	NI-USRP 2953R, 1.2 GHz - 6 GHz frequency, 256x256 MIMO capability, 160 MHz maximum real-time bandwidth, 200 MS/s.
UE	COTS Cat4 Smartphone.

the split 8 option, as depicted in Figure 5.1 while other functions for the DL direction including antenna-air interfacing, analog RF functionalities (up-and down-conversion, amplification, filtering, beamforming) and digital to analog (D/A) or analog to digital (A/D) conversion functions are performed at the DU which is at the proximity of the antenna. However, for the UL, the digitized radio samples are directly transmitted over the fronthaul for full remote processing at the CU. Other functionalities at the UL include

### 5.3. Experimental Setup

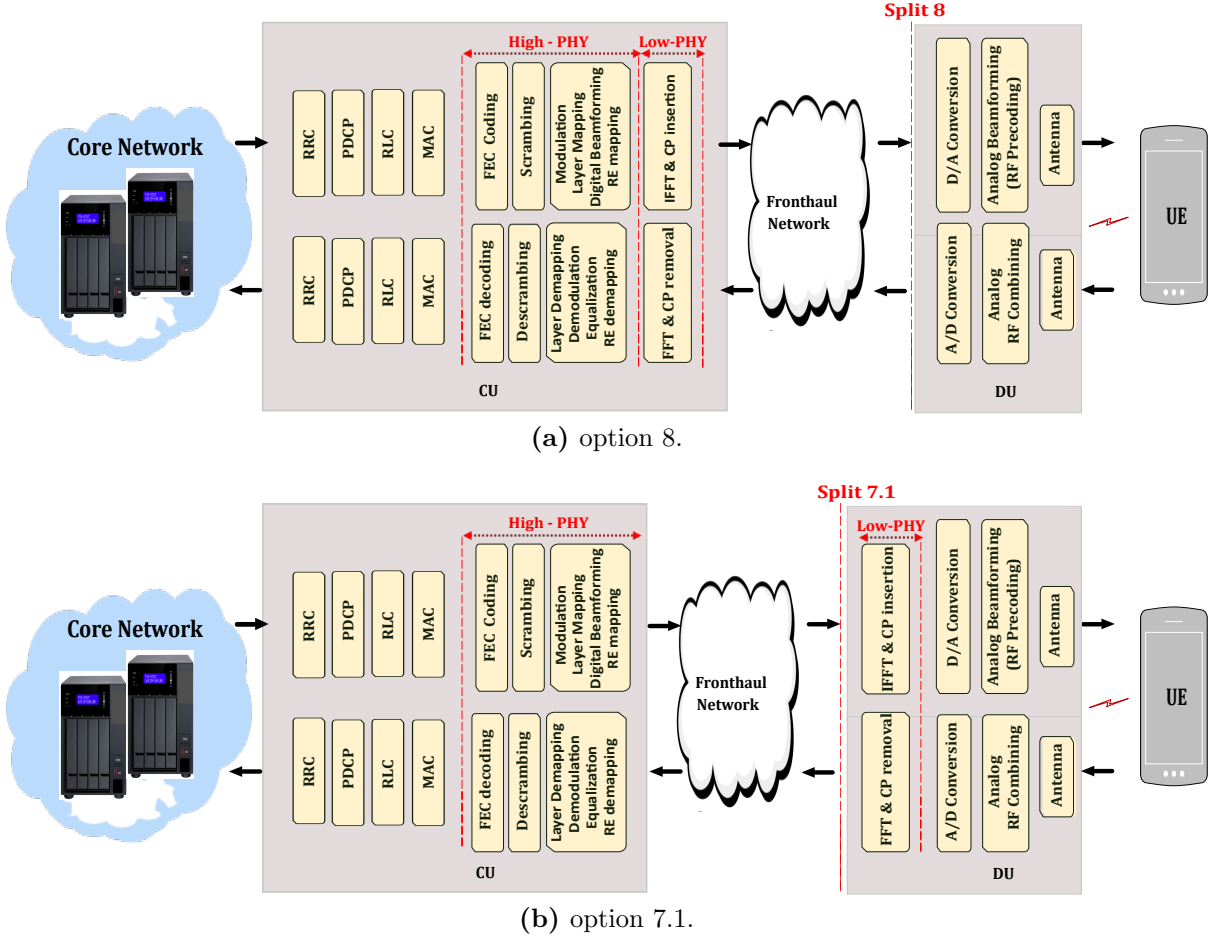


**Figure 5.1:** Emulated RAN with functional splits adopted for the experimental setup.

the entire physical layer (PHY) processing, data link layer processing of media access control (MAC), radio link control (RLC), packet data convergence protocol (PDCP) and network layer functions that include radio resource control (RRC) and internet protocol (IP) for control plane and user plane respectively.

For split option 7.1, extra functions are performed at the DU and these include: part of the low physical layer (Low-PHY) processing of the digitized waveform (fast Fourier transform (FFT)/ inverse fast Fourier transform (IFFT) and cyclic prefix insertion/removal), while the remaining PHY layer (High-PHY) functions, which include resource element (RE) mapping, digital beamforming, layer mapping, modulation, scrambling and forward error correction (FEC) coding are handled at the CU. However, it should be noted that single-input single-output (SISO) transmission mode is considered for this experiment, although the setup of Figure 5.1 can effectively supported MIMO processing and digital beamforming features. Meanwhile, the two E2E LTE networks are configured to operate with 5 MHz bandwidth for the purpose of mixing the generated signals with 5G to achieve joint transmission over an OWC link. The 4G yields a maximum throughput of 8 Mbps for the UL and 16 Mbps for the DL, the transport rates over the fronthaul are approximately 248 Mbps and 140 Mbps for split 8 and split

7.1, respectively, as measured by Wireshark protocol analyzer.

### 5.3.2 Optical–Wireless Mobile Fronthaul

To investigate the suitability of FSO transport solution as a MFH and analyze the performance of a coexisting 5G service with diverse 4G traffics, the experimental setup in Figure 5.2 is proposed. The 5G signal is designed off-line using Keysight’s Signal Studio and only implemented for the downlink direction for this work. Furthermore, a 100 MHz bandwidth 64QAM 5G signal located in the 3.5 GHz band is provided by a VSG which comprises an M8190A Arbitrary Waveform Generator (AWG) and E8267D PSG (both from Keysight). The 5G signal is transmitted on a single component carrier and in full compliance with the 3GPP specifications, having all the standardized channels, which include: primary synchronization signal (PSS), secondary synchronization signal (SSS), physical broadcast channel (PBCH), PBCH demodulation reference signal (DMRS), physical data shared channel (PDSCH) and PDSCH DMRS. Binary phase shift keying (BPSK) is employed for the PSS and SSS channels, quadrature phase shift keying (QPSK) is used for the PBCH and DMRS, while quadrature amplitude modulation with 64 symbols (64-QAM) is applied to the PDSCH.

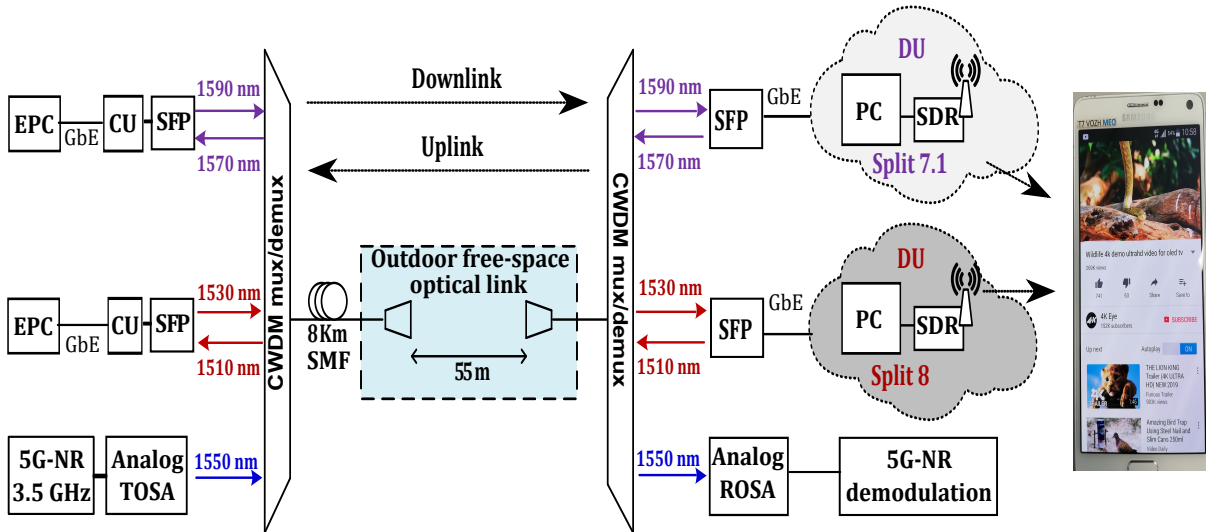


**Figure 5.2:** Experimental setup for the demonstration of heterogeneous 5G and 4G LTE fronthaul over a hybrid fiber-FSO link. The inset shows a photo of a mobile terminal downloading a 4K video using our E2E OAI-based LTE implementation.

Coarse wavelength division multiplexing (CWDM) technology is adopted to enable seamless coexistence of these radio signals over a single optical link. In addition, the small form-factor pluggable (SFP) transceivers and low-cost optical-to-electrical (O/E) converters provide interface with the optical fronthaul which is designed to demonstrate a hybrid fiber-wireless scenario. The transmission link consists of an 8 km single-mode fiber (SMF) which has about 2 dB loss and an outdoor FSO link; which is composed of two fiber collimators that are operating in the 1550 nm band with a full-angle divergence of  $0.017^\circ$  and a 24 mm lens diameter. To achieve a total transmission distance (55 m),



**Figure 5.3:** Snapshot of the FSO devices consisting of two fiber collimators and a two-inch mirror.

---

two-inch mirror is located half-way through the link at 27.5 m to double the transmission distance. At the antenna side, a CWDM mux / demux splits the signals for the different services along the UL and DL directions. Also included in the experimental setup are uncooled and directly modulated transmitter optical sub-assembly (TOSA) and a receiver optical sub-assembly (ROSA). The RF power driving the TOSA is about 3 dBm, which has been optimized for the experienced link loss. While the transmitted optical power is -3 dBm, the corresponding optimum received power at the ROSA is about -13 dBm, making an approximately 10 dB power budget. Since turbulence is normally expected to affect FSO transmission, therefore, to evaluate the performance degradation due to this effect, a wide bandwidth vector signal analyzer (Keysight's N9041B) is used to demodulate the received 5G signal after the ROSA. Finally, two COTS mobile terminals are connected to both on split 8 and split 7.1 4G LTE networks.

## 5.4 Experimental results

The mobile terminal is monitored during the experiment and continuous download of 4K video is observed throughout the measurement time, as can be seen in Figure 5.2 (a), while the 5G traffic is concurrently transmitted. Apparently, the coexistence of the 4G and 5G networks is noted from the RF spectrum captured by an antenna combined with the detected 5G spectrum is shown in Figure 5.4.

Also, it can be noted that the power fluctuations caused by FSO do not create any impact on the user experience because sufficient power budget is provided by the optical transceivers to tolerate these variations without any errors, since the FSO link for the 4G LTE services is located within a digital Ethernet-based fronthaul interface. Moreover, the SFP power budget is specified to be more than 30 dB, which is much larger than the overall loss consisting of 7.5 dB link loss, 1 dB loss in each CWDM mux/demux and

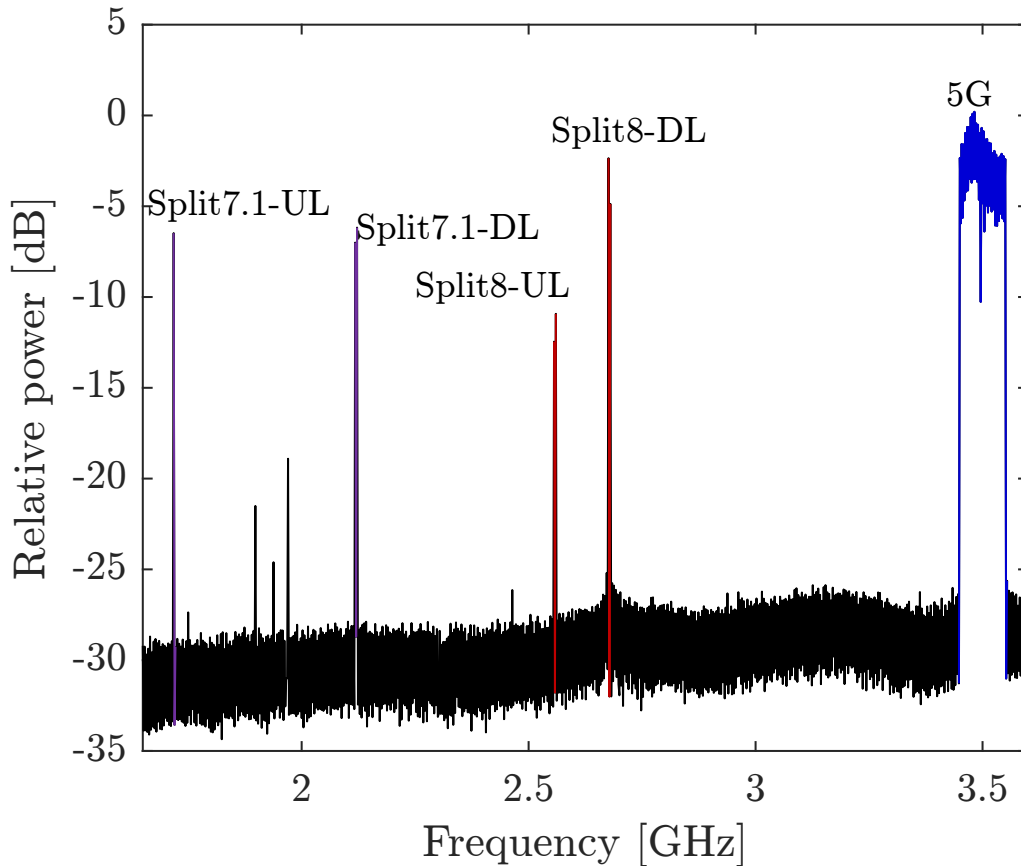


**Figure 5.4:** Measured spectra of both LTE signals measured with an antenna combined with the 5G signal after the photodetector.

the additional FSO loss due to atmospheric turbulence, pointing errors and mechanical vibrations. Conversely, since we are performing analog transmission of the 5G signal, the loss variations reflect on the measured Error Vector Magnitude (EVM) after detection.

To study the resilience of the 5G service against FSO power fluctuations, we present EVM measurements taken during 1 hour and a half in Figure 5.5. For performance benchmark, we compare these measurements to the case of a fronthaul link of only fiber transmission over 8 km. As noted in Fig. 5.5, a very stable EVM performance of 3.9% has been obtained throughout the entire measurement time without FSO. This EVM is limited by the performance of the low-cost optical transceivers. Conversely, the measured EVM shows significant variations over time when the FSO extension is utilized. Furthermore, it is observed that the EVM is below 5% in most cases and only in one measurement out of more than 250 measurements the obtained EVM is above the specified limit of 8% for a 64QAM signal [39]. For that extreme case, the power of the 5G signal measured after the ROSA was about 8 dB lower than that of fiber only transmission, as shown in Figure 5.6. It is also worth mentioning that we have not found any visible impact between the 5G and 4G systems in terms of throughput performance or reliability, as expected given the large guard band provided by the CWDM grid.



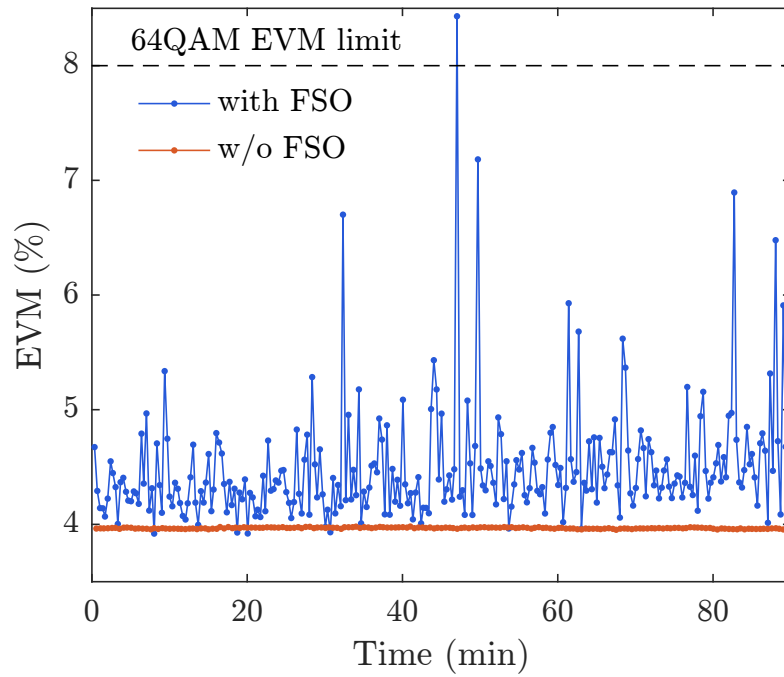


**Figure 5.5:** Measured EVM vs time for the 64QAM, 100 MHz 5G signal.

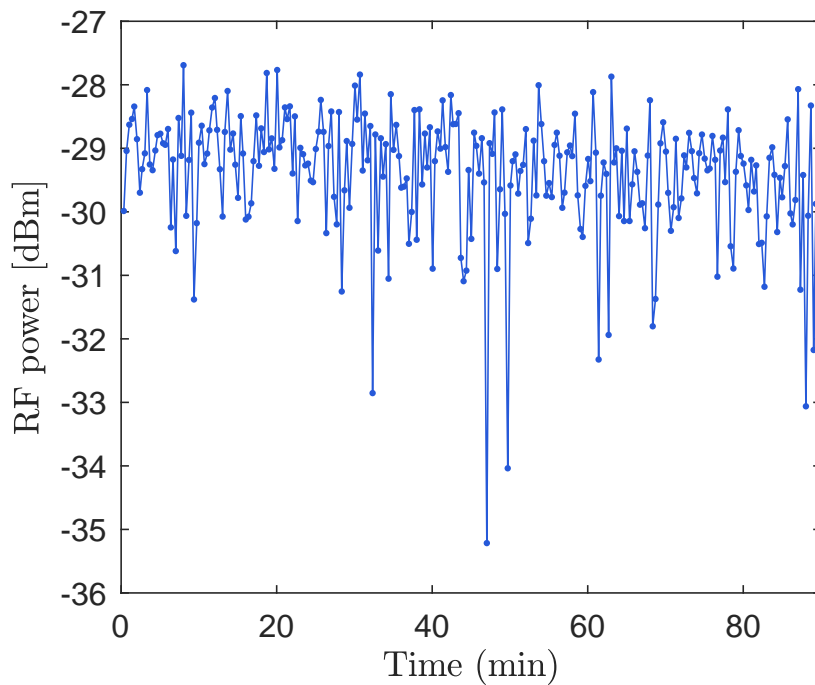


**Figure 5.6:** RF power vs time for the 5G signal.

---

In Figure 5.7, an example of the measured constellations with the different data and

---

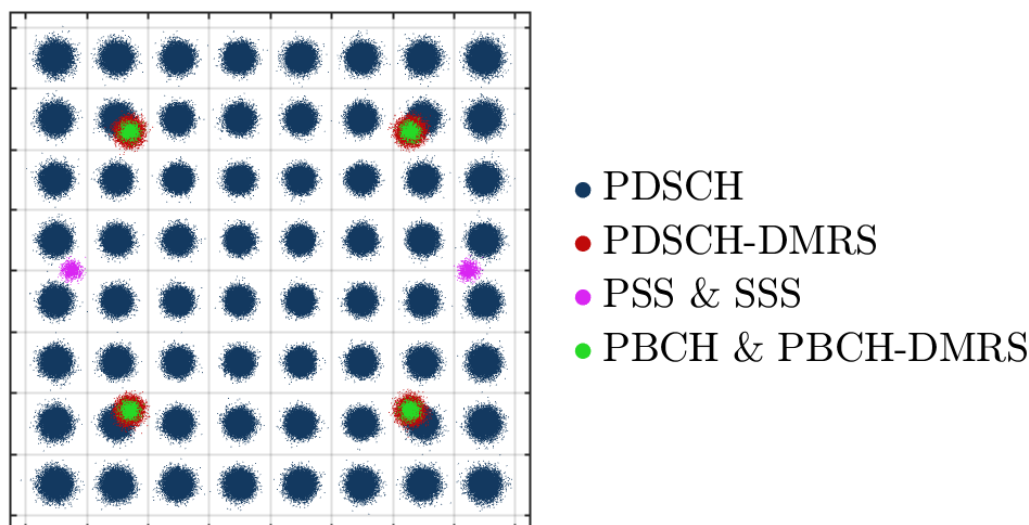


**Figure 5.7:** Measured constellation of the 5G signal after 8 km fiber and 55 m free-space optics link. The different points correspond to user data in the physical downlink shared channel (PDSCH), PDSCH demodulation reference signal (PDSCH-DMRS), primary and secondary synchronization channels (PSS and SSS), and physical broadcast channel (PBCH).

synchronization channels is presented, which corresponds to a case with a minor effect of FSO distortions which has a measurement of 4.1% EVM, although larger noise is observed in the outer points of the constellation. Moreover, the transceiver could be optimized to compensate for non-linearity to possibly enable a further reduction of the EVM, thereby allowing possible transmission of 256 QAM (limit EVM of 3.5%) when the turbulence effect on the FSO channel is low. However, the overall performance could be improved by using more advanced transceivers, e.g. using external modulation and/or avalanche photodiodes (APD).

## 5.5 Summary

In this chapter we have proposed a hybrid digital-analog fiber-wireless fronthaul architecture supporting a full-fledged 4G LTE network together with an analog 5G downlink, according to the corresponding 3GPP recommendations (Release 12 for 4G and Release 15 for 5G). By using commercially available low-cost CWDM-compliant components and extending the fiber link with free space optical channel, we propose and experimentally assess the coexistence of both digital and analog radio-over-fiber (ARoF) fronthauling to seamlessly achieve the joint transmission of an analog 100 MHz 64QAM-modulated 5G signal with digital 4G LTE signals of different functional splits specifically, options 8 and 7.1 over a hybrid link consisting of 8 km fiber and 55 m FSO. In addition, the robustness of outdoor RoFSO transmission was demonstrated following the results

## 5.5. Summary

---

of the EVM measurements taken over long period.

In a nutshell, the results presented do not only demonstrate the benefits of employing hybrid analog-digital transmission of heterogeneous, but it also validates their compatibility with a high-capacity FSO-based wireless fronthaul extension, thus paving the way for a sustainable development of novel 5G and beyond scenarios coexisting with legacy RAN deployments.

## References

- [1] L. C. Alexandre, A. L. De Souza Filho, and A. C. Sodr e, “Indoor Coexistence Analysis Among 5G New Radio, LTE-A and NB-IoT in the 700 MHz Band,” *IEEE Access*, vol. 8, pp. 135 000–135 010, 2020.
- [2] L. Wan, Z. Guo, and X. Chen, “Enabling Efficient 5G NR and 4G LTE Coexistence,” *IEEE Wireless Communications*, vol. 26, no. 1, pp. 6–8, 2019.
- [3] L. Wan *et al.*, “4G/5G Spectrum Sharing: Efficient 5G Deployment to Serve Enhanced Mobile Broadband and Internet of Things Applications,” *IEEE Vehicular Technology Magazine*, vol. 13, no. 4, pp. 28–39, 2018.
- [4] I. A. Alimi, A. L. Teixeira, and P. P. Monteiro, “Toward an Efficient C-RAN Optical Fronthaul for the Future Networks: A Tutorial on Technologies, Requirements, Challenges, and Solutions,” *IEEE Communications Surveys Tutorials*, vol. 20, no. 1, pp. 708–769, Firstquarter 2018.
- [5] A. O. Mufutau *et al.*, “Demonstration of a hybrid optical fiber–wireless 5g fronthaul coexisting with end-to-end 4g networks,” *IEEE/OSA Journal of Optical Communications and Networking*, vol. 12, no. 3, pp. 72–78, 2020.
- [6] 3GPP, “Technical Specification Group Services and System Aspects (Release 15),” 3rd Generation Partnership Project, Tech. Rep., 2019.
- [7] T. Nakamura, “5g evolution and 6g,” in *2020 IEEE Symposium on VLSI Technology*, 2020, pp. 1–5.
- [8] C. Song *et al.*, “Hierarchical edge cloud enabling network slicing for 5G optical fronthaul,” *IEEE/OSA Journal of Optical Communications and Networking*, vol. 11, no. 4, pp. B60–B70, April 2019.
- [9] W. Lee, T. Na, and J. Kim, “How to Create a Network Slice? - A 5G Core Network Perspective,” in *21st International Conference on Advanced Communication Technology (ICACT)*, Feb 2019, pp. 616–619.
- [10] C. Bockelmann *et al.*, “Towards Massive Connectivity Support for Scalable mMTC Communications in 5G Networks,” *IEEE Access*, vol. 6, no. ii, pp. 28 969–28 992, 2018.
- [11] A. Ghosh, A. Maeder, M. Baker, and D. Chandramouli, “5G Evolution: A View on 5G Cellular Technology Beyond 3GPP Release 15,” *IEEE Access*, vol. PP, pp. 1–1, 09 2019.
- [12] B. Imanilov, M. Sauer, and A. Kobayakov, “Optical Fiber in Wireless Networks: From Radio-over-Fiber DAS to 5G RAN,” in *2019 IEEE Photonics Conference (IPC)*, Sep. 2019, pp. 1–2.

- [13] P. Perry *et al.*, “All-Optical Network Capacity for 5G Cellular Fronthaul,” in *21st International Conference on Transparent Optical Networks (ICTON)*, 07 2019, pp. 1–4.
- [14] K. Zeb, X. Zhang, and Z. Lu, “High Capacity Mode Division Multiplexing Based MIMO Enabled All-Optical Analog Millimeter-Wave Over Fiber Fronthaul Architecture for 5G and Beyond,” *IEEE Access*, vol. 7, pp. 89 522–89 533, 2019.
- [15] D. Chitimalla, K. Kondepu, L. Valcarenghi, M. Tornatore, and B. Mukherjee, “5G Fronthaul–Latency and Jitter Studies of CPRI Over Ethernet,” *Journal of Optical Communications and Networking*, vol. 9, no. 2, p. 172, 2017.
- [16] CPRI, “Common Public Radio Interface,” <https://orcip.pt/>, Common Public Radio Interface, 2021, accessed: 2021-05-06.
- [17] 3GPP, “Technical specification group radio access network; study on cu-du lower layer split for nr; (release 15),” 3rd Generation Partnership Project, Tech. Rep., 2017.
- [18] M. Gilson, R. Mackenzie, A. Sutton, and J. Huang, “NGMN Overview on 5G RAN Functional Decomposition by NGMN Alliance,” Next Generation Mobile Networks Ltd, Tech. Rep., 2018.
- [19] G. Otero Pérez, D. Larrabeiti López, and J. A. Hernández, “5G New Radio Fronthaul Network Design for eCPRI-IEEE 802.1CM and Extreme Latency Percentiles,” *IEEE Access*, vol. 7, pp. 82 218–82 230, 2019.
- [20] D. Novak *et al.*, “Radio-Over-Fiber Technologies for Emerging Wireless Systems,” *IEEE Journal of Quantum Electronics*, vol. 52, no. 1, pp. 1–11, Jan 2016.
- [21] S. Yao *et al.*, “Non-orthogonal uplink services through co-transport of d-rof/a-rof in mobile fronthaul,” *Journal of Lightwave Technology*, vol. 38, no. 14, pp. 3637–3643, 2020.
- [22] T. Salgals, I. Kurbatska, V. Bobrovs, and S. Spolitis, “Research of pam-4 modulated wdm-pon architecture for 5g millimeter-wave hybrid photonics-wireless interface,” in *2019 Photonics Electromagnetics Research Symposium - Fall (PIERS - Fall)*, 2019, pp. 728–734.
- [23] J. J. Vegas Olmos, T. Kuri, and K. Kitayama, “60-ghz-band 155-mb/s and 1.5-gb/s baseband time-slotted full-duplex radio-over-fiber access network,” *IEEE Photonics Technology Letters*, vol. 20, no. 8, pp. 617–619, 2008.
- [24] M. A. Vázquez, L. Blanco, and A. I. Pérez-Neira, “Hybrid Analog–Digital Transmit Beamforming for Spectrum Sharing Backhaul Networks,” *IEEE Transactions on Signal Processing*, vol. 66, no. 9, pp. 2273–2285, May 2018.

- 
- [25] R. G. Stephen and R. Zhang, "Joint Millimeter-Wave Fronthaul and OFDMA Resource Allocation in Ultra-Dense CRAN," *IEEE Transactions on Communications*, vol. 65, no. 3, pp. 1411–1423, March 2017.
- [26] T. Kawanishi, "THz and Photonic Seamless Communications," *Journal of Lightwave Technology*, vol. 37, no. 7, pp. 1671–1679, April 2019.
- [27] P. T. Dat, A. Kanno, N. Yamamoto, and T. Kawanishi, "Seamless Convergence of Fiber and Wireless Systems for 5G and Beyond Networks," *Journal of Lightwave Technology*, vol. 37, no. 2, pp. 592–605, Jan 2019.
- [28] I. Alimi *et al.*, "Challenges and Opportunities of Optical Wireless Communication Technologies," *Optical Communication Technology*, 2017.
- [29] N. A. Gunathilake and M. Z. Shakir, "Empirical performance evaluation of FSO availability under different weather conditions," in *2017 8th International Conference on the Network of the Future (NOF)*, Nov 2017, pp. 156–158.
- [30] I. A. Alimi, A. O. Mufutau, A. L. Teixeira, and P. P. Monteiro, "Performance Analysis of Space-Air-Ground Integrated Network (SAGIN) Over an Arbitrarily Correlated Multivariate FSO Channel," *Wireless Personal Communications*, vol. 100, no. 1, pp. 47–66, May 2018.
- [31] Y. Dong, M. Z. Hassan, J. Cheng, M. J. Hossain, and V. C. M. Leung, "An Edge Computing Empowered Radio Access Network with UAV-Mounted FSO Fronthaul and Backhaul: Key Challenges and Approaches," *IEEE Wireless Communications*, vol. 25, no. 3, pp. 154–160, JUNE 2018.
- [32] J. Bohata *et al.*, "24–26 GHz radio-over-fiber and free-space optics for fifth-generation systems," *Optics Letters*, vol. 43, 02 2018.
- [33] O. Alkhalifah, O. Alrabiah, A. Ragheb, M. A. Esmail, and S. Alshebeili, "Investigation and demonstration of 5G signal transmission over fiber/FSO/wireless links," in *2017 International Conference on Electrical and Computing Technologies and Applications (ICECTA)*, Nov 2017, pp. 1–4.
- [34] A. Lorences-Riesgo *et al.*, "200 Gbit/s Free-Space Optics Transmission using a Kramers-Kronig Receiver," in *2019 Optical Fiber Communications Conference and Exhibition (OFC)*, March 2019, pp. 1–3.
- [35] Y. Alfadhli *et al.*, "Real-Time FPGA Demonstration of Hybrid Bi-Directional MMW and FSO Fronthaul Architecture," in *2019 Optical Fiber Communications Conference and Exhibition (OFC)*, March 2019, pp. 1–3.
- [36] L. M. P. Larsen, A. Checko, and H. L. Christiansen, "A Survey of the Functional Splits Proposed for 5G Mobile Crosshaul Networks," *IEEE Communications Surveys Tutorials*, vol. 21, no. 1, pp. 146–172, Firstquarter 2019.
-

- [37] C. Y. Chang, N. Nikaein, R. Knopp, T. Spyropoulos, and S. S. Kumar, “FlexCRAN: A flexible functional split framework over ethernet fronthaul in Cloud-RAN,” *IEEE International Conference on Communications*, 2017.
- [38] OpenAirInterface Software Alliance (OSA), “OpenAirInterface: 5G Software Alliance for Democratising Wireless Innovation,” <https://openairinterface.org/getting-started/openairinterface-an-open-cellular-ecosystem/>, [Online; accessed 2021-10-06].
- [39] 3GPP, “User Equipment (UE) radio transmission and reception; Part 1: Range 1 Standalone (Release 15),” 3rd Generation Partnership Project, Tech. Rep., 2018.





# Chapter 6

## Conclusions and Future Work

Technology-driven services and applications are increasingly embedded in all aspects of global society going by the increasing volume of data traffic generated from proliferation of connected devices worldwide. Mobile networks, as key enablers, are constantly being redesigned to meet new service requirements. In addition, future networks are expected to involve heterogeneous communication systems that can support multiple radio access technologies. Considering the diversity of services to be supported, it becomes imperative to have robust radio access networks with the required flexibility.

While there is significant research work aimed at achieving good quality of service delivery, tremendous efforts are also being made to design and deploy the radio access network (RAN) architecture for 5G and B5G [1, 2]. Obviously, the transport segment of the mobile network needs to be positioned appropriately to support these different services. In this context, various mobile backhaul/fronthaul solutions have been investigated aiming at upgrading existing mobile networks to improve their overall performance. This work therefore contributes to the scope of research efforts on the suitability of mobile fronthaul for diverse mobile services. In this final chapter, the most relevant conclusions are summarized and the future research topics are discussed.

### 6.1 Conclusions

The first major contribution of this thesis is presented in Chapter 5 where a hybrid mobile fronthaul is proposed that takes advantage of both fiber and free space optical links to provide a robust transport solution for joint transmission of 4G and 5G signals. For the demonstration, an analog 100 MHz 64QAM modulated 5G signal is transmitted along with digital 4G LTE signals of different functional splits, namely options 8 and 7.1, over a hybrid link consisting of 8 km optical fiber and 55 m FSO. Moreover, in this work, we have experimentally demonstrated an architectural option for the transition from 4G to 5G, where the coexistence of 4G and 5G services is supported. Based on this, we have also proposed and experimentally demonstrated a coarse wavelength-division multiplexing-compatible optical access network for joint provisioning of 4G/5G RAN services to seamlessly support the coexistence of digital and analog radio-over-fiber (ARoF) fronthauling. The result of EVM measurements over a long period of time

shows the robustness of outdoor RoFSO transmission over this period under relatively unperturbed weather conditions. As far as we know, the technology described above has never been reported before the publication of our article [3].

We also demonstrated the transmission of real-time radio signals over a passive optical network (RFoPON) as part of the contribution of this thesis as reported in Chapter 4 and published in [4]. In this work, a NG-PON based fronthaul, which is integrated to a SDR based radio access network that is developed on open-source platform to provide real-time signal, is experimentally validated. While successful transmission is achieved, the results presented show that the performance of C-RAN is limited by the delay overhead requirement of the passive optical network. A unique feature of the developed testbed is that it can be ease integration with different fronthaul solutions. In view of the continuous need to improve on the aforementioned transport solutions, it is therefore desirable to develop a testbed platform as contribution to research infrastructure for validating and testing of various optical-wireless transport solutions. In this regard, this thesis has presented the exploitation of softwarization and virtualization technologies to develop an open-source based testbed built on a modified C-RAN architecture to test mobile fronthaul solutions as a significant contribution of this work. This testbed has also facilitated the research work reported in [5] and contributed to [6].

In addition to the above main contributions, thesis has presented a comprehensive review of RAN architectures particularly modifications to the widely studied C-RAN which is characterised by challenges associated with the stringent requirements on the fronthaul when transmitting IQ signals. As a measure to ameliorate this challenge, proposals on functional split options have been extensively reviewed in this thesis, while concepts leading to flexibility of RAN to meeting different categories of services has also been discussed. Furthermore, thesis has presented basic techniques for transporting RF signal over fiber, involving analog and digital signal RF transmission over fiber schemes and highlighting the strengths and weaknesses of each scheme. Advancing the aforementioned transmission schemes to MFH in RAN architecture, a number of possible adoptable mobile transport solutions have been discussed with emphasis on technologies that could enable high bit rate and low-latency traffic while achieving high capacity as envisioned for 5G and future networks.

## 6.2 Future Work

Due to rapid advancement in innovative services supported by evolving telecommunication technologies, 5G is reaching full maturity while extensive research efforts are focused on studying the upcoming sixth generation (6G) network. Be that as it may, a reliable and efficient transmission system is key towards delivering of the envisioned services and should therefore not only support the current mobile network, but also allow for seamless upgrades, optimization and reconfiguration to meet the demands of future networks. Therefore, mobile transport solutions based on OWC transmission and PON systems, among others, can provide the required support for the Beyond 5G network. In view of the above, the research presented in this thesis has opened new possibilities and research directions for a mobile transport solution are open for investigation. Hence, it would be interesting to exploit the following challenging topics:

- As advance optical technologies is pertinent for full implementation of full 5G and upcoming 6G mobile network [7], FSO communication link combined with RF channel can be a promising technique to support the required demand for high speed transmission while equipping the entire transmission system with resiliency. Although, hybrid RF/FSO and relay-assisted RF/FSO have been extensively studied, mostly focusing on theoretical modelling and analysis of techniques to mitigate atmospheric impairments like fog and scintillation by optimising the pointing error (PE), angular fluctuations, bit error rate (BER), average symbol error rate (ASER) and the outage probability, etc. When applied to supporting ultra-low-latency and high rate dependent services like augmented reality (AR) and haptic communication, the link state switching that is associated with the hybrid RF/FSO transmission scheme is critical and this remains a challenge. Therefore, a novel robust system that is built on machine learning and artificial intelligence (AI) is desirable not only to enable fast and intelligent RF/FSO switching but to also optimise the PE and BER, and thus, improving the overall system perform. In addition, the proposed system will be practically demonstrated for transporting real-time 5G signal and validated using the testbed presented in this thesis.
- The PON systems have been extensively studied and have found widespread application in broadband deployment for mobile network capacity enhancement and high speed transmission. However, these gains come at a cost of latency and jitter overheads normally associated with PON systems which reflected on the results presented in Chapter 4. Moreover, to address the stringent requirements, several optimization techniques involving dynamic wavelength and bandwidth allocation algorithms have been proposed. One recent approach reported in [8] involving orthogonal and non-orthogonal multi-access resources is interesting and this could be improved upon by proposing an holistic algorithm for high speed PON systems.

## References

- [1] C. Barjau, M. Säily, and D. G. Barquero, “Enabling sfn transmissions in 5g cloud-ran deployments,” in *2019 IEEE International Symposium on Broadband Multimedia Systems and Broadcasting (BMSB)*, 2019, pp. 1–5.
- [2] J. Pedreno-Manresa, P. S. Khodashenas, J. Izquierdo-Zaragoza, and P. Pavon-Marino, “Improved User Experience by Dynamic Service Handover and Deployment on 5G Network Edge,” in *2019 21st International Conference on Transparent Optical Networks (ICTON)*, 2019, pp. 1–4.
- [3] A. O. Mufutau *et al.*, “Demonstration of a hybrid optical fiber–wireless 5g fronthaul coexisting with end-to-end 4g networks,” *IEEE/OSA Journal of Optical Communications and Networking*, vol. 12, no. 3, pp. 72–78, 2020.
- [4] A. O. Mufutau, F. P. Guiomar, A. Oliveira, and P. P. Monteiro, “Software-defined radio enabled cloud radio access network implementation using openairinterface,” *Wireless Personal Communications*, Sep 2021.
- [5] A. O. Mufutau, F. P. Guiomar, M. A. Fernandes, A. Oliveira, and P. P. Monteiro, “On the suitability of vlc enabled fronthaul for future mobile network,” in *2021 Telecoms Conference (ConfTELE)*, 2021, pp. 1–4.
- [6] P. P. Monteiro *et al.*, “Flexible optical and wireless testbed for 5g and beyond communication systems,” in *OSA Advanced Photonics Congress (AP) 2019 (IPR, Networks, NOMA, SPPCom, PVLED)*. Optical Society of America, 2019, p. JT4A.15.
- [7] L. U. Khan, I. Yaqoob, M. Imran, Z. Han, and C. S. Hong, “6g wireless systems: A vision, architectural elements, and future directions,” *IEEE Access*, vol. 8, pp. 147 029–147 044, 2020.
- [8] E. Inaty, R. J. Raad, and M. Maier, “Generalized multi-access dynamic bandwidth allocation scheme for future generation pons: A solution for beyond 5g delay/jitter sensitive systems,” *Journal of Lightwave Technology*, pp. 1–1, 2021.

## Appendix A

# OpenAirInterface Monolithic eNB with USRP NI-2953R

### **Abstract**

The goal of this document is to guide its reader on the installation of OpenAirInterface (OAI) eNodeB software in a given PC with specific consideration for USRP NI-2953R RF device setup. This document assumes user has acquired the required hardware. The configuration of the OAI EPC or UE is not addressed here.

## **1 Introduction**

OpenAirInterface (OAI), developed by EURECOM, is an open-source software-based implementation of the LTE system spanning the full protocol stack of 3GPP standard both in E-UTRAN and EPC. It can be used to build and customize a LTE base station (OAI eNB), a user equipment (OAI UE) and a core network (OAI EPC) on a PC. OpenAirInterface is equipped with facility to monitor in real-time the entire network, including mobile devices. Hardware and source requirement can be found in [1]. In addition, real physical interface can be created when used with transceivers or network's part can be emulated using its OASIM (OpenAirInterface System Emulation) module.

Structured as an hand-on installation manual, this document helps to mitigate the complex tasks of installing OAI and also guide on how to easily configure it. The next sections describe the installation procedure with particular focus on OAI setup with National Instrument NI-2953R USRP.

---

## 2 Setting up the Hardware and Kernel

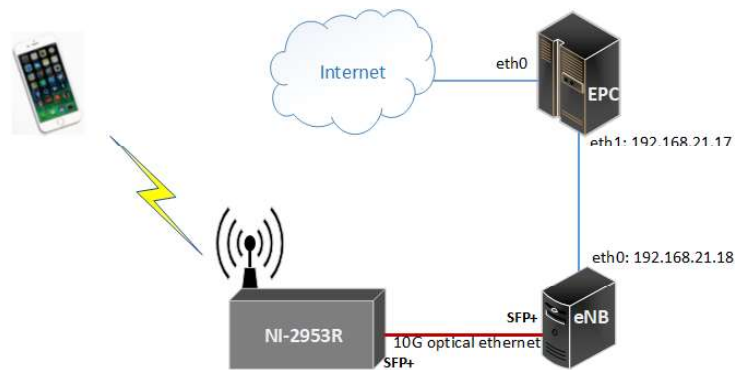


Figure 1: Example network

This guide assumes the user has acquired a PC of the model:  
Ultra Compact PC Kit Gigabyte Brix S GB-Bki7HA-7500 BWEK  
It is assumed that the user also has another PC capable of running the EPC  
and also an USRP B210. Figure 1 illustrates the network setup.  
The operating system used in this guide is:  
64-bit Ubuntu 16.04.2 LTS.  
Proceed to install the operating system in the PC.

### 2.1 Low latency kernel

After installing the Ubuntu operating system, proceed to install a low latency kernel. To do this, write at the command line:

```
sudo apt-get install linux-image-4.15.0.23-lowlatency linux-headers-4.15.0.23-lowlatency linux-image-4.13.0.46-lowlatency linux-headers-4.13.0.46-lowlatency
```

Restart PC and press "Esc" at boot.  
Select "Advanced options for Ubuntu"  
Select "Ubuntu, with Linux 4.8.0-58-lowlatency"  
At the command line write:

```
uname -a
```

to verify that the system has booted with the low-latency kernel  
If desirable, you may remove the generic kernel to avoid always having to select the low-latency kernel at startup. Write at the command line:

```
dpkg --list | grep linux-image
```

to see the installed kernels. Remove all of them except the low-latency kernel. To do this, for example, to remove these two kernels write at the command line:

```
sudo apt-get purge linux-image-4.10.0-28-generic  
sudo apt-get purge linux-image-4.13.0-37-generic
```

Then write:

```
sudo update-grub2
```

and reboot.

REMEMBER to boot first in low-latency kernel before removing the other kernels!

## 2.2 Power management

Next we proceed to ensure that the CPU cores are always at full speed.

Restart PC and Press “Del” to enter BIOS configuration.

At “Advanced” tab select “CPU Configuration”.

At “CPU C states” select “Disabled”.

At “CPU P states” select “Disabled”.

At “Turbo Mode” select “Disabled”.

Proceed to save and exit BIOS configuration.

To disable hyperthreading on Ubuntu write at the command line:

```
sudo nano /etc/rc.local
```

```
for CPU in /sys/devices/system/cpu/cpu[0-9]*; do  
  CPUID=$(basename $CPU | cut -b4-  
  echo -en "CPU: $CPUID\t"  
  [ -e $CPU/online ] && echo "1" > $CPU/online  
  THREAD1=$(cat $CPU/topology/thread_siblings_list | cut -f1 -d  
  ↪ ,'  
  if [ $CPUID = $THREAD1 ]; then
```



---

```
    echo "-> enable"
    [ -e $CPU/online ] && echo "1" > $CPU/online
else
    echo "-> disable"
    echo "0" > $CPU/online
fi
done
```

Proceed to reboot the PC.

To disable frequency scaling write at the command line:

```
sudo apt-get install cpufrequtils
```

Edit the following file:

```
sudo nano /etc/default/cpufrequtils
```

Add the following line to it:

```
GOVERNOR="performance"
```

Save and exit.

Then enter at the command line:

```
sudo update-rc.d ondemand disable
sudo /etc/init.d/cpufrequtils restart
```

We can check that the CPU cores are at the maximum speed by writing at the command line:

```
cpufreq-info
```

Next, we need to disable p-states and c-states in Linux. To do that write at the command line:

```
sudo nano /etc/default/grub
```

and replace the line:

```
GRUB_CMDLINE_LINUX_DEFAULT ...
```

with the following line:

```
GRUB_CMDLINE_LINUX_DEFAULT="quiet intel_pstate=disable
↪ processor.max_cstate=1 intel_idle.max_cstate=0 idle=poll
↪ "
```

Save and exit. Write in the command line:

```
sudo update-grub
```

Next, we need to disable powerclamp. To do that, write in the command line:

```
sudo nano /etc/modprobe.d/blacklist.conf
```

and add the following line at the end of the file:

```
blacklist intel_powerclamp
```

Save, exit and reboot

Install i7z utility to check the CPU with:

```
sudo apt-get install i7z
sudo i7z
```

The C0 states should be at 100% and the other states should be at 0%.  
WARNING: In the hardware tested we could not bring C1 states to 0 (they were at 7.24%).

### 3 Setting up the OAI eNB software

To get the OAI eNB source code, install git first by writing at the command line:

```
sudo apt-get update
sudo apt-get install subversion git
```

Add a certificate from gitlab.eurecom.fr to your Ubuntu installation:

```
echo -n | openssl s_client -showcerts -connect gitlab.eurecom.
↪ fr:443 2\textgreater{/dev/null | sed -ne '/-BEGIN
↪ CERTIFICATE-/,/-END CERTIFICATE-/p' | sudo tee -a /etc/
↪ ssl/certs/ca-certificates.crt
```

If you do not have root access to /etc/ssl directory, disable certificate check with (you probably don't need to do this):

```
git config --global http.sslverify false
```

---

Then proceed to checkout RAN repository (eNB RAN + UE RAN) by writing at the command line:

```
git clone https://gitlab.eurecom.fr/oai/openairinterface5g.git
```

### 3.1 Conversion of NI-2953R to Ettus X310: Uploading of X310 firmware

OAI does not directly support NI-2953R USRP, so there is need to convert it to its Ettus equivalent (X310) by uploading X310 firmware. Essentially, it is advised to do this after coning the OAI eNB software in your system.

To load FPGA firmware through 10G Ethernet connection. The SFP+ transceiver module must be in port 1 of the USRP. Ensure that your PC network interface is set to

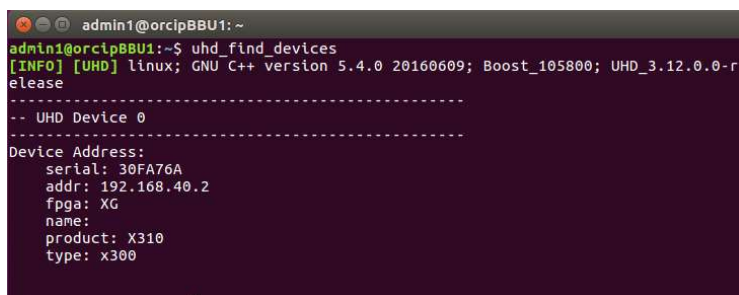
```
192.168.40.1
mtu 9000      #for 10 GigE
```

Then, type :

```
uhd_image_loader --args="type=x310,addr=192.168.40.2" --fpga-
↪ path="/usr/share/uhd/images/usrp_x310_fpga_XG.bit"
```

Next step is to check if the USRP device is communicating with the host PC. This can be done bu using the two commands below and the responses should be similar to Figures 2 and 3.

```
sudo uhd_find_devices
```



```
admin1@orcipBBU1: ~
admin1@orcipBBU1:~$ uhd_find_devices
[INFO] [UHD] linux; GNU C++ Version 5.4.0 20160609; Boost_105800; UHD_3.12.0.0-r
elease
-----
-- UHD Device 0
-----
Device Address:
  serial: 30FA76A
  addr: 192.168.40.2
  fpga: XG
  name:
  product: X310
  type: x300
```

Figure 2: Expected response of usrp find command

```
sudo uhd_usrp_probe
```

```
admin1@orcipBBU1: ~
-----
Name: ad9146
Gain Elements: None
-----
TX Dboard: B
ID: CBX-120 (0x0084)
Serial: 30F1ECB
-----
TX Frontend: 0
Name: CBX-120 TX
Antennas: TX/RX, CAL
Sensors: lo_locked
Freq range: 1200.000 to 6000.000 MHz
Gain range PGA0: 0.0 to 31.5 step 0.5 dB
Bandwidth range: 120000000.0 to 120000000.0 step 0.0 Hz
Connection Type: QI
Uses LO offset: No
-----
TX Codec: B
Name: ad9146
Gain Elements: None
-----
RFNoC blocks on this device:
* DmaFIFO_0
* Radio_0
* Radio_1
* DDC_0
* DDC_1
* DUC_0
* DUC_1
admin1@orcipBBU1:~$
```

Figure 3: Expected response of usrp probe command

It is recommended that the network be tuned to optimize the performance of the link. This could be achieved by performing the following task:

---

```
sudo ethtool -g enp2s0f1 ;# enp2s0f1 is the interface name

sudo ethtool -G enp2s0f1 tx 4096 rx 4096 # if 4096 is the
    ↪ maximum obtained for the above command

sudo gedit /etc/sysctl.conf ;
#add the following to any line in the file:

net.core.rmem_max=33554432
net.core.wmem_max=33554432
```

### 3.2 Compiling and Editing soft-modem script file

It is important to upgrade the oai software to the latest developed version to obtain good performance of the setup.

```
cd openairinterface5g # Press ENTER key
git checkout develop
git pull
```

Edit eNB config file:

```
nano ~/openairinterface5g/targets/PROJECTS/GENERIC-LTE-EPC/CONF
    ↪ /enb.band7.tm1.usrpX310.conf
```

and replace the following parameters with the values given below:

```
mobile_country_code = "268";
mobile_network_code = "08";
```

Then replace the mme\_ip\_address with your configured ip address of mme. Replace the enB interface names and ip addresses for S1\_MME and for S1U. The edited eNB config file should have similar lines to this:

```
Active_eNBs = ( "eNB_Eurecom_LTEBox");
# Asn1_verbosity, choice in: none, info, annoying
Asn1_verbosity = "none";
```

```
eNBs =
(
{
////////// Identification parameters:
eNB_ID = 0xe00;

cell_type = "CELL_MACRO_ENB";

eNB_name = "eNB_Eurecom_LTEBox";

// Tracking area code, 0x0000 and 0xffff are reserved
  ↪ values
tracking_area_code = "1";

mobile_country_code = "268";

mobile_network_code = "08";

tr_s_preference = "local_mac"
.
.
.
////////// MME parameters:
mme_ip_address = ( { ipv4 = "192.168.21.17";
                    ipv6 = "192:168:30::17";
                    active = "yes";
                    preference = "ipv4";
                    }
                );

NETWORK_INTERFACES :
{

    ENB_INTERFACE_NAME_FOR_S1_MME = "enp0s31f6";
    ENB_IPV4_ADDRESS_FOR_S1_MME = "192.168.21.18/24";
```

where `mme_ip_address` is the network interface's IP address of your EPC/HSS, and `NETWORK_INTERFACE` is your eNB related network interface infor-

---

mation.

### 3.3 Building the OAI eNB

Build and run OAI eNB by typing at the command line:

```
cd ~/openairinterface5g
source oaienv
./cmake_targets/build_oai -w USRP -x -c --eNB
cd cmake_targets/lte_build_oai/build
sudo -E ./lte-softmodem -O $OPENAIR_DIR/targets/PROJECTS/
↳ GENERIC-LTE-EPC/CONF/enb.band7.tm1.usrpX310.conf
```

If all went well, you should have an OAI eNB configured in your PC and may proceed to test it in a network similar to the one displayed in Figure 1!

## 4 Running the OAI eNB and Testing the Setup

Ensure that the eNB host PC has physical Ethernet connection to the epc. At this juncture, ssh already installed will be used to remotely run the hss, mme and spgw in that order on separate terminal.

On hss terminal, do:

```
cd openair-cn
source oaienv
cd scripts
./run_hss
```







## 4.2 likely problems and resolutions

eNB reporting spontaneous 'LLLL'

- Check if the power management and clock frequency scaling is properly configured.
- Reduce the rx gain in the eNB script file to 105,95 or 85.
- Set the RB parameter to 25, then try 50
- Adjust the CPU affinity or reduce the graphics processing workload of the CPU. A simple way of doing this is to boot your Ubuntu to recovery mode

## Appendix B

### OpenAirInterface with Functional Split 7.2

### Abstract

The goal of this document is to guide the user in the installation of OpenAirInterface NGFI with RCC/RRU Functional Split. The configuration of the OAI EPC or UE is not addressed here.

## 1 Introduction

OpenAirInterface (OAI) is an open-source software-based implementation of the LTE system spanning the full protocol stack of 3GPP standard both in E-UTRAN and EPC. It can be used to build and customize a LTE base station (OAI eNB), a user equipment (OAI UE) and a core network (OAI EPC) on a PC. Additionally it allows the functional split of the eNB in two systems: the RCC and the RRU. This document is meant to aid the user in installing OAI RCC/RRU functional split "NGFI IF4.5" with 25 Resource Blocks. The next sections describe the procedure followed to install and run the software in the RCC and in the RRU.

## 2 Setting up the Hardware and Kernel

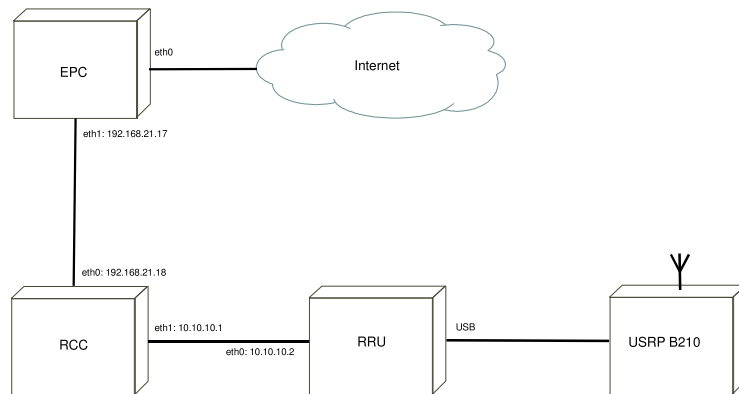


Figure 1: Example network

This guide assumes the user has acquired two PCs of the model: Ultra Compact PC Kit Gigabyte Brix S GB-Bki7HA-7500 BWEK, one for the RRU and the other for the RCC.

---

It is assumed that the user also has another PC capable of running the EPC and also an USRP B210. Figure 1 illustrates the network setup.

The operating system used in this guide is:

64-bit Ubuntu 16.04.2 LTS.

Proceed to install the operating system in the both the RRU and the RCC PCs.

## 2.1 Low latency kernel

After installing the Ubuntu operating system, proceed to install a low latency kernel. To do this, write at the command line:

```
sudo apt-get install linux-image-4.8.0-58-lowlatency linux-headers-4.8.0-58-lowlatency
```

Restart PC and press "Esc" at boot.

Select "Advanced options for Ubuntu"

Select "Ubuntu, with Linux 4.8.0-58-lowlatency"

At the command line write:

```
uname -a
```

to verify that the system has booted with the low-latency kernel

You can remove the generic kernel to avoid always having to select the low-latency kernel at startup. Write at the command line:

```
dpkg --get-selections | grep linux-image
```

to see the installed kernels. Remove all of them except the low-latency kernel. To do this, for example, to remove these two kernels write at the command line:

```
sudo apt-get purge linux-image-4.10.0-28-generic  
sudo apt-get purge linux-image-4.13.0-37-generic
```

Then write:

```
sudo update-grub2
```

and reboot.

REMEMBER to boot first in low-latency kernel before removing the other kernels!

## 2.2 Power management

Next we proceed to ensure that the CPU cores are always at full speed.

Restart PC and Press “Del” to enter BIOS configuration.

At “Advanced” tab select “CPU Configuration”.

At “CPU C states” select “Disabled”.

At “CPU P states” select “Disabled”.

At “Turbo Mode” select “Disabled”.

Proceed to save and exit BIOS configuration.

To disable hyperthreading on Ubuntu write at the command line:

```
sudo nano /etc/rc.local
```

and enter the following script (change the `cpu[0-9]` with the range of present CPUs - e.g.: `cpu[0-9]` for 10 CPUs):

```
for CPU in /sys/devices/system/cpu/cpu[0-9]*; do
  CPUID='basename $CPU | cut -b4-'
  echo -en "CPU: $CPUID\t"
  [ -e $CPU/online ] && echo "1" > $CPU/online
  THREAD1='cat $CPU/topology/thread_siblings_list | cut -f1 -d
  ↪ , '
  if [ $CPUID = $THREAD1 ]; then
    echo "-> enable"
    [ -e $CPU/online ] && echo "1" > $CPU/online
  else
    echo "-> disable"
    echo "0" > $CPU/online
  fi
done
```

Proceed to reboot the PC.

To disable frequency scaling write at the command line:

```
sudo apt-get install cpufrequtils
```

Edit the following file:

```
sudo nano /etc/default/cpufrequtils
```

Add the following line to it:

```
GOVERNOR="performance"
```

---

Save and exit.

Then enter at the command line:

```
sudo update-rc.d ondemand disable
sudo /etc/init.d/cpufrequtils restart
```

We can check that the CPU cores are at the maximum speed by writing at the command line:

```
cpufreq-info
```

Next, we need to disable p-states and c-states in Linux. To do that write at the command line:

```
sudo nano /etc/default/grub
```

and replace the line:

```
GRUB_CMDLINE_LINUX_DEFAULT ...
```

with the following line:

```
GRUB_CMDLINE_LINUX_DEFAULT="quiet intel_pstate=disable
    ↪ processor.max_cstate=1 intel_idle.max_cstate=0 idle=poll
    ↪ "
```

Save and exit. Write in the command line:

```
sudo update-grub
```

Next, we need to disable powerclamp. To do that, write in the command line:

```
sudo nano /etc/modprobe.d/blacklist.conf
```

and add the following line at the end of the file:

```
blacklist intel_powerclamp
```

Save, exit and reboot

Install i7z utility to check the CPU with:

```
sudo apt-get install i7z
sudo i7z
```

The C0 states should be at 100% and the other states should be at 0%.  
WARNING: In the hardware tested we could not bring C1 states to 0 (they were at 7.24%).

The procedures described up to this point should be followed for both the RCC and the RRU PCs.

### 3 Setting up OAI RRU and OAI RCC

To get the OAI eNB source code, install git first by writing at the command line:

```
sudo apt-get update
sudo apt-get install subversion git
```

Add a certificate from gitlab.eurecom.fr to your Ubuntu installation:

```
echo -n | openssl s\client -showcerts -connect gitlab.eurecom.
  ↪ fr:443 2\textgreater{/dev/null | sed -ne '/-BEGIN
  ↪ CERTIFICATE-/,/-END CERTIFICATE-/p' | sudo tee -a /etc/
  ↪ ssl/certs/ca-certificates.crt
```

If you do not have root access to /etc/ssl directory, disable certificate check with (you probably don't need to do this):

```
git config --global http.sslverify false
```

Then proceed to checkout RAN repository (eNB RAN + UE RAN) by writing at the command line:

```
git clone https://gitlab.eurecom.fr/oai/openairinterface5g.git
cd ~/openairinterface5g
git checkout develop
git pull
```

This will download the developer branch of OAI5G. The version used in this guide was "2018.w15". The instructions up to this point should be followed for both the RRU and the RCC PCs.



---

### 3.1 Setting up the OAI RRU

Proceed to the RRU PC. Build OAI RRU by writing at the command line:

```
cd ~/openairinterface5g
source oaienv
cd cmake_targets
./build_oai -I --eNB -w USRP
```

Then edit the configuration file with:

```
nano ~/openairinterface5g/targets/PROJECTS/GENERIC-LTE-EPC/CONF
  ↪ /rru.oaisim.conf
```

The file should be similar to this:

```
RUs = (
  {
    local_if_name = "enp0s31f6";
    remote_address = "10.10.10.1"
    local_address = "10.10.10.2";
    local_portc = 50000;
    remote_portc = 50000;
    local_portd = 50001;
    remote_portd = 50001;
    local_rf = "yes"
    tr_preference = "udp_if4p5";
    nb_tx = 1;
    nb_rx = 1;
    max_pdschReferenceSignalPower = -15;
    max_rxgain = 120;
    bands = [7]; # [7,13]
  }
);

log_config = {
  global_log_level ="info";
  ...
  rrc_log_verbosity ="medium";
};
```

In this file we need to change:

"local\_if\_name" to the name of the ethernet interface of the RRU;  
"remote\_address" to the IP address of the ethernet interface of the RCC that connects to the RRU;  
"local\_address" to the IP address of the ethernet interface of the RRU;  
"tr\_preference" to "udp\_if4p5" to signalize functional split NGFI IF4.5;  
"bands" to "[7]" to select band 7;  
"global\_log\_level" to "info";  
"phy\_log\_level" to "info";  
"mac\_log\_level" to "info".

The three last variables are not obligatory but allow for smoother performance of the RRU.

To run OAI RRU execute the following commands:

```
cd ~/openairinterface5g
source oaienv
cd cmake_targets/lte_build_oai/build
sudo -E ./lte-softmodem -O $OPENAIR_DIR/targets/PROJECTS/
↳ GENERIC-LTE-EPC/CONF/rru.oaisim.conf
```

---

## 3.2 Setting up the OAI RCC

Proceed to the RCC PC. Build OAI RCC by writing at the command line:

```
cd ~/openairinterface5g
source oaienv
cd cmake_targets
./build_oai -I --eNB -w USRP
./build_oai -w None -t ETHERNET -x -c --eNB
```

Because in this git branch there is no configuration file for 25 Resource Blocks (RBs), we proceed to make a copy of the configuration file for 50 RBs to use 25 RBs with:

```
cd ~/openairinterface5g/targets/PROJECTS/GENERIC-LTE-EPC/CONF
cp rcc.band7.tm1.if4p5.50PRB.conf rcc.band7.tm1.if4p5.25PRB.
  ↪ conf
nano rcc.band7.tm1.if4p5.25PRB.conf
```

This configuration file is for 25 Resource Blocks (5MHz) and functional split "NGFI IF4.5". The file should be similar to this:

```
...
eNBs =
(
{
  # real_time choice in {hard, rt-preempt, no}
  real_time = "no";
  ////////////// Identification parameters:
  eNB_ID = 0xe00;
  cell_type = "CELL_MACRO_ENB";
  eNB_name = "eNB-Eurecom-LTEBox";
  // Tracking area code, 0x0000 and 0xffff are reserved
  ↪ values
  tracking_area_code = "1";
  mobile_country_code = "268";
  mobile_network_code = "08";
  tr_s_preference = "local_mac"
  ////////////// Physical parameters:
  component_carriers = (
  {
```

```

node_function = "NGFI_RCC_IF4p5";
...
downlink_frequency = 2660000000L;
...
N_RB_DL = 25;
...
pdsch_referenceSignalPower = -24;
...
rach_preambleInitialReceivedTargetPower = -104;
...
////////// MME parameters:
mme_ip_address = ( { ipv4 = "192.168.21.17";
                    ipv6 = "192:168:30::17";
                    active = "yes";
                    preference = "ipv4";
                    }
                  );

NETWORK_INTERFACES :
{

    ENB_INTERFACE_NAME_FOR_S1_MME = "enx00e04c534458";
    ENB_IPV4_ADDRESS_FOR_S1_MME = "192.168.21.18/24";
    ENB_INTERFACE_NAME_FOR_S1U = "enx00e04c534458";
    ENB_IPV4_ADDRESS_FOR_S1U = "192.168.21.18/24";
    ENB_PORT_FOR_S1U = 2152; # Spec 2152
};
}
);
...
RUs = (
{
    local_if_name = "enp0s31f6";
    remote_address = "10.10.10.2";
    local_address = "10.10.10.1";
    local_portc = 50000;
    remote_portc = 50000;
    local_portd = 50001;

```

---

```

        remote_portd = 50001;
        local_rf = "no"
        tr_preference = "udp_if4p5"
        nb_tx = 1
        nb_rx = 1
        att_tx = 0
        att_rx = 0;
        eNB_instances = [0];
    }
);
...

```

In this file we need to change:

- "tracking\_area\_code" to "1";
- "mobile\_country\_code" to "268";
- "mobile\_network\_code" to "08";
- "node\_function" to "NGFI\_RCC\_IF4p5";
- "downlink\_frequency" to 2660000000L;
- "N\_RB\_DL" to 25;
- "pdsch\_referenceSignalPower" to -24;
- "rach\_preambleInitialReceivedTargetPower" to -104;
- in "mme\_ip\_address", "ipv4" to "192.168.21.17" (the IP address of the EPC); in "NETWORK\_INTERFACES":
- "ENB\_INTERFACE\_NAME\_FOR\_S1\_MME" to "enx00e04c534458" (name of the ethernet interface to the EPC);
- "ENB\_IPV4\_ADDRESS\_FOR\_S1\_MME" to "192.168.21.18/24" (IP address of the ethernet interface to the EPC);
- "ENB\_INTERFACE\_NAME\_FOR\_S1U" to "enx00e04c534458" (same as above);
- "ENB\_IPV4\_ADDRESS\_FOR\_S1U" to "192.168.21.18/24" (same as above);
- in "RUs":
- "local\_if\_name" to "enp0s31f6" (name of the ethernet interface of the RCC that connects to the RRU);
- "remote\_address" to "10.10.10.2" (IP address of the RRU);
- "local\_address" to "10.10.10.1" (IP address of the interface of the RCC that connects to the RRU);
- "tr\_preference" to "udp\_if4p5" (the functional split).

To run OAI RCC execute the following commands:

```
cd ~/openairinterface5g
source oaienv
cd cmake_targets/lte_build_oai/build
sudo -E ./lte-softmodem -O $OPENAIR_DIR/targets/PROJECTS/
↳ GENERIC-LTE-EPC/CONF/rcc.band7.tm1.if4p5.25PRB.conf
```

If all went well, you should have both RRU and RCC up and running and may proceed to test them in a network similar to the one displayed in Figure 1!

## Appendix C

### Sample of OAI eNB, CU, DU and gNB Configuration files

## C.1 OAI eNB Configuration script

```
,
Active_eNBs = ("eNB_Eurecom_LTEBox");
# Asn1_verbosity, choice in: none, info, annoying
Asn1_verbosity = "none";

eNBs =
(
{
////////// Identification parameters:
eNB_ID = 0xe00;

cell_type = "CELL_MACRO_ENB";

eNB_name = "eNB_Eurecom_LTEBox";

// Tracking area code, 0x0000 and 0xfffe are reserved values
tracking_area_code = "1";

mobile_country_code = "268";

mobile_network_code = "08";

////////// Physical parameters:

component_carriers = (
{
node_function = "eNodeB_3GPP";
node_timing = "synch_to_ext_device";
node_synch_ref = 0;
frame_type = "FDD";
tdd_config = 3;
tdd_config_s = 0;
prefix_type = "NORMAL";
eutra_band = 7;
downlink_frequency = 2660000000L;
uplink_frequency_offset = -120000000;
Nid_cell = 0;
N_RB_DL = 25; # 25RB=5MHz, 50RB=10MHz, 100RB=20MHz
Nid_cell_mbsfn = 0;
nb_antenna_ports = 2;
nb_antennas_tx = 2;
nb_antennas_rx = 2;
tx_gain = 90;
rx_gain = 125;
prach_root = 0;
```



### C.1. OAI eNB Configuration script

---

```
Active_eNBs = ("eNB_Eurecom_LTEBox");
# Asn1_verbosity, choice in: none, info, annoying
Asn1_verbosity = "none";

eNBs =
(
{
////////// Identification parameters:
eNB_ID = 0xe00;

cell_type = "CELL_MACRO_ENB";

eNB_name = "eNB_Eurecom_LTEBox";

// Tracking area code, 0x0000 and 0xfffe are reserved values
tracking_area_code = "1";

mobile_country_code = "268";

mobile_network_code = "08";

////////// Physical parameters:

component_carriers = (
{
node_function = "eNodeB_3GPP";
node_timing = "synch_to_ext_device";
node_synch_ref = 0;
frame_type = "FDD";
tdd_config = 3;
tdd_config_s = 0;
prefix_type = "NORMAL";
eutra_band = 7;
downlink_frequency = 2660000000L;
uplink_frequency_offset = -120000000;
Nid_cell = 0;
N_RB_DL = 25; # 25RB=5MHz, 50RB=10MHz, 100RB=20MHz
Nid_cell_mbsfn = 0;
nb_antenna_ports = 2;
nb_antennas_tx = 2;
nb_antennas_rx = 2;
tx_gain = 90;
rx_gain = 125;
prach_root = 0;
```

```

prach_config_index           = 0;
prach_high_speed             = "DISABLE";
prach_zero_correlation       = 1;
prach_freq_offset            = 2;
pucch_delta_shift            = 1;
pucch_nRB_CQI                = 1;
pucch_nCS_AN                 = 0;
pucch_n1_AN                  = 32;
pdsch_referenceSignalPower   = -24;
pdsch_p_b                    = 1;
pusch_n_SB                   = 1;
pusch_enable64QAM            = "DISABLE";
pusch_hoppingMode            = "interSubFrame";
pusch_hoppingOffset          = 0;
pusch_groupHoppingEnabled    = "ENABLE";
pusch_groupAssignment        = 0;
pusch_sequenceHoppingEnabled = "DISABLE";
pusch_nDMRS1                 = 1;
phich_duration               = "NORMAL";
phich_resource                = "ONESIXTH";
srs_enable                   = "DISABLE";
/* srs_BandwidthConfig        =;
srs_SubframeConfig           =;
srs_ackNackST                =;
srs_MaxUpPts                 =;*/

pusch_p0_Nominal             = -90;
pusch_alpha                   = "AL1";
pucch_p0_Nominal             = -96;
msg3_delta_Preamble          = 6;
pucch_deltaF_Format1         = "deltaF2";
pucch_deltaF_Format1b        = "deltaF3";
pucch_deltaF_Format2         = "deltaF0";
pucch_deltaF_Format2a        = "deltaF0";
pucch_deltaF_Format2b        = "deltaF0";

rach_numberOfRA_Preambles    = 64;
rach_preamblesGroupAConfig   = "DISABLE";
/*
rach_sizeOfRA_PreamblesGroupA =;
rach_messageSizeGroupA       =;
rach_messagePowerOffsetGroupB =;
*/
rach_powerRampingStep        = 4;

```

### C.1. OAI eNB Configuration script

---

```
rach_preambleInitialReceivedTargetPower    = -104;
rach_preambleTransMax                      = 10;
rach_raResponseWindowSize                  = 10;
rach_macContentionResolutionTimer          = 48;
rach_maxHARQ_Msg3Tx                       = 4;

pcch_default_PagingCycle                   = 128;
pcch_nB                                    = "oneT";
bcch_modificationPeriodCoeff               = 2;
ue_TimersAndConstants_t300                 = 1000;
ue_TimersAndConstants_t301                 = 1000;
ue_TimersAndConstants_t310                 = 1000;
ue_TimersAndConstants_t311                 = 10000;
ue_TimersAndConstants_n310                 = 20;
ue_TimersAndConstants_n311                 = 1;

    ue_TransmissionMode                     = 2;
}
);

srb1_parameters :
{
    # timer_poll_retransmit = (ms) [5, 10, 15, 20,... 250, 300, 350, ... 500]
    timer_poll_retransmit = 80;

    # timer_reordering = (ms) [0,5, ... 100, 110, 120, ... ,200]
    timer_reordering = 35;

    # timer_reordering = (ms) [0,5, ... 250, 300, 350, ... ,500]
    timer_status_prohibit = 0;

    # poll_pdu = [4, 8, 16, 32 , 64, 128, 256, infinity(>10000)]
    poll_pdu = 4;

    # poll_byte = (kB) [25,50,75,100,125,250,375,500,750,1000,1250,1500,2000,3000,infinity(>10000)]
    poll_byte = 99999;

    # max_retx_threshold = [1, 2, 3, 4 , 6, 8, 16, 32]
    max_retx_threshold = 4;
}

# ----- SCTP definitions
SCTP :
{
```

```
# Number of streams to use in input/output
SCTP_INSTREAMS = 2;
SCTP_OUTSTREAMS = 2;
};

////////// MME parameters:
mme_ip_address = { {   ipv4   = "192.168.21.17";
                      ipv6   = "192:168:30::17";
                      active  = "yes";
                      preference = "ipv4";
                      }
                  };

NETWORK_INTERFACES :
{

    ENB_INTERFACE_NAME_FOR_S1_MME   = "eno2";
    ENB_IPV4_ADDRESS_FOR_S1_MME     = "192.168.21.17/24";
    ENB_INTERFACE_NAME_FOR_S1U     = "eno2";
    ENB_IPV4_ADDRESS_FOR_S1U       = "192.168.21.17/24";
    ENB_PORT_FOR_S1U                = 2152; # Spec 2152
};

log_config :
{
    global_log_level      = "info";
    global_log_verbosity  = "medium";
    hw_log_level          = "info";
    hw_log_verbosity      = "medium";
    phy_log_level         = "debug";
    phy_log_verbosity     = "medium";
    mac_log_level         = "info";
    mac_log_verbosity     = "high";
    rlc_log_level         = "info";
    rlc_log_verbosity     = "medium";
    pdcp_log_level       = "info";
    pdcp_log_verbosity   = "medium";
    rrc_log_level        = "info";
    rrc_log_verbosity    = "medium";
};
}
);
```

## C.2 OAI CU Configuration script

```
Active_eNBs = ( "eNB-CU-Eurecom-LTEBox");
# Asnl_verbosity, choice in: none, info, annoying
Asnl_verbosity = "none";

eNBs = (
{
  /////////////// Identification parameters:
  eNB_ID      = 0xe00;

  cell_type = "CELL_MACRO_ENB";

  eNB_name = "eNB-CU-Eurecom-LTEBox";

  // Tracking area code, 0x0000 and 0xfffe are reserved values
  tracking_area_code = 1;
  plmn_list = ( { mcc = 268; mnc = 08; mnc_length = 2; } )

  nr_cellid = 12345678L

  tr_s_preference = "f1"

  local_s_if_name = "enp95s0f1";
  remote_s_address = "10.10.30.2";
  local_s_address = "10.10.30.1";
  local_s_portc = 501;
  remote_s_portc = 500;
  local_s_portd = 601;
  remote_s_portd = 600;

  /////////////// Physical parameters:

  component_carriers = (
  {
    node_function           = "3GPP_eNodeB";
    node_timing             = "synch_to_ext_device";
    node_synch_ref         = 0;
    frame_type              = "FDD";
    tdd_config              = 3;
    tdd_config_s            = 0;
    prefix_type             = "NORMAL";
    eutra_band              = 7;
    downlink_frequency      = 2680000000L;
    uplink_frequency_offset = -120000000;
    Nid_cell                = 0;
    N_RB_DL                 = 25;
    pbch_repetition        = "FALSE";
    prach_root              = 0;
    prach_config_index      = 0;
    prach_high_speed        = "DISABLE";
    prach_zero_correlation = 1;
    prach_freq_offset       = 2;
    pucch_delta_shift       = 1;
    pucch_nRB_CQI           = 0;
    pucch_nCS_AN            = 0;
    pucch_n1_AN             = 0;
    pdsch_referenceSignalPower = -25;
    pdsch_p_b               = 0;
  }
);
};
);
```

---

*Appendix C. Sample of OAI eNB, CU, DU and gNB Configuration files*

---

```
Active_eNBs = ( "eNB-CU-Eurecom-LTEBox");
# Asnl_verbosity, choice in: none, info, annoying
Asnl_verbosity = "none";

eNBs = (
{
////////// Identification parameters:
eNB_ID      = 0xe00;

cell_type   = "CELL_MACRO_ENB";

eNB_name    = "eNB-CU-Eurecom-LTEBox";

// Tracking area code, 0x0000 and 0xffff are reserved values
tracking_area_code = 1;
plmn_list = ( { mcc = 268; mnc = 08; mnc_length = 2; } )

nr_cellid = 12345678L

tr_s_preference = "f1"

local_s_if_name = "enp95s0f1";
remote_s_address = "10.10.30.2";
local_s_address = "10.10.30.1";
local_s_portc = 501;
remote_s_portc = 500;
local_s_portd = 601;
remote_s_portd = 600;

////////// Physical parameters:
component_carriers = (
{
    node_function           = "3GPP_eNodeB";
    node_timing             = "synch_to_ext_device";
    node_synch_ref          = 0;
    frame_type              = "FDD";
    tdd_config              = 3;
    tdd_config_s            = 0;
    prefix_type             = "NORMAL";
    eutra_band              = 7;
    downlink_frequency      = 2680000000L;
    uplink_frequency_offset = -1200000000;
    Nid_cell                = 0;
    N_RB_DL                 = 25;
    pbch_repetition        = "FALSE";
    prach_root              = 0;
    prach_config_index     = 0;
    prach_high_speed       = "DISABLE";
    prach_zero_correlation = 1;
    prach_freq_offset      = 2;
    pucch_delta_shift      = 1;
    pucch_nRB_CQI          = 0;
    pucch_nCS_AN           = 0;
    pucch_n1_AN            = 0;
    pdsch_referenceSignalPower = -25;
    pdsch_p_b              = 0;

```

## C.2. OAI CU Configuration script

---

```
pusch_n_SB = 1;
pusch_enable64QAM = "DISABLE";
pusch_hoppingMode = "interSubFrame";
pusch_hoppingOffset = 0;
pusch_groupHoppingEnable = "ENABLE";
pusch_groupAssignment = 0;
pusch_sequenceHoppingEnabled = "DISABLE";
pusch_nDMRS1 = 1;
phich_duration = "NORMAL";
phich_resource = "ONESIXTH";
srs_enable = "DISABLE";
/*
srs_BandwidthConfig =;
srs_SubframeConfig =;
srs_ackNackST =;
srs_MaxUpPts =;
*/

pusch_p0_Nominal = -96;
pusch_alpha = "AL1";
pucch_p0_Nominal = -104;
msg3_delta_Preamble = 6;
pucch_deltaF_Format1 = "deltaF2";
pucch_deltaF_Format1b = "deltaF3";
pucch_deltaF_Format2 = "deltaF0";
pucch_deltaF_Format2a = "deltaF0";
pucch_deltaF_Format2b = "deltaF0";

rach_numberOfRA_Preambles = 64;
rach_preamblesGroupAConfig = "DISABLE";
/*
rach_sizeOfRA_PreamblesGroupA = ;
rach_messageSizeGroupA = ;
rach_messagePowerOffsetGroupB = ;
*/
rach_powerRampingStep = 4;
rach_preambleInitialReceivedTargetPower = -108;
rach_preambleTransMax = 10;
rach_raResponseWindowSize = 10;
rach_macContentionResolutionTimer = 48;
rach_maxHARQ_Msg3Tx = 4;

pcch_default_PagingCycle = 128;
pcch_nB = "oneT";
bcch_modificationPeriodCoeff= 2;
ue_TimersAndConstants_t300 = 1000;
ue_TimersAndConstants_t301 = 1000;
ue_TimersAndConstants_t310 = 1000;
ue_TimersAndConstants_t311 = 10000;
ue_TimersAndConstants_n310 = 20;
ue_TimersAndConstants_n311 = 1;
ue_TransmissionMode = 1;

//Parameters for SIB18
rxPool_sc_CP_Len = "normal";
rxPool_sc_Period = "sf40";
rxPool_data_CP_Len = "normal";
```

*Appendix C. Sample of OAI eNB, CU, DU and gNB Configuration files*

```

rxPool_ResourceConfig_prb_Num           = 20;
rxPool_ResourceConfig_prb_Start        = 5;
rxPool_ResourceConfig_prb_End          = 44;
rxPool_ResourceConfig_offsetIndicator_present = "prSmall";
rxPool_ResourceConfig_offsetIndicator_choice = 0;
rxPool_ResourceConfig_subframeBitmap_present = "prBs40";
rxPool_ResourceConfig_subframeBitmap_choice_bs_buf =
"000000000000000000000000";
rxPool_ResourceConfig_subframeBitmap_choice_bs_size = 5;
rxPool_ResourceConfig_subframeBitmap_choice_bs_bits_unused = 0;
/*
rxPool_dataHoppingConfig_hoppingParameter = 0;
rxPool_dataHoppingConfig_numSubbands =
"ns1";
rxPool_dataHoppingConfig_rbOffset = 0;
rxPool_commTxResourceUC-ReqAllowed =
"TRUE";
*/

// Parameters for SIB19
discRxPool_cp_Len =
"normal"
discRxPool_discPeriod =
"rf32"
discRxPool_numRetx = 1;
discRxPool_numRepetition = 2;
discRxPool_ResourceConfig_prb_Num = 5;
discRxPool_ResourceConfig_prb_Start = 3;
discRxPool_ResourceConfig_prb_End = 21;
discRxPool_ResourceConfig_offsetIndicator_present =
"prSmall";
discRxPool_ResourceConfig_offsetIndicator_choice = 0;
discRxPool_ResourceConfig_subframeBitmap_present =
"prBs40";
discRxPool_ResourceConfig_subframeBitmap_choice_bs_buf =
"f0ffffff";
discRxPool_ResourceConfig_subframeBitmap_choice_bs_size = 5;
discRxPool_ResourceConfig_subframeBitmap_choice_bs_bits_unused = 0;
}
);

srb1_parameters :
{
# timer_poll_retransmit = (ms) [5, 10, 15, 20,... 250, 300, 350, ...
500]
timer_poll_retransmit = 80;

# timer_reordering = (ms) [0,5, ... 100, 110, 120, ... ,200]
timer_reordering = 35;

# timer_reordering = (ms) [0,5, ... 250, 300, 350, ... ,500]
timer_status_prohibit = 0;

# poll_pdu = [4, 8, 16, 32 , 64, 128, 256, infinity(>10000)]
poll_pdu = 4;

```



## C.2. OAI CU Configuration script

---

```
# poll_byte = (kB)
[25,50,75,100,125,250,375,500,750,1000,1250,1500,2000,3000,infinity(>10000)]
poll_byte = 99999;

# max_retx_threshold = [1, 2, 3, 4, 6, 8, 16, 32]
max_retx_threshold = 4;
}

# ----- SCTP definitions
SCTP :
{
# Number of streams to use in input/output
SCTP_INSTREAMS = 2;
SCTP_OUTSTREAMS = 2;
};

////////// MME parameters:
mme_ip_address = (
{
    ipv4 = "192.168.21.17";
    ipv6 = "192:168:30::17";
    port = 36412 ;
    active = "yes";
    preference = "ipv4";
}
);

NETWORK_INTERFACES : {
    ENB_INTERFACE_NAME_FOR_S1_MME = "eno2";
    ENB_IPV4_ADDRESS_FOR_S1_MME = "192.168.21.17";
    ENB_INTERFACE_NAME_FOR_S1U = "eno2";
    ENB_IPV4_ADDRESS_FOR_S1U = "192.168.21.17";
    ENB_PORT_FOR_S1U = 2152; # Spec 2152
    ENB_IPV4_ADDRESS_FOR_X2C = "192.168.21.17";
    ENB_PORT_FOR_X2C = 36422; # Spec 36422
};
}
);

log_config = {
    global_log_level = "info";
    global_log_verbosity = "medium";
    pdcp_log_level = "info";
    pdcp_log_verbosity = "high";
    rrc_log_level = "info";
    rrc_log_verbosity = "medium";
    flexran_agent_log_level = "info";
    flexran_agent_log_verbosity = "medium";
    gtp_log_level = "info";
    gtp_log_verbosity = "medium";
};

NETWORK_CONTROLLER : {
    FLEXRAN_ENABLED = "no";
    FLEXRAN_INTERFACE_NAME = "lo";
    FLEXRAN_IPV4_ADDRESS = "CI_FLEXRAN_CTL_IP_ADDR";
```

*Appendix C. Sample of OAI eNB, CU, DU and gNB Configuration files*

---

```
FLEXRAN_PORT          = 2210;  
FLEXRAN_CACHE         = "/mnt/oai_agent_cache";  
FLEXRAN_AWAIT_RECONF = "no";  
};
```

## C.3 OAI DU Configuration script

```
Active_eNBs = ( "eNB-Eurecom-DU");
# Asnl_verbosity, choice in: none, info, annoying
Asnl_verbosity = "none";

eNBs =
(
  {
    //////////// Identification parameters:
    eNB_CU_ID = 0xe00;

    eNB_name = "eNB-Eurecom-DU";

    // Tracking area code, 0x0000 and 0xfffe are reserved values
    tracking_area_code = 1;
    plmn_list = ( { mcc = 268; mnc = 08; mnc_length = 2; } )

    nr_cellid = 12345678L

    //////////// Physical parameters:

    component_carriers = (
      {
        node_function           = "3GPP_eNODEB";
        node_timing             = "synch_to_ext_device";
        node_synch_ref          = 0;
        frame_type              = "FDD";
        tdd_config              = 3;
        tdd_config_s            = 0;
        prefix_type             = "NORMAL";
        eutra_band              = 7;
        downlink_frequency      = 2680000000L;
        uplink_frequency_offset = -120000000;
        Nid_cell                = 0;
        N_RB_DL                 = 25;
        Nid_cell_mbsfn          = 0;
        nb_antenna_ports        = 1;
        nb_antennas_tx          = 1;
        nb_antennas_rx          = 1;
        tx_gain                  = 90;
        rx_gain                  = 125;

        pucch_deltaF_Format1    = "deltaF2";
        pucch_deltaF_Format1b   = "deltaF3";
        pucch_deltaF_Format2    = "deltaF0";
        pucch_deltaF_Format2a   = "deltaF0";
        pucch_deltaF_Format2b   = "deltaF0";
      }
    );

    # ----- SCTP definitions
    SCTP :
    {
      # Number of streams to use in input/output
      SCTP_INSTREAMS = 2;
      SCTP_OUTSTREAMS = 2;
    };
  }
);
```

---

Appendix C. Sample of OAI eNB, CU, DU and gNB Configuration files

---

```
Active_eNBs = ( "eNB-Eurecom-DU");
# Asnl_verbosity, choice in: none, info, annoying
Asnl_verbosity = "none";

eNBs =
(
{
////////// Identification parameters:
eNB_CU_ID = 0xe00;

eNB_name = "eNB-Eurecom-DU";

// Tracking area code, 0x0000 and 0xffffe are reserved values
tracking_area_code = 1;
plmn_list = ( { mcc = 268; mnc = 08; mnc_length = 2; } )

nr_cellid = 12345678L

////////// Physical parameters:
component_carriers = (
{
node_function           = "3GPP_eNODEB";
node_timing             = "synch_to_ext_device";
node_synch_ref          = 0;
frame_type              = "FDD";
tdd_config              = 3;
tdd_config_s            = 0;
prefix_type             = "NORMAL";
eutra_band               = 7;
downlink_frequency      = 2680000000L;
uplink_frequency_offset = -120000000;
Nid_cell                 = 0;
N_RB_DL                  = 25;
Nid_cell_mbsfn           = 0;
nb_antenna_ports         = 1;
nb_antennas_tx           = 1;
nb_antennas_rx           = 1;
tx_gain                  = 90;
rx_gain                  = 125;

pucch_deltaF_Format1    = "deltaF2";
pucch_deltaF_Format1b   = "deltaF3";
pucch_deltaF_Format2    = "deltaF0";
pucch_deltaF_Format2a   = "deltaF0";
pucch_deltaF_Format2b   = "deltaF0";
}
);

# ----- SCTP definitions
SCTP :
{
# Number of streams to use in input/output
SCTP_INSTREAMS = 2;
SCTP_OUTSTREAMS = 2;
};
```

### C.3. OAI DU Configuration script

---

```
    }
);

MACRLCs = (
{
    num_cc          = 1;
    tr_s_preference = "local_L1";
    tr_n_preference = "f1";
    local_n_if_name = "enp1s0f0";
    remote_n_address = "10.10.30.1";
    local_n_address  = "10.10.30.2";
    local_n_portc    = 500;
    remote_n_portc   = 501;
    local_n_portd    = 600;
    remote_n_portd   = 601;
}
);

Lls = (
{
    num_cc = 1;
    tr_n_preference = "local_mac";
}
);

RUs = (
{
    local_rf          = "yes";
    nb_tx             = 1;
    nb_rx             = 1;
    att_tx            = 10;
    att_rx            = 10;
    bands              = [7];
    max_pdschReferenceSignalPower = -25;
    max_rxgain        = 125;
    eNB_instances     = [0];
}
);

log_config = {
    global_log_level      = "info";
    global_log_verbosity = "medium";
    hw_log_level          = "info";
    hw_log_verbosity     = "medium";
    phy_log_level         = "info";
    phy_log_verbosity    = "medium";
    mac_log_level         = "info";
    mac_log_verbosity    = "high";
    rlc_log_level         = "info";
    rlc_log_verbosity    = "medium";
    flexran_agent_log_level = "info";
    flexran_agent_log_verbosity = "medium";
};

NETWORK_CONTROLLER : {
    FLEXRAN_ENABLED      = "no";
    FLEXRAN_INTERFACE_NAME = "lo";
};
```

---

*Appendix C. Sample of OAI eNB, CU, DU and gNB Configuration files*

---

```
FLEXRAN_IPV4_ADDRESS = "CI_FLEXRAN_CTL_IP_ADDR";
FLEXRAN_PORT         = 2210;
FLEXRAN_CACHE        = "/mnt/oai_agent_cache";
FLEXRAN_AWAIT_RECONF = "no";
};

THREAD_STRUCT = (
{
    #three config for level of parallelism "PARALLEL_SINGLE_THREAD",
    "PARALLEL_RU_L1_SPLIT", or "PARALLEL_RU_L1_TRX_SPLIT"
    parallel_config = "PARALLEL_SINGLE_THREAD";
    #           #two option for worker "WORKER_DISABLE" or "WORKER_ENABLE"
    worker_config   = "WORKER_ENABLE";
}
);
```

## C.4 OAI gNB Configuration script

```

Active_gNBs = ( "gNB-Eurecom-5GNRBox");
# Asnl_verbosity, choice in: none, info, annoying
Asnl_verbosity = "none";
Num_Threads_PUSCH = 8

gNBs =
(
{
////////// Identification parameters:
gNB_ID      = 0xe00;

cell_type = "CELL_MACRO_GNB";
gNB_name  = "gNB-Eurecom-5GNRBox";

// Tracking area code, 0x0000 and 0xfffe are reserved values
tracking_area_code = 1;
plmn_list = ({mcc = 222; mnc = 01; mnc_length = 2;});

tr_s_preference      = "local_mac"

////////// Physical parameters:

ssb_SubcarrierOffset      = 31; //0;
pdsch_AntennaPorts        = 1;
pusch_TargetSNRx10        = 200;
pucch_TargetSNRx10        = 200;

servingCellConfigCommon = (
{
#spCellConfigCommon

    physCellId              = 0;

# downlinkConfigCommon
#frequencyInfoDL
    # this is 3600 MHz + 84 PRBs@30kHz SCS (same as initial BWP)
    absoluteFrequencySSB    = 641272; //641032;
#641968; 641968=start of ssb at 3600MHz + 82 RBs    641032=center of SSB at center of cell
    dl_frequencyBand        = 78;
    # this is 3600 MHz
    dl_absoluteFrequencyPointA = 640000;
    #scs-SpecificCarrierList
    dl_offstToCarrier        = 0;
# subcarrierSpacing
# 0=kHz15, 1=kHz30, 2=kHz60, 3=kHz120
    dl_subcarrierSpacing    = 1;
    dl_carrierBandwidth     = 106;
#initialDownlinkBWP
#genericParameters
    # this is RBstart=84,L=13 (275*(L-1))+RBstart
    initialDLBWPlocationAndBandwidth = 6366;
//28875; //6366; #6407; #3384;
# subcarrierSpacing
# 0=kHz15, 1=kHz30, 2=kHz60, 3=kHz120
    initialDLBWPsubcarrierSpacing = 1;
#pdcch-ConfigCommon
    initialDLBWPcontrolResourceSetZero = 0;
    initialDLBWPsearchSpaceZero = 0;
#pdsch-ConfigCommon
    #pdschTimeDomainAllocationList (up to 16 entries)
    initialDLBWPk0_0 = 0;

```

---

## Appendix C. Sample of OAI eNB, CU, DU and gNB Configuration files

---

```
Active_gNBs = ( "gNB-Eurecom-5GNRBox");
# Asn1_verbosity, choice in: none, info, annoying
Asn1_verbosity = "none";
Num_Threads_PUSCH = 8

gNBs =
(
{
////////// Identification parameters:
gNB_ID      = 0xe00;

cell_type = "CELL_MACRO_GNB";
gNB_name  = "gNB-Eurecom-5GNRBox";

// Tracking area code, 0x0000 and 0xfffe are reserved values
tracking_area_code = 1;
plmn_list = ({mcc = 222; mnc = 01; mnc_length = 2;});

tr_s_preference      = "local_mac"

////////// Physical parameters:

ssb_SubcarrierOffset      = 31; //0;
pdsch_AntennaPorts        = 1;
pusch_TargetSNRx10        = 200;
pucch_TargetSNRx10        = 200;

servingCellConfigCommon = (
{
#spCellConfigCommon

physCellId                = 0;

# downlinkConfigCommon
#frequencyInfoDL
# this is 3600 MHz + 84 PRBs@30kHz SCS (same as initial BWP)
absoluteFrequencySSB      = 641272; //641032;
#641968; 641968=start of ssb at 3600MHz + 82 RBs    641032=center of SSB at center of cell
dl_frequencyBand          = 78;
# this is 3600 MHz
dl_absoluteFrequencyPointA = 640000;
#scs-SpecificCarrierList
dl_offstToCarrier         = 0;
# subcarrierSpacing
# 0=kHz15, 1=kHz30, 2=kHz60, 3=kHz120
dl_subcarrierSpacing      = 1;
dl_carrierBandwidth       = 106;
#initialDownlinkBWP
#genericParameters
# this is RBstart=84,L=13 (275*(L-1))+RBstart
initialDLBWPlocationAndBandwidth = 6366;
//28875; //6366; #6407; #3384;
# subcarrierSpacing
# 0=kHz15, 1=kHz30, 2=kHz60, 3=kHz120
initialDLBWPsubcarrierSpacing = 1;
#pdcch-ConfigCommon
initialDLBWPcontrolResourceSetZero = 0;
initialDLBWPsearchSpaceZero      = 0;
#pdsch-ConfigCommon
#pdschTimeDomainAllocationList (up to 16 entries)
initialDLBWPk0_0                 = 0;
```



#### C.4. OAI gNB Configuration script

---

```
#initialULBWPmappingType
#0=typeA,1=typeB
  initialDLBWPmappingType_0          = 0;
  #this is SS=1,L=13
  initialDLBWPstartSymbolAndLength_0 = 40;

  initialDLBWPk0_1                   = 0;
  initialDLBWPmappingType_1          = 0;
  #this is SS=2,L=12
  initialDLBWPstartSymbolAndLength_1 = 53;

  initialDLBWPk0_2                   = 0;
  initialDLBWPmappingType_2          = 0;
  #this is SS=1,L=12
  initialDLBWPstartSymbolAndLength_2 = 54;

  initialDLBWPk0_3                   = 0;
  initialDLBWPmappingType_3          = 0;
  #this is SS=1,L=4 //5 (4 is for 43, 5 is for 57)
  initialDLBWPstartSymbolAndLength_3 = 57; //43; //57;
#uplinkConfigCommon
#frequencyInfoUL
  ul_frequencyBand                    = 78;
#scs-SpecificCarrierList
  ul_offstToCarrier                   = 0;
# subcarrierSpacing
# 0=kHz15, 1=kHz30, 2=kHz60, 3=kHz120
  ul_subcarrierSpacing                = 1;
  ul_carrierBandwidth                 = 106;
  pMax                                = 20;
#initialUplinkBWP
#genericParameters
  initialULBWPlocationAndBandwidth    = 6366;
//28875; //6366; #6407; #3384;
# subcarrierSpacing
# 0=kHz15, 1=kHz30, 2=kHz60, 3=kHz120
  initialULBWPsubcarrierSpacing       = 1;
#rach-ConfigCommon
#rach-ConfigGeneric
  prach_ConfigurationIndex           = 98;
#prach_msg1_FDM
#0 = one, 1=two, 2=four, 3=eight
  prach_msg1_FDM                     = 0;
  prach_msg1_FrequencyStart           = 0;
  zeroCorrelationZoneConfig          = 13;
  preambleReceivedTargetPower         = -100;
#preambleTransMax (0..10) = (3,4,5,6,7,8,10,20,50,100,200)
  preambleTransMax                   = 6;
#powerRampingStep
# 0=dB0,1=dB2,2=dB4,3=dB6
  powerRampingStep                   = 1;
#ra_ReponseWindow
#1,2,4,8,10,20,40,80
  ra_ResponseWindow                  = 5;
#ssb_perRACH_OccasionAndCB_PreamblesPerSSB_PR
#1=oneeighth,2=onefourth,3=half,4=one,5=two,6=four,7=eight,8=sixteen
  ssb_perRACH_OccasionAndCB_PreamblesPerSSB_PR = 4;
#oneHalf (0..15) 4,8,12,16,...60,64
  ssb_perRACH_OccasionAndCB_PreamblesPerSSB = 14; //15;
#ra_ContentionResolutionTimer
#(0..7) 8,16,24,32,40,48,56,64
  ra_ContentionResolutionTimer       = 7;
  rsrp_ThresholdSSB                  = 19;
```

## Appendix C. Sample of OAI eNB, CU, DU and gNB Configuration files

---

```

#prach-RootSequenceIndex_PR
#1 = 839, 2 = 139
    prach_RootSequenceIndex_PR                = 2;
    prach_RootSequenceIndex                    = 1;
    # SCS for msg1, can only be 15 for 30 kHz < 6 GHz, takes precedence over the one
derived from prach-ConfigIndex
    #
    msg1_SubcarrierSpacing                      = 1,

# restrictedSetConfig
# 0=unrestricted, 1=restricted type A, 2=restricted type B
    restrictedSetConfig                          = 0,
    # pusch-ConfigCommon (up to 16 elements)
    initialULBWPk2_0                            = 2;
    initialULBWPmappingType_0                    = 1
    # this is SS=0 L=11
    initialULBWPstartSymbolAndLength_0          = 55;

    initialULBWPk2_1                            = 2;
    initialULBWPmappingType_1                    = 1;
    # this is SS=0 L=12
    initialULBWPstartSymbolAndLength_1          = 69;

    initialULBWPk2_2                            = 7;
    initialULBWPmappingType_2                    = 1;
    # this is SS=10 L=4
    initialULBWPstartSymbolAndLength_2          = 52;

    msg3_DeltaPreamble                          = 1;
    p0_NominalWithGrant                         = -90;

# pucch-ConfigCommon setup :
# pucchGroupHopping
# 0 = neither, 1= group hopping, 2=sequence hopping
    pucchGroupHopping                          = 0;
    hoppingId                                    = 40;
    p0_nominal                                   = -90;
# ssb_PositionsInBursts_BitmapPR
# 1=short, 2=medium, 3=long
    ssb_PositionsInBurst_PR                     = 2;
    ssb_PositionsInBurst_Bitmap                 = 1; #0x80;

# ssb_periodicityServingCell
# 0 = ms5, 1=ms10, 2=ms20, 3=ms40, 4=ms80, 5=ms160, 6=spare2, 7=spare1
    ssb_periodicityServingCell                  = 2;

# dmrs_TypeA_position
# 0 = pos2, 1 = pos3
    dmrs_TypeA_Position                         = 0;

# subcarrierSpacing
# 0=kHz15, 1=kHz30, 2=kHz60, 3=kHz120
    subcarrierSpacing                           = 1;

#tdd-UL-DL-ConfigurationCommon
# subcarrierSpacing
# 0=kHz15, 1=kHz30, 2=kHz60, 3=kHz120
    referenceSubcarrierSpacing                  = 1;
    # pattern1
    # dl_UL_TransmissionPeriodicity
    # 0=ms0p5, 1=ms0p625, 2=ms1, 3=ms1p25, 4=ms2, 5=ms2p5, 6=ms5, 7=ms10
    dl_UL_TransmissionPeriodicity              = 6;

```

## C.4. OAI gNB Configuration script

---

```
nrofDownlinkSlots           = 7; //8; //7;
nrofDownlinkSymbols        = 6; //0; //6;
nrofUplinkSlots            = 2;
nrofUplinkSymbols          = 4; //0; //4;

ssPBCH_BlockPower          = -25;
}

);

# ----- SCTP definitions
SCTP :
{
    # Number of streams to use in input/output
    SCTP_INSTREAMS = 2;
    SCTP_OUTSTREAMS = 2;
};

////////// MME parameters:
mme_ip_address = ( { ipv4      = "192.168.21.17";
                    ipv6      = "192:168:30::17";
                    port      = 36412 ;
                    active    = "yes";
                    preference = "ipv4";
                    }
                );

//x2
enable_x2 = "yes";
t_reloc_prep      = 1000;    /* unit: millisecond */
tx2_reloc_overall = 2000;    /* unit: millisecond */
t_dc_prep         = 1000;    /* unit: millisecond */
t_dc_overall      = 2000;    /* unit: millisecond */
target_enb_x2_ip_address = (
    { ipv4      = "192.168.21.17";
      ipv6      = "192:168:30::17";
      preference = "ipv4";
    }
);

NETWORK_INTERFACES :
{
    GNB_INTERFACE_NAME_FOR_S1_MME      = "eth0";
    GNB_IPV4_ADDRESS_FOR_S1_MME        = "192.168.21.17";
    GNB_INTERFACE_NAME_FOR_S1U         = "eth0";
    GNB_IPV4_ADDRESS_FOR_S1U           = "192.168.21.17";
    GNB_PORT_FOR_S1U                   = 2152; # Spec 2152
    GNB_IPV4_ADDRESS_FOR_X2C           = "192.168.21.17";
    GNB_PORT_FOR_X2C                   = 36422; # Spec 36422
};
};

MACRLCs = (
{
    num_cc = 1;
    tr_s_preference = "local_L1";
    tr_n_preference = "local_RRC";
}
);
```

---

Appendix C. Sample of OAI eNB, CU, DU and gNB Configuration files

---

```
L1s = (
    {
        num_cc = 1;
        tr_n_preference = "local_mac";
    }
);

RUs = (
    {
        local_rf      = "yes"
        nb_tx         = 1
        nb_rx         = 1
        att_tx        = 0
        att_rx        = 0;
        bands         = [7];
        max_pdschReferenceSignalPower = -27;
        max_rxgain    = 114;
        eNB_instances = [0];
        clock_src     = "external";
    }
);

THREAD_STRUCT = (
    {
        #three config for level of parallelism "PARALLEL_SINGLE_THREAD",
        "PARALLEL_RU_L1_SPLIT", or "PARALLEL_RU_L1_TRX_SPLIT"
        parallel_config = "PARALLEL_RU_L1_TRX_SPLIT";
        //parallel_config = "PARALLEL_SINGLE_THREAD";
        #two option for worker "WORKER_DISABLE" or "WORKER_ENABLE"
        worker_config = "WORKER_ENABLE";
    }
);

log_config :
{
    global_log_level      = "info";
    global_log_verbosity = "medium";
    hw_log_level          = "info";
    hw_log_verbosity     = "medium";
    phy_log_level         = "info";
    phy_log_verbosity    = "medium";
    mac_log_level         = "info";
    mac_log_verbosity    = "high";
    rlc_log_level         = "info";
    rlc_log_verbosity    = "medium";
    pdcp_log_level       = "info";
    pdcp_log_verbosity  = "medium";
    rrc_log_level        = "info";
    rrc_log_verbosity   = "medium";
};

uicc: {
    opc = "testopc";
};
```